

Stochastic Energy Management and Cyber-Physical Security of Battery Energy Storage Systems in Smart Distribution Systems

by

Peng Zhuang

A thesis submitted in partial fulfillment of the requirements for the degree of

Doctor of Philosophy
in
Energy Systems

Department of Electrical and Computer Engineering
University of Alberta

©Peng Zhuang, 2020

Abstract

Battery energy storage systems (BESSs) are vital for improving the sustainability, efficiency, and resiliency of smart distribution systems (SDSs). With the proper energy management, BESSs can provide a wide range of applications for both demand-side and grid-scale services in SDSs. However, there are various elements in SDSs with randomnesses, such as renewable energy sources (RES) power output, load demand, electricity price, and the mobility of residential electric vehicles (EVs) and electric buses (EBs), which can significantly affect the performance of energy management of BESSs. Moreover, due to the highly coupled cyber and physical systems in SDSs, the cyber-physical attacks that leverage common cyber attacks to stealthily cause cascaded physical failures seriously threaten the effective and reliable energy management of BESSs. In this thesis, the stochastic energy management and cyber-physical security of BESSs in SDSs are investigated from four main aspects to improve BESS integration in SDSs.

Firstly, to improve the performance of BESSs in demand-side electricity usage cost reductions under randomness, the stochastic energy management of demand-side BESSs is investigated with its application in greenhouses. Specifically, a stochastic multi-timescale energy management scheme for greenhouses with RES and electrical/thermal energy storage systems is proposed. The optimal energy management problem is formulated as a multi-timescale Markov decision process (MMDP) to address the randomness of RES and the outside weather conditions. In particular, a fast-timescale (FTS) process is used to model the rapidly changing electrical process with fine granularity, while a slow-timescale (STS) process is used to model the gradually varying thermal process to reduce the computational complexity. The exact solution of the optimal energy management problem is derived to minimize the greenhouse operating cost. Then, an approximation solution is developed to reduce the computational complexity further. The proposed energy management scheme is evaluated by case studies based on a commercial greenhouse structure from Bonnyville Forest Nursery Inc. for spruce and real data of weather conditions, photovoltaic (PV) generation, combined heat and power (CHP) unit, and energy storage

systems.

In SDSs, the highly penetrated demand-side BESSs that are driven by the objective of electricity usage cost reductions can unintentionally induce residential electricity usage to negatively impact power system operations. In the second work, the stochastic energy management of residential BESSs at high penetration levels in SDSs is studied. A hierarchical and decentralized stochastic energy management scheme is proposed. This energy management problem is formulated in a two-layer hierarchical architecture and is solved in a decentralized manner. In the lower layer, individual BESS's energy management problem is formulated as a Markov decision process (MDP) to minimize the electricity usage cost. In the upper layer, the solutions of individual BESS energy management problems are used by the system operator to minimize the line losses and maintain the voltage levels within the required range, which is formulated as a decentralized partially observable MDP (POMDP) and is solved through dynamic programming with exhaustive backups. A heuristic search and pruning method is proposed to reduce the computational complexity for practical applications. The case study results based on IEEE 5-bus test feeder and IEEE European low voltage test feeder have validated the effectiveness and efficiency of the proposed energy management scheme.

The EVs and EBs with vehicle-to-grid (V2G) and bus-to-grid (B2G) capabilities can function as mobile BESSs to provide energy storage capabilities. However, the mobility of EVs and EBs introduces great challenges to efficient energy management. In the third work, the stochastic energy management of electric bus charging stations (EBCSs) for EBs with B2G capabilities that function as mobile BESSs is investigated. The RES with integrated BESSs are included for the sustainable charging of EBs with reduced costs. By treating B2G-enabled EBCSs as flexible energy prosumers, the day-ahead dynamic prices are used to mitigate charging impacts on SDSs. This problem is formulated as a distributionally robust MDP (DRMDP) to address the inaccuracies of probability density function estimations of random variables. An event-based ambiguity set with combined statistical distance and moment information is developed to achieve *minimax-regret* criterion for robust solutions that are less conservative. To facilitate practical applications and reduce the computational complexity, a heuristic regret function is proposed for tractable solutions, based on which the day-ahead dynamic prices are determined. Case studies based on real EB data from St. Albert Transit and IEEE test feeder indicate that the proposed method can minimize EB charging costs with mitigated impacts on SDSs.

For the cyber-physical security analysis, the understanding of attack structure is es-

essential as it provides helpful guidance for the development of effective countermeasures. Thus, in the fourth work, the mechanisms of cyber-physical attacks against BESSs in SDSs are analyzed. More specifically, a numerical model of false data injection attacks (FDIAs) against distribution system states estimation (DSSE) of SDSs is developed, which is used to construct stealthy cyber attacks targeting system information integrity of SDSs. In the developed FDIAs, the three-phase feeder model is leveraged to consider the unbalanced loads and unsymmetrical line parameters of practical SDSs. The virtual self admittance is added to address the missing phase(s) in practical multiphase SDSs. Further, based on the developed FDIAs, the mechanism of FDIAs against the state of charge (SoC) estimation of BESSs in SDSs is studied. The results of the case study based on real data of the modified IEEE 13 bus test feeder and parameters of Lithium-ion battery pack show that an adversary can use the well-constructed FDIAs to cause significant errors in SoC estimation of BESSs that will not be detected. Also, the scalability of the proposed FDIAs against SoC estimation in SDSs is validated using the IEEE 37 bus test feeder.

Preface

The material presented in this thesis is based on the original work by Peng Zhuang. As detailed in the following, materials from some chapters of this thesis have been published as journal articles under the supervision of Dr. Hao Liang in concept formation and by providing comments and corrections to the article manuscript.

Chapter 2 includes the results published in the following journal paper:

- P. Zhuang, H. Liang, and M. Pomphrey, "Stochastic multi-timescale energy management of greenhouses with renewable energy sources," *IEEE Trans. Sustain. Energy*, vol. 10, no. 2, pp. 905-917, Apr. 2019.

The materials presented in Chapter 3 are published in the following journal paper:

- P. Zhuang and H. Liang, "Hierarchical and decentralized stochastic energy management for smart distribution systems with high BESS penetration," *IEEE Trans. Smart Grid*, vol. 6, no. 6, pp. 9583-9595, Dec. 2019.

Chapter 4 includes the contents that have been submitted for publication as follow:

- P. Zhuang and H. Liang, "Stochastic energy management of electric bus charging stations with renewable energy integration and B2G capabilities," submitted to *IEEE Trans. Sustain. Energy*, under 2nd round review.

Chapter 5 includes the results in the following journal papers that have been published or submitted for publication:

- P. Zhuang, R. Deng, and H. Liang, "False data injection attacks against state estimation in multiphase and unbalanced smart distribution systems," *IEEE Trans. Smart Grid*, vol. 10, no. 6, pp. 6000-6013, Nov. 2019.
- P. Zhuang and H. Liang, "False data injection attacks against state of charge estimation of battery energy storage systems in smart distribution networks," submitted to *IEEE Trans. Smart Grid*, under 2nd round review.

Acknowledgements

I would like to express my deepest appreciation to my supervisor *Prof. Hao Liang* for his supportive attitude, encouragement, and guidance through my research at the University of Alberta. Undoubtedly, without his constant help and supervision, this dissertation would not have been possible.

It is an honor for me to extend my gratitude to all my Ph.D. committee members for reviewing my thesis and providing thoughtful comments to improve it. Also, I thank all my colleagues and friends at the Intelligent Energy Systems Lab with whom I had a wonderful time during my Ph.D. program.

In addition, I would like to express my great gratitude to my parents and my wife for their great understanding and support throughout my research.

Table of Contents

1	Introduction	1
1.1	Background	1
1.2	General Terms and Definitions	6
1.2.1	Quality of Supply Voltage	6
1.2.2	Stochastic Dynamic Programming	6
1.2.3	Markov Decision Process	7
1.2.4	Distributionally Robust Markov Decision Process	7
1.2.5	Power System State Estimation	7
1.2.6	Battery State of Charge Estimation	8
1.2.7	Cyber-Physical System Security	9
1.3	Research Definition and Literature Review	9
1.3.1	Stochastic Energy Management in Greenhouses with RES and Energy Storage Systems	9
1.3.2	Stochastic Energy Management of BESSs at High Penetration Level in SDSs	11
1.3.3	Stochastic Energy Management of Electric Bus Charging Stations with B2G Capabilities	12
1.3.4	Cyber-Physical Security Analysis of BESSs in SDSs	13
1.4	Thesis Motivation and Contributions	16
1.5	Thesis Outline	20
2	Stochastic Energy Management in Greenhouses with RES and Energy Storage Systems	22
2.1	System Model	23
2.1.1	The Mathematical Model of Greenhouses	24
2.1.2	The Load Model of Greenhouses	27
2.1.3	The Stochastic Models of Weather Conditions	27
2.1.4	The Models of Energy Conversion Module	28
2.2	Formulation of the Stochastic Multi-timescale Energy Management Problem	30
2.2.1	Slow-timescale Thermal Process	30
2.2.2	Fast-timescale Electrical Process	31

2.2.3	The Formulation of Stochastic Multi-timescale Energy Management Problem as a MMDP	33
2.3	Solution of the Stochastic Multi-timescale Energy Management Problem . .	34
2.4	Case Study	36
2.5	Summary	44
3	Stochastic Energy Management of BESSs at High Penetration Level in SDSs	45
3.1	System Model	46
3.1.1	Distribution System Model	47
3.1.2	Battery Model	48
3.1.3	PV System and Residential Load Model	49
3.2	Problem Formulation	49
3.2.1	BESS Energy Management	49
3.2.2	Hierarchical and Decentralized Stochastic Energy Management BESSs in SDSs	50
3.3	The Energy Management Scheme with Exhaustive Backups	52
3.4	Energy Management Scheme with Heuristic Solution	55
3.5	Case Study	55
3.6	Summary	61
4	Stochastic Energy Management of Electric Bus Charging Stations with B2G Capabilities	62
4.1	System Model	63
4.1.1	Battery Models for EBs and BESS	64
4.1.2	Stochastic Modeling for Individual EB	64
4.1.3	Stochastic Modeling for EBCS with BESS and PV	65
4.1.4	Linearized AC Power Flow Model	66
4.2	Problem Formulations	66
4.2.1	Stochastic EBCSs Energy Management	66
4.2.2	An Event-Based Ambiguity Set with Combined Statistical Distance and Moment Information	67
4.2.3	SCOPF with EBCSs as Flexible Energy Prosumers	68
4.3	Solutions based on Heuristic Regret Function	69
4.3.1	Tractable Solutions based on Heuristic Regret Function	69
4.3.2	Derivations of State-Wise Dynamic Prices	71
4.4	Case Studies	72
4.5	Summary	78
5	Cyber-Physical Security Analysis of BESSs in SDSs	79
5.1	The Construction Principle of False Data Injection Attacks in SDSs	80

5.1.1	Local State-Based Linear DSSE for Multiphase and Unbalanced Smart Distribution Systems	80
5.1.2	The Principles of FDIAs Against DSSE	85
5.1.3	The Construction of Attack Vectors	90
5.1.4	Case Study	93
5.2	False Data Injection Attacks Against State of Charge Estimation of BESSs in SDSs	101
5.2.1	System Model	102
5.2.2	Sequential FDIAs against SoC Estimation of BESSs within SDSs	108
5.2.3	Case Studies	112
5.3	Summary	117
6	Conclusions and Future Works	118
6.1	Contributions of Thesis	119
6.2	Directions for Future Work	120
	Bibliography	123

List of Tables

2.1	THE COMPARISON RESULTS OF EIGHT CASES	42
3.1	NUMBER AND TYPES OF LOADS CONNECTED	56
3.2	ELECTRICITY COST REDUCTION (CASE I)	58
3.3	ELECTRICITY COST REDUCTION (CASE II)	61
4.1	CONFIGURATION PARAMETERS FOR EB, BESS, AND PV	74
4.2	PERFORMANCE OF PROPOSED HEURISTIC REGRET FUNCTION	78
5.1	BATTERY PACK RATINGS	113

List of Figures

1.1	The typical architecture of an SNS with integrated BESSs.	3
1.2	The diagram of a BESS.	3
2.1	The architecture of energy management system.	23
2.2	An illustration of the thermal and electrical processes.	24
2.3	The simulation results of inside temperature and humidity in comparison with measurement data.	26
2.4	An illustration of the evolving process of MMDP.	33
2.5	The greenhouse for case study.	37
2.6	The measured response of inside temperature.	37
2.7	Weather conditions for a summer day and a winter day.	39
2.8	Regulated inside environment for a winter day.	39
2.9	Optimal control strategies for a winter day.	40
2.10	Electricity and natural gas consumption for a winter day.	41
2.11	The January wind speed data.	43
2.12	The inside temperature error caused by using multi-timescale process.	44
3.1	An illustration of the smart distribution system.	47
3.2	The solution procedures of proposed scheme.	52
3.3	An illustration of the algorithm for exhaustive backups.	54
3.4	IEEE 5-node test feeder (Case I).	56
3.5	The comparison of SoC profiles for three households at bus 5 (Case I).	57
3.6	Voltage profile of bus 3 (Case I).	58
3.7	The computation time for Case I.	59
3.8	IEEE European low voltage test feeder (Case II).	60
3.9	Voltage profile of bus 45 (Case II).	60
4.1	System architecture for stochastic energy management of EBCSs in power distribution system.	64
4.2	St. Albert transit systems.	73
4.3	Modified IEEE 123-node test feeder with integrated EBCSs.	73
4.4	Spot prices for reference node \bar{h}	74
4.5	EBCS demand without using dynamic prices.	75

4.6	EBCS demand with dynamic prices.	76
4.7	Charging cost for one day.	76
4.8	Ou-of-sample performance for different number of events.	77
4.9	Out-of-sample performance for different radius.	77
4.10	Out-of-sample performance for different cases.	77
5.1	A single-line diagram of smart distribution system with different types of measurements.	81
5.2	IEEE 13 Bus Test Feeder (Case I)	94
5.3	IEEE 37 Bus Test Feeder (Case II)	95
5.4	The estimation results under no attacks.	95
5.5	The LNR results for 100 MC simulations (Case I).	96
5.6	The LNR results for 100 MC simulations (Case II).	96
5.7	The bus voltage profile under attacks for Case I (The lines in blue are for the voltage profile under no attacks, and the boxplots in red are for the voltage profile under attacks).	97
5.8	The LNR results for 100 MC simulations of Case I.	98
5.9	The LNR results for 100 MC simulations of Case II.	99
5.10	The LNR results for 100 MC simulations under attacks (Case I).	99
5.11	The LNR results for 100 MC simulations under attacks (Case II).	100
5.12	The required number of measurements to be compromised (Case I).	100
5.13	The required number of measurements to be compromised (Case II).	101
5.14	The probabilities of successful imperfect three-phase decoupled random attack (Case I).	101
5.15	The probabilities of successful imperfect three-phase decoupled random attack (Case II).	102
5.16	A typical architecture of SDSs with BESSs.	102
5.17	Unit model of battery pack.	105
5.18	Modified IEEE 13 bus test feeder with BESS at bus 632.	112
5.19	Active power setpoints for BESS.	113
5.20	Static FDIA against SoC estimation.	114
5.21	Measurement residual under static FDIA.	114
5.22	Innovation under static FDIA.	114
5.23	Sequential FDIA against SoC estimation.	115
5.24	Innovation under sequential FDIA.	115
5.25	Innovations for different time slots under sequential FDIA.	115
5.26	Sequential FDIA with post-attack compromising.	116
5.27	Innovations for different time slots under sequential FDIA with post-attack compromising.	116

List of Acronyms

AC	Alternating Current
ADP	Approximate Dynamic Programming
AMI	Advanced Metering Infrastructure
BESS	Battery Energy Storage System
BES	Building Energy System
BMS	Battery Management System
B2G/B2B	Bus-to-Grid/Bus-to-Building
CAN	Controller Area Network
DAU	Data Aggregation Unit
CHP	Combined Heat and Power
DC	Direct Current
DLI	Daily Light Integral
DoD	Depth of Discharge
CPS	Cyber-Physical System
DRMDP	Distributionally Robust Markov Decision Process
DRSDP	Distributionally Robust Stochastic Dynamic Programming
DSE	Dynamic State Estimation
DSL	Digital Subscriber Line
DSO	Distribution System Operator
DSSE	Distribution System State Estimation
DER	Distributed Energy Resources
DES	Distributed Energy System
EB	Electric Bus
EBCS	Electric Bus Charging Station
EKF	Extended Kalman Filter
EMS	Energy Management System
EV	Electric Vehicle
EVCS	Electric Vehicle Charging Station
FASE	Forecasting-Aided State Estimation
FDIA	False Data Injection Attacks
FTS	Fast-Timescale
HES	Home Energy Systems
HPF	High Pressure Fogging
HPS	High Pressure Sodium
ICT	Information and Communication Technology
IED	Intelligent Electronic Device
IoT	Internet of Things
MDP	Markov Decision Process

MMDP	Multi-Timescale Markov Decision Process
RL	Reinforcement Learning
RSDP	Robust Stochastic Dynamic Programming
PCC	Point of Common Coupling
PLC	Power-Line Communication
PMU	Phasor Measurement Unit
POMDP	Partially Observable Markov Decision Process
PV	Photovoltaics
RES	Renewable Energy Sources
RF	Radio Frequency
RTU	Remote Terminal Unit
SCADA	Supervisory Control and Data Acquisition
SDP	Stochastic Dynamic Programming
SDS	Smart Distribution System
SoC	State of Charge
SoH	State of Health
SSE	Static State Estimation
STS	Slow-Timescale
TSSE	Transmission System State Estimation
VSC	Voltage Source Converter
V2G/V2H	Vehicle-to-Grid/Vehicle-to-Home
WLS	Weighted-Least Square

Nomenclature

Chapter 2

- η^{bat} Peukert's constant for lithium-ion battery, 1.05
- η^{pv} Combined efficiency of PV system with dual-axis solar tracker, 0.8256
- η^{solar} Conversion efficiency of solar irradiation to light intensity, $4.6065 \mu moles/m^2/s/W$
- κ Cycle-depth influencing factor of battery, 3.664
- ω DoD of battery
- $\pi_t^f(\pi_n^s)$ Nonhomogeneous policy of FTS(STS) MDP for time slot t (n)
- ψ SoH of battery
- ρ^{air} Dry density of air, $1.1455 kg/m^3$
- τ Battery round-trip efficiency, 0.92
- \bar{C} Battery nominal capacity, $45000 Ah$
- \bar{D}^{bat} Deployment cost of battery, $2.1 \$/Ah$
- \bar{D}^{fuel} Natural gas rate
- \mathbf{q}_i^{chp} Range of CHP thermal power within feasible region i
- \dot{C}^{plant} Plants CO₂ generation rate
- \dot{C}^{vent} CO₂ mass exchange rate through natural and forced ventilation
- \dot{W}^{hpf} Droplets mass rate of HPF system
- \dot{W}^{plant} Plants transpiration rate in term of water evaporation
- \dot{W}^{vent} Water content exchange rate through natural and forced ventilation
- A^{pv} Total effective area of PV system, $550 m^2$
- $a_1 - a_5$ Coefficients of CHP cost function, 1.45, 0.00345, 0.0031, 0.42, 0.003

$b_1 - b_3$ Coefficients of battery degradation cost function, 2600, -0.5318, -2426
 $BL_i^{l(u)}$ Lower(upper) linear boundary function of CHP feasible region i
 c^{air} Air specific heat capacity, 1000J/kg/K
 $C^{in}(C)$ Greenhouse inside(outside) CO₂ concentration
 D^{bat} Degradation cost function of battery
 D^{chp} Cost function of the usage of CHP
 $D^{cp}(D^{ch})$ Cost function of the electrical (thermal) power generation of CHP
 G Plants weight
 $H^{in}(H)$ Greenhouse inside(outside) humidity
 $J^f(J^s)$ Action vector of FTS(STS) MDP
 L^{hps} Light intensity of HPS lamps
 $L^{in}(L)$ Greenhouse inside(outside) light intensity(solar irradiation)
 L_{DLI}^{in} Required DLI
 L_{min}^{in} Minimum light intensity required by the photosynthesis
 $p(q)$ Greenhouse electrical(thermal) demand
 $p(q)^{chp}$ Electrical power supplied by CHP
 $p(q)^{ef}$ Electrical(thermal) power of exhaust fans
 $p(q)^{eh}$ Electrical(thermal) power of electric heaters
 $p(q)^{hpf}$ Electrical(thermal) power of HPF
 $p(q)^{hps}$ Electrical(thermal) power of HPS
 p^{bat} Power exchange of battery
 p^{pv} Electrical output of PV system
 p^{sh} Electrical power of shutters
 P_n^{fs} Nonhomogeneous initial state transition function of FTS MDP for time slot n
 $P_t^f(P_n^s)$ Nonhomogeneous state transition function of FTS(STS) MDP for time slot t (n)
 q_{ramp}^{chp} Ramping rate of CHP thermal heater

q^{con}	Thermal loss through the cover and ground
q^{ex}	External heat supply
q^h	Thermal power of the thermal storage devices
q^{plant}	Heat absorption by plants
q^{solar}	Thermal power of solar irradiation
q^{vent}	Heat exchange through natural and forced ventilation
R	Immediate cost function of MMDP
$R^f(R^s)$	Immediate cost function of FTS(STS) MDP
s	SoC of battery
$S^f(S^s)$	State vector of FTS(STS) MDP
s^h	Available thermal energy stored
$T^{in}(T)$	Greenhouse inside(outside) temperature
U	Battery nominal voltage, 120V
V	Value function
v	Wind velocity
V^{gh}	Greenhouse volume, 37747.2m ³
W^{in}	Inside air water content
Y	C rate of battery, C10

Chapter 3

γ	Electricity price
ν	Virtual battery state
ω	Battery state of charge change
$\Pi(\cdot)$	Policy
ϖ	BESS state vector
S	System state vector
$C(\cdot)$	Cost function

$c^b(\cdot)$	Battery cost function
$C^{d(g)}$	Cost of battery degradation (electricity)
E	Battery degradation factor
$f(\cdot)(g(\cdot))$	Battery discharging(charging) function
$P(\cdot)$	State transition function
p^b	Action of battery
$p^{d(c)}$	Battery discharging(charging) power
p^g	Power to/from grid
p^l	Residential load
p^s	PV power generation
$Q^c(\cdot)$	Correlated controller
q^c	Correlated controller variable
$R(\cdot)$	Immediate cost function
s	Battery state of charge

Chapter 4

$\alpha_{1,\dots,12}^{0-2}/\beta_{1,\dots,12}^{0-2}$	Linear coefficients of polygonal approximation for quadratic constraints
\bar{C}	Nominal capacity of battery
ι_z	Location dependent route-level EB bus loads
Π	Policy set
π_s	Policy for state s , $\pi_s \in \Pi$
p_s	State transition vector for state s , $p_s \in \mathcal{P}$
Δt	Length of discrete time slot
$\eta/\chi/\xi/\zeta/\varepsilon$	Dual variables
η^{pv}	Efficiency of PV system
\bar{h}	Reference node, i.e., slack bus
ι_z	EB bus loads at location z

κ	Battery degradation function parameter with varying average SoC
$\mathcal{D}/\mu/\varphi/\varrho$	Support/mean/absolute distance from mean/radius of Wasserstein metric
\mathcal{M}_s	State-wise ambiguity set for state s
ν	EB velocity
σ	Charging availability of EB
τ	Round-trip efficiency of battery
θ	SoC change
$\tilde{\mathbf{r}}_s$	Immediate cost vector for state s , $\tilde{\mathbf{r}}_s \in \tilde{\mathbf{r}}$
a	EB acceleration
A^{pv}	Area of PV system
$b_1 - b_3$	Battery degradation function parameter with average SoC of 50%
c_b	Peukert's constant for battery
$c_m/c_d/c_r/c_{tr}/c_{con}$	Factor of EB rotating components/aerodynamic constant/rolling resistance coefficient/efficiency of power transmission/efficiency of power conversion
d	Index of driver
D_{lp}/D_{lq}	Transfer factor of active/reactive power injection
D_{vp}/D_{vq}	Sensitivity factor of active/reactive power injection
F^p/F^q	Active/reactive power flow in line
$h^{p,\tilde{h}}$	Spot price at reference node \tilde{h}
h^p	Dynamic price
i	Index of EB
l	Index of route
m	Index of road segment
P/Q	Active/Reactive power injection
P^{bat}	Battery power
P^b	EB electricity energy consumption

P^{pv}	PV generation
s	State of EBCS energy management problem, $s \in \mathcal{S}$
t	Index of time slot
u	Action vector of EBCS energy management problem, $u \in \mathcal{U}$
x	Index of EBCS
Y	Nominal C-rate of battery
z	EB location

Chapter 5, Section 5.1

σ	Measurement standard deviation
\mathbf{a}	FDI attack vector for the linear DSSE
\mathbf{e}	Measurement error set
\mathbf{H}	Linear measurement functions
$\mathbf{h}(\cdot)$	Nonlinear measurement functions
\mathbf{H}_d	Three-phase decoupled linear measurement functions
\mathbf{H}'_d	Linear compensation measurement functions for three-phase decoupling
\mathbf{I}_{br_equ}	Equivalent three-phase measurements in rectangular form of complex branch current flows
\mathbf{I}_{br_mea}	Three-phase measurements in rectangular form of complex branch current flows
\mathbf{I}_{bus_equ}	Equivalent three-phase measurements in rectangular form of complex bus current injections
\mathbf{R}	Covariance matrix of measurement errors
\mathbf{r}	Measurement residual vector
\mathbf{r}^N	Normalized measurement residual vector
\mathbf{r}_a	Measurement residual vector after attacks
\mathbf{S}	Measurement sensitivity functions
\mathbf{S}_{br_mea}	Three-phase measurements in rectangular form of complex branch power flows
\mathbf{S}_{bus_mea}	Three-phase measurements in rectangular form of complex bus power injections

V_{bus_equ}	Equivalent three-phase measurements in rectangular form of complex bus voltages
V_{bus_mea}	Three-phase measurements in rectangular form of complex bus voltages
V_{kl}	Bus voltage drop between bus k and l for all three phases in rectangular form
W	Weight matrix
x	System state set
x_a	System state set after attacks
Y_{kl}	Admittance matrix of line between bus k and l
Y_{kl}^c	Compensation admittance matrix of line between bus k and l
Y_{kl}^d	Decoupled admittance matrix of line between bus k and l
Y_k	Equivalent bus primitive admittance matrix of bus k
z	Original measurement set
Δz	FDI attack vector for the original nonlinear DSSE
\tilde{x}	Estimated system state set
\tilde{z}	Equivalent measurement set
\tilde{z}_a	Equivalent measurement set after attacks
$I_{k.re(im)}^{a,b,c}$	Real (imaginary) part of bus k current injection in phase a, b, and c
$I_{kl.re(im)}^{a,b,c}$	Real (imaginary) part of branch current between bus k and l in phase a, b, and c
$V_{k.re(im)}^{a,b,c}$	Real (imaginary) part of bus k voltage in phase a, b, and c

Chapter 5, Section 5.2

β	Constant slope of linearized open-circuit voltage function
δ	Measurement noises
ε	Attack vector
ϑ	Manipulations on estimation states
$\Delta\theta^{abc}$	Three-phase phase-displacement angles of VSC
\mathcal{A}_i	Set of buses adjacent to bus i

\mathcal{C}_{bat}	Nominal capacity of battery pack
\mathcal{P}	Estimation error variance in EKF
\mathcal{Q}	Variance of Gaussian white process noise in EKF
\mathcal{R}	Assumed measurement noise variance in EKF
Φ	SoC of battery pack
σ	Variance of measurement noise
θ_i^α	Voltage phase angles of bus i in phase α
$\mathbf{h}()$	Nonlinear system measurement functions
\mathbf{m}^{abc}	Three-phase magnitude modulation indexes of VSC
\mathbf{W}	Weight matrix
\mathbf{x}	System state vector
\mathbf{Y}^{abc}	Nodal admittance matrix in three phases
\mathbf{z}	Measurement vector
I	Current injection
K	Kalman gain
R_{ac}/R_{dc}	AC-side/DC-side resistor of VSC
R_{bat}	Battery parameter
V	Bus voltage

1

Introduction

In this thesis, the stochastic energy management and cyber-physical security of battery energy storage systems (BESSs) in smart distribution systems (SDSs) are investigated. For the stochastic energy management of BESSs in SDSs, the main focus is on the development of efficient stochastic energy management algorithms for effective BESSs operations under various uncertainties. By investigating the cyber-physical security of BESSs in SDSs, the main focus of this thesis is on the exploration of the vulnerability of BESSs to severe cyber-physical attacks to provide theoretical guidelines for the development of effective countermeasures.

1.1 Background

To better accommodate the ever-increasing load demand and environmental concerns, the conventional power distribution systems are undergoing massive shifts towards the more efficient, reliable, sustainable, and intelligent systems, i.e., the SDSs [1]. Under the context of SDSs, a large number of renewable energy sources (RES), such as solar, wind, hydro, biomass, and geothermal, are being integrated.

However, due to the intermittent and fluctuating nature, most RES provide variable and non-dispatchable generation, which, at high penetration level, impose significant challenges for the distribution system operators (DSOs) in maintaining power quality, security, and reliability of SDSs. For example, the conventional generation must be increased rapidly around the time of sunset to compensate for the loss of solar generation, which results in a high ramping rate of generators. Also, the time and amount of RES generation can hardly match that of load demand, and the peak of RES output can cause congestion, which eventually leads to a system overload. Further, the fluctuation of RES requires ad-

ditional balancing power. As shown in [2], to maintain the stability of system operation, a 2% to 4% balancing generation is required for every 10% penetration of wind generation. Also, the proliferation of residential electric vehicles (EVs) and electric buses (EBs) in SDSs introduces new energy consumption patterns, leading to more random and concentrated loads with high power. This will cause severe impacts on the efficiency and stability of SDS operation, e.g., line congestion, generation cost increment, and voltage issues. Thus, there is an urgent need to develop practical solutions to facilitate the development of SDSs.

Due to the high versatility, energy density, and efficiency, the integration of BESSs in SDSs has been seen as a promising solution [3–5]. With proper energy management, the optimally sized and located BESSs can provide a wide range of services, e.g., arbitrage, operating reserves, and ancillary services, for DSOs to improve the power quality, security, and reliability of SDSs. For example, the BESSs can store the energy during off-peak periods and supply demand during on-peak periods for peak shaving and system upgrading deferral. The high peak of RES generation can be stored by the BESSs, instead of being transported by the system, which can release the congestion and avoid overloading. The BESSs can also provide balancing power to limit the fluctuations of feed-in RES generation. For the operation of electric vehicle charging stations (EVCSs) or electric bus charging stations (EBCSs), the BESSs can be utilized to support energy resource allocations and charging demand shifting to fulfill the charging requirements of massive-diffused EVs or EBs with reduced charging costs and mitigated impacts on SDSs. Also, the EVs/EBs equipped with bi-directional power inverters can function as mobile BESSs to provide vehicle-to-grid (V2G)/bus-to-grid (B2G) and vehicle-to-home (V2H)/bus-to-building (B2B) functions. Further, the BESSs can store or feed in energy to balance the supply and demand instantaneously to maintain the frequency. The BESSs can also feed in energy when the voltage is low and store energy when the voltage is high for voltage control. Moreover, the BESSs can benefit small and medium-size customers through time-shift for self-consumption, time-shift for feed-in via “storing-selling-consumption” trading to local utility [6].

The typical architecture of an SDS with BESSs is shown in Fig. 1.1. The BESSs are integrated into different systems within SDSs to provide different types of services. Within the household/building energy systems (HESs/BESs), the BESSs can store the energy from RES, e.g., photovoltaics (PV), and supply the demand of electrical appliances, EVs, and building automation systems. Within HESs and BESs, the home area networks and building area networks, via the Z-wave, Wi-Fi, or ZigBee technologies, are constructed for communications among different devices, based on which the energy management systems (EMSs) are used for optimal energy management. Within the distributed energy systems (DESs), the BESSs are controlled by the EMSs through distributed energy resources (DER) local area networks to regulate the feed-in power of RES. Within the EVCSs and EBCSs, the EMSs control the charging processes of EVs and EBs via EV charging networks or EB

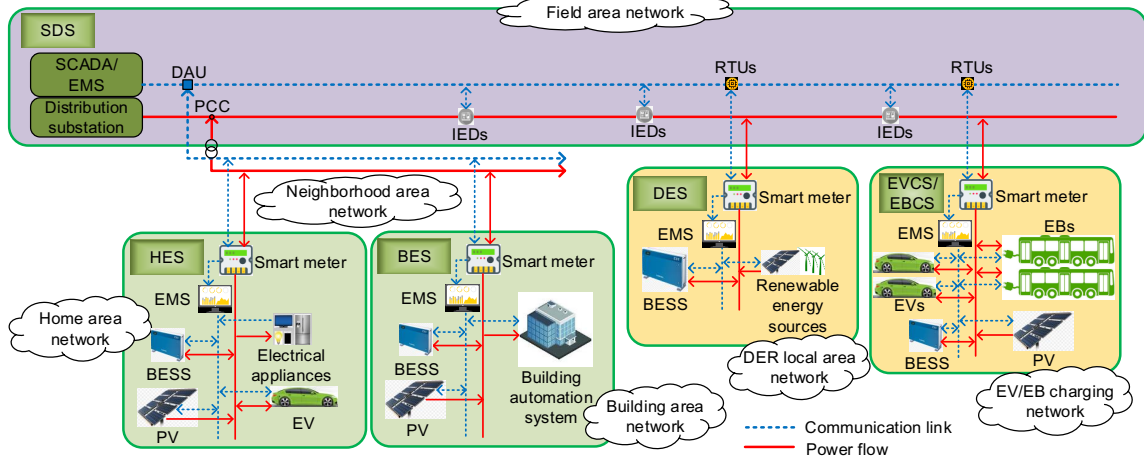


Figure 1.1: The typical architecture of an SNS with integrated BESSs.

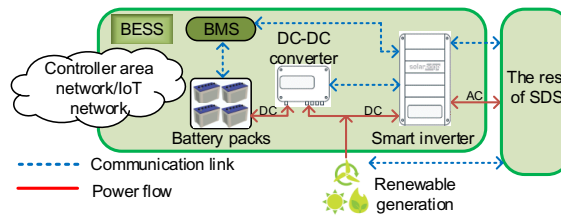


Figure 1.2: The diagram of a BESS.

charging networks, respectively. The EV charging networks can also be established among the EVs of households within secondary distribution networks to coordinate the charging among EVs. The communication links, via power-line communication (PLC), digital subscriber line (DSL), coaxial cable, or radiofrequency (RF) mesh technologies, are established among different HESs/BESs based on the geographical locations, to form neighborhood area networks. Within the SDSs, the data aggregator units (DAUs), remote terminal units (RTUs), smart meters, intelligent electronic devices (IEDs), and other information and communication technology (ICT) devices communicate with the distribution supervisory control and data acquisition (SCADA) systems and the distribution EMSs based on field area networks. Also, in the field area networks, the BESSs within the HESs, BESs, DESs, EVCSs, and EBCSs can be managed by the DSO to improve the stability and sustainability of the systems. As shown in Fig. 1.2, within individual BESS, the controller area network (CAN) or Internet of Things (IoT) network is constructed for the communications among battery management system (BMS), battery packs, DC-DC converter, and smart inverter, which helps to achieve the real-time monitoring and control of BESSs.

With the wide deployments of the advanced monitoring and control devices and well-established communication networks, the SDSs are becoming complicated cyber-physical systems, which improve the observability of SDSs for improved system operation. Also, the proliferation of BESSs in SDNs requires more advanced BMSs to ensure the safety, reli-

ability, and optimal performance of BESSs with more accurate SoC estimation. Also, BMS developers have focused on minimizing cost, weight, size, and manufacturing complexity of BMSs [7]. To better meet these requirements, the BMSs are undergoing massive revolutions to integrate Internet of Things (IoT) technologies and cloud computing services [8,9], and the BESSs are becoming complex cyber-physical systems (CPSs) with communications with the external communication systems and the internet [11, 12]. However, this exposes the SDSs and BESSs to severe cyber-physical attacks [7, 13–15]. Unlike pure cyber attacks, the cyber-physical attacks are based on cyber attacks; however, they are restricted by the physical constraints and can have severe impacts on the physical systems based on these constraints. Compared with physical attacks, the cyber-physical attacks are typically stealthy and can last for a long time. Nowadays, cyber-physical attacks have been recognized as one of the major threats to power systems. For example, the cyber-physical attacks targeting the SCADA systems of Ukrainian power grid opened circuit breakers and caused a power outage of 225,000 customers [16]. Also, some incidents related to BESSs have revealed the impacts of cyber-physical attacks on the operation of BESSs which imposes new security and safety issues. For example, in 2011, a security researcher hacked the firmware of a smart battery by penetrating the communication channel and alternating the BMS to report low SoC [17]. The attacked BESSs may operate in conditions violating both mechanical and electrical safety requirements and threaten the physical safety of BESSs, especially maliciously intending to explode batteries. For example, in 2019, the counterfeit BMSs caused several BESSs in Korean on fire [8].

To fully explore the benefits of integrated BESSs in SDSs, it is critical for the energy management of BESSs to consider the RES generation, the demand of households and commercial buildings, EVs with V2G and V2H capabilities, EBs with B2G and B2B capabilities, and operating rules of power systems and battery devices in SDSs. The energy management problem of BESSs in SDSs is generally formulated as a sequential decision-making problem [18, 19]. However, there are different sources of randomness in SDSs, for example, the demand of households and commercial buildings, RES generation, mobility of EVs and EBs, which can significantly affect the performance of energy management of BESSs in SDSs. In literature, there are numerous research works related to addressing the randomness in the energy management of BESSs in SDSs by using stochastic dynamic programming (SDP) approaches. In [20], the SDP approach is used to formulate the energy management of BESSs under randomness in HESs, based on a non-homogeneous Markov chain model. The Markov decision process (MDP) is also utilized to solve the stochastic energy management problem of BESSs in SDSs in [21, 22]. However, the SDP approaches in [20–22] suffer from high computational complexity for practical applications as more control variables (e.g., for HESs or BESs that involve the control of thermal appliances [23]) or BESS units (e.g., for a high penetration level of residential BESSs and EVs at dispersed locations) are involved [24]. Also, it is commonly assumed that the prob-

ability distribution functions (PDFs) of random variables can be estimated precisely for SDP. The estimation errors of PDFs will degrade the performance of the stochastic energy management of BESSs in SDSs by using SDP approaches. Moreover, with the development of SDSs, an increasing number of ICT devices are being embedded, as shown in Fig. 1.1 and 1.2. The stochastic energy management of BESSs relies heavily on the real-time system information obtained through the ICT devices, which makes the stochastic energy management of BESSs in SDSs prone to cyber-physical attacks. In literature, several works have revealed the vulnerability of BESSs to cyber-physical attacks, such as unauthorized source code changing, unauthorized access to data, and insecure network protocol [8–10]. This imposes great threats to the data integrity of BESSs [25]. It has been shown in [8] that the tampered real-time terminal voltage measurement can lead to overcharging and cause permanent damage to the battery. As an important function in DSSE, bad data detection (BDD) can detect bad measurements introduced by various sources, including the data tampering induced by cyber-physical attacks [26,27]. The BDD can easily detect the cyber-physical attacks that target the measurements within BESSs. However, a class of cyber-physical attacks named false data injection attacks (FDIAs) that can stealthily tamper measurements in SDSs still imposes great threats to the SoC estimation [28]. The FDIAs in power systems have been studied extensively. In [29], the FDIAs against the operation of the deregulated electricity market is investigated. Considering the load redistribution in security-constrained economic dispatch, the FDIAs driving the power system to operate on an uneconomic state is studied in [30]. With the high penetration level of DER, the FDIAs targeting the distributed energy routing processes are analyzed in [31]. In [33], the authors investigate the coordinated cyber and physical attacks, and the FDIAs designated to compromise the launched physical attacks are considered. A novel FDIA that aims at causing induced cascade failure of physical systems is studied in [34]. However, to the authors' best knowledge, the vulnerability analysis of FDIAs against SoC estimation of BESSs in SDSs has been barely studied. Moreover, there are strong temporal correlations among battery pack terminal voltage measurements at different time slots due to the inherent relationship between terminal voltage and SoC of a battery [35]. The FDIAs in [29–31,33,34] are mainly investigated targeting one snapshot, i.e., single time slot, and they have not considered the temporal correlations of measurements. This type of FDIAs can be detected using the temporal correlation of measurements [36]. Although the FDIAs considering the temporal correlation of measurements is studied in [36–38], the constructed FDIAs result in the modifications on measurements with small values and have the least impacts on power systems [39].

In summary, extensive research efforts are still required for the stochastic energy management and cyber-physical security enhancement of BESSs in SDSs. In particular, the following four topics will be discussed in this thesis.

1. Stochastic energy management in greenhouses with RES and energy storage systems;

2. Stochastic energy management of BESSs at high penetration level in SDSs;
3. Stochastic energy management of electric buses charging stations with B2G capabilities;
4. Cyber-physical security analysis of BESSs in SDSs.

1.2 General Terms and Definitions

In this section the important terms used in this thesis are defined to clearly identify the scope of work done in this research.

1.2.1 Quality of Supply Voltage

In low-voltage distribution networks, the quality of supply voltage implies the compliance of the voltage magnitude and frequency with statutory limits, resilience to continual fluctuation within those statutory limits, uninterrupted power supply, except for scheduled maintenance shutdowns, and preservation of a near-sinusoidal waveform. In this thesis, the maintenance of voltage magnitude in the statutory limit is mainly considered in preserving the quality of supply voltage in SDSs. Most national standards recommend that the low-voltage electrical appliances be designed to have a satisfactory performance within the limits of $\pm 5\%$ of nominal voltage. Then, this leaves a margin of 5% allowable voltage drop/rise at the service point of consumers along the feeder under the worst conditions. Thus, there is a statutory obligation to maintain the level of voltage at the service point within the limits of $\pm 5\%$ of the nominal value.

1.2.2 Stochastic Dynamic Programming

The energy management problem of BESSs, which is a typical sequential decision-making problem, is usually formulated and solved using the multistage stochastic programming approach, to address the impacts of random perturbations, e.g., RES generation, load demand, and electricity price, in the future [40]. However, due to the non-anticipative constraint, the multistage stochastic programming often suffers from the curse of dimensionality, which makes it computationally intractable [41]. One way to address this issue is to compress the information of non-anticipative constraints inside a state. Then, the multistage stochastic programming problem can be reformulated dynamically as a sequence of time-decomposed subproblems and is solved recursively. This technique was initially introduced by Richard E. Bellman [42] in 1957 as stochastic dynamic programming (SDP). The solution of an SDP problem is formally defined as a policy, which is a look-up table prescribing how to act optimally in response to random perturbations. The SDP can be solved optimally by using backward recursion or forward recursion algorithms based on the Bellman equation's formation. To improve the computational efficiency of SDP, the

memorization technique in computing has been widely applied. Also, there are numerous research works on reinforcement learning (RL) for model-free problems and approximate dynamic programming (ADP) in large or continuous-space, infinite-horizon problems, to reduce computational complexity and facilitate the practical application of SDP.

1.2.3 Markov Decision Process

An MDP is featured as a stationary and discrete-time stochastic control process. MDP is a particular class of stochastic dynamic programs in which the underlying stochastic process is an extension of the Markov chain. Different from the Markov chain, the outcomes of an MDP partly depend on the endogenous Markov property and partly depend on the actions of decision maker. MDP is a helpful model of random processes in SDP and RL, which has been widely studied and applied in different disciplines, such as automatic control, economics, and manufacturing. At each time step, the MDP is in some state, and the decision maker may choose any feasible action in this state. Then, the MDP will transit to a new state following a random process with defined transition probabilities and receive a reward according to the defined immediate reward function at the next time step.

1.2.4 Distributionally Robust Markov Decision Process

For an MDP, it is commonly assumed that the parameters, e.g., transition probabilities and immediate reward function, are estimated accurately. However, in practice, there may be a significant deviation of the estimated parameters from actual values, which introduce significant uncertainties into the parameters and significantly degrade the performance of obtained policy [43]. In order to address this issue, many research works have devoted significant efforts in minimizing the performance variation by using robust MDP [44–46]. In the context of robust MDP, the solution is defined as the optimal policy against the worst case of the realizations of all possible parameters of an MDP. However, due to the lack of consideration of the statistical information of uncertainties of parameters, the solutions of robust MDP are usually overly conservative. In contrast to robust MDP, the distributionally robust Markov decision process (DRMDP), which considers the statistical information of uncertainties of MDP parameters, has been widely studied, recently [47]. Instead of considering all the possible parameters arising from estimation deviation as deterministic events, the DRMDP treats them as random variables with an ambiguous probability distribution function that belongs to an ambiguity set described by *a priori* statistical information. The DRMDP has been studied as a successful approach to address the neglect of probability cognitive bias, whose solutions are robust and less conservative.

1.2.5 Power System State Estimation

For most power system energy management functions, e.g., the stochastic energy management of BESSs, the complete and consistent real-time power system operating condition

is required. The power system state estimation techniques, which were first proposed by Fred Schweppe in 1969 [49], have been widely studied to obtain the operating conditions of power systems based on the current set of measurements. The power system state estimation is generally referred to as static state estimation (SSE) to consider the quasi-steady state operating conditions of power systems, in which only the static states, e.g., system bus angles and magnitudes, are considered, and the dynamic characteristics of systems are not involved. However, the stochastic nature of demand and generation, integration of DER, and complex demand-response technologies have resulted in significant concerns about the increased uncertainties of the power system dynamics. The SSE is unable to capture these dynamics in operating conditions of power systems. Thus, based on different dynamic phenomena in power systems at multiple timescales, different extensions of SSE have been made to capture the dynamics in operating conditions for power system state estimation [37]. For the transient operating conditions of power systems, the dynamic state estimation (DSE) is adopted, in which the dynamic state variables, e.g., rotor angles and angular speeds of generators, are considered. For quasi-steady-state operating conditions that involve the changes in operating conditions caused by smooth and slow load/generation changes, the forecasting-aided state estimation (FASE) has been developed. In FASE, the state-transition model is used to capture the dynamics of quasi-steady-state operating conditions due to smooth evolution.

1.2.6 Battery State of Charge Estimation

The state of charge (SoC) is a critical battery parameter that reflects the amount of available energy stored in a battery. For optimal utilization and protection of the battery, the accurate information of SoC is important [12]. Due to the complex and nonlinear electrochemical reactions within a battery, the SoC is typically estimated, instead of being directly measured [50]. In literature, the methods for battery SoC estimation can be mainly classified into three categories, i.e., book-keeping estimation, data-driven estimation, and model-based estimation approaches [51]. The book-keeping estimation approach keeps tracking the charging/discharging currents and computes the accumulated charges in the battery. The book-keeping approach is low-cost and easy to implement; however, it is sensitive to the accumulated errors of current measurements and initial SoC estimation, which requires frequent calibrations during operation. The data-driven approach uses techniques such as fuzzy logic, artificial neural network, and support vector machines to extract SoC estimation information from data and automatically adapt to changing battery operating conditions, without relying on the configuration of complex electrochemical reactions in a battery. However, the data-driven approach is currently limited to experimental usages due to the high requirements for computational capabilities in data processing. The most used approach for battery SoC estimation is the model-based estimation, which utilizes the real-time measurements of battery, e.g., terminal voltage, current, and temperature,

to estimated battery SoC based on battery equivalent circuit model [52]. Considering the nonlinear property of battery, the Kalman filter's nonlinear variants, e.g., extended Kalman filter (EKF) and central difference Kalman filter (CDKF), are usually used for model-based SoC estimation [53].

1.2.7 Cyber-Physical System Security

The cyber-physical system (CPS) is an integrated system that consists of computing units and physical objects that are deeply intertwined through the network [13], where the SDSs and the BESSs are typical examples of CPSs. The integration of cyber and physical systems enhances the performance of CPS operation and control. However, it also introduces a new security threat, i.e., the cyber-physical security threat, to CPS [14]. The cyber-physical security threat combines both information security threats to the cyber system and engineering security threats to the physical system. Since the physical systems are typically closed and have well-established engineering security protection schemes, they are usually assumed to be resilient to a variety of cyber and physical threats. However, due to the requirements for efficiency and compatibility, the engineering physical systems typically lack proper information security protection schemes. With the deep interaction between cyber and physical systems in CPS, cyber intrusion will have significant impacts on the engineering security of the physical system. Also, conventional engineering security protection schemes in the physical system are mainly designed against naturally occurred faults. However, in CPS, the well-coordinated cyber-physical attacks are stealthy and can easily bypass these protection schemes [15]. Also, in CPS, the cyber-physical attacks are well constructed based on the physical system's property and can lead to devastating physical effects. In the CPS security analysis, it is crucial to consider the interaction between cyber and physical systems.

1.3 Research Definition and Literature Review

In this section, the research problems will be defined for the four research topics in this thesis. Moreover, the existing research works in literature will be discussed.

1.3.1 Stochastic Energy Management in Greenhouses with RES and Energy Storage Systems

In this research, the stochastic multi-timescale energy management of commercial greenhouses with RES, including a PV system, combined heat and power (CHP) unit, and energy storage systems, is studied. The objective of this studied optimal energy management problem is to minimize the operating cost of commercial greenhouses, while precisely conditioning plant environments.

In literature, commercial greenhouses' energy management problems are addressed in [56–65]. In [56–58], the authors investigate the energy usage reductions of greenhouses by increasing the efficiency of energy generation facilities, upgrading the architectures of greenhouses to reduce energy losses, and optimizing the inside greenhouse environment. However, the research works have not involved the optimization of the greenhouse control, based on the mathematical models of greenhouses, which are critical for greenhouse energy management [59]. Approaches are proposed to optimize the control of commercial greenhouse energy-consuming facilities based on the mathematical greenhouse models [59–61]. However, the approaches in [59–61] are deterministic approaches, such that the randomness of the weather conditions can degrade their performance. In [62], a model-based energy management system is developed for greenhouses to optimize energy utilization. Moreover, the randomness of the weather conditions is addressed by considering the forecasting results. However, this work does not consider the utilization of RES and energy storage, which, in [63–65], has been proven to be an effective way towards the sustainable development of commercial greenhouse industry. However, in [63–65], the utilization of renewable energy is limited to solar energy, and the research works focus on redesigning the shape of the greenhouses and introducing thermal/solar curtain into the greenhouses. To the best of our knowledge, there is no existing research work investigating the optimal energy management strategy for greenhouses with RES and energy storage. On the other hand, the integration of RES results in greater randomness, and the traditional forecasting-based optimization method can degrade the performance of energy management in real-time control. As a result, the uncertainty in weather conditions and RES must be considered in a dynamic way for more efficient real-time control [66]. However, by considering the stochastic greenhouses energy management as a dynamic problem, the computational complexity increases significantly due to the high dimension of the solution caused by the great number of controllable loads for electrical and thermal appliances and time slots in the period of optimization [67]. In [23], the timescale characteristics of home thermal and electrical energy management are investigated. The results indicate that, given the two-dimensional (thermal and electrical) energy pathway, the computational complexity can be potentially reduced by considering different timescales for each of the two pathways.

In summary, the existing methods for stochastic energy management of greenhouses are subject to the curse of dimensionality, due to the large number of controllable loads and time slots. Although the usage of different timescales for each of the two pathways can significantly reduce the computational complexity, the interaction between these two processes at different timescales in a greenhouse environment still needs to be investigated.

1.3.2 Stochastic Energy Management of BESSs at High Penetration Level in SDSs

To mitigate the impacts of residential BESSs at high penetration level on the reliable operation of SDSs, the hierarchical and decentralized stochastic energy management for SDSs with high BESSs penetration is studied in this research. The objective of this studied energy management problem is to improve the overall social welfare by jointly minimizing the electricity usage cost for residential customers and the operating cost associated with line losses for DSO while maintaining the voltage levels within the required range.

In literature, considerable works have been devoted to the stochastic energy management of BESSs in SDSs [68–76], which consider the stochastic energy management of BESSs from both DSO and customers perspectives for demand-side electricity cost reduction with mitigated impacts on SDS operation. In [68] and [69], decentralized energy management approaches are investigated. The Lyapunov approach [68] and the Lagrangian multiplier method [69] are used to solve these problems through the economic duality between decentralized and centralized control. However, the proposed decentralized schemes mainly consider the total cost minimization of customers under the distribution system operational constraints. Moreover, in the planning of decentralized schemes, the DSO still requires all the information of individual BESSs [70]. SDS stochastic energy management schemes in a hierarchical structure are proposed in [70] and [71], which are designated to reduce the costs of both DSO and customers, while maintaining the power quality. However, these hierarchical approaches rely on the predetermined setpoints of powers of the DSO, and if the information of all the individual BESS is unknown by the DSO, the solutions of individual BESS cannot be guaranteed to be optimal.

The decentralized or hierarchical approaches proposed in [68–71] consider the stochastic energy management of BESSs from both DSO and customer perspectives. However, these approaches either consider the optimization problem of DSO or customers as the main problem, and the overall benefit of DSO and customers has not been considered. In the future energy system, different entities, e.g., the transmission system operator (TSO), DSO, demand side management participants, and operators of distributed energy resources, are supposed to coordinate with each other to improve the system overall benefit [72]. It has been well studied that, by considering the joint optimization of TSO and DSO, the overall benefit of TSO and DSO can be significantly improved through the coordination between TSO and DSO [73]. With the integration of BESS, the customers are becoming more active in distribution system energy management, and the coordination between DSO and customers will be beneficial, in social cost and technical aspects, for smart distribution system energy management [74–76]. In [75] and [76], the energy management of multiple customers in a smart distribution system is investigated. The centralized energy management schemes are proposed for the coordination between DSO and customers, considering the joint cost of DSO and customers, to minimize the overall electricity usage

and generation cost for the improvement of the distribution system overall benefit. However, the centralized schemes require all the computations being performed at a central unit of DSO, which significantly increases the computational complexity of DSO at high BESS penetration.

In summary, the existing decentralized or hierarchical approaches either consider the optimal utility of DSO or customers. They have degraded performance in improving the overall social welfare, which requires a joint utility optimization of both DSO and customers. Although the hierarchical approaches with complete information about customers and the centralized schemes can jointly optimizing the utilities of both DSO and customers, they cannot be applied in SDSs with high BESS penetration practically due to the high computational complexity.

1.3.3 Stochastic Energy Management of Electric Bus Charging Stations with B2G Capabilities

In this research, the stochastic energy management of EBCSs is investigated, where the RES with integrated BESSs and B2G capabilities are considered. The objective of the stochastic energy management is to minimize the charging costs of EBs while mitigating the charging impacts of EBCSs on SDSs.

In literature, the stochastic energy managements of EBCSs [81–83] and EVCSs [84–86] are usually formulated using SDP, which assumes that the PDFs of random variables can be accurately estimated [87]. As EBs have fixed routes and schedules, they are more statistical, and the PDF estimations of random EB energy consumption and charging duration are more accurate compared with EVs [88]. This makes SDP a suitable method for stochastic energy management of EBCSs. However, different from EVs with relatively constant loads, the bus loads of EBs vary significantly over time and are highly random, significantly affecting the accuracy of PDF estimation of EB energy consumption [89]. To address this issue, several methods have been proposed to incorporate PDF estimation of random bus loads for stochastic energy management of EBCSs [90]. However, due to varying real situations, such as weather and activities of passengers, the PDF estimation of random bus loads is usually inaccurate, which introduces significant errors to PDF estimation of EB energy consumption [91]. This results in degraded performance of stochastic energy management of EBCSs using SDP, or even cause reliability issues of public transit systems, as it has no robustness to PDF estimation errors [92]. To guarantee the reliability of transit services, the application of robust stochastic dynamic programming (RSDP) to stochastic energy management of EBCSs has been studied in [93]. In which only the support of random bus loads is considered, and the solution against the worst-case bus loads is obtained. Compared with SDP, RSDP is more robust and has a better guarantee of the reliability of public transit systems. However, without considering the statistical information of random variables, RSDP admits broad unrealistic single-point distribution on the support set,

with overly-conservative solutions [94].

The distributionally robust SDP (DRSDP) has been extensively studied as an intermediate method between SDP and RSDP. DRSDP uses ambiguity set to address the PDF estimation errors while considering the statistical information for robust solutions that are less conservative [43]. DRSDP has wide applications in power system disciplines, including unit commitment [95], optimal power flow [96], and system planning [97]. However, its application to stochastic energy management of EVCSs and EBCSs has not been studied. In [95–97], the objective functions are based on *minimax* criterion, where the consideration of the worst case usually gives conservative solutions [98], such as the newsvendor problem in [99]. To address this issue, the *minimax-regret* criterion (i.e., worst-case conditional value at risk of regret) has been extensively studied for RSDP [100, 101]. However, its application to DRSDP usually results in an NP-hard problem with intractable solutions [98]. Also, the ambiguity sets used in [95–97] are either based on moment or statistical distance information. The moment-based ambiguity set usually leads to conservative solutions, as all the distributions with the same moment are considered. The statistical distance-based ambiguity set leverages the reference PDF obtained from empirical data for good robustness and controllable conservatism [43]. However, the lack of consideration of moment information may result in overly conservative solutions [47]. Moreover, in [95–97], the uncertainties of approximated statistical information used for the ambiguity set have not been considered, which may result in solutions with less robustness [48].

In summary, the SDP approaches based on PDF estimations are commonly used for the stochastic energy management of both EBCSs and EVCSs in literature. However, due to varying real situations, the PDF estimations of the random variables, such as RES generation, charging demands, and charging availability, usually have significant errors, which will affect the energy management performance. Although the RSDP and DRSDP have been extensively studied to improve the energy management performance by considering the PDF estimation errors in the formulation of stochastic optimization problems using ambiguity set, they usually result in an NP-hard problem that cannot be solved analytically, and their solutions are usually either overly conservative or less robust.

1.3.4 Cyber-Physical Security Analysis of BESSs in SDSs

In this research, the cyber-physical security of BESSs in SDSs is studied by investigating the vulnerability of SoC estimation of BESSs in SDSs to typical cyber-physical attacks, i.e., the FDIAs, through a series of two research topics. For the first research topic, the construction principle of FDIAs in practical SDSs is investigated, where the objective is to numerically construct FDIAs that can tamper the targeting measurements while bypassing the existing measurement residual-based BDD schemes in practical SDSs. Then, the mechanism of FDIAs against SoC estimation of BESSs in SDSs is investigated based on the construction principle proposed in the first research topic, and the objective is to stealthily tamper the

measurements of BESSs in SDSs using FDIAs to maximize the SoC estimations errors.

The Construction Principle of False Data Injection Attacks in SDSs

In literature, the FDIAs for power transmission systems have been investigated extensively. The FDIAs are explicitly designed against the SSE to corrupt the outcome of power system controls. Moreover, the study on impacts of FDIAs in power transmission systems has been well-conducted [105]. As concluded in [105], in power transmission systems, the FDIAs attacks can inject malicious data stealthily, without being detected by the BDD function of transmission system state estimation (TSSE), and affect the outcome of system controls. Based on the well-constructed FDIAs attack models in power transmission systems, different countermeasures are proposed to protect the power transmission systems from FDIAs by protecting a small subset of the measurements [34, 106–108]. In [107], an intrusion detection method is proposed to detect the anomalous power flows in power transmission systems by using the optimal power flow functions. By leveraging the linear FDIAs attack models in power transmission systems, the authors in [34] propose a fast screening method to detect the high-risk line in power transmission systems that is more vulnerable to FDIAs. Moreover, in [108], a corrective dispatch scheme is proposed for dispatching generators in power transmission systems to mitigate the impacts of FDIAs. In the future SDSs, as there is more reliance on the measurements deployed at dispersed locations, the potential impacts of FDIAs on SDSs need to be investigated extensively. Furthermore, the numerical models of potential FDIAs in SDSs are required for the deployment of effective and efficient countermeasures.

Also, due to the limited number of real-time measurements in power distribution systems, the system observability cannot be achieved unless the pseudo measurements are used. For example, the pseudo power injection measurements that are determined using customer billing information and typical load profiles or defined as Gaussian distributions with their means at half the transformer ratings [33]. However, due to the uncertainty in load demand, these pseudo measurements obtained based on load forecasts or historical data are much less accurate than real-time measurements [110]. These low-accuracy pseudo measurements may degrade the performance of DSSE. The benefits of introducing more accurate real-time measurements such as phasor measurement units (PMUs), IEDs, and advanced metering infrastructure (AMI) systems to improve system observability have been well demonstrated [109]. Unlike power transmission systems, the dimension of power distribution systems in terms of the number of measurement points is typically very high, so it is impractical to telemeter all points using the expensive real-time measurement devices. The optimal placement of real-time measurements, concerning system observability improvement and state estimation error minimization in DSSE, has been well studied in [111]. However, the optimal placement of real-time measurements for DSSE considering the vulnerability of DSSE to FDIAs still requires extensive research [27]. This

is mainly due to the lack of numerical models of FDIAs in power distribution systems.

In [112–114], the FDIAs against linear power system SSE are proposed, in which the SSE investigated is formulated based only on the bus voltage measurements. Since the developed SSE is linear, it facilitates the attackers to construct an FDIAs attack against SSE. However, with the development of smart grid measurement infrastructures, different types of measurements are being deployed in both transmission and distribution systems. The integration of more real-time measurements, especially the power measurements, leads to the generally nonlinear SSE, making the FDIAs based on linear SSE infeasible.

Due to the nonlinearity of general SSE, it is difficult for the attacker to construct an FDIA by analyzing the complicated nonlinear system numerically. In the transmission system, the authors in [115–117] analyze the construction of FDIAs against nonlinear TSSE based on the AC model of the transmission system. The FDIAs is constructed by finding a fixed system state set after the injection of FDIAs that does not change the measurement residuals during each iteration. However, these methods require that the attackers have the information of the entire estimated system states for each iteration, or the convergence of iterations cannot be guaranteed [118]. Also, the attackers cannot find the fixed system state set numerically. Thus, in power transmission systems, the nonlinear TSSE is usually relaxed to linear TSSE as in [119–122]. This relaxation is based on the observation that, in transmission systems, the x/r ratio of transmission lines are typically high. Then, the voltage phase angle differences can be approximated by using the real power flow, and the voltage magnitude differences can be estimated based on the reactive power flow. However, this relaxation cannot be implemented in DSSE directly due to the low x/r ratio of distribution lines. We believe that the difficulty in dealing with the nonlinear DSSE has limited the research on FDIAs against DSSE.

Recently, the authors in [33] investigate the FDIAs against DSSE in a smart distribution system. The nonlinearity of the DSSE is relaxed based on the observation that, within a distribution system, the changes of voltage phase angles are typically small, and the voltage drops are usually much smaller than the nominal voltages. Then, the FDIAs against nonlinear DSSE can be obtained based on power flow or injection measurements without too much effort. However, the investigated distribution system model is simplified to a single-phase feeder model. In practice, the distribution systems are typically constructed with three-phase lines. Also, the distribution systems usually have unbalanced load distributions and unsymmetrical line parameters, which cause the coupling among the three phases. Moreover, there are one- and two-phase branches in most distribution systems. Due to the complex system model of distribution systems and the coupling among three phases, it seems difficult for the attackers to construct FDIAs against DSSE in an SDS with varying measurements.

False Data Injection Attacks Against State of Charge Estimation of BESSs in SDSs

In the discipline of power systems, the mechanisms of FDIAs have been studied extensively. In [29], the mechanism of FDIAs against the operation of the deregulated electricity market is investigated. Considering the load redistribution in a security-constrained economic dispatch, the mechanism of FDIAs that drive the power system to operate on an uneconomic state is studied in [30]. With the high penetration level of DER, the mechanism of FDIAs targeting on affecting the distributed energy routing processes is analyzed in [31]. In [33], the authors investigate the coordination between cyber and physical attacks, and the mechanism of FDIAs designated to compromise the launched physical attacks is considered. Recently, a novel FDIA that aims at causing induced failure of physical systems is proposed, and the corresponding mechanism is studied in [34].

However, to the best of our knowledge, the mechanism of FDIAs against SoC estimation of BESSs in SDSs has been barely studied. Moreover, there are strong temporal correlations among battery pack terminal voltage measurements at different time instances due to the inherent relationship between terminal voltage and SoC of a battery [35]. The mechanisms of FDIAs in [29–31, 33, 34] are mainly investigated targeting one snapshot, i.e., single time instant, and have not considered the temporal correlations of measurements. This type of FDIAs can be detected by considering the temporal correlations of measurements [36]. Although the mechanism of FDIAs considering measurement temporal correlations is studied in [36–38], the constructed FDIAs result in the modifications on measurements with small values and have the least impacts on power systems [39].

In summary, the existing research works on the construction principles of FDIAs are mainly studied for the power transmission systems. However, due to the low x/r ratio in SDSs, the construction principles of FDIAs in power transmission systems cannot be directly applied to SDSs. Although some methods have been proposed to construct FDIAs in SDSs with low x/r ratio, they have not considered the existence of one- and/or two-phase branches, unbalanced load distributions, and unsymmetrical line parameters in practical SDSs. Moreover, the existing FDIAs targeting on one snapshot of SE can be easily detected by considering the temporal correlations of measurements for SoC estimation of BESSs. Although the impacts of temporal correlations of measurements on FDIAs have been studied for some works, the proposed FDIAs in these works usually result in the least impacts of FDIAs, which has less practical meaning.

1.4 Thesis Motivation and Contributions

As discussed above, the development of stochastic energy management of BESSs in SDSs still faces great challenges. On the demand side, the stochastic energy management of BESSs is subject to high computational complexity, especially for the application in large-scale facilities, e.g., the commercial greenhouses that contain a large number of control

variables arising from coupled electrical and thermal processes and time slots. Also, the lack of consideration for the BESS charging/discharging impacts on SDSs in stochastic energy management of residential BESSs at a high penetration level can significantly affect the economics and stability of SDS operation. Moreover, for the stochastic energy management of B2G-enabled EBCs with BESSs and RES integration, the PDF estimation errors of random variables can degrade the performance of energy management, or even affect the reliability of public transit services. Although some stochastic energy management approaches for BESSs leverage the robust optimization methods to address the impacts of PDF estimation errors on the reliability on public transit services, the consideration of the single-point distribution of extreme condition in robust optimization usually results in overly conservative solutions, which will significantly affect the economics of stochastic energy management of BESSs. Further, the implementation of a variety of ICT devices in SDSs leads to the development of SDSs and BESSs towards CPSs, which greatly facilitate the efficient and reliable management and operation of BESSs in SDSs. However, it also exposes the physical systems of SDSs and BESSs to severe cyber-physical attacks and results in new cyber-physical security threats to SDSs and BESSs. Therefore, exploring the efficiency, reliability, and security of stochastic energy management of BESSs in SDSs constitutes the main motivation of this thesis. This thesis proposes the novel approaches of the multi-timescale Markov decision process (MMDP) with interactions, hierarchical and decentralized management scheme using Dec-POMDP, and a distributionally robust Markov decision process (DRMDP) are proposed for effect and optimal energy management of BESSs. Also, an equivalent measurement-based method for constructing FDIAs against DSSE and a novel sequential FDIA is proposed. Moreover, the finished research works also have significant contributions in the case studies, where experiments and tests based on real industrial data are conducted. The detailed motivation and contributions of this thesis are described as follows:

- **Stochastic Multi-Timescale Energy Management of Greenhouses**

For the stochastic energy management of demand-side BESSs, the optimization problem is usually formulated in a single timescale. However, for the application in commercial greenhouses, the consideration of both electrical and thermal processes using the fastest timescale will increase the number of control variables and time slots involved and results in high computational complexity. The usage of the slowest timescale can significantly reduce the number of time slots; however, it results in degraded performance of stochastic energy management for the energy process with faster timescale. In this thesis, a novel stochastic multi-timescale energy management scheme of BESSs with application in greenhouses with RES integration is proposed to address this issue. In this proposed scheme, the energy management problem is formulated as a MMDP, consisting of two coupled MDPs with different timescales for the electrical and thermal processes. More specifically, the MDP with

a fast timescale is defined for the electrical process that changes rapidly, while the MDP with a slow timescale is defined for the gradually varying thermal processes. In this way, the number of control variables and time slots in the optimization period for each process will be less, and the dimension of the solution can be reduced, which can help reduce the computational complexity.

- **Hierarchical and Decentralized Stochastic Energy Management of BESSs**

The approaches for stochastic energy management of residential BESSs in SDSs from both DSO and customer perspectives can be mainly classified into centralized, decentralized, or hierarchical approaches. Compared with the centralized approaches, the decentralized and hierarchical approaches are more efficient in large-scale systems. However, the existing stochastic energy management of BESSs in SDSs using decentralized or hierarchical approaches either considers the optimization problem of DSO or customers as the main problem, and the overall benefit of DSO and customers has not been considered. In this thesis, a hierarchical and decentralized stochastic energy management scheme is proposed to address the aforementioned issues. The energy management problem of smart distribution systems is formulated based on a two-layer architecture and is solved in a decentralized manner. In this way, most of the computations are processed by the end-users, which will significantly reduce the DSO's computational complexity. Simultaneously, the hierarchical control structure allows the DSO to regulate the energy management decisions of end-users with simple instruction signals.

- **Distributionally Robust Stochastic Energy Management of BESSs**

For SDP approaches, the errors in random variable PDF estimations can significantly affect the performance of stochastic energy management of BESSs in SDSs. To address the errors of random variable PDF estimation, the usage of robust optimization method in SDP approaches has been well studied to improve the robustness of solutions to extreme conditions. However, considering the single-point distribution of extreme conditions will lead to overly conservative solutions that can affect the economics of stochastic energy management of BESSs. In this thesis, the stochastic energy management of B2G-enabled EBCSs with RES and integrated BESS is investigated to address the errors in PDF estimations of random RES power output and EBs that are highly statistical. This problem is formulated as a DRMDP with uncertain parameters, i.e., transition probabilities and costs, to consider both the highly statistical random RES and EBs with fixed routes and schedules for less conservative solutions, and random bus loads with inaccurate PDF estimation for improved robustness. To utilize both the approximated reference PDF and moment information obtained from empirical data, while considering the uncertainties of this approximated information, an event-based ambiguity set with combined statistical distance and moment information is developed to achieve *minimax-regret* criterion for robust

solutions that are less conservative. Moreover, a heuristic regret function is proposed to obtain tractable solutions, based on which the day-ahead dynamic prices, used for the mitigation of EB charging impacts, are derived from the optimality conditions of reduced mixed-integer linear programming (MILP) problems.

- **Vulnerability Analysis of Cyber-Physical Security of BESSs in SDSs**

Along with the development of ICTs in SDSs and BESSs, the future SDSs and BESSs will become typical CPSs, which can facilitate the development of efficient and effective stochastic energy management of BESSs in SDSs. However, this also exposes the BESSs in SDSs to severe cyber-physical attacks and cause new cyber-physical threats, where the FDIAs that targets on the system information integrity has been seen as one of the most severe threats. Thus, there is an urgent need to develop adequate protection and countermeasures against the new cyber-physical threats, where a better understanding of the construction principles and mechanisms of cyber-physical threats to BESSs in SDSs is essential. In this thesis, the vulnerability analysis of BESSs in SDSs to FDIAs is conducted. More specifically, the construction principle of practical FDIAs in SDSs is investigated. The existing DSSE is extended to multiphase and unbalanced linear DSSE, based on the local states (i.e., the complex voltage of local bus) only. Then, the construction of three-phase coupled FDIAs, considering the coupling among phases, is introduced. To reduce the number of required measurements, the weak three-phase coupling for DSSE is investigated, which decouples the multiphase systems into independent single-phase systems. Moreover, the construction of perfect three-phase decoupled FDIAs is developed. For DSSE with strong three-phase coupling, which cannot be decoupled into independent single-phase systems, the probabilities of successful three-phase decoupled FDIAs is derived numerically, which can be used to find an FDIA against DSSE with the least efforts. Further, the mechanism of FDIAs in SDSs targeting on the SoC function of BESSs is studied. The mechanism of static FDIAs targeting on one snapshot of SoC estimation of BESSs is analyzed, which can significantly affect the accuracy of SoC estimation without being detected by the conventional measurement residual-based BDD in DSSE. According to temporal correlations of real-time terminal voltage measurements within BESSs, a detection method based on the innovation test of measurements is developed to detect the static FDIAs against SoC estimation. Next, the mechanisms of sequential FDIAs against SoC estimation of BESSs is studied. The proposed sequential FDIAs can bypass the conventional measurement residual-based BDD and innovation test-based detection, with significant impacts on SoC estimation accuracy. Further, an online approach is proposed for the practical construction of a sequential FDIA. From the vulnerability analysis of cyber-physical security of BESSs in SDSs, it can be observed that for practical sequential FDIAs, there is an assumption about the insignificant changes of lumped parameters. Thus, one of the possible directions

for countermeasures against sequential FDIAs is to insert watermarks to alternate the lumped parameter by leveraging the concept of coordinated parameter variation defense (CPVD). However, there still exist great challenges in designing optimal watermarks that can cause significant variations of lumped parameters while imposing the least impacts on the performance of SoC estimation.

1.5 Thesis Outline

In this thesis, the stochastic energy management and cyber-physical security of BESSs in SDSs are studied. For the stochastic energy management of BESSs, the MDP-based techniques, which are inherently developed for sequential decision-making problems under randomness, are mainly considered. Firstly, the energy management of single demand-side BESS, with a specific application in greenhouses, is studied for electricity usage cost reductions. In this study, the MMDP is used to accommodate the multiple energy pathways with distinct timescale characteristics in greenhouses. Then, inspired by the MDP-based stochastic energy management of individual BESS, a hierarchical and decentralized energy management scheme using Dec-POMDP for stochastic energy management of multiple BESSs is proposed to mitigate the impacts of BESSs on quality of supply voltage in SDSs. Moreover, by considering the EBs with B2G capabilities as mobile BESSs, the stochastic energy management of EBCSs is studied to reduce EB charging costs with mitigated charging impacts on SDSs. In this study, the DRMDP is leveraged to address the high degree of randomness caused by the mobility of EBs for robust solutions that are less conservative. Considering the dependency of effective energy management of BESSs on the communication networks in SDSs and the vulnerability of SDS communication networks to common cyber attacks, the cyber-physical security of BESSs in SDSs is analyzed by investigating the mechanism of typical cyber-physical attacks, i.e., FDIAs, against BESSs in SDSs. More specifically, this thesis consists of six chapters and is organized as follows:

- **Chapter 1: Introduction** - The research background is first introduced in this chapter to address the importance of this research. Then, the general terms used in this thesis are described to highlight the scope of the research. Also, the research problems are defined, followed by a review of relevant literature to highlight each research problem's research challenges. In the end, the motivation and contributions of this thesis are presented.
- **Chapter 2: Stochastic Energy Management in Greenhouses with RES and Energy Storage Systems** - This chapter presents a stochastic multi-timescale energy management scheme of greenhouses with RES and energy storage systems. An optimal energy management problem is formulated using MMDP, where both the optimal solution and approximation solution with less computational complexity are derived.

The performance of this proposed energy management scheme is evaluated using case studies based on real data.

- **Chapter 3: Stochastic Energy Management of BESSs at High Penetration Level in SDSs** - This chapter presents a hierarchical and decentralized stochastic energy management scheme for smart distribution systems with high BESS penetration. An energy management problem is formulated based on a two-layer hierarchical architecture and an energy management scheme based on Dec-POMDP is proposed to solve the formulated problem in a decentralized manner. Also, a heuristic search and pruning method is proposed to reduce the computational complexity. The performance of the proposed scheme is evaluated using case studies based on IEEE 5-bus test feeder and IEEE European low voltage test feeder.
- **Chapter 4: Stochastic Energy Management of Electric Bus Charging Stations with B2G Capabilities** - In this chapter, the stochastic energy management of EBCSs with RES, BESSs, and B2G capabilities, using day-ahead dynamic prices is investigated, where the problem is formulated as a DRMDP with an event-based ambiguity set to achieve *minimax-regret* criterion for robust solutions that are less conservative. Further, a heuristic regret function is proposed for tractable solutions with less computational complexity. The performance of the proposed method is evaluated using case studied based on real EB data and IEEE test feeders.
- **Chapter 5: Cyber-Physical Security Analysis of BESSs in SDSs** - This chapter presents the construction principle of FDIAs in multiphase and unbalanced SDSs. The construction of three-phase coupled FDIAs is introduced. To reduce the number of required measurements, the perfect three-phase decoupled FDIAs are investigated with the probabilities of successful attacks derived numerically. Based on the proposed construction principle of FDIAs in SDS, the mechanism of FDIAs against SoC estimation of BESSs in SDSs is studied by considering the temporal correlations of BESS measurements. The analytical results are verified by simulations.
- **Chapter 6: Conclusions and Future Works** - The contributions of this thesis and the future works are summarized in this chapter.

2

Stochastic Energy Management in Greenhouses with RES and Energy Storage Systems

In this chapter, the stochastic energy management of demand-side BESSs is studied with its application in commercial greenhouses. In commercial greenhouses, the CHP units and electric heaters are generally equipped to reduce the overall energy costs. The stochastic energy management of commercial greenhouses needs to consider the coupled electrical and thermal processes. In practice, the electrical and thermal processes have distinct timescale characteristics, due to different response times [23].

This phenomena is very common in CHP systems with cogeneration of electrical and thermal powers [123]. For the energy management of CHP systems, the distinct timescale characteristics are addressed by formulating two coupled optimization problems with different timescales for electrical and thermal processes, receptively. Then, based on the operating mode, i.e., the thermal-demand leading mode or electrical-demand leading mode, either the optimal thermal power dispatch or electrical power dispatch is determined primarily [124]. Then, the dispatch of the rest power will be performed according to the feasible operation region of CHP. However, this approach cannot guarantee the optimality of the energy management for the whole energy system [125]. The optimal dispatches of CHP systems can be achieved by formulating these two processes into one process in either the slow timescale of thermal process or the fast timescale of electrical process. However, by considering these two processes in a slow timescale, the dispatch for electrical process usually results in high electrical generation, due to the fluctuation of electrical demand. On the other hand, the usage of fast timescale for both processes will increase the computational complexity significantly [126,127]. In this chapter, a novel stochastic multi-timescale

energy management scheme of greenhouses with RES and electrical/thermal storage systems is presented, where the electrical grid, PV system with dual-axis solar trackers, and CHP unit are used as the energy sources. A comprehensive mathematical model is developed for a greenhouse with the integration of electrical/thermal energy storage systems and RES to investigate the coupling between the electrical and thermal processes with distinct timescale characteristics. A stochastic multi-timescale energy management problem is formulated by using MMDP, which involves two energy processes at different timescales, i.e. a fast-timescale (FTS) process for electrical process and a slow-timescale (STS) process for thermal process. And these two energy processes are coupled to consider the interaction between the electrical and thermal processes. An approximation method is proposed by considering the monotonicity of daily MMDP problem and the homogeneity of optimal policy from day to day, to increase the computational efficiency of the energy management problem for large-scale facilities.

2.1 System Model

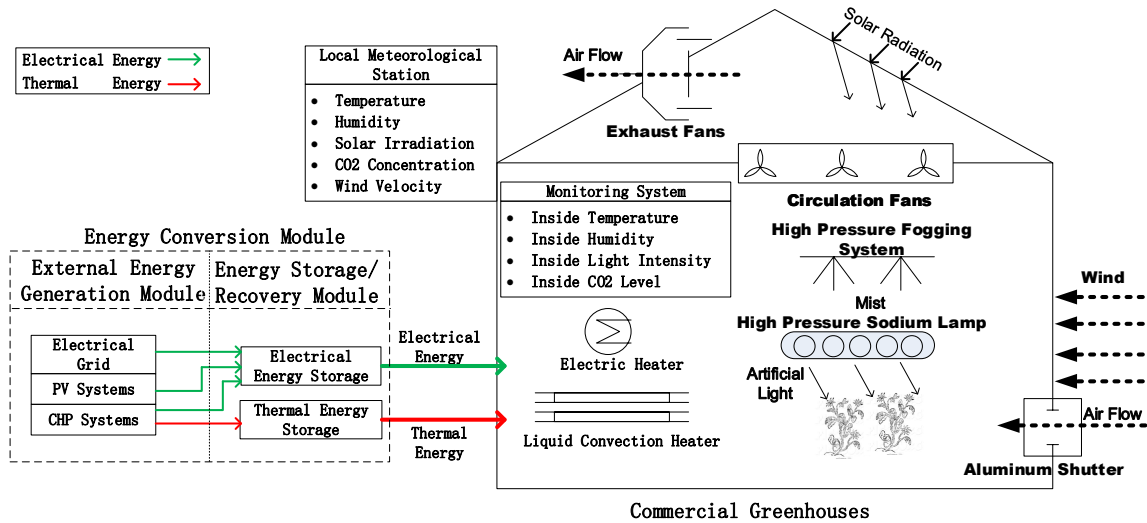


Figure 2.1: The architecture of energy management system.

A typical greenhouse structure from [62] is shown in Fig. 2.1, where the inside environment and weather conditions are monitored and recorded. Exhaust fans, aluminum shutters, high pressure sodium (HPS) lamps, high pressure fogging (HPF) system, and electric and liquid convection heaters are implemented to regulate the inside environment. To service and manage such electrical and thermal demands, an external energy system consisting of generation, storage and recovery components is integrated. For generation, a PV system and CHP unit are used to increase the energy efficiency of the greenhouse [63]. Thermal and electrical energy storage is used to respond to the real-time greenhouse demands and recover underutilized heat and power. The system is further connected to

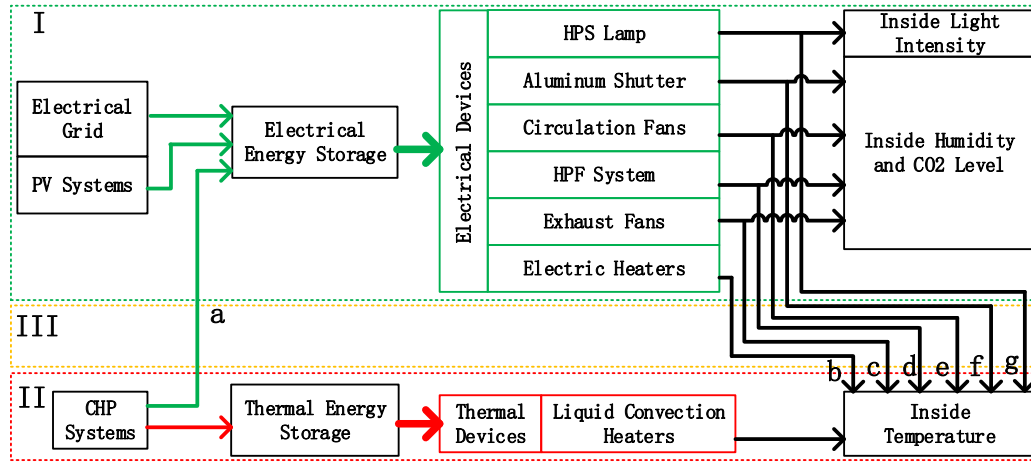


Figure 2.2: An illustration of the thermal and electrical processes.

the electrical grid for the stability of operation. An illustration of the interaction between thermal and electrical processes is shown in Fig. 2.2. The proposed energy management system consists of three sectors. Sector I is for the electrical process, in which the electrical grid and PV systems, combined with the electrical energy storage, provide electrical power for the electrical devices, i.e. HPS lamp, aluminum shutter, circulation fans, HPF system, and exhaust fans, to regulate the inside light intensity, humidity, and CO₂ level. Sector II represents the thermal process, where the CHP systems are utilized, together with the thermal energy storage, to supply thermal power for the thermal devices, i.e. liquid convection heaters, to regulate the inside temperature. The paths *a* – *g* enclosed by sector III indicate the interaction between the thermal and electrical processes. In particular, path *a* represents the interaction between thermal and electrical supply caused by the cogeneration property of CHP systems. Path *b* indicates that the electric heaters consume electric power to generate thermal power, which also introduces the interaction between the thermal and electrical processes. Paths *c* – *g* represent the interaction caused by the thermal effects of the operations of HPS lamp, aluminum shutter, circulation fans, HPF system, and exhaust fans. In the rest of this section, the mathematical models of each components and the interaction between thermal and electrical processes are discussed. For analytical tractability, the time horizon is divided into consecutive time slots with equal duration Δt . In this section, the timescale characteristics of electrical and thermal processes are not considered and Δt is used for both electrical and thermal processes.

2.1.1 The Mathematical Model of Greenhouses

The mathematical model of the inside greenhouse environment, i.e., temperature, humidity, light intensity, and CO₂ concentration, is presented. The discrete first-order heat equa-

tion is used to describe the inside temperature as follows [62]:

$$(T_{t+1}^{in} - T_t^{in})\rho^{air} c^{air} V^{gh} = (q_t^{ex} + q_t^{eh} + q_t^{hps} + q_t^{solar} - q_t^{con} - q_t^{plant} - q_t^{hpf} - q_t^{vent})\Delta t, \quad (2.1)$$

where the term $(T_{t+1}^{in} - T_t^{in})\rho^{air} c^{air} V^{gh}$ represents the total thermal energy required to increase the inside temperature of a greenhouse with volume V^{gh} , from T_t^{in} to T_{t+1}^{in} . This amount of thermal energy is provided by the external heat supply q_t^{ex} and the thermal power of electric heaters q_t^{eh} , at time slot t . It is also affected by the thermal power of HPS lamps q_t^{hps} , solar irradiation q_t^{solar} , thermal loss through cover and ground q_t^{con} , heat absorption by plants q_t^{plant} , evaporation heat of HPF system q_t^{hpf} , and the heat exchange through natural and forced ventilation q_t^{ef} . The heat absorption by plants depends on the inside light intensity, temperature, and humidity [57]. In a greenhouse with a large air space, the natural ventilation is affected by the forced ventilation, variable (on or off) of shutters, and wind velocity, while the forced ventilation depends mainly on the fan staging [145]. The inside humidity, light intensity, and CO₂ concentration are modeled based on the agricultural practices and greenhouse structural properties described in [57].

The inside humidity is evaluated by the inside temperature and air water content, and the inside air water content is determined by

$$(W_{t+1}^{in} - W_t^{in})V^{gh} = (\dot{W}_t^{vent} + \dot{W}_t^{hpf} + \dot{W}_t^{plant})\Delta t, \quad (2.2)$$

where the total inside water content change $(W_{t+1}^{in} - W_t^{in})V^{gh}$ of a greenhouse with volume V^{gh} is determined based on the water content exchange rate between the inside and outside air through the natural and forced ventilation \dot{W}_t^{vent} and the water content generation rate of the HPF system \dot{W}_t^{hpf} . Also, the plants will increase the inside water content at the rate of \dot{W}_t^{plant} , through the transpiration process. The plants transpiration rate is a function of the plants weight, inside temperature and air water content [57]. The plants weight is modeled by using the plants CO₂ generation rate as in [146]. The inside light intensity received by the plants during time slot t depends on the solar irradiation and the light intensity of HPS lamps for time slot t , as

$$L_t^{in} = \eta^{solar} L_t + L_t^{hps}. \quad (2.3)$$

Based on the mass balance of open system, the inside CO₂ concentration is calculated as

$$(C_{t+1}^{in} - C_t^{in})V^{gh} = (\dot{C}_t^{vent} + \dot{C}_t^{plant})\Delta t, \quad (2.4)$$

where the total amount of CO₂ change $(C_{t+1}^{in} - C_t^{in})V^{gh}$ for a greenhouse with volume V^{gh} , depends on the CO₂ mass exchange rate between the inside and outside air through the natural and forced ventilation \dot{C}_t^{vent} and the CO₂ generation rate of the plants \dot{C}_t^{plant} . For all the time periods t , the following constraints are applied,

$$M_{min} \leq M_t \leq M_{max}, \quad (2.5)$$

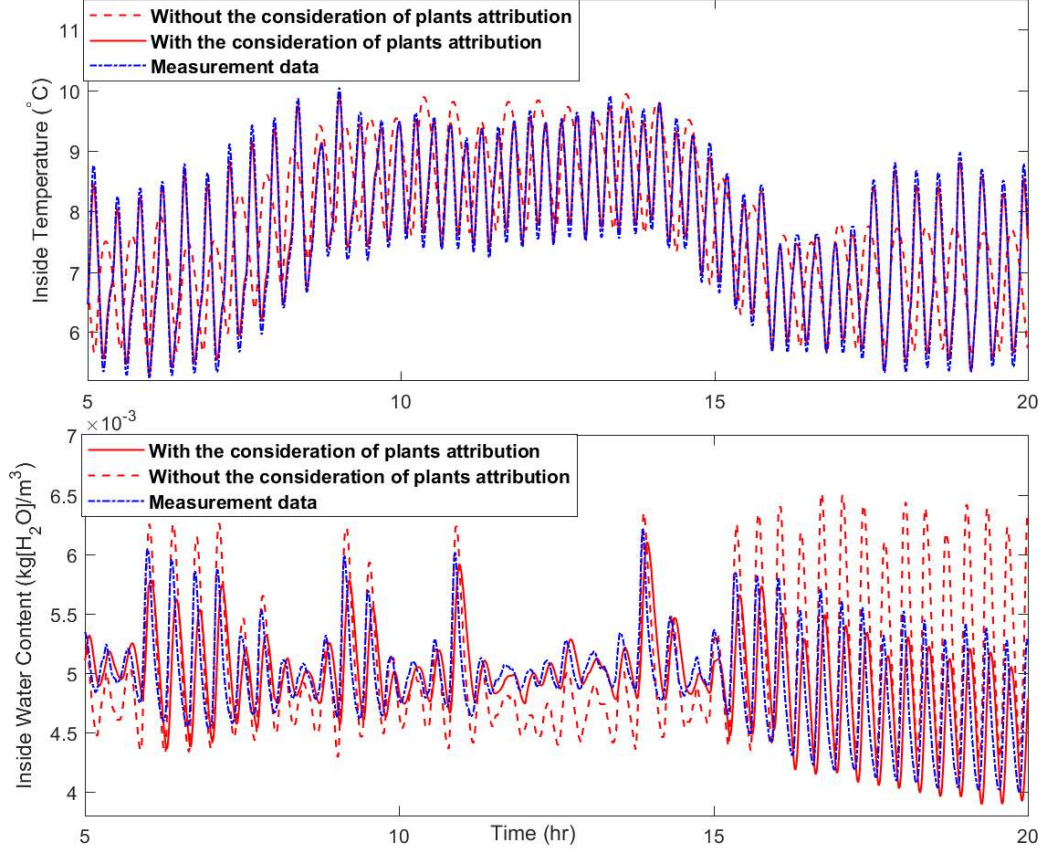


Figure 2.3: The simulation results of inside temperature and humidity in comparison with measurement data.

where M denotes T^{in} , H^{in} , and C^{in} . Also, the daily light integral (DLI) has to be met [56], which is expressed as, for all time t within one day,

$$\sum_t (\max\{0, L_t^{in} - L_{min}^{in}\}) \geq L_{DLI}^{in}. \quad (2.6)$$

The above equation indicates that the aggregated useful light intensity, that is greater than or equal to a threshold L_{min}^{in} (i.e., the minimum light intensity that can activate the photosynthesis process of plants) should be greater than or equal to the required DLI (L_{DLI}^{in}) to guarantee the yield of plants. Different from the other research works on greenhouses energy management [59–62], which only consider the attribution of the botanical characteristics of the plants to the inside CO₂ concentration (i.e. \dot{C}^{plant}), in this work, we also consider the attributions of the plants to the inside temperature q^{plant} and humidity \dot{W}^{plant} . As shown in Fig. 2.3, by considering the attributions of the plants to the inside temperature and humidity, the model accuracy can be improved, which will further improve the accuracy of proposed energy management scheme. The details of the parameters used in this case study are presented in Section 2.4.

2.1.2 The Load Model of Greenhouses

For a well-controlled greenhouse, the electrical power demand arises from the power consumption of the electric heaters, the exhaust fans, the shutters, the HPS lamps, and the HPF system. While the thermal power demand is from the required external and electric heaters thermal power supply. The total electrical and thermal demand of a greenhouse can be expressed, respectively, as

$$p_t = p_t^{eh} + p_t^{ef} + p_t^{hpf} + p_t^{sh} + p_t^{hps} \quad (2.7)$$

$$q_t = q_t^{ex} + q_t^{eh}. \quad (2.8)$$

In this work, we consider a typical setup of commercial greenhouses, such as the one used by Bonnyville Forest Nursery Inc. In particular, due to the consideration of the capital costs of greenhouses construction, the exhaust fans and aluminum shutters are not equipped with variable-frequency drives (VFDs). This makes the control variables of the exhaust fans and aluminum shutters to be either on or off. Also, the high-pressure sodium lamps are controlled to be turned on/off simultaneously to guarantee the even distribution of light intensity within greenhouses [56]. The existing high-pressure fogging systems for greenhouses usually uses the pressure from the city water system, and the only power consumption is to move the fogging systems horizontally at a constant speed. So, in our study, for the exhaust fans, p^{ef} is zero if they are off, and p^{ef} equals to the rating power of exhaust fans if they are on. In addition, p^{sh} equals to the shutter motors rating power, when the aluminum shutters are controlled to be fully opened from fully closed, and vice versa. Currently, all the HPS lamps are controlled simultaneously to be turned on or off, and p^{hps} represents the total power of all the HPS lamps if they are turned on. The HPF system uses the city water pressure to generate the water content, and the only power consumption is the motor used to move the fogging pipes horizontally at a constant speed, when the HPF system is turned on. Some recent research works indicate that, the energy efficiency of greenhouses operation can be improved by adding VFDs. And with the implementation of accurate Photosynthesis Activation Radiation (PAR) sensors, the high-pressure sodium lamps can be controlled individually to further improve the energy efficiency of greenhouses [147]. An extension to consider the control of exhaust fans and aluminum shutters with VFDs and the individual controls of HPS lamps for different PAR sensor monitored areas is left for future work.

2.1.3 The Stochastic Models of Weather Conditions

In the energy management problem of greenhouses with RES, the randomness arises from the PV system, which uses the solar irradiation to generate electricity, and the greenhouses load caused by the inside environment regulation, which is affected by the weather conditions, i.e. the outside temperature, humidity, solar irradiation, wind speed, and CO2 concentration. Then, the randomness of the RES and greenhouses can be addressed by

a proper stochastic model of the weather conditions. The Markov chain with nonhomogeneous state transition probabilities [148] is used to model the stochastic outside temperature, humidity, solar irradiation, wind speed, and CO₂ concentration, individually. Then, by using the segmentation methods [149], one day can be divided into several time segments, with homogeneous state transition probabilities for each of them. While, for different time segments, the state transition probabilities are nonhomogeneous. And the nonhomogeneous state transition probabilities of the weather conditions are denoted as $P_t(T_{t+1}|T_t)$, $P_t(H_{t+1}|H_t)$, $P_t(L_{t+1}|L_t)$, $P_t(v_{t+1}|v_t)$, and $P_t(C_{t+1}|C_t)$, respectively. Instead of forecasting the weather conditions ahead, in our research work, we use the Markov decision process to include the randomness of the weather conditions in the formulation of the stochastic energy management problem, which will be discussed in detail in Section 2.2.

For an arbitrary time segment o , the intra-segment homogeneous transition probability of state X , $P(X'|X)$, can be calculated by using the historical data, through the maximum likelihood estimation [148], where the maximum likelihood estimation for the homogeneous transition probability can be obtained through either parameter elimination or Lagrange multiplier method, which is given as [150]

$$P(X' = x_{o,2}|X = x_{o,1}) = \frac{N_{o,12}}{N_{o,1}}, \quad (2.9)$$

where $N_{o,12}$ is the total number of occurrences of the transitions from state $x_{o,1}$ to $x_{o,2}$, and $N_{o,1}$ is the total number of occurrences of the transitions from state $x_{o,1}$, within the time segment o . For the inter-segment transition from time segment o to time segment $o + 1$, the state at the end of time segment o is the state at the beginning of time segment $o + 1$. The transition probability of the state at the end of time segment o should follow the intra-segment transition probability of time segment $o + 1$ [149], which is the inter-segment nonhomogeneous transition probability, and can be expressed as

$$P_{t_{o,end}}(X' = x_{o+1,2}|X = x_{o,1}) = \frac{N_{o+1,12}}{N_{o+1,1}}, \quad (2.10)$$

where $t_{o,end}$ is the time slot at the end of time segment o , $N_{o+1,12}$ is the total number of occurrences of the transitions from state $x_{o,1}$ to $x_{o+1,2}$, and $N_{o+1,1}$ is the total number of occurrences of the transitions from state $x_{o,1}$, within the time segment $o + 1$.

2.1.4 The Models of Energy Conversion Module

In this work, the multi-stage steam turbine CHP is considered, in which the feasible combinations of electrical power and thermal power are enclosed by the conceptual feasible region [151]. The combined electrical and thermal outputs of the multi-stage steam turbine CHP can be expressed in piece-wise function as

$$BL_i^l(q^{chp}) \leq p^{chp} \leq BL_i^u(q^{chp}), \text{ for } q^{chp} \in \mathbf{q}_i^{chp}. \quad (2.11)$$

The above equation indicates that the extractable electrical power from a multi-stage turbine CHP p^{chp} , which runs at q^{chp} thermal power output, can be any value between the lower boundary $BL_i^l(q^{chp})$ and upper boundary $BL_i^u(q^{chp})$. Then, the cost of the CHP for the generation of feasible amounts of electrical and thermal powers is given by [152]

$$D^{chp} = D^{cp}(p^{chp}, q^{chp}) + D^{ch}(q^{chp}), \quad (2.12)$$

where the electrical generation cost is $D^{cp}(p^{chp}, q^{chp}) = [a_1 p^{chp} + a_2 (p^{chp})^2 + a_3 p^{chp} q^{chp}] \bar{D}^{fuel} \Delta t$ and the thermal generation cost is $D^{ch}(q^{chp}) = [a_4 q^{chp} + a_5 (q^{chp})^2] \bar{D}^{fuel} \Delta t$. The thermal generator ramping model is defined in [153].

The Lithium-ion battery can be modeled based on the state of health (SoH), depth of discharge (DoD), and state of charge (SoC) [154]. Based on Peukert's law, the battery effective discharging power, $p^{bat} < 0$, is given by

$$p_t^{bat} = \psi_t U \bar{C} \left[\frac{\Delta t}{Y} \right]^{\frac{\tau-1}{\tau}} (\omega_t \eta^{bat})^{\frac{1}{\tau}}. \quad (2.13)$$

This equation indicates that the effective discharging power depends on the DoD ω_t , SoH ψ_t , and the real discharging time Δt . The effective charging power $p^{bat} > 0$ can be determined based on Coulomb's law, given by $p_t^{bat} = U \bar{C} \omega_t Y / \Delta t$. For each discharging/charging cycle, the SoH is reduced, due to the degradation of battery lifetime, as

$$\psi_{t'} = \psi_t - [e^{(\bar{s}_t - 0.5)\kappa}] / [b_1 |\omega_t|^{b_2} + b_3], \quad (2.14)$$

where the average SOC $\bar{s}_t = \frac{s_{t'} + s_t}{2}$, and $s_{t'} = s_t + \omega_t$. Also, $b_1 |\omega_t|^{b_2} + b_3$ is the battery lifetime degradation function for average SOC resides at 50%, and $e^{(\bar{s}_t - 0.5)\kappa}$ compensates for the varying average SOC. The cost due to battery lifetime degradation is expressed as

$$D^{bat}(s_t, \omega_t) = \bar{D}^{bat} \left(\frac{e^{(\bar{s}_t - 0.5)\kappa}}{b_1 |\omega_t|^{b_2} + b_3} \right). \quad (2.15)$$

The available thermal energy stored in kWh , of the thermal storage devices depends on the injected thermal power and extracted thermal power [155], and is determined as

$$s_{t'}^h - s_t^h = q_t^h \Delta t, \quad (2.16)$$

where $q^h < 0$ and $q^h > 0$ represent the thermal power extracted from and injected into the storage device, respectively. The PV system with dual-axis solar tracker is modeled with combined efficiency, which includes the PV module and power inverter efficiencies, system losses, and tracking efficiency. At time t , the electrical output of the PV system is given by

$$p_t^{pv} = \eta^{pv} A^{pv} L_t. \quad (2.17)$$

2.2 Formulation of the Stochastic Multi-timescale Energy Management Problem

Greenhouses' energy management problem with integrated RES and energy storage systems is essentially a sequential decision-making problem under uncertainties, which can be formulated as an SDP problem. Also, for the modeling of stochastic weather forecasting and battery degradation, the Markov chain model is well studied and has a good performance [156–159]. Moreover, the state transitions in the SDP problem of greenhouse energy management are partly random due to the uncertainties of RES and weather conditions, and partly under the control of energy storage systems and other environment regulating devices. So, the stochastic greenhouse energy management can be better formulated using Markov decision process (MDP). The conventional MDP only considers a single timescale. However, in practical greenhouse energy management problem, the regulation of inside environment usually refers to multiple timescales. The operation of heating equipment always needs to consider the slow ramping rate of the temperature change. And the operation of electricity equipment usually happens in a relatively faster process. By considering all these processes in a single fast timescale, the dimension of solution is too high to be valid in practice [160]. And the electricity process modeling is less accurate if a single slow timescale is considered. So, it is necessary to consider multiple timescales for different processes, and formulate the greenhouse energy management problem in a MMDP.

Inspired by the multi-timescale problem of real-time operation and long-term planning in processing industry [161], we formulate the stochastic multi-timescale energy management problem of greenhouses as a MMDP, to account for the different timescales of electrical and thermal processes, and the stochastic RES and weather conditions. Due to the interaction between thermal and electrical processes, different from traditional MMDP problem, the formulated MMDP consists of two coupled single-timescale MDPs, i.e. an STS MDP and an FTS MDP for thermal and electrical processes, respectively. The traditional MMDP considers the solving of the STS MDP first, then the FTS MDP is solved for each time slot of the STS MDP. This solution will be valid if the solution of the STS MDP is independent of the solution of the FTS MDP. However, in our case, the regulation of the inside temperature, which is of the STS MDP, will also depend on the operation of all the electrical devices in the FTS MDP. So, the proposed MMDP formulation considers the STS and FTS MDP as two parallel processes that have interaction.

2.2.1 Slow-timescale Thermal Process

Typically, the thermal process varies gradually due to the relatively slow heat exchange and CHP ramping. Therefore, a STS MDP is used to model the thermal process. The time horizon is divided into consecutive time slots with equal duration Δt^s , and the time slots are denoted by $n = [0, 1, 2, \dots]$. Then the STS thermal process is defined as a single-

timescale MDP that operates at timescale Δt^s with finite state space \mathbb{S}^s and finite action space \mathbb{J}^s . In this work, since the energy storage systems are considered to be operated at rated powers with discrete values, for the simplicity of analysis with analytical solutions, the MDP-based energy management problem states and actions are segmented into discrete values [162]. The actions can be easily discretized based on the rated powers. To effectively discretize the states, the state space is first transformed into grids with the vertices representing the discrete states. Then, the transition process of continuous states can be simplified to the states' transitions at the nearest vertex or the neighboring vertices [156]. Since the usage of neighboring vertices has better performance in many experiments for our problem, the state space is discretized based on neighboring vertices in this work. At an arbitrary time n , the state and action are vectors of variables in the form of

- $S_n^s = \langle T_n^{in}, T_n, L_n, s_n^h \rangle, S_n^s \in \mathbb{S}^s;$
- $J_n^s = \langle q_n^{chp}, q_n^h, q_n^{eh} \rangle, J_n^s \in \mathbb{J}^s,$

where $q_n^{ex} = q_n^{chp} - q_n^h$. And, by taking the action J_n^s with state S_n^s at time n , the STS MDP has a bounded immediate cost $R_n^s(J_n^s) = D_n^{ch}(q_n^{chp})$, and the STS MDP nonhomogeneous state transition function $P_n^s(S_{n+1}^s | S_n^s, J_n^s)$ is defined as

$$P_n^s(S_{n+1}^s | S_n^s, J_n^s) = \begin{cases} P_n(T_{n+1} | T_n) P_n(L_{n+1} | L_n), & \text{if (2.1) and } s_{n+1}^h - s_n^h = q_n^h \Delta t^s \text{ hold} \\ 0, & \text{otherwise.} \end{cases} \quad (2.18)$$

In the STS process, the T_{n+1}^{in} is determined by S_n^s and J_n^s . Also, the following constraints applied, for any time $n \geq 0$:

$$q_{n-1}^{chp} - q_{ramp}^{chp} \Delta t^s \leq q_n^{chp} \leq q_{n-1}^{chp} + q_{ramp}^{chp} \Delta t^s \quad (2.19)$$

$$s_{min}^h \leq s_n^h \leq s_{max}^h \quad (2.20)$$

$$q_{min}^h \leq q_n^h \leq q_{max}^h \quad (2.21)$$

$$T_{min}^{in} \leq T_n^{in} \leq T_{max}^{in}, \quad (2.22)$$

where the constraint (2.19) implies the ramping rate constraint of thermal generator. The constraints (2.20) and (2.21) are the constraints of the thermal energy storage capacity and operating limits, respectively. The constraint (2.22) represents the regulation requirement of inside temperature.

2.2.2 Fast-timescale Electrical Process

The electrical process usually has a short response time of operation. Therefore, a FTS MDP is used to model the electrical process. The discrete time slots, with equal duration Δt^f , are denoted as $t = [t_0, t_1, t_2, \dots]$. It is assumed that one time slot of the STS process contains m time slots of the FTS process, i.e. $\Delta t^s = m \Delta t^f$. And the time slot t_{nm} of the

FTS process denotes the same real time as time slot n of the STS process. Then, within each time slot of the STS process, the FTS process is defined as a finite-horizon MDP with length m , finite state space \mathbb{S}^f and action space \mathbb{J}^f . The state and action of the FTS MDP at time t are defined as

- $S_t^f = \langle \psi_t, s_t, T_t^{in}, H_t, H_t^{in}, L_t, L_t^{in}, v_t, C_t, C_t^{in}, p_t^g \rangle, S_t^f \in \mathbb{S}^f$;
- $J_t^f = \langle \omega_t, p_t^{chp}, p_t^{ef}, p_t^{hpf}, p_t^{sh}, p_t^{hps} \rangle, J_t^f \in \mathbb{J}^f$,

where $T_{tmm}^{in} = T_n^{in}$ and p_t^g is the peak demand before time t . By definition, within one time slot of the STS MDP, the state and action of the STS MDP will remain unchanged, and the power of electric heaters depends on q_n^{eh} , which is the action of STS MDP. Then, the bounded immediate cost of the FTS MDP is given by

$$R_t^f(S_t^f, J_t^f, J_n^s) = D^{cp}(p_t^{chp}, q_n^{chp}) + D^{bat}(s_t, \omega_t) + \bar{D}^{el}(p_t - p_t^{pv} - p_t^{chp} + p_t^{bat})\Delta t^f + \bar{D}^{peak} \max\{0, p_t - p_t^{pv} - p_t^{chp} + p_t^{bat} - p_t^g\} \quad (2.23)$$

where \bar{D}^{el} is the electricity price, \bar{D}^{peak} is the peak demand electricity rate, and p_t is the same as (2.7) with p_t^{eh} replaced by p_n^{eh} . And, the nonhomogeneous state transition function of the FTS MDP is denoted as $P_t^f(S_{t+1}^f | S_t^f, J_t^f, S_n^s, J_n^s)$ with the following expression:

$$P_t^f(S_{t+1}^f | S_t^f, J_t^f, S_n^s, J_n^s) = \begin{cases} P_t(H_{t+1}|H_t)P_t(L_{t+1}|L_t)P_t(C_{t+1}|C_t)P_t(v_{t+1}|v_t), & \text{if } s_{t+1} = s_t + \omega_t, p_{t+1}^g \\ = \max\{p_t^g, p_t - p_t^{pv} - p_t^{chp} + p_t^{bat}\}, & \text{(2.1)-(2.4), and (2.14) hold} \\ 0, & \text{otherwise} \end{cases} \quad (2.24)$$

which states that the state transition of FTS MDP depends on the state and action of the STS MDP.

Based on the discussion above, it can be concluded that the FTS MDP is, inherently, induced by the STS MDP. We define a nonhomogeneous policy for the FTS MDP as $\pi_t^f(S_t^f, S_n^s, J_n^s) = J_t^f$, with $S_t^f \in \mathbb{S}^f$, $S_n^s \in \mathbb{S}^s$, $J_n^s \in \mathbb{J}^s$, and $J_t^f \in \mathbb{J}^f$. For all time slots t within STS MDP time slot n , the FTS MDP is subjected to the following constraints:

$$BL_i^l(q_n^{chp}) \leq p_t^{chp} \leq BL_i^u(q_n^{chp}), \text{ for } q_n^{chp} \in \mathbf{q}_i^{chp} \quad (2.25)$$

$$s^{min} \leq s_t \leq s^{max} \quad (2.26)$$

$$p_{min}^{bat} \leq p_t^{bat} \leq p_{max}^{bat} \quad (2.27)$$

$$M_{min} \leq M_t \leq M_{max}, \quad (2.28)$$

where the constraint (2.25) is the constraint of the CHP electrical power at a specific thermal power output. The constraints (2.26) and (2.27) are the constraints of the electrical energy storage capacity and operating limits, respectively. The constraint (2.28) represents the regulation requirement of inside temperature, humidity, CO₂ concentration, and light intensity.

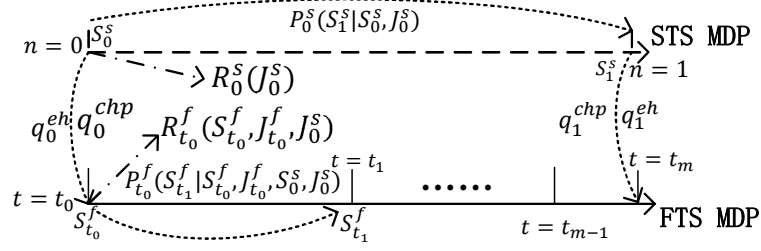


Figure 2.4: An illustration of the evolving process of MMDP.

2.2.3 The Formulation of Stochastic Multi-timescale Energy Management Problem as a MMDP

As shown in Fig. 2.4, the STS MDP and FTS MDP evolve simultaneously in a MMDP. And for an MMDP, over one time slot of the STS MDP, the total cost consists of the STS MDP immediate cost and the m -slot cost of the FTS MDP. Therefore, a function R can be defined such that for all $n \geq 0$ and $t = t_{nm}, \dots, t_{(n+1)m-1}$, $S_t^f \in \mathbb{S}^f$, $S_n^s \in \mathbb{S}^s$, $J_n^s \in \mathbb{J}^s$, and π_t^f , we have

$$R_n(S^f, \pi_{nm}^f, S_n^s, J_n^s) = R_n^s(J_n^s) + \mathbb{E}\left[\sum_{t=t_{nm}}^{t_{(n+1)m-1}} R_t^f(S_t^f, \pi_t^f, J_n^s) \mid S_{t_{nm}}^f = S^f\right], \quad (2.29)$$

where S^f is the initial state of this m -horizon FTS MDP, π_{nm}^f is a sequence of FTS MDP nonhomogeneous policies within the horizon from nm to $(n+1)m-1$, i.e. $\pi_{nm}^f = \{\pi_{t_{nm}}^f, \pi_{t_{nm+1}}^f, \dots, \pi_{t_{(n+1)m-1}}^f\}$, and the expectation term represents the expected total cost of the m -horizon FTS MDP with given S^f and π_{nm}^f . Also, the cost incurred at time $n+1$ of the STS MDP is considered only in the next time slot of STS MDP. Therefore, R is an induced cost function of the MMDP, through the coupling of the FTS MDP iterations that occur during a single STS MDP time step. The above discussion implies that by following a sequence of FTS MDP nonhomogeneous policies, the initial state of the FTS MDP can affect the cost, R . Then, we define the nonhomogeneous policy of the STS MDP, π_n^s , as a function $\pi_n^s(S_{t_{nm}}^f, S_n^s) = J_n^s$ for each time n . Next, we formulate the stochastic multi-timescale energy management problem as a finite-horizon MMDP with a period of one month, and value function defined as

$$V(S^f, S^s) = \mathbb{E}\left\{\sum_n \left[R_n^s(\pi_n^s) + \mathbb{E}\left(\sum_{t=t_{nm}}^{t_{(n+1)m-1}} R_t^f(S_t^f, \pi_t^f, \pi_n^s)\right) \mid S_{t_0}^f = S^f, S_0^s = S^s \right]\right\}, \quad (2.30)$$

with the objective to minimize the total expected cost of the MMDP over infinite horizon with constraints (2.6), (2.19) - (2.22), and (2.25) - (2.28).

2.3 Solution of the Stochastic Multi-timescale Energy Management Problem

For the proposed stochastic multi-timescale energy management problem, which is formulated as a MMDP, the solution is the optimal policy sets for STS and FTS processes, at each time slot, for a definite time horizon. We would like to emphasize that the time horizon required for the optimization can be adjusted based on the electricity pricing scheme of utility company, the accuracy of weather forecasting, and the computational complexity. The corresponding MMDP only needs to adapt the length of the definite time horizon required for optimization. For the commercial greenhouse considered in this work, a popular industrial electricity pricing scheme called demand billing is used. The demand billing contains three components for distribution-connected customers, i.e., customer charge, demand charge, and energy charge. The customer charge is charged at \$/day for customers with distribution services connected to. The demand charge at \$/kW and energy charge at \$/kWh are charged over a monthly billing period [163]. Accordingly, the time horizon required for the optimization is selected as one month. Then, based on the definition of the policy for MDP, as described in Section 2.2, the optimal policy sets can be used in real-time operation, i.e., for each time slot in real time. The corresponding optimal action can be determined based on the actual state vectors and the optimal policy sets of this time slot. In the rest of this section, the derivation of the optimal solution for the proposed MMDP problem will be presented.

From (2.30), it can be observed that for any given $S_n^s \in \mathbb{S}^s$ and $J_n^s \in \mathbb{J}^s$ at time n , the m -horizon FTS MDP has a total expected cost R_{nm}^f for a nonhomogeneous policies set π_{nm}^f and initial state S^f , in the form

$$R_{nm}^f(S^f, \pi_{nm}^f, S_n^s, J_n^s) = \mathbb{E}\left[\sum_{t=t_{nm}}^{t_{(n+1)m-1}} R_t^f(S_t^f, \pi_t^f, J_n^s) | S_{t_{nm}}^f = S^f\right]. \quad (2.31)$$

Based on the principle of optimality [164], the m -horizon FTS MDP with any policy set π_{nm}^f , has a backward recursion of the value function, and the corresponding Bellman equation for the FTS MDP, given $S_n^s \in \mathbb{S}^s$ and $J_n^s \in \mathbb{J}^s$, can be defined for $t = t_{(n+1)m-2}, \dots, t_{nm}$ as

$$V_t^{\pi_{nm}^f*}(S_t^f, S_n^s, J_n^s) = \min_{\pi_t^f} \left\{ R_t^f(S_t^f, \pi_t^f, J_n^s) + \sum_{S_{t+1}^f \in \mathbb{S}^f} [P_t^f(S_{t+1}^f | S_t^f, \pi_t^f, S_n^s, J_n^s) V_{t+1}^{\pi_{nm}^f*}(S_{t+1}^f, S_n^s, J_n^s)] \right\}. \quad (2.32)$$

For $t = t_{(n+1)m-1}$, the Bellman equation is given by

$$V_t^{\pi_{nm}^f*}(S_t^f, S_n^s, J_n^s) = \min_{\pi_t^f} \left\{ R_t^f(S_t^f, \pi_t^f, S_n^s, J_n^s) \right\}. \quad (2.33)$$

Since the FTS process is a finite-horizon MDP at given $S_n^s \in \mathbb{S}^s$ and $J_n^s \in \mathbb{J}^s$, with a simple adaption of MDP theory [165], the following theorem holds.

Theorem 1. For given $S_n^s \in \mathbb{S}^s$ and $J_n^s \in \mathbb{J}^s$ the nonhomogeneous policies set π_{nm}^{f*} that satisfies

$$V_{t_{nm}}^{\pi_{nm}^{f*}} = V_{t_{nm}}^{\pi_{nm}^{f*}}, \forall S_{t_{nm}}^f \in \mathbb{S}^f \quad (2.34)$$

is an optimal nonhomogeneous policies set for the n^{th} m -horizon FTS MDP.

And this finite-horizon FTS MDP can be solved by using a backward induction algorithm as follows [161].

Definition 1. (Initial state transition function) in the form of $P_n^{fs}(S_{t_{(n+1)m}}^f | S_{t_{nm}}^f, \pi_{nm}^f, S_n^s, J_n^s)$ defines the initial state transition function between consecutive m -horizon FTS MDPs.

Starting with initial state $S_{t_{nm}}^f$ of the n^{th} m -horizon FTS MDP and S_n^s and J_n^s of the STS MDP, the n^{th} FTS MDP behaves under π_{nm}^f as a Markov chain. This results in a deterministic state and action of the FTS MDP at time $t_{(n+1)m-1}$. Then, the distribution of FTS MDP states at time $t_{(n+1)m}$, which is the initial state of next m -horizon FTS MDP, can be obtained from the transition function $P_{t_{(n+1)m-1}}^f$.

It should be noted that, for finite-horizon MDP, the value function of the starting point is the reward-to-go function of this finite-horizon MDP, i.e. $V_{t_{nm}}^{\pi_{nm}^f}(S_{t_{nm}}^f, S_n^s, J_n^s) = R_{nm}^f(S^f, \pi_{nm}^f, S_n^s, J_n^s)$ given $S_{t_{nm}}^f = S^f$. Then, the cost function (2.29) can be rewritten as

$$R_n(S_{t_{nm}}^f, \pi_{nm}^f, S_n^s, J_n^s) = R_n^s(J_n^s) + V_{t_{nm}}^{\pi_{nm}^f}. \quad (2.35)$$

Then, the finite-horizon MMDP has the corresponding Bellman equation in the form

$$V_n^*(S_{t_{nm}}^f, S_n^s) = \min_{\pi_{nm}^f, \pi_n^s} \left\{ R_n^s(\pi_n^s) + V_{t_{nm}}^{\pi_{nm}^f} + \sum_{S_{t_{(n+1)m}}^f \in \mathbb{S}^f} \sum_{S_{n+1}^s \in \mathbb{S}^s} \{ P_n^{fs}(S_{t_{(n+1)m}}^f | S_{t_{nm}}^f, \pi_{nm}^f, S_n^s, \pi_n^s) \right. \\ \left. P_n^s(S_{n+1}^s | S_n^s, \pi_n^s) V_{n+1}^*(S_{t_{(n+1)m}}^f, S_{n+1}^s) \} \right\}. \quad (2.36)$$

Due to its nonhomogeneity, it should be noticed that $V_n^*(S^f, S^s) \neq V_{n'}^*(S^f, S^s)$ for $n \neq n'$. With the expression of the Bellman equation of the MMDP in (2.36), this finite-horizon MMDP can be solved by using backward induction algorithm for a horizon of N , which represents one month, with the FTS MDP being computed in parallel. The computational complexity of the FTS MDP is $O(m|\mathbb{J}^f|(|\mathbb{S}^f|)^2)$ for each given pair of $S^s \in \mathbb{S}^s$ and $J^s \in \mathbb{J}^s$. And the total computational time for the finite-horizon MMDP is $O(Nm|\mathbb{J}^f||\mathbb{J}^s|(|\mathbb{S}^f||\mathbb{S}^s|)^2)$. The computational complexity is acceptable for growers with a single or a small number of greenhouses. However, in order to find the optimal energy management policies for a large number of greenhouses, the computational complexity still needs to be reduced. To this end, an approximated solution method is proposed in the following.

From (2.24) and (2.29), it can be observed that by expressing the peak demand p^g and peak demand cost at any time t as $p_t^g = \max\{p_{t-1}^g, p_t - p_t^{pv} - p_t^{chp} + p_t^{bat}\}$ and $\bar{D}^{peak} \max\{0, p_t - p_t^{pv} - p_t^{chp} + p_t^{bat} - p_t^g\}$, respectively. We can use the peak demand and peak demand cost at the end of one day to represent the peak demand and peak demand cost occurred over this

day. Also, the final states of one day should be the initial states of the next day. The energy and peak demand cost decreases as p^{pv} and p^g increase. The battery has lower degradation cost at higher SoC, but faster SoH changes at either higher SoC or deeper DoD. Based on these properties, the MMDP problem for one-day energy management has a monotone optimal policy set [166]. This means that by giving the initial states of one day, the final states of this day are unique. Further, based on the cyclical changes in day to day weather conditions, we assume that the unique optimal policy set for any initial states is homogeneous from day to day. Then, with the unique optimal daily value function V^* and policy set $\{\pi^{f*}, \pi^{s*}\}$ for a month with K days, an approximated solution method, as shown in **Algorithm 1**, can be used to find the minimal total monthly cost V_K . In **Algorithm I**, the same daily optimal value function V^* is used for all days within the same month. For a given peak demand, $p_{1,1}^g$, and the first time slot of the first day of a month, the optimal daily cost for the first day is $V_1^*(p_{1,1}^g) = V^*(p_{1,1}^g)$. The peak demand for the first time slot of the next day, $p_{1,2}^g$, can be determined and is unique, given by $V_2^*(p_{1,2}^g) = V^*(p_{1,2}^g)$. The same process can be applied to the remaining days of the same month. Then, the object is to find the value of $p_{1,1}^g$ that minimizes the summation of the daily costs within a month.

Algorithm 1 Approximation method (for a month with K days)

Input: V^* and $\{\pi^{f*}, \pi^{s*}\}$ obtained by using backward induction algorithm

Output: the optimal initial value of $p_{1,1}^g$

- 1: **for all** $p_{1,1}^g$ **do**
 - 2: $V_K^*(p_{1,1}^g) = 0$
 - 3: **for** $j = 1 \dots K$ **do**
 - 4: $V_K^*(p_{1,1}^g) = V_K^*(p_{1,1}^g) + V^*(p_{1,j}^g)$
 - 5: $p_{1,j+1}^g$ is determined based on $\{\pi^{f*}, \pi^{s*}\}$ and $p_{1,j}^g$
 - 6: **end for**
 - 7: **end for**
 - 8: **return** $p_{1,1}^g$ that has the minimum value of $V_K^*(p_{1,1}^g)$.
-

2.4 Case Study

The case study is performed based on a commercial greenhouse structure from Bonnyville Forest Nursery Inc. [167]. The structure of this greenhouse, the electrical data measurement and recording system for panel A, and the PV system with dual-axis solar tracker from Pomphrey Industries Corporation [168], are shown in Fig. 2.5. Originally, this greenhouse was operated with 24 natural gas unit heaters with a nominal thermal power of 300,000 BTU/hr for each unit heater, 24 horizontal ventilation fans, 96 HPS lamps, 12 aluminum shutters with a total area of $20m^2$, and 3 exhaust fans with $1720cfm$ air flow each at rated power. The inside humidity is regulated by the natural and forced ventilation. In our case study, the horizontal ventilation is designed to operate routinely to guarantee the uniform distribution of air content inside greenhouse. Spruce botany data is considered. And for

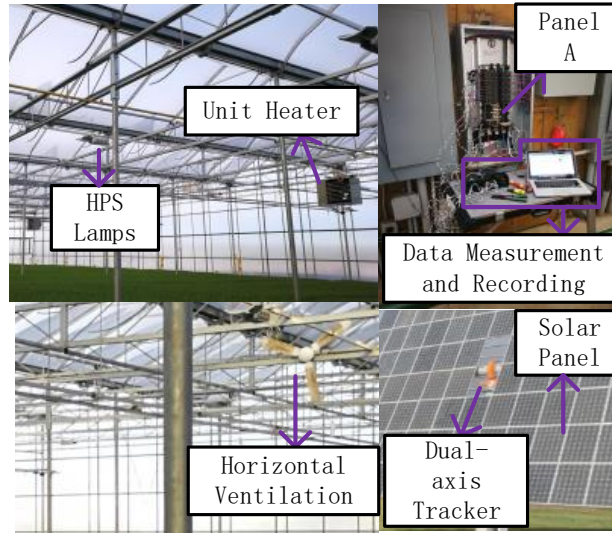


Figure 2.5: The greenhouse for case study.

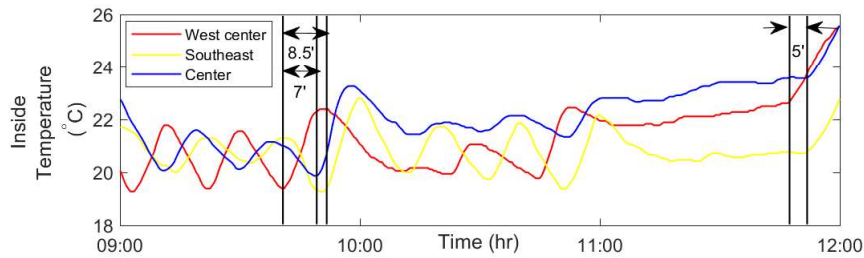


Figure 2.6: The measured response of inside temperature.

spruce, the minimum light intensity required by the photosynthesis is $1850 \mu\text{moles}/\text{m}^2/\text{s}$. The desired DLI is $75 \text{moles}/\text{m}^2/\text{day}$. The inside temperature is regulated between 12°C and 22°C , while the inside humidity and CO_2 are desired within the ranges of $65\% - 68\%$ and $330 \text{ppm} - 1000 \text{ppm}$, respectively. A 1.5MW CHP is selected based on the peak heat demand of this greenhouse which is 1055kW . And the ramping rate of the CHP thermal heater is $15 \text{kW}/\text{min}$. The parameters of the battery are obtained by using the curve-fitting method as in [169]. The electricity rate structure from BC Hydro for General Service [170] is used, which is composed of an energy charge at $0.08 \text{\$/kWh}$ and demand charge at $5.81 \text{\$/kW}$ over one billing period. And the flat rate $0.024 \text{\$/kWh}$ of natural gas from ATCOEnergy [171] is used. For the timescale, we choose $\Delta t^f = 30 \text{sec}$ and $\Delta t^s = 10 \Delta t^f = 5 \text{min}$.

The selection of the above time slot duration for FTS process is because the supervisory control and data acquisition (SCADA) system, used to monitor and control the greenhouse inside environment, has the finest resolution of 30 seconds. To determine the time slot duration for the STS process, it can be observed from Fig. 2.6 that the measured temperatures of the three areas, i.e. the west center area, southeast area, and center area, of the green-

house under study, have relative slow variations due to the large space of the greenhouse and the time that the heat transfer needs to reach different areas. From Fig. 2.6, we can approximate the time required for all three area of this greenhouse to response to the same scenario of heater operation and solar irradiation. It can be observed that the fastest heat transfer comes from the solar irradiation, due to the even distribution of the solar irradiation over the greenhouse space. It takes about 5 minutes, as shown in Fig. 2.6, to increase the temperature of the entire greenhouse space. The time required to increase the temperature of the entire greenhouse space by heaters is much slower, which is about 7-10 minutes, as shown in Fig. 2.6. To reduce the computational complexity of MMDP while maintaining acceptable accuracy of inside environment regulation results, we can set the time slot duration of the STS process as $\Delta t^s = 5\text{min}$.

The on-site weather conditions are monitored and used. As an example, the weather conditions for a winter day and a summer day are shown in Fig. 2.7. We can see that the fluctuations of temperature are relatively small for both winter and summer days. However, the solar irradiation, humidity, CO₂ concentration, and wind speed have large fluctuations. Due to the low temperature and solar irradiation in winter, which results in high energy consumption, the case study is performed for the planting of spruce in winter. The Fig. 2.8 shows the inside environment regulated by the proposed stochastic multi-timescale energy management with an approximation solution. It can be observed that the inside environment is regulated properly within the desired ranges. At night, the temperature is regulated to a low value, which intends to reduce the heat losses caused by the difference between the inside and outside temperatures. Also, the low temperature can reduce the transpiration rate of plants which reduces the fluctuation of inside humidity and CO₂ concentration.

The corresponding operations of the greenhouse equipment are shown in Fig. 2.9, and the energy consumption is shown in Fig.2.10. It can be observed that the HPS is turned on during the time periods of high temperature. The main reason is that during high temperature time periods, the heat requirement is low or close to zero. Accordingly, the CHP, PV system, and battery can be used to reduce the peak electricity demand. Also, the HPS is controlled to be turned on when the solar irradiation is less than but close to $1850\mu\text{moles}/\text{m}^2/\text{s}$, which increases the utilization of solar radiation for plants photosynthesis. And the total photosynthesis time is reduced from 12 hours to 8 hours, with a DLI of $75.012\text{moles}/\text{m}^2/\text{day}$. The exhaust fans and aluminum shutters are used only for the cooling at noon. While the HPF system is operated to increase the humidity when ventilation is on and/or temperature is high. Due to the flat electricity pricing rate, the battery is controlled to shift the PV generation, which increases the utilization of RES. Also, the battery is used to provide thermal power through electric heaters for time period with low heat demand, since a high degradation cost is incurred if the battery is discharged at a high power for a long period of time. On the other hand, the battery is used for peak

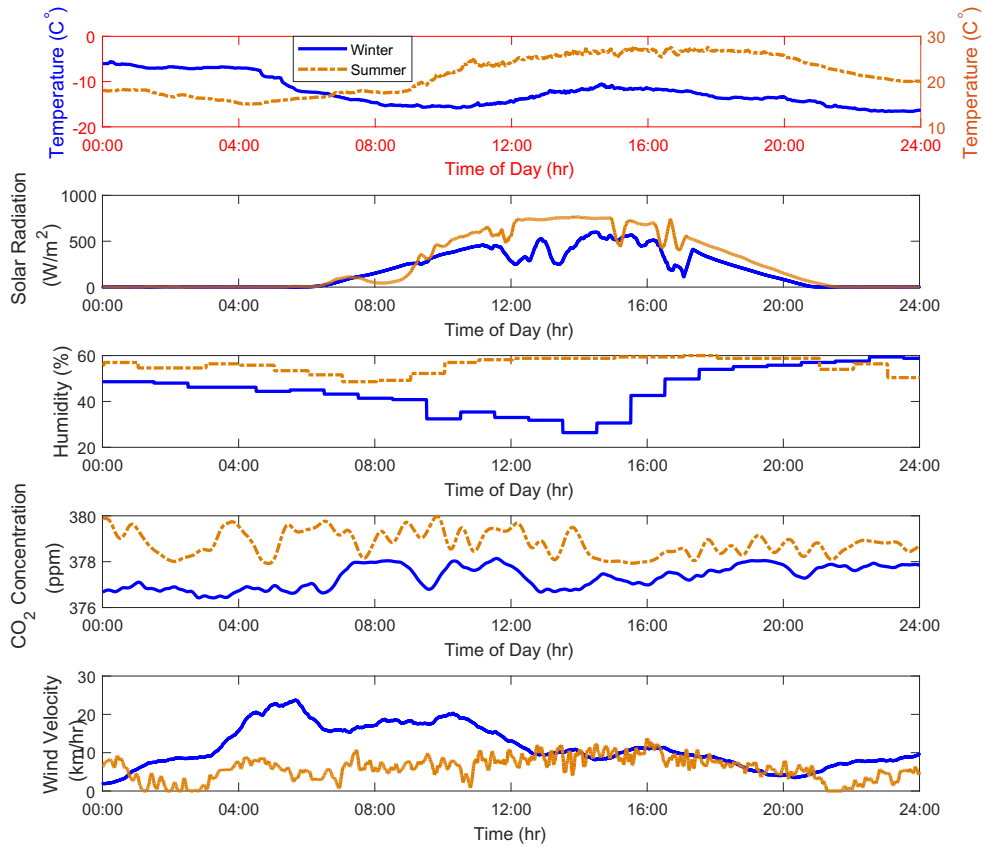


Figure 2.7: Weather conditions for a summer day and a winter day.

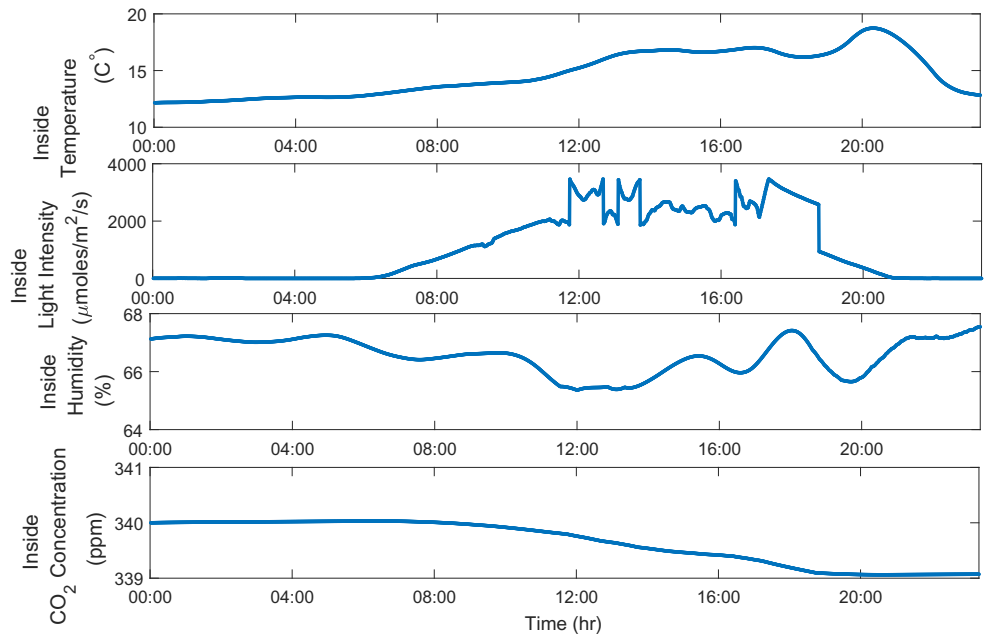


Figure 2.8: Regulated inside environment for a winter day.

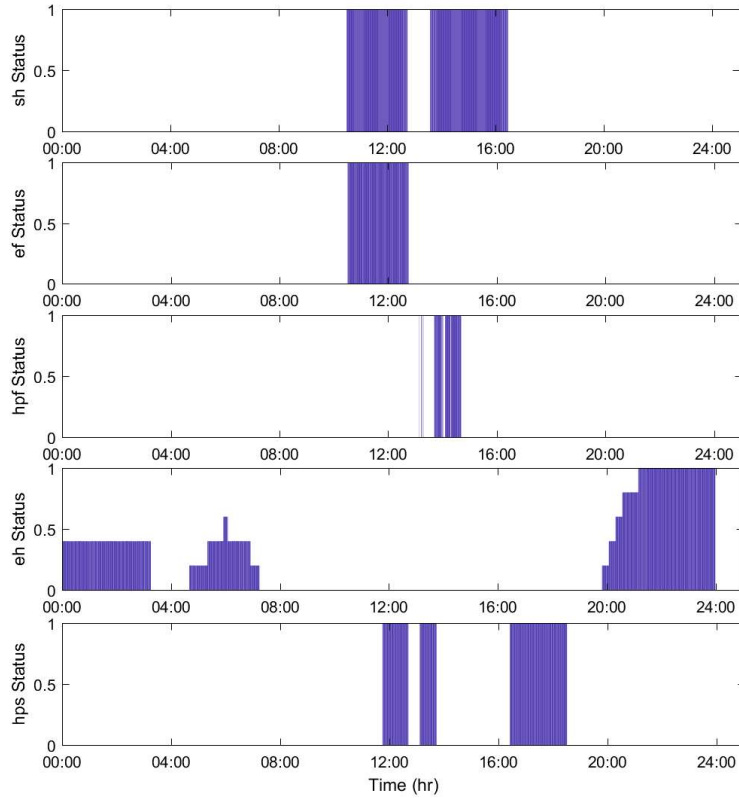


Figure 2.9: Optimal control strategies for a winter day.

demand reduction for a short duration. So, the battery is mainly used during the time periods when the electrical devices are operated, which may cause high peak demand. The battery is only charged by using the excessive PV and CHP electrical power. And it is not necessary to charge the battery by using the grid power to maintain a high SoC at the end of a day, for the next day usage. Similarly, the thermal storage shifts the wasted thermal energy (produced when the CHP is operated to reduce peak demand) to night time. Further, it can be observed that the CHP always tries to provide thermal power by combining the direct heat supply and the heat supplied by electric heaters, due to the fact that CHP has higher efficiency than thermal generator.

To further evaluate the performance of our proposed method, the following cases are considered for comparison:

- Case 0: The greenhouse does not have the RES and is controlled based on setpoint manually setup by the greenhouse grower;
- Case 1: The greenhouse with RES is controlled based on the setpoint;
- Case 2: The greenhouse with RES is controlled by using the forecasting-based method in [62], and is formulated as a single FTS process;
- Case 3: The greenhouse with RES is controlled by using our proposed stochastic

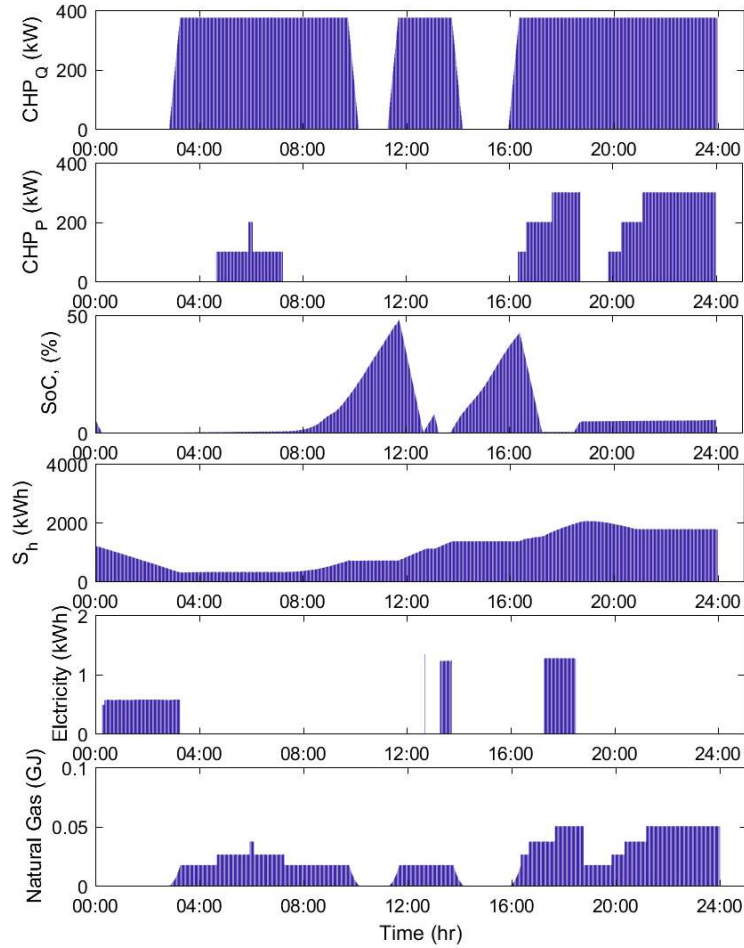


Figure 2.10: Electricity and natural gas consumption for a winter day.

method, and is formulated as a single FTS process;

- Case 4: The greenhouse with RES is controlled by using our proposed stochastic method, and is formulated as a single STS process;
- Case 5: The greenhouse with RES is controlled by using our proposed stochastic method with approximation solution, and is formulated as a multi-timescale process.
- Case 6: The greenhouse with RES is controlled by using our proposed stochastic method with exact solution, and is formulated as a multi-timescale process.
- Case 7: The greenhouse with RES is controlled by using the stochastic multi-timescale method in [23], with approximation solution.

These cases are compared in terms of the natural gas and electricity energy consumption, peak demand, energy cost, demand cost, and computation time. In this work, a PC with Intel CORE i7-4770 3.4 GHz CPU and 8 GB DDR3 RAM is used as a test platform. The results are shown in Table 2.1. By comparing the results of Case 1 and the Case 0, it can be

Table 2.1
THE COMPARISON RESULTS OF EIGHT CASES

	Gas (GJ)	Electricity (kWh)	Peak Demand (kW)	Energy Cost (\$)	Peak Demand Cost (\$)
Case 0	126.46	672.66	126.29	896.88	733.77
Case 1	89.89	230.89	109.72	615.71	637.49
Case 2	52.36	229.65	59.18	367.43	343.84
Case 3	44.32	194.37	30.27	310.99	175.88
Case 4	48.14	445.75	47.93	356.59	278.46
Case 5	48.18	225.45	31.12	339.20	180.80
Case 6	45.32	198.77	31.12	318.03	180.80
Case 7	50.18	220.11	46.45	352.17	269.88
	Energy Cost Reduction (%)	Peak Demand Reduction (%)	Total Cost Reduction (%)	Computation Time (Hr)	
Case 0	0.00	0.00	0.00	0.00	
Case 1	31.35	13.12	23.15	0.00	
Case 2	59.03	53.14	56.38	2.16	
Case 3	65.32	76.03	70.14	14.42	
Case 4	60.24	62.05	61.05	2.67	
Case 5	62.18	75.36	68.11	2.74	
Case 6	64.54	75.36	69.41	7.05	
Case 7	60.73	63.22	61.85	2.71	

observed that by adding RES, the total cost can be reduced to 23.15%. However, the peak demand cost is only reduced by 13.12%, due to the low ramping rate of CHP. Moreover, the energy cost reduction is only 31.35%, and this reduction is less than the price difference of natural gas and electricity which is 70%, this is due to the inefficient operation of CHP. From the comparison between Case 2 and Case 1, we can see that by using the forecasting-based optimization method, the total cost reduction is improved. However, by comparing Case 2 and Case 3, it can be observed that the forecasting-based optimization has low performance than stochastic method, in terms of both energy cost reduction and peak demand reduction. And the stochastic method has obvious advantage in peak demand reduction, since the forecasting typically has higher accuracy in long term and a relative low accuracy in short term. However, the stochastic method consumes more computation time than the forecasting-based method. From the comparison between Case 3 and Case 4, by increasing the time slot duration, i.e. change the process from single FTS process to single STS process, the computation time is reduced significantly. However, the performance of energy and peak demand cost reductions is worse, although it is still better than the forecasting-based method. The results of Case 5 indicate that by using a multi-timescale process, the energy cost and peak demand cost reductions are as good as Case 4, and the computation time is reduced by 81%. The time saving is significant for growers with multiple greenhouses. The comparison between Case 5 and Case 6 indicates that the approximation solution method has total cost reduction that is close to the reduction by using exact solution method, and the relative difference is about 1.87%. However, the time consumption reduction, by using

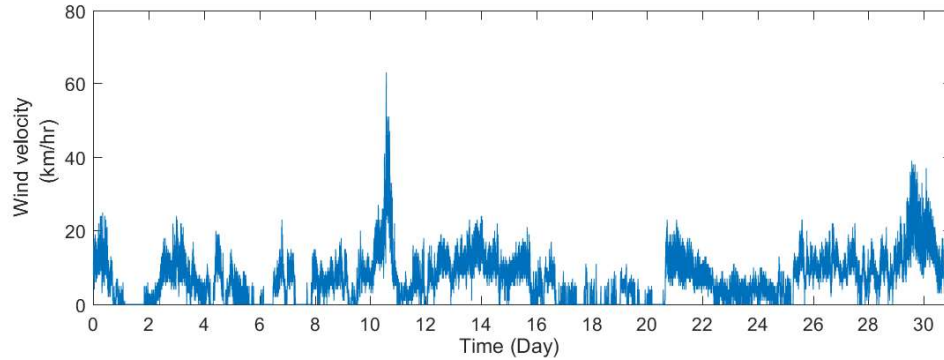


Figure 2.11: The January wind speed data.

the approximation method, is about 61.13%. The peak demands of Case 5 and Case 6 are the same, while the only differences are the gas and electricity consumption, which are caused by the decision of the devices' operating duration. As an example, from the measurement data of wind speed in January (as shown in Fig. 2.11) it can be observed that, the general statistics/trends of wind speed is similar from day to day. However, some days may have unusually high wind speed at several time slots. The exact solution method is able to consider the contribution of such unusual wind speed and reduce the duration of the operations of exhaust fans and/or aluminum shutters. However, this will not affect the occurrences and values of peak demands, since the operation duration reduction only affects the opening percentage of the aluminum shutters and the on-time duration of the exhaust fans. The peak demand occurs at the moment when the aluminum shutter motor and/or the exhaust fans are turned on. Also, by comparing the results of Case 5 and Case 7, it can be observed that the method in Case 7 can reduce the total energy cost by 60.73%, which is close to the cost reduction of our proposed method that is 62.18%; however, the performance on peak demand reduction of the method in Case 7 is inferior to our method, and the difference is about 16%. The main reason is that the method in Case 7 does not consider the interaction between the STS and FTS processes by simply decoupling them into two independent processes. On the other hand, a main contribution of our work is to formulate the stochastic multi-timescale energy management problem by using an MMDP which involves two coupled energy processes at different timescales. Accordingly, the total cost reduction of Case 7 is smaller than that of our method by about 9%, while the computation time is almost the same.

Also, from the results of Cases 1-7, it can be observed that all the energy cost reductions are less than 70%, which is due to the tradeoff between energy cost reduction and peak demand cost reduction. The peak demand cannot be reduced to zero, since the power provided to reduce the peak demand has to last for certain duration. If the time duration is long enough, it is more economic to increase the peak demand. Also, we compare the inside temperature regulated by using a single FTS process and a multi-timescale process, and the results are shown in Fig. 2.12. We can see that the variations of inside temperature

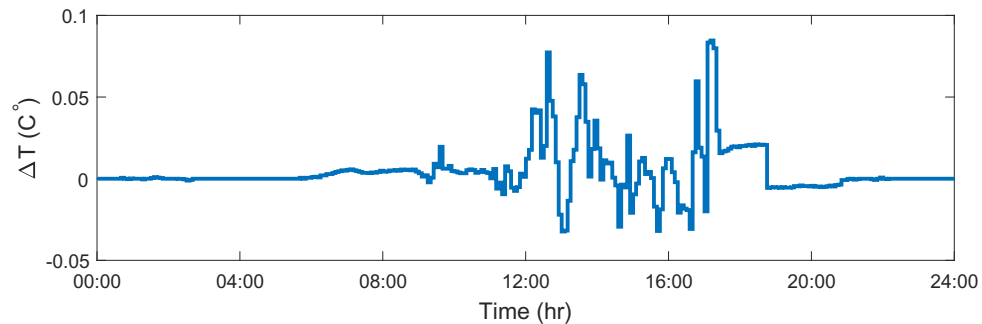


Figure 2.12: The inside temperature error caused by using multi-timescale process.

are low, and the maximum error is limited to 1.42%. The main reason is that the electrical process can affect the thermal process; however, the impact is limited.

2.5 Summary

This chapter presents a multi-timescale stochastic energy management scheme for large facility with RES integration and energy storage systems, with its application in commercial greenhouses. This proposed multi-timescale stochastic energy management scheme is able to reduce the computational complexity significantly by formulating the whole optimization problem into two coupled optimization problems for electrical and thermal processes, respectively. In this way, the number of control variables and time slots in optimization period can be reduced, which results in low dimension of solution.

3

Stochastic Energy Management of BESSs at High Penetration Level in SDSs

The grid-tied residential BESSs with bidirectional power flows can benefit the customers through time-shift for self-consumption, time-shift for feed-in of arbitrage service, smoothing of RES feed-in, and other functionalities [172]. However, with the proliferation of residential BESSs in SDSs, the stochastic energy management of BESSs that is lack of proper regulation may cause active power loss increase, voltage profile variation, and other impacts on the efficiency and stability of SDS operation [173]. For example, at high penetration level, the energy management of BESSs based on pricing incentives may cause the loss of load diversity or even cause new peak during the off-peak period. Thus, there is an urgent need to investigate the stochastic energy management of BESSs at high penetration in SDSs, which considers both the economics of demand-side electricity energy usages and the efficiency and stability of SDS operation.

In the literature, the existing approaches for stochastic energy management of BESSs at high penetration level can be classified into centralized, decentralized, and hierarchical approaches. As the most direct, the centralized energy management of BESSs in SDSs can be easily implemented and can achieve the joint optimization of DSO and customers, simultaneously [73]. However, at high penetration level, the large amount of residential BESSs will increase the number of control variables significantly, which will cause high computational complexity issue for centralized approaches. To reduce the computational complexity, the decentralized approaches and hierarchical approaches have been proposed and evaluated to distribute the computation to different agents in SDSs [68–71]. However, due to the limitation of information in these two approaches, i.e., for the decentralized approaches, the local agents are not aware of the system information or only have partial system information, while for the hierarchical approaches, the agents in the top layer do

not have the complete information of the agents in the next-level layers. Then, the decentralized approaches or hierarchical approaches for stochastic energy management of BESSs either consider the optimization problem of DSO or customers as the main problem, and the overall benefit of DSO and customers has not been considered. Recently, the analysis of hierarchical and decentralized control methods in the applications of battery pack management [174] and frequency control [175] indicates that the hierarchical and decentralized control methods can achieve the coordination among different power system devices at a low computational complexity. This property is particularly desirable for the efficient energy management of residential BESS, for the joint optimization of DSO and customers, at a high penetration level. However, how to apply it to the energy management for smart distribution systems still requires extensive research. Also, to the best of our knowledge, no research works have considered the nonhomogeneous stochastic renewable power generation and residential load during the formulations of optimal energy management problems at the distribution system level.

In this chapter, an energy management scheme that can reduce the computational complexity of DSO while considering the joint optimization of DSO and customers is proposed. In the lower layer, the stochastic information of individual BESS is processed locally to reduce the computational complexity of DSO, and optimal policies are generated for the minimization of customers electricity cost. In the upper layer, based on the optimal policies of individual BESS, the DSO minimizes the line losses while maintaining the voltage levels within required range. System state information is generated to regulate the decentralized control of individual BESS. A heuristic search and pruning method is proposed to further reduce the computational complexity for SDSs with high BESS penetration.

3.1 System Model

An illustration of the smart distribution system considered is shown in Fig. 3.1. In particular, a group of households connected to the same service transformer form a secondary distribution system. Three types of households in terms of Configurations I, II, and III, respectively, are considered [176]. The definitions of these three configurations are:

- Configuration I: The node with grid-tied PV is modeled as PQ node with capabilities of drawing/injecting power;
- Configuration II: The node with residential load only is modeled as PQ node, which can only draw power;
- Configuration III: The node with grid-tied BESS is modeled as adjustable PQ node, where the drawing/injecting active power can be controlled by EMS.

We consider a typical configuration of communication links for smart distribution systems [129]. Two-way communication links are established within the smart distribution

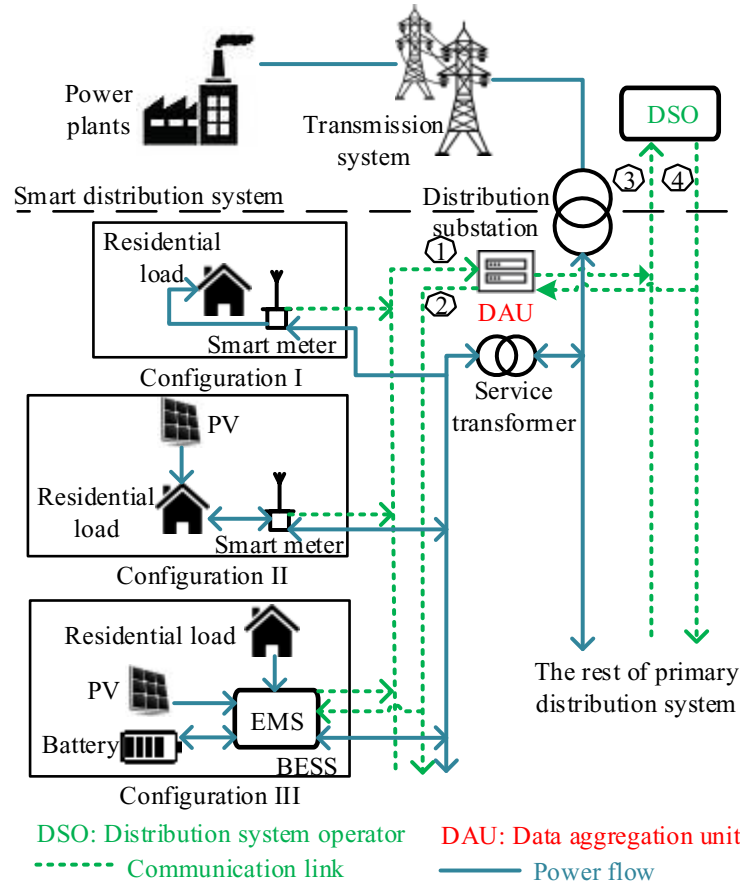


Figure 3.1: An illustration of the smart distribution system.

system between the individual households and DSO through the DAUs. Within a secondary distribution system, the EMS for households with BESS and smart meters for households without BESS communicate with the DAU through communication link ①. And the DAU can broadcast system information to the EMS through communication link ②. Also, the DAU communicates with DSO through communication links ③ and ④. In a hierarchical and decentralized energy management framework, the feedback from DSO to DAU is general system information such as the system voltage levels, rather than the direct control signals for each EMS. In this way, the computational complexity at DSO can be significantly reduced [177]. For the tractability of analysis, the time is partitioned into time slots with equal duration T . The electricity price γ varies over time and is known *a priori*. In the rest of this section, the detailed models of the distribution system, battery, PV system, and residential load are presented.

3.1.1 Distribution System Model

In this research, we consider the smart distribution system as a balanced system which can be represented by an equivalent single-line diagram. The equations in [178] are used

to calculate the voltage levels and line losses. The relationship between the magnitudes of primary-side voltages v_i and v_j of service transformers i and j , respectively, can be expressed as

$$v_j^2 - v_i^2 = \frac{(r_{ij}^2 + x_{ij}^2)(p_i^2 + q_i^2)}{v_i^2} - 2(p_i r_{ij} + q_i x_{ij}), \quad (3.1)$$

where p_i and q_i are, respectively, the effective active and reactive powers from service transformer i flowing through branch ij that connects service transformers i and j . And r_{ij} and x_{ij} are the resistance and reactance of branch ij , respectively. The active power loss of branch ij can be calculated as

$$p_{ij}^{loss} = r_{ij}(p_i^2 + q_i^2)/v_i^2. \quad (3.2)$$

3.1.2 Battery Model

In this research, the battery is modeled based on the degradation cost and effective charging and discharging powers. The charging and discharging processes are considered having equivalent degradation effect but opposite power flow directions [179], i.e., negative for charging and positive for discharging. The charging/discharging processes cause the degradation of battery lifetime, and the battery lifetime degradation is quantified by the degradation factor (E) which is the percentage of lost active capacity to the nominal active capacity. For an arbitrary time slot t , the degradation factor can be calculated base on Millner's model [154] as

$$E_t = (\alpha|\omega_t|^\beta + \mu)^{-1} e^{|s_t + \frac{\omega_t}{2} - 0.5|\kappa} \times \psi_t, \quad (3.3)$$

where the parameters α , β , and μ can be calculated by using the curve-fitting method. And the parameter κ for Lithium-ion battery is 3.446 [154]. The state of charge (SoC) and SoC change are denoted by s and ω , respectively, while ψ_t is the remaining active capacity. The battery degradation cost (C_t^d) is calculated as $C_t^d = \varepsilon \times E_t$, where ε is the unit cost of battery in $\$/Ah$. And, for the next time slot $t + 1$, values of s and ψ are updated, respectively, as $s_{t+1} = s_t + \omega_t$ and $\psi_{t+1} = \psi_t - E_t/\psi_t$. Based on Peukert's law, the effective discharging power p^d , for given ψ and w , is given by

$$p^d = f(\psi, \omega) = \psi U \tilde{C} (H/T^2)^{\frac{1-\iota}{\iota}} (|\omega|\tau)^{\frac{1}{\iota}}, \quad (3.4)$$

where U is the battery terminal voltage, \tilde{C} is the nominal battery capacity, H and T are, respectively, the nominal and actual discharging time. Also, ι is the Peukert's constant, and τ is the round-trip efficiency of battery. The charging processes of residential batteries in a short duration can be represented by constant voltage processes [180]. So, the power p^c , required to increase the SoC by w , is calculated as

$$p^c = g(\omega) = U \tilde{C} |\omega|/T. \quad (3.5)$$

For a given ψ , (3.4) and (3.5) are monotonous with respect to ω . This allows us to calculate ω from p^d and p^c by using the inverse functions f^{-1} and g^{-1} , respectively.

3.1.3 PV System and Residential Load Model

In this research, the PV power generation is considered as a function of the solar irradiation, and the equation in [181] is utilized. At time slot t , the PV power generation can be calculated as $p_t^s = \sigma A \xi_t$, where σ is the efficiency of PV system, A is the total area of PV panels, and ξ is the solar irradiation in kW/m^2 . The stochastic solar irradiation is modeled by nonhomogeneous Markov chain model [182]. For each time slot, the solar irradiation is denoted as a state of the Markov chain. And the Bayesian approach can be used to estimate the state transition probability $P(\xi_{t+1}|\xi_t)$ of solar irradiation. To deal with the nonhomogeneity of the solar irradiation, one day is partitioned into several time segments, for each time segment the solar irradiation is treated as homogeneous Markov chain [182]. So, the time-partitioned solar irradiation transition model can be expressed as $P_t(\xi_{t+1}|\xi_t)$. Moreover, the state transition probability of the PV power generation can be determined as $P_t(p_{t+1}^s|p_t^s) = P_t(p_{t+1}^s = \sigma A \xi_{t+1} | p_t^s = \sigma A \xi_t) = P_t(\xi_{t+1}|\xi_t)$, which indicates that the transition of the PV power generation follows the nonhomogeneous Markov chain model of solar irradiation. In [134], it has been discussed that the residential load is associated with the nonhomogeneous stochastic activity of daily life, which is modeled by the Markov chain. So, the time-partitioned homogeneous Markov chain model is also used to model the residential load with the nonhomogeneous transition probability $P_t(p_{t+1}^l|p_t^l)$, where p^l is the residential load.

3.2 Problem Formulation

In this research, the stochastic energy management problem is formulated based on a two-layer hierarchical architecture. In the lower layer, each BESS has its own policy for stochastic BESS management to minimize the electricity cost. The battery power is determined locally by the EMS based on the policy, PV power generation, residential load, and system information. In the upper layer, the DSO considers the aggregated power at each service transformer and tries to minimize the line losses while maintaining the voltage levels within required range. The BESS are controlled in a decentralized manner with partial communications among the households within a smart distribution system, and there are no control signals sent by DSO directly to any BESS. Next, the detailed formulations of the hierarchical and decentralized stochastic energy management problem will be presented.

3.2.1 BESS Energy Management

The BESS can be implemented by the customers to increase the efficiency of installed PV systems and reduce the electricity costs [184]. In this configuration, the PV power generation supplies the residential load first, and the surplus can be fed back to the electrical grid or stored in the battery. Then, at time slot t , the power balance equation is given by $p_t^l = p_t^s + p_t^b + p_t^g$. The cost C_t^g for buying/selling energy from/to the electrical grid is

given by $C_t^g = p_t^g \gamma_t = (p_t^l - p_t^s - p_t^b) T \gamma_t$. As discussed in Subsection 3.1.2, with the given values of ψ_t and p_t^b of battery, the SoC change ω_t can be calculated by using the inverse functions of (3.4) and (3.5). Also, we have $s_{t+1} = s_t + \omega_t$ and $\psi_{t+1} = \psi_t - E_t / \psi_t$. So, the values of s_{t+1} and ψ_{t+1} at time slot $t + 1$, and the battery degradation cost C_t^d at time slot t can be determined explicitly from s_t , ψ_t , and p_t^b of time slot t . For notation clarity, we define the battery state transition function as $P(s_{t+1}, \psi_{t+1} | s_t, \psi_t, p_t^b)$ and battery degradation cost function as $c^b(s_t, \psi_t, p_t^b)$. Then, the immediate cost at time slot t , by taking action p_t^b with state vector $\varpi_t = \{p_t^s, p_t^l, s_t, \psi_t\}$, is the summation of C_t^g and C_t^d , and can be expressed as $R_t(\varpi_t, p_t^b) = (p_t^l - p_t^s - p_t^b) T \gamma_t + c^b(s_t, \psi_t, p_t^b)$. Also, at time slot $t + 1$, the state vector transits to $\varpi_{t+1} = \{p_{t+1}^s, p_{t+1}^l, s_{t+1}, \psi_{t+1}\}$ with probability $P_t(p_{t+1}^s | p_t^s) P_t(p_{t+1}^l | p_t^l)$, since PV power generation and residential load state transition processes are independent, and the transition of battery state is determined deterministically by transition function $P(s_{t+1}, \psi_{t+1} | s_t, \psi_t, p_t^b)$. Based on the discussion above, the immediate cost and state transition of the stochastic BESS energy management problem can be described explicitly by the current states and action taken. This allows the usage of MDP to formulate the stochastic BESS energy management problem. For time slot t , with state vector ϖ_t and action p_t^b , the total expected cost function $C_t(\varpi_t, p_t^b)$, i.e., the cost-to-go function for time slot t , can be calculated as

$$\begin{aligned}
 C_t(\varpi_t, p_t^b) &= R_t(\varpi_t, p_t^b) + \sum_{p_{t+1}^s, p_{t+1}^l} P_t(p_{t+1}^s | p_t^s) P_t(p_{t+1}^l | p_t^l) P(s_{t+1}, \psi_{t+1} | s_t, \psi_t, p_t^b) C_{t+1}(\varpi_{t+1}, p_{t+1}^b),
 \end{aligned} \tag{3.6}$$

where $c_{t+1}(\varpi_{t+1}, p_{t+1}^b)$ is the cost-to-go function for time slot $t + 1$. The objective is to minimize the total expected cost, given by

$$\min_{p_t^b} C_t(\varpi_t, p_t^b), \tag{3.7}$$

and the constraints of this problem are related to the battery SoC, current, and SoC change, respectively, given by

$$SoC_{min} \leq s_t \leq SoC_{max} \tag{3.8}$$

$$-|\bar{I}^c| < p_t^b / U < |\bar{I}^d| \tag{3.9}$$

$$0 \leq |\omega_t| \leq 1. \tag{3.10}$$

3.2.2 Hierarchical and Decentralized Stochastic Energy Management BESSs in SDSs

In this research, the decentralized partially observable Markov decision process (Dec-POMDP) with a stochastic controller (SC) [183] is implemented to reformulate the general Dec-POMDP to consider the stochastic information of individual households. We define

each household as a single SC. The system state (\mathbf{S}_t) is defined as the set of PV power generation, residential loads, and battery states of all households, i.e., $\mathbf{S}_t = \{\dots, p_t^{s,n}, p_t^{l,n}, s_t^n, \psi_t^n, \dots, p_t^{s,N}, p_t^{l,N}, s_t^N, \psi_t^N, \dots, p_t^{s,m}, p_t^{l,m}, \dots, p_t^{s,M}, p_t^{l,M}\}$, where n is the n^{th} household with BESS, m is the m^{th} household without BESS, and $N + M$ is the total number of households. Also, we define the action vector (\mathbf{p}_t^b) of the system as the set of actions taken by all the households with BESS, given by $\mathbf{p}_t^b = \{\dots, p_t^{b,n}, \dots, p_t^{b,N}\}$. Further, we define $P_t(\mathbf{S}_{t+1}|\mathbf{S}_t, \mathbf{p}_t^b)$ and $R(\mathbf{S}_t, \mathbf{p}_t^b)$, respectively, as the nonhomogeneous system state transition function and system immediate cost. As discussed in [75], to reduce the operating cost of smart distribution systems through the coordination between the DSO and customers, the system cost includes the electricity usage cost and electricity generation cost. The electricity usage cost is the cost of purchasing the total net energy from the grid, i.e., $\gamma T[\sum_{l=1}^L p_l^{\text{loss}} + \sum_{n=1}^N (p^{l,n} - p^{s,n} - p^{b,n}) + \sum_{m=1}^M (p^{l,m} - p^{s,m})]$, where L is the number of total lines and p_l^{loss} is the line loss of single branch calculated in (3.2). Since we only consider the renewable power generation, the electricity generation cost contains only the battery degradation cost c^b . Then, the immediate cost of system with electricity price γ can be calculated as

$$\begin{aligned} R(\mathbf{S}, \mathbf{p}^b) &= \gamma T \sum_{l=1}^L p_l^{\text{loss}} + \gamma T \sum_{m=1}^M (p^{l,m} - p^{s,m}) + \gamma T \sum_{n=1}^N (p^{l,n} - p^{s,n} - p^{b,n}) + \sum_{n=1}^N c^{b,n} \\ &= \gamma T \sum_{l=1}^L p_l^{\text{loss}} + \sum_{y=1}^{N+M} R^y(\varpi, p^b). \end{aligned} \quad (3.11)$$

In centralized energy management scheme, the DSO controls the individual BESS directly which results in high computational complexity. To reduce the computation complexity by using decentralized energy management scheme, we define a virtual battery state (ν) as system information given by the DSO to individual BESS. The battery state given in ν may or may not be the same as the actual battery state, and the actual battery state is the constraint of BESS energy management problem. Further, we define $P(\nu_{t+1}|\nu_t, p_t^b)$ as the virtual battery state transition function. Then, the system total expected cost function of this formulated energy management problem is given by

$$C_t(\mathbf{S}_t, \nu_t) = \sum_{\mathbf{p}_t^b} \Pi(\mathbf{p}_t^b|\nu_t) [R(\mathbf{S}_t, \mathbf{p}_t^b) + \sum_{\mathbf{S}_{t+1}} P(\mathbf{S}_{t+1}|\mathbf{S}_t, \mathbf{p}_t^b) P(\nu_{t+1}|\nu_t, \mathbf{p}_t^b) C_{t+1}], \quad (3.12)$$

where $\Pi(\mathbf{p}_t^b|\nu_t)$ is the set of distributions of actions for BESS with given ν . And the objective function is given by

$$\min_{\nu_t, P(\nu_{t+1}|\nu_t, \mathbf{p}_t^b)} C_t(\mathbf{S}_t, \nu_t), \quad (3.13)$$

with the following constraints applied to:

1. The voltage magnitude of each service transformer has to be within required voltage range $[v^{\text{min}}, v^{\text{max}}]$;
2. BESS energy management constraints (3.8) - (3.10).

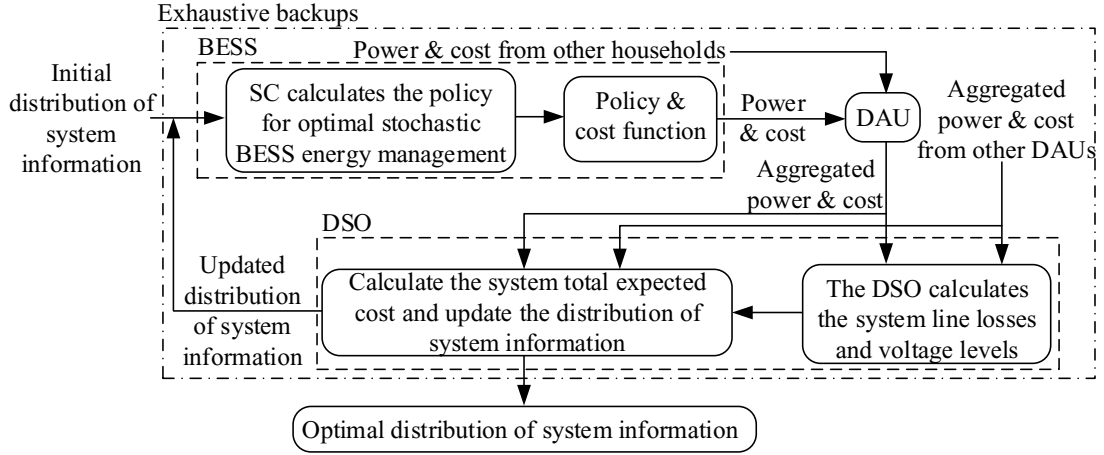


Figure 3.2: The solution procedures of proposed scheme.

3.3 The Energy Management Scheme with Exhaustive Backups

In this section, we derive the solution of the proposed energy management problem for smart distribution systems based on dynamic programming method with exhaustive backups. An illustration of the solution procedures is shown in Fig. 3.2. In the lower level, each SC determines the policy for optimal BESS energy management at given initial distribution of system information, e.g., the initial virtual battery states and the system voltage levels. Then, the power and cost determined by individual SC are aggregated at the DAU. In the upper level, the aggregated power from different DAUs are used by the DSO to calculate the line losses and voltage levels. Then, the system total expected cost is calculated based on the aggregated cost and system line losses. The exhaustive backups are performed, with updated distribution of system information, to find the minimized system total expected cost under constraints and the perspective distribution of system information, i.e., the optimal distribution of system information. The optimal distribution of system information is used by individual BESS to determine the actual battery power based on the local information, i.e., the actual battery states, PV power generation, and residential load. To address the inaccuracy of long-term forecasting and guarantee the convergence of nonhomogeneous MDP and Dec-POMDP for smart distribution system energy management [185], a discount factor, $\eta \in (0, 1)$, is introduced to update the recursive cost C_{t+1} , in (3.6) and (3.12), as ηC_{t+1} .

As discussed in Subsection 3.2.1, the solution of individual BESS energy management problem, for given state ϖ , is the action p^{b*} that minimizes the total expected cost $C(\varpi, p^b)$. The dynamic programming with exhaustive backups is operated on $C_t(\varpi_t, p_t^b)$, for all possible ϖ_t , to find p_t^{b*} that minimizes $C_t(\varpi_t, p_t^b)$ for perspective state ϖ_t , while subjecting to the constraints (3.8)-(3.10). We define $\Pi^*(p^b|\varpi)$ as the policy of BESS energy management problem that maps the optimal battery action with respect to the BESS state, i.e.,

the local information. As discussed in Subsection 3.2.2, for the decentralized coordination among BESS, each BESS is defined as a SC with virtual battery states ν . In conventional Dec-POMDP, the policy $\Pi(p^b|\nu)$ for individual SC is unknown and has to be solved for. However, in this research work, the formulation of smart distribution systems energy management problem in a two-layer hierarchical architecture with the individual BESS functioning as a SC allows us to use the policy of individual BESS to represent the policy of individual SC, and the policy of individual SC can be rewritten as $\Pi^*(p^b|p^s, p^l, \nu)$, which considers both the local information and system information ν . For a given set of initial virtual battery states $\nu_t = [\nu_t^1, \dots, \nu_t^n, \dots, \nu_t^N]$, each household has the corresponding battery power based on $\Pi^{n*}(p_t^{b,n}|p_t^{s,n}, p_t^{l,n}, \nu_t^n)$ as discussed above. At the service transformer, the powers are aggregated by the DAU based on the battery power, PV power generation, and residential load. For example, the aggregated power p_t^k at time t of service transformer k is $p_t^k = \sum_{n,m \in k} (p_t^{l,n} - p_t^{s,n} + p_t^{l,m} + p_t^{s,m}) - \sum_{n \in k} p_t^{b,n}$. Then, equations (5.7) and (3.2) are used to calculate the voltage levels and line loss, respectively, based on the aggregated power. Due to the independence among households and the dependence of battery state transition on current battery states and action taken, the nonhomogeneous system state transition $P(\mathcal{S}_{t+1}|\mathcal{S}_t, \mathbf{p}_t^b)$ can be expressed as

$$P(\mathcal{S}_{t+1}|\mathcal{S}_t, \mathbf{p}_t^b) = \prod_{m,n \in k} P(p_{t+1}^{s,n}|p_t^{s,n})P(p_{t+1}^{l,n}|p_t^{l,n})P(p_{t+1}^{s,m}|p_t^{s,m})P(p_{t+1}^{l,m}|p_t^{l,m})P(s_{t+1}^n, \psi_{t+1}^n|s_t^n, \psi_t^n, p_t^n), \quad (3.14)$$

where K is the total number of service transformers. Due to the decentralized formulation of energy management problem for smart distribution systems, there is no system belief state for the coordination among BESS [186]. In this research work, a correlated controller Q^c is formulated as nonhomogeneous random variables with variable q^c , to coordinate BESS based on the information of system voltage levels, and is given as

$$Q_t^c(q_t^c) = \begin{cases} P_t^{c,l}, & \text{if } q_t^c = V_l \\ P_t^{c,h}, & \text{if } q_t^c = V_h \\ P_t^{c,s}, & \text{if } q_t^c = V_s \end{cases} \quad (3.15)$$

where $P_t^{c,l} + P_t^{c,h} + P_t^{c,s} = 1$. The events V_l , V_h , and V_s are

- $V_l = [\min\{v_{t+1}^1, \dots, v_{t+1}^k, \dots, v_{t+1}^K\} < v^{min}]$;
- $V_h = [\max\{v_{t+1}^1, \dots, v_{t+1}^k, \dots, v_{t+1}^K\} > v^{max}]$;
- $V_s = [\forall k \in K, v_{t+1}^k \in [v^{min}, v^{max}]]$.

Then, the virtual battery states transition function in (3.12) is now revised to $P_t(\nu_{t+1}|\nu_t, \mathbf{p}_t^b, q_t^c)$ to consider the information of system voltage levels. Different from the conventional dynamic programming that updates the cost function, in our problem, we solve

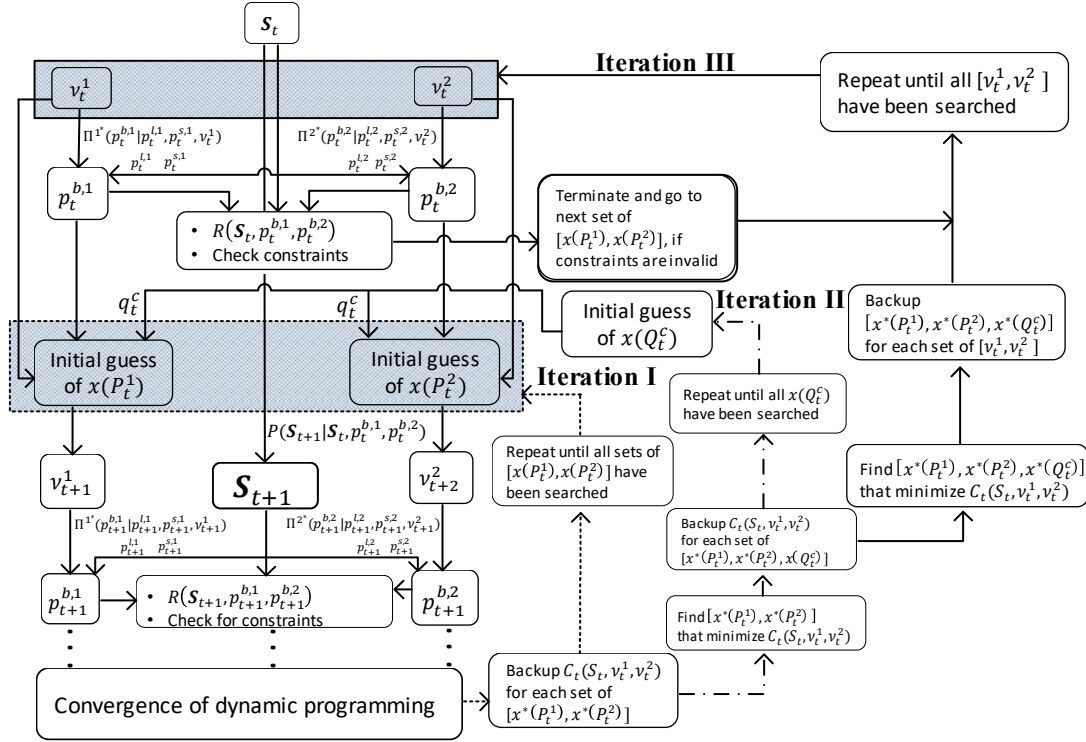


Figure 3.3: An illustration of the algorithm for exhaustive backups.

the proposed hierarchical and decentralized stochastic energy management problem by solving the nonhomogeneous variables for distribution of system information, i.e., $x(\boldsymbol{\nu}_t)$, $x(Q_t^c) = Q_t^c(q_t^c)$, and $x(P_t) = P_t(\boldsymbol{\nu}_{t+1} | \boldsymbol{\nu}_t, \mathbf{p}_t^b, q_t^c)$. Further, in our problem, $x^*(\boldsymbol{\nu}_t)$ is determined by $x^*(P_{t-1})$. Then the variables to be solved at time slot t are reduced to $x(Q_t^c)$ and $x(P_t)$, and the objective function is now given as $\min_{x(Q_t^c), x(P_t)} C_t(S_t, x^*(\boldsymbol{\nu}_t))$. Note that the same constraints as in (3.13) are also applied here. The optimal distributions of $x(Q_t^c)$ and $x(P_t)$ can be solved by performing dynamic programming with exhaustive backups as shown in Fig. 3.3, for an example of a simplified system with two households. The Iteration I is designed to search all possible expected total cost, $C_t(S_t, \nu_t^1, \nu_t^2)$, for different $x(P_t^1)$ and $x(P_t^2)$. After the convergence of dynamic programming, we have $x^*(P_t^1)$ and $x^*(P_t^2)$ that minimize $C_t(S_t, \nu_t^1, \nu_t^2)$, which is the joint optimal distributions of $x(P_t^1)$ and $x(P_t^2)$ for ν_t^1, ν_t^2 , and $x(Q_t^c)$ at given S_t . Then, Iteration II is performed for an exhaustive search on all possible distributions of $x(Q_t^c)$, by changing the variables $P^{c,l}$, $P^{c,h}$, and $P^{c,s}$ discretely, with repeated Iteration I. And Iteration II returns $[x^*(P_t^1), x^*(P_t^2), x^*(Q_t^c)]$, which is the joint optimal distributions of $x(P_t^1)$, $x(P_t^2)$, and $x(Q_t^c)$ for ν_t^1 and ν_t^2 , at given S_t . Finally, Iteration III finds the joint optimal distributions of $x(P_t^1)$, $x(P_t^2)$, and $x(Q_t^c)$ for all possible sets of ν_t^1 and ν_t^2 at given S_t . By applying the exhaustive backups, the optimal solution can be found with a computational complexity of $O(N^3 |x(\boldsymbol{\nu})| |x(\mathbf{P})| |x(Q^c)| \epsilon |\varpi| |p^b|^2)$, where ϵ is the iterations the dynamic programming takes, and it is upper bounded by the value of

$\frac{1}{1-\eta} \log \frac{\eta^2}{1-\eta}$ [183]. As we can see, this algorithm has a high computational complexity for the DSO, especially with high BESS penetration level, i.e., when the value of N is large.

3.4 Energy Management Scheme with Heuristic Solution

In order to reduce the computational complexity, we firstly reduce the size of virtual battery states needed to be searched by exhaustive backups, i.e., the value of $|x(\boldsymbol{\nu})|$, which is based on the convexity of a discounted Dec-POMDP with denumerable states [187]. The linear programming is used to find the approximated piecewise linear convex function of the Dec-POMDP, for all $\nu_t^{n'}$, which is given as

$$C_t(\mathbf{S}_t, \nu_t^n, \nu_t^{n'})|_{(x^*(\mathbf{P}_t), x^*(Q_t^c))} + \varrho \leq \sum_{\hat{\nu}_t^n} x(\hat{\nu}_t^n) C_t(\mathbf{S}_t, \hat{\nu}_t^n, \nu_t^{n'})|_{(x^*(\mathbf{P}_t), x^*(Q_t^c))}, \quad (3.16)$$

where $\sum_{\hat{\nu}_t^n} x(\hat{\nu}_t^n) = 1$ and for all $\nu_t^{n'}$, $x(\hat{\nu}_t^n) > 0$, where $\nu_t^{n'}$ is the initial virtual battery states at time slot t for all BESS except for n . Solving the linear program in (3.16) for each household by finding the maximum value of ϱ , an approximated piecewise linear convex distribution, $x(\hat{\nu}_t^n)$, can be found. This prunes initial battery states at each time slot, and replaces the original distribution by piecewise linear convex function, and for an arbitrary BESS n , $|x(\hat{\nu}_t^n)| \leq |x(\nu_t)|$. Due to the coordination among BESS, the computational complexity of exhaustive backups is in the power of three of the BESS penetration level. So, we further reduce the computational complexity for high BESS penetration by using the heuristic search method. According to our definition, the virtual battery states transition function $P_t(\nu_{t+1} | \nu_t, \mathbf{p}_t^b, q_t^c)$ depends on the information of system voltage levels Q^c , and the coordination of BESS can be achieved by adjusting the distribution function of Q^c . Then, the heuristic search method is conducted by performing Iteration I and the pruning method, described by (3.16), on each SC, i.e., the BESS, independently by keeping the $x(\mathbf{P})$ and $x(\nu^{n'})$ of other SC unchanged. This approach reduces the computational complexity to $O(N|x(\boldsymbol{\nu})||x(\mathbf{P})||x(Q^c)|\epsilon|\varpi||p^b|^2)$, which is linear with respect to the BESS penetration level.

3.5 Case Study

In this work, a PC with Intel CORE i7-4770 3.4 GHz CPU and 8 GB DDR3 RAM is used as a test platform. And the case study is performed based on the IEEE 5-node test feeder (Case I) and IEEE European low voltage test feeder (Case II) [188]. For both cases, the residential loads are considered as distributed load with data obtained from the Australia government open-data center [189]. The solar irradiation data, over four years, are obtained from NREL for Colorado south park mountain [190]. In this work, the sizes of the defined action space and state space are 56 and 630, respectively. For the BESS, we consider two types of batteries, i.e., the Tesla Powerwall [191] and Samsung SDI [192]. The

round-trip efficiency τ of these two batteries are 92% and 95%, respectively. And the unit cost ε of these two batteries are 0.25\$/Ah and 0.23\$/Ah, respectively. The Time-of-Use electricity pricing scheme in [189] is used. For summer time, the on-peak period is 11:00 to 17:00, the mid-peak periods are 7:00-11:00 and 17:00-19:00, while the off-peak period is 19:00-7:00. The electricity rate for on-peak, mid-peak, and off-peak periods are 13.2, 9.5, and 6.5 ¢/kWh, respectively. Based on ANSI C84.1 standard [193], the National Steady State Voltage Regulation requires $\pm 5\%$ voltage variations for electricity distribution service. To analyze the performance of proposed energy management scheme, four existing energy management schemes are considered for comparison:

1. The energy management scheme proposed in [133], which considers only the maximization of customers' utilities. This scheme does not involve the coordination between the DSO and customers;
2. The decentralized energy management scheme proposed in [68], which maximizes the customers' profits with the voltage regulation as a constraint;
3. The hierarchical energy management scheme proposed in [70]. In this scheme, the DSO predetermines the power set points, based on the statistical information of PV power generation and residential load, to minimize the line losses while maintaining the voltage levels within required range. The optimization problem of individual BESS is solved based on the predetermined power set points;
4. The centralized energy management scheme proposed in [75], in which the DSO coordinate the BESS for cost reduction of both DSO and customers. And the stochastic information of individual BESS is processed at the DSO.

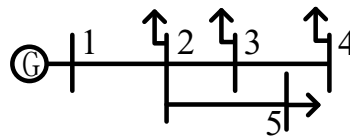
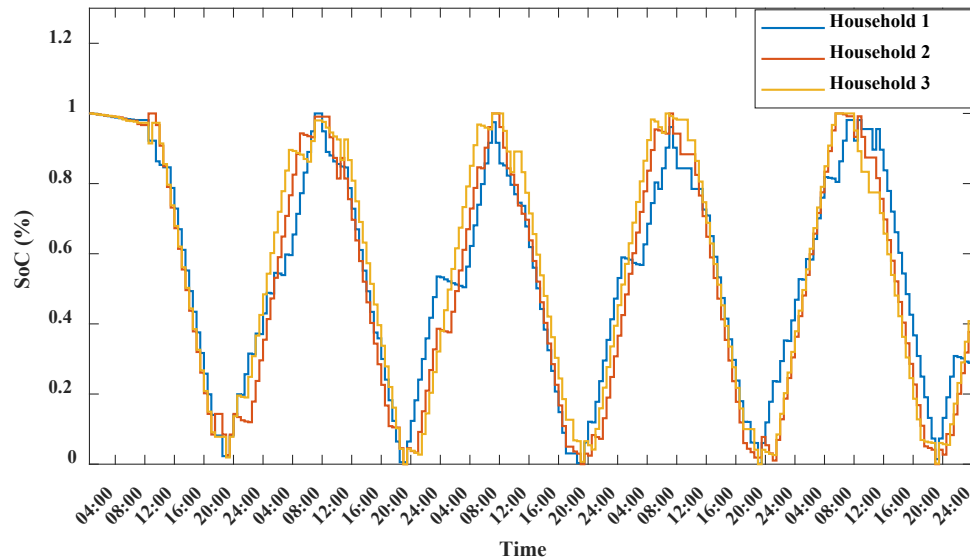


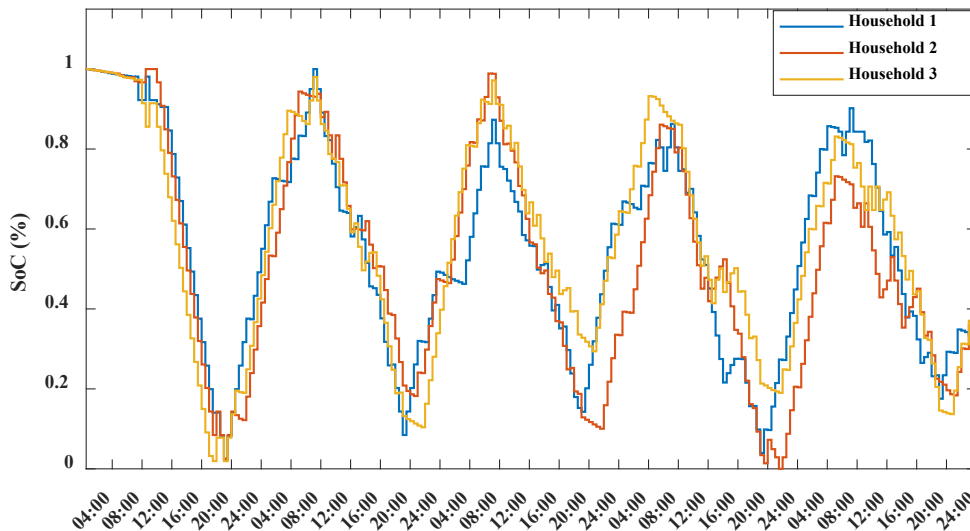
Figure 3.4: IEEE 5-node test feeder (Case I).

Table 3.1
NUMBER AND TYPES OF LOADS CONNECTED

	Bus ID				
	1	2	3	4	5
Loads with PV	-	6	4	3	5
Loads with BESS	-	4	4	1	3
Conventional PQ loads	-	2	1	1	1
Total loads	-	12	9	5	9



(a) Energy management scheme 1)



(b) Proposed scheme with heuristic search and pruning

Figure 3.5: The comparison of SoC profiles for three households at bus 5 (Case I).

The single-line diagram of Case I is shown in Fig. 3.4. The number and types of loads connected to each bus are shown in Table 3.1. The bus 1 connected to the main grid is selected as the slack bus. The Fig. 3.5(a) shows the SoC profiles of three households at bus 5 for 5 days by using scheme 1). It can be observed that, for the maximization of customers' profits, the BESS strategies of these three households are similar. The BESS charges the battery during off-peak periods and discharges the battery during mid-peak and on-peak periods, which maximizes the customers' revenue from selling power. Also, for some off-peak time, the BESS discharges the battery to supply residential load. This

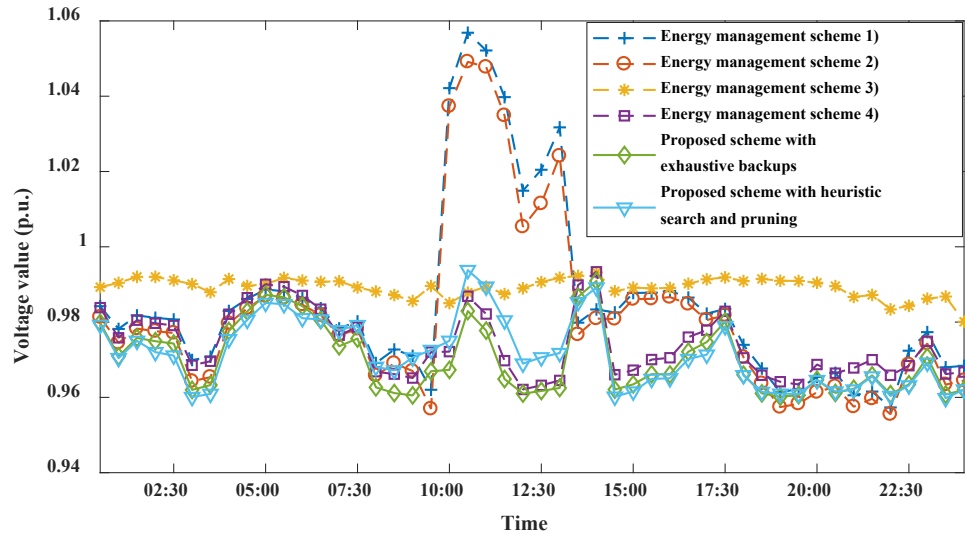


Figure 3.6: Voltage profile of bus 3 (Case I).

Table 3.2
ELECTRICITY COST REDUCTION (CASE I)

	Customers	DSO	Total
Energy management scheme 2)	32.1	-19.01	25.95262
Energy management scheme 3)	29.1	26	29.83178
Energy management scheme 4)	46	25	44.62617
Proposed scheme with exhaustive backups	45.96	22	44.39252
Proposed scheme with heuristic search and pruning	45.28	21.61	43.7315

is due to the fact that the PV surplus during mid-peak periods can be used to charge the battery. The decision of charging the battery using PV power generation during mid-peak periods is to maximize the revenue of selling power by shifting the PV surplus to on-peak period which has the highest selling price. This results in the similar SoC profiles, which leads to the concentrated power injections/drawings to/from the grid. This is the main reason for the significant drops and rises of voltage levels with high BESS penetration. It can be observed from Fig. 3.5(b) that, by using the proposed scheme with heuristic search and pruning, the SoC profiles of these three BESS are differentiated from each other. This can avoid the concentrated power injections and drawings.

As shown in Fig. 3.6, with energy management scheme 1), due to the concentrated power injections to the grid during on-peak periods, the voltage level is greater than the upper bound (1.05 p.u.) of required voltage variations. By using the energy management scheme 2), the voltage levels follow the similar trend of the voltage levels of scheme 1), and it regulates the voltage levels only when they are out of the required range. On the contrary, the energy management scheme 3) regulates the voltage levels with less fluctuations

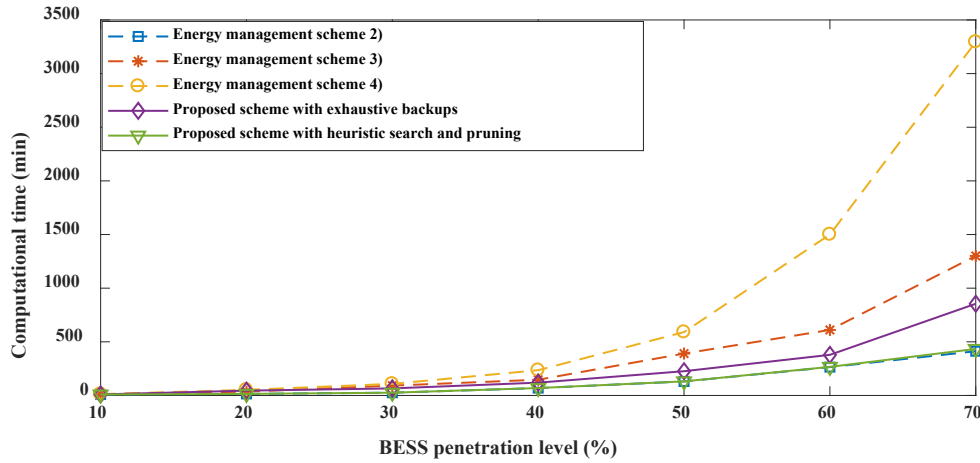


Figure 3.7: The computation time for Case I.

to minimize the line losses. The voltage profile after using our proposed schemes, with exhaustive backups and heuristic search and pruning, are almost the same as the voltage profile of energy management scheme 4). This indicates that the performance of our proposed schemes in terms of voltage regulation is close to the centralized scheme, i.e., scheme 4), which is the optimal one. Also, from Table 3.2, it can be observed that, due to the lack of the consideration of stochastic PV power generation and residential load, schemes 2) and 3) have much lower total cost reduction, compared with scheme 4) and our proposed schemes. Also, the scheme 2) can achieve a higher customer cost reductions compared with scheme 3). However, it results in the significant line losses increment. By comparing the results of our proposed schemes with the results of the scheme 4), our proposed schemes can achieve almost the same results as that of scheme 4). This indicates that our proposed schemes have the similar cost reduction performance as that of the centralized scheme. Also, the performance of our proposed scheme with heuristic search and pruning is close to the one with exhaustive backups. With regard to the computational complexity, we study the above schemes at different BESS penetration levels. The results are shown in Fig. 3.7. It can be observed that, as the penetration level increases, the computational times of scheme 4) and 3) increase dramatically, with that of the scheme 4) being the highest one. And the computational time of the decentralized scheme, i.e., scheme 2), is the lowest one. Compared with scheme 2), our proposed scheme with exhaustive backups requires significantly longer computational time; however, it requires significantly shorter computational time than schemes 4) and 3).

The single-line diagram of Case II is shown in Fig. 3.8. For Case II, we consider 20 buses, out of the total 55 buses, having customers with BESS installed. And each of these 20 buses has 5-15 customers connected to, with 4-8 customers being equipped with BESS. Since the solar irradiation data are measured at discrete stations, we assign the solar irradiation based on areas, according to the locations of measurement stations, as illustrated

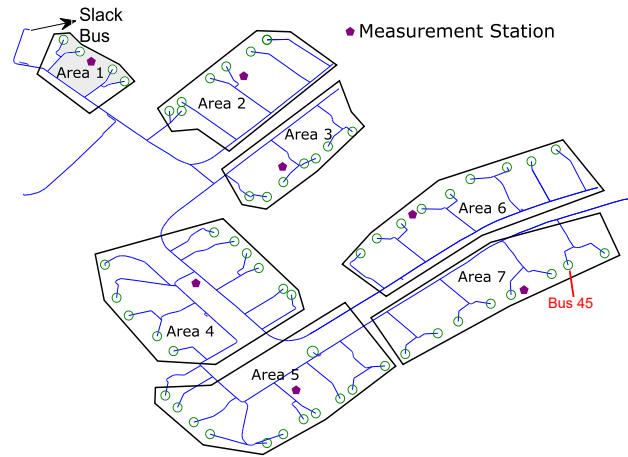


Figure 3.8: IEEE European low voltage test feeder (Case II).

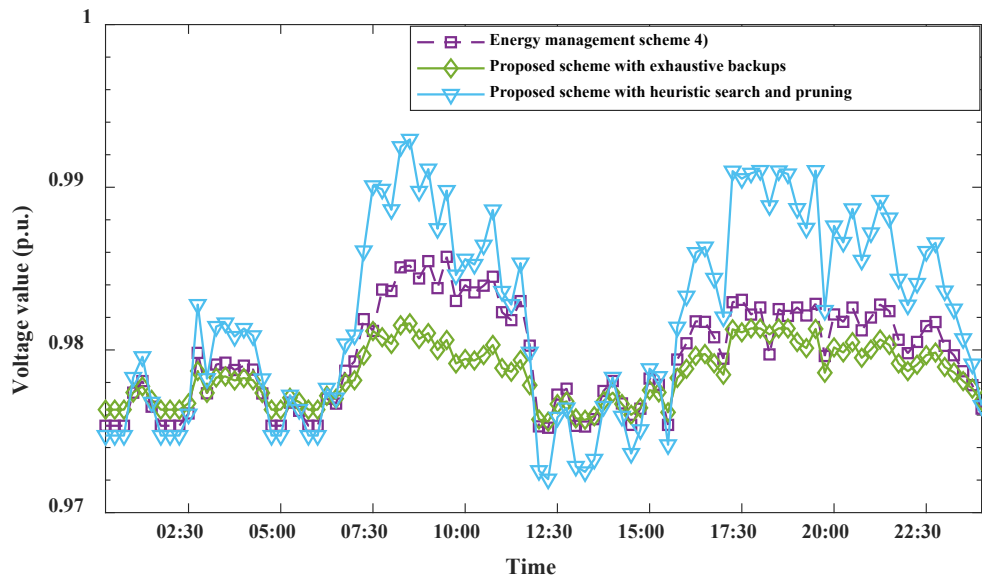


Figure 3.9: Voltage profile of bus 45 (Case II).

in Fig. 3.8. From Fig. 3.9 and Table 3.3, it can be observed that our proposed schemes with exhaustive backups and heuristic search and pruning, for a larger case, have similar performance as the optimal centralized scheme 1). However, the computational time of the centralized energy management scheme for a 30% penetration of BESS is around 1740 minutes, while that of our proposed scheme with exhaustive backups is 910 minutes, which is almost the half of the computational time required by centralized scheme. By using the proposed scheme with heuristic search and pruning, the computational time is further reduced to 407 minutes. It can be concluded that our proposed schemes can achieve similar performances as that of the optimal centralized scheme, with significantly reduced computational complexity.

Table 3.3
ELECTRICITY COST REDUCTION (CASE II)

	Customers	DSO	Total
Energy management scheme 4)	32.5	18.1	31.55794
Proposed scheme with exhaustive backups	31.9	16.7	30.90561
Proposed scheme with heuristic search and pruning	31.2	16.1	30.21215

3.6 Summary

In this chapter, the stochastic energy management of BESSs at high penetration level in SDSs is investigated to mitigate the impacts of BESSs operations on SDSs. Comparing with the existing approaches in literature, the hierarchical and decentralized stochastic energy management approach proposed in this chapter is able to distribute most the computations to local end-user EMSs, which can significantly reduce the computation burdens at the DSO. Also, by leveraging the hierarchical structure, the decisions of end-user EMSs can be well regulated by using system signals given by DSO. The integration of hierarchical control structure and decentralized optimization is a promising solution to address the stochastic energy management problems in large-scale energy systems.

4

Stochastic Energy Management of Electric Bus Charging Stations with B2G Capabilities

In this chapter, the stochastic energy management of EBCSs with B2G capabilities is investigated, where the impacts of PDF estimation errors of random variables are considered and addressed by using distributionally robust optimization approaches. Due to the high energy efficiency and zero-emission, EBs have attracted considerable attention for the sustainable development of public transit systems [194]. As of 2017, there are more than 385,000 EBs in China, which is 17% of China's public transit buses [195]. By 2025, Paris and Amsterdam expect to achieve fully electrified public transit systems [196]. To further promote EBs' adoption, the integration of RES with BESSs at EBCSs has been widely studied for cost-effective and sustainable charging of EBs [81–83]. The publicly owned EBCSs of EBs with B2G capabilities can function as mobile BESSs, which can help the EBCSs reduce their operating costs through arbitrage services and provide a variety of ancillary services DSO with extended flexibility and stability [199]. However, the randomnesses of RES generation and mobility of EBs, e.g., random charging duration and energy consumption, will result in inefficient RES usage and unstable B2G capabilities. Also, the charging power of EBs is usually several times higher than that of residential EVs, the uncoordinated EB charging can have severe negative impacts, e.g., load fluctuations, generation costs increments, congestion, and voltage issues, on electric grids, especially in power distribution systems. Thus, there is an urgent need to investigate the stochastic energy management of EBCSs with B2G capabilities. However, in literature, there are no such works for EBCSs.

For EVs, the energy management of EVCSs are considered in market environments by using price signals to relieve the congestion and regulate voltage levels [197, 198]. However, as discussed in [199], for the charging scheduling management and charging station resource allocation, one of the issues is the multi-stage solutions, since the EV charg-

ing requirements cannot be fulfilled in only one-time slot considering the distribution system constraints. For the charging scheduling management involving multiple stages, the stochastic and dynamic futures will significantly affect the current decisions. The stochastic multi-stage quadratic programming [199] and chance-constrained multi-stage optimization [200] are proposed to address the stochastic and dynamic futures with known distributions of EV arriving and departures. However, the scenario tree of stochastic multi-stage optimization often suffers from the curse of dimensionality, due to the consideration of entire history [41]. Also, the linear interpolation is usually required for future expectation value approximation and the solutions of multi-stage stochastic programmings are usually intractable [201]. Recently, for the stochastic EV charging problems considering multiple stages, the SDP has attracted great interests.

SDP requires accurate PDF estimation of random variables. Unlike residential EVs with relatively constant loads, the varying bus loads can significantly affect the accuracy of EBs stochastic models, especially for the power consumption estimation during regular operation. As concluded in [89], the power consumption of standard EB in on-peak periods can be 2.3 times higher than that in off-peak periods. Due to multiple external factors, such as weather, characteristics of time dimension, activities of individual passenger, and regional demographics, the PDF of random bus loads cannot be precisely estimated [91]. The SDP is not risking aware of the large errors of PDF estimation of random bus loads.

RSDP for EV charging is investigated in [87], which shows that by considering high degree of uncertainties introduced by wind generation, the SDP will cause a significant reduction of the charging performance for EVs. However, the RSDP in [87] usually results in overly conservative solutions, due to the considering of single-point distribution of extreme condition. Also, the solution in [87] is not tractable, and obtaining a global optimal solution is not guaranteed. Also, how to determine the price signals by considering stochastic dynamic programming problem under large errors of PDF estimation still requires intensive researches. To address the above issues, in this thesis, a stochastic energy management approach for EBCSs with B2G capabilities is proposed based on the distributionally robust optimization methods.

4.1 System Model

The system architecture considered in this research is shown in Fig. 4.1. The EBCSs are located at the depot and transit center. The photovoltaic (PV) and battery energy storage systems (BESS) are considered for RES and ESS, respectively. Both EBs parking at EBCSs and running on roads are considered. With B2G capabilities, the EBCSs connect to power distribution system through bidirectional power flows and behave as energy prosumers. With two-way communication links, EBs report their real-time information, e.g., locations, velocities, and bus loads, to EBCSs for energy management. The EBCSs transmit information of PV, BESS, and EBs to DSO for charging impact mitigation. For the tractability of

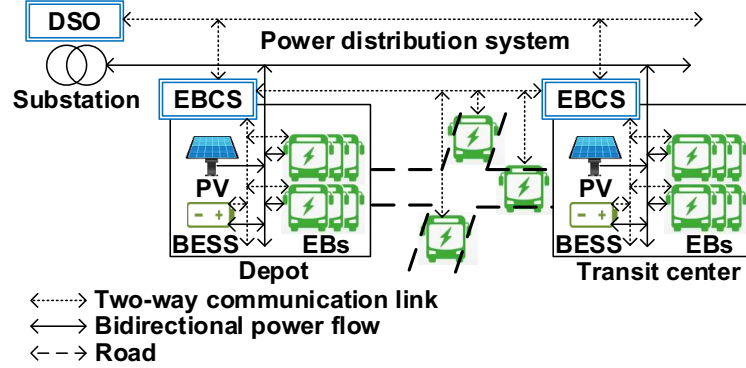


Figure 4.1: System architecture for stochastic energy management of EBCSs in power distribution system.

analysis, one day is divided into multiple time slots with equal length of Δt . $(a_n)_{n \in \mathcal{N}}$ is a vector of $\mathbb{R}^{|\mathcal{N}| \times 1}$ and $\langle N \rangle$ is a running index set. Next, the system models will be presented in detail.

4.1.1 Battery Models for EBs and BESS

For both EBs and BESS, the LiFePO4 battery model in [154] is used, where charging and discharging are equivalent processes with positive/negative values, respectively. The state of charge (SoC) change θ with battery power P_t^{bat} is determined as

$$\theta_{t+1} - \theta_t = (P_t^b)^\tau Y^{\tau-1} / (c_b \bar{C}^\tau \Delta t^{\tau-1}), \quad (4.1)$$

where c_b is Peukert's constant, \bar{C} is nominal capacity, τ is round trip efficiency, and Y is C-rate. Then, the battery degradation cost is calculated as

$$C_t^{bat}(\theta_t, P_t^{bat}) = \bar{C}^b e^{(\kappa|\bar{\theta}_t - 0.5|)} / (b_1 |\theta_{t+1} - \theta_t|^{b_2} + b_3), \quad (4.2)$$

where average SoC $\bar{\theta}_t = (\theta_{t+1} + \theta_t)/2$. κ is estimated based on experimental lifetime data with $\bar{\theta}_t = 50\%$, while b_1 - b_3 are estimated from data with $\bar{\theta}_t$ varying from 50%.

4.1.2 Stochastic Modeling for Individual EB

Considering traffic conditions and shifted drivers, the segmented Markov velocity acceleration emission probabilities of EBs in [203] are considered. For EB i with driver d along route l on road segment m , the emission probability from velocity ν to acceleration a' in time slot k is denoted as $p_{m,k}^{i,d,l}(a'|\nu)$, which is estimated using maximum likelihood. With route information, the velocity, location, and energy consumption in next time slot are estimated based on acceleration, respectively, as [204]

$$\nu_t^i = \nu_{t-1}^i + a_{t-1}^i \Delta t \quad (4.3)$$

$$z_t^i = z_{t-1}^i + \nu_{t-1}^i \Delta t + a_{t-1}^i \Delta t^2 / 2 \quad (4.4)$$

$$P_t^{b,i} = [c_m a_t^i (\tilde{m} + \bar{m} \nu_z) (a_t^i \Delta t^2 + \nu_t^i) + c_d (a_t^i c_r + \nu_t^i)^4 / (21.15 \times 2 a_t^i)] \Delta t c_{tr} c_{con} / 2, \quad (4.5)$$

where c_m is mass factor of rotating components, c_d is aerodynamic constant, c_r is rolling resistance coefficient, and c_{tr} and c_{con} are efficiencies of power transmission and battery power conversion, respectively. EB mass \tilde{m} and passenger weight \bar{m} are constant, while location-dependent bus loads ν_z is random. In this research, for given combination $(z^i)_{i \in \mathcal{I}}$ of locations of all EBs, the route-level bus loads $\nu_z = (\nu_{z^i}^i)_{i \in \mathcal{I}}$, i.e., combination of bus loads of all EBs, is defined. Battery power P^{bat} of EB i depends on $P^{b,i}$ and charging power $P^{b,i,x}$ at EBCS x .

In this work, the individual EB is modeled stochastically by considering the impacts of traffic conditions on EB energy consumption using location-dependent aerodynamic constant and rolling resistance coefficient based on the fixed route information of EBs. In the real world, the traffic conditions, e.g., the congestion delay, also impact the velocity acceleration emission probabilities of EBs. In [205], the authors have investigated the impacts of congestion delay on the modeling of trucks serving as mobile energy storage systems (MESSs), in which a transition scenario-based transit delay model is proposed for the transit delay caused by congestion delay. However, in [205], it is assumed that the congestion delay can be estimated, and a suboptimal solution is obtained through solving a deterministic problem for the instant transition of a MESS. Extensive research is still needed to model the transit delay stochastically by considering the uncertainties of traffic conditions in the real world, which will be studied in future work.

4.1.3 Stochastic Modeling for EBCS with BESS and PV

PV generation P^{pv} is calculated based on efficiency η^{pv} , area A^{pv} , and solar radiation L_t as $P_t^{pv} = \eta^{pv} A^{pv} L_t$ [256]. The random PV generation is modeled using segmented Markov chain transition probability $p_w^{pv}(P^{pv'} | P^{pv})$, which is calculated using maximum likelihood of solar radiation as in [207]. For B2G-enabled EBCS, P^{bat} is the charging/discharging power $P^{b,x}$ of BESS at EBCS x . The charging cost for EBCS consists of battery degradation and electricity costs, which can be expressed as

$$C_t^{cs} = \sum_i \sum_x [C_t^{bat}(\theta_t^i, \sigma_t^{i,x} P_t^{b,i,x}, P_t^{b,i}) + C_t^{bat}(\theta_t^x, P_t^{b,x}) + (\sigma_t^{i,x} P_t^{b,i,x} + P_t^{b,x} + P_t^{pv,x}) (h_t^{p,h} + h_t^{p,x})], \quad (4.6)$$

where the charging availability $\sigma_t^{i,x} \in [0, 1]$ of EB i at EBCS x depends on the location and driving velocity [208]. $h_t^{p,h}$ is the spot price for reference node and $h_t^{p,x}$ is the dynamic price for EBCS x connecting node which is used to regulate the demand of EBCS x to mitigate the charging impacts on power distribution systems [200].

4.1.4 Linearized AC Power Flow Model

The substation is selected as reference node h . To have a tractable solution, the AC power flow is linearized as [198]

$$V_{i'} = V_h - \sum_i (D_{vp}^{i'} P_i - D_{vq}^{i'} Q_i), \quad (4.7)$$

$$F_\ell^p = \sum_i D_{lp}^{\ell i} P_i, \quad F_\ell^q = \sum_i D_{lq}^{\ell i} Q_i, \quad (4.8)$$

where P_i/Q_i and F_ℓ^p/F_ℓ^q are the active/reactive power injections at node i and powers in line ℓ , respectively. Sensitivity ($D_{vp}^{i'}/D_{vq}^{i'}$) and transfer ($D_{lp}^{\ell i}/D_{lq}^{\ell i}$) factors represent the impacts of power injection at node i to voltage magnitude $V_{i'}$ at node i' and powers in line ℓ , respectively.

4.2 Problem Formulations

Under the market environment in [200], the objective of EBCSs energy management is to minimize charging cost based on dynamic prices, which is determined by DSO to alleviate congestion and support voltage levels with EBCSs as flexible energy prosumers. In this section, the problem formulations of stochastic EBCSs energy management and security-constrained optimal power flow (SCOPF) of DSO for dynamic price determination will be presented.

4.2.1 Stochastic EBCSs Energy Management

In this research, a DRMDP with tuple $\langle \mathcal{S}, \mathcal{U}, \mathbf{p}, \tilde{\mathbf{r}}, \mathbf{\Pi} \rangle$ is defined for stochastic energy management of EBCSs, where discrete state space \mathcal{S} includes SoC, velocities, EB locations, PV generation, and remaining time slots ϕ , i.e., $s = (\theta^i, \nu^i, z^i, \theta^x, P^{pv,x}, \phi)_{i \in \mathcal{I}, x \in \mathcal{X}}$, where \mathcal{I} and \mathcal{X} are the number of EBs and EBCSs, respectively. \mathcal{U} is action space for battery powers of EBs and BESS, i.e., $u = (P^{b,i,x}, P^{b,x})_{i \in \mathcal{I}, x \in \mathcal{X}}$. \mathcal{U}_s is the state-wise action set for s . \mathbf{p} is state transition probability vector with $\mathbf{p} = (\mathbf{p}_s)_{s \in \mathcal{S}}$ and $\mathbf{p}_s = (p_{s',s,u})_{u \in \mathcal{U}_s, s' \in \mathcal{S}}$. $\tilde{\mathbf{r}}$ denotes immediate cost vector with $\tilde{\mathbf{r}} = (\tilde{\mathbf{r}}_s)_{s \in \mathcal{S}}$, where $\tilde{\mathbf{r}}_s = (\tilde{r}_{s,u})_{u \in \mathcal{U}_s}$ and $\tilde{r}_{s,u}$ is calculated through (4.6). $\mathbf{\Pi}$ is policy set, $\pi_{s,u}$ is the probability of selecting u for s and $\boldsymbol{\pi}_s = (\pi_{s,u})_{u \in \mathcal{U}_s}$. In this research, the deterministic policy is considered. Also, due to the state-dependency feature of policies, the state-wise dynamic price $h_{s_t}^{p,x}$ is used.

For any given route-level bus loads ν_z , parameter $\tilde{\mathbf{r}}_s$ can be determined by calculating $\tilde{r}_{s,u}$ through (4.6). Also, parameter \mathbf{p}_s can be determined explicitly by calculating $p_{s',s,u}$ as

$$p_{s',s,u} = \begin{cases} \prod_i p_{m,k}^{i,d,l}(a^{i'}|\nu^i) \prod_x p_w^{pv,x}(P^{pv,x'}|P^{pv,x}), & \text{if (4.1), (4.3), (4.4), and} \\ & \text{(4.5) hold } \forall i, \text{ and (4.1) holds } \forall x \\ 0, & \text{otherwise.} \end{cases} \quad (4.9)$$

However, since $\boldsymbol{\nu}_z$ is random, the parameters $\tilde{\boldsymbol{r}}_s$ and \boldsymbol{p}_s are uncertain in our problem. To address this issue, the uncertain parameters $(\boldsymbol{p}_s, \tilde{\boldsymbol{r}}_s) \in \mathbb{R}^{|\mathcal{S}||\boldsymbol{U}_s|+|\boldsymbol{U}_s|}$ is considered and whose empirical data are obtained based on (4.6) and (4.9) using the empirical data of $\boldsymbol{\nu}_z$. The joint PDF of $(\boldsymbol{p}_s, \tilde{\boldsymbol{r}}_s)$ is described by state-wise ambiguity set \mathcal{M}_s . Since, for any s , there is always a $\boldsymbol{\nu}_z$ giving the worst-case distribution of $(\boldsymbol{p}_s, \tilde{\boldsymbol{r}}_s)$ from \mathcal{M}_s , regardless of the worst-case distributions for other states, which satisfies the s-rectangularity [267]. Then, the ambiguity set \mathcal{M}_S for \mathcal{S} is defined using Cartesian product [43]. Under *minimax-regret* criterion in [100], the stochastic EBCSs energy management problem with ambiguity set \mathcal{M}_S is expressed as

$$\begin{aligned} & \min_{\boldsymbol{\pi}} \max_{\mathbb{P} \in \mathcal{M}_S} \mathbb{E}_{\mathbb{P}} \left(\mathbb{E}_{\mathcal{H}_{\boldsymbol{p}_{s_1}^{\boldsymbol{\pi}}}} \sum_t \tilde{r}_{s_t, u_t} - \mathbb{E}_{\mathcal{H}_{\boldsymbol{p}_{s_1}^{\hat{\boldsymbol{\pi}}^*}}} \sum_t \tilde{r}_{s_t, u_t} \right) \iff \\ & \min_{\boldsymbol{\pi}} \max_{\mathbb{P} \in \mathcal{M}_S} \mathbb{E}_{\mathbb{P}} [v(\boldsymbol{p}, \tilde{\boldsymbol{r}}, \boldsymbol{\pi}, s_1) - v(\boldsymbol{p}, \tilde{\boldsymbol{r}}, \hat{\boldsymbol{\pi}}^*, s_1)] \end{aligned} \quad (4.10)$$

subject to

$$\mathbf{1}^\top \boldsymbol{\pi}_s = 1, \quad \forall s \in \mathcal{S} \quad (4.11)$$

$$\pi_{s,u} \in [0, 1], \quad \forall u \in \boldsymbol{U}_s \quad \forall s \in \mathcal{S}, \quad (4.12)$$

where $s_1 \in \mathcal{S}$ is the initial state. $\boldsymbol{\pi} = (\boldsymbol{\pi}_s)_{s \in \mathcal{S}}$ is an arbitrary policy, while $\hat{\boldsymbol{\pi}}^* = (\hat{\boldsymbol{\pi}}_s^*)_{s \in \mathcal{S}}$ is the optimal policy under realization of $(\boldsymbol{p}, \tilde{\boldsymbol{r}})$. $\hat{\boldsymbol{\pi}}^*$ may not be equal to the optimal policy $\boldsymbol{\pi}^*$ of (4.10). $\mathcal{H}_{\boldsymbol{p}_{s_1}^{\boldsymbol{\pi}}}$ and $\mathcal{H}_{\boldsymbol{p}_{s_1}^{\hat{\boldsymbol{\pi}}^*}}$ are probability measures on stochastic processes $\{(s_t, u_t)\} \forall t \geq 1$ for policies $\boldsymbol{\pi}$ and $\hat{\boldsymbol{\pi}}^*$, respectively. The optimal value $v(\boldsymbol{p}, \tilde{\boldsymbol{r}}, \hat{\boldsymbol{\pi}}^*, s_1)$ is obtained under realization of $(\boldsymbol{p}, \tilde{\boldsymbol{r}})$. While the value $v(\boldsymbol{p}, \tilde{\boldsymbol{r}}, \boldsymbol{\pi}, s_1)$ is obtained by taking $\boldsymbol{\pi}$ under \mathcal{M}_S [100]. The difference of them, i.e., the regret, measures the disappointment for not taking $\hat{\boldsymbol{\pi}}^*$ due to the ambiguity set. Different $\hat{\boldsymbol{\pi}}^*$ can be taken for different realizations of $(\boldsymbol{p}, \tilde{\boldsymbol{r}})$, while single $\boldsymbol{\pi}$ has to be taken.

4.2.2 An Event-Based Ambiguity Set with Combined Statistical Distance and Moment Information

In this research, the ambiguity set \mathcal{M}_s is constructed to include combined statistical distance, more specifically the Wasserstein distance, and moment information to leverage the approximated reference PDF and statistical information obtained from empirical data for robust solutions that are less conservative. Also, considering the uncertainties of approximated reference PDF and moment information obtained from empirical data of $(\boldsymbol{p}_s, \tilde{\boldsymbol{r}}_s)$. An event-based ambiguity set \mathcal{M}_s^E is developed based on the structure of lifted ambiguity set [201], which is expressed as

$$\mathcal{M}_s^E = \left\{ \begin{array}{l} \mathbb{P} \in \left\{ \begin{array}{l} \mathcal{P}_0(\mathbb{R}^{|\mathcal{S}|}) \\ \times \mathbb{R}^{|\boldsymbol{U}_s|} \\ \times \langle N_s \rangle \end{array} \right\} \left| \begin{array}{l} ((\boldsymbol{p}_s, \tilde{\boldsymbol{r}}_s), \tilde{n}_s) \sim \mathbb{P} \\ \mathbb{P}[(\boldsymbol{p}_s, \tilde{\boldsymbol{r}}_s) \in \mathcal{D}_{n_s} | \tilde{n}_s] = 1, \\ \mathbb{E}_{\mathbb{P}}[(\boldsymbol{p}_s, \tilde{\boldsymbol{r}}_s) | \tilde{n}_s] = \boldsymbol{\mu}_{n_s}, \\ \mathbb{E}_{\mathbb{P}}[\|\mathbf{1}^\top((\boldsymbol{p}_s, \tilde{\boldsymbol{r}}_s) - \boldsymbol{\mu}_{n_s})\| | \tilde{n}_s] \leq \varphi_{n_s}, \\ \mathbb{E}_{\mathbb{P}}[\|(\boldsymbol{p}_s, \tilde{\boldsymbol{r}}_s) - (\boldsymbol{p}_s, \tilde{\boldsymbol{r}}_s)_{\tilde{n}_s}^\dagger\|_2 | \tilde{n}_s] \leq \varrho_{n_s}, \\ \mathbb{P}[\tilde{n}_s] = \varpi_{n_s}, \quad \forall \tilde{n}_s \in \langle N_s \rangle \end{array} \right. \end{array} \right\}, \quad (4.13)$$

where $\mathcal{P}_0(\cdot)$ is Borel distribution. Each $\mathbb{P} \in \mathcal{M}_s^E$ can be expressed as $\mathbb{P} = \sum_{n_s} \varpi_{n_s} \mathbb{P}_{n_s}$, where \mathbb{P}_{n_s} is any PDF that satisfies statistical information defined in (4.13). $\tilde{n}_s \in N_s$ is index of event, i.e., components in mixture of PDFs. On the realization of \tilde{n}_s , the second, third, and fourth constraints are for finite support \mathcal{D}_{n_s} , mean μ_{n_s} , and absolute deviation from mean φ_{n_s} . The absolute deviation, instead of variance, is used to incorporate the data-driven feature of Wasserstein metric [43]. The fifth constraint is Wasserstein metric in the form of lifted ambiguity set using Euclidean norm [201] with reference PDF $(\mathbf{p}_s, \tilde{\mathbf{r}}_s)_{\tilde{n}_s}^\dagger$ and radius $\varrho_{n_s} \in \mathbb{R}_+$. ϖ_{n_s} the probability of realization of event n_s . As following typical DR optimization, the parameters of \mathcal{M}_s^E is restricted to satisfy the conditions in [267] for Slater's condition.

4.2.3 SCOPF with EBCSs as Flexible Energy Prosumers

DSO determines day-ahead dynamic prices through minimizing system generation cost, consisting of responsive cost of flexible generation/demand and electricity cost, using SCOPF [210]. Since B2G-enabled EBCSs behave as energy prosumers to provide flexible generation/demand, the responsive cost is the charging cost of EBCSs. The electricity cost is calculated as $h_t^{p,h}(\sum_i P_{i,t}^d + \sum_x P_{s_t,u_t}^x) + h_t^{q,h} \sum_i Q_{i,t}^d$ [199], where $P_{s_t,u_t}^x = \sum_i \sigma_t^{i,x} P_t^{b,i,x} + P_t^{b,x} + P_t^{pv,x}$ is flexible power injection at node EBCS x connecting to. $\mathbf{P}_s^x = (P_{s,u}^x)_{u \in U_s}$ is state-wise flexible power injections. $P_{i,t}^d/Q_{i,t}^d$ are expected conventional demands [197]. Then, the system generation cost is calculated as $\hat{r}_{s_t,u_t} + \sum_i (h_t^{p,h} P_{i,t}^d + h_t^{q,h} Q_{i,t}^d)$, where \hat{r} is similar to \tilde{r} in (4.10) without dynamic price $h_s^{p,x}$. Since $h_t^{p,h} P_{i,t}^d + h_t^{q,h} Q_{i,t}^d$ is constant, it is only considered in constraints. Then, with (4.7) and (4.8), the DRMDP problem for SCOPF considering line congestion and voltage levels is expressed as

$$\min_{\boldsymbol{\pi}} \max_{\mathbb{P} \in \mathcal{M}_s^E} \mathbb{E}_{\mathbb{P}} [v(\mathbf{p}, \hat{\mathbf{r}}, \boldsymbol{\pi}, s_1) - v(\mathbf{p}, \hat{\mathbf{r}}, \hat{\boldsymbol{\pi}}^*, s_1)] \quad (4.14)$$

subject to

$$\underline{V} - S_t^a \leq - \sum_x D_{vp}^{ix} \mathbf{P}_{s_t}^{x\top} \boldsymbol{\pi}_{s_t} \leq \bar{V} - S_t^a, \forall i \forall s_t \forall t \quad (4.15)$$

$$\sum_x \alpha_c^0 D_{lp}^{\ell x} \mathbf{P}_{s_t}^{x\top} \boldsymbol{\pi}_{s_t} \leq -(S_t^\ell + \alpha_c^2 \bar{S}_\ell^f), \forall \ell \forall s_t \forall t \quad (4.16)$$

$$\sum_x \beta_c^0 \mathbf{P}_{s_t}^{x\top} \boldsymbol{\pi}_{s_t} \leq -(S_t^h + \beta_c^2 \bar{S}_c^h), \forall s_t \forall t \quad (4.17)$$

constraints (4.11) and (4.12),

where $S_t^a = V_h - \sum_{i'} (D_{vp}^{i'} P_{i',t}^d - D_{vq}^{i'} Q_{i',t}^d)$, $S_t^\ell = \sum_i (\alpha_c^0 D_{lp}^{\ell i} P_{i,t}^d + \alpha_c^1 D_{lq}^{\ell i} Q_{i,t}^d)$, and $S_t^h = \sum_i (\beta_c^0 P_{i,t}^d + \beta_c^1 Q_{i,t}^d)$. α_c^{0-2} and β_c^{0-2} , for all $c \in \{1, \dots, 12\}$, are linear coefficients of polygonal approximation [211] for quadratic constraints. Since $\boldsymbol{\pi}_{s_t}$ is deterministic policy, different from violation risk constraints in [257], the solutions of (4.14) satisfy constraints (4.15)-(4.16), certainly. With (4.17) that limits the power exchange with transmission system, $h_t^{p,h}/h_t^{q,h}$ can be treated as *a priori* [199]. It is worth noting that (4.14) is not constrained

MDP, since constraints (4.15)-(4.17) do not involve conflicting objectives [213]. The constraints (4.15)-(4.17) restrain the set of feasible actions for all states and time slots. The existence and optimality of the Markov policies for DRMDP has been proved in [43]. However, solving the DRMDP with *minimax-regret* criterion is typically NP hard.

4.3 Solutions based on Heuristic Regret Function

For (4.10) and (4.14), the sequential sub-problems do not exist, which make them NP-hard [101]. To facilitate the practical applications and reduce the computational complexity, in this section, a heuristic regret function is proposed to formulate (4.10) and (4.14) into sequential subproblems with tractable solutions. Then, the dynamic prices $h_s^{p,x}$ determined by DSO will be derived.

4.3.1 Tractable Solutions based on Heuristic Regret Function

The regret $\mathcal{R}(\pi)$, with regret function $v(\mathbf{p}, \tilde{\mathbf{r}}, \pi, s_1) - v(\mathbf{p}, \tilde{\mathbf{r}}, \hat{\pi}^*, s_1)$, cannot be evaluated dynamically [101]. Inspired by simple regret [214], a state-wise heuristic regret function $\tilde{r}_{s_t, u_{s_t}} - \tilde{r}_{s_t}^*$ with s-rectangularity is defined. Under a $(\mathbf{p}_{s_t}, \tilde{\mathbf{r}}_{s_t})$, $\tilde{r}_{s_t}^*$ depends only on state s_t and is calculated as

$$\tilde{r}_{s_t}^* = \min_{\pi'_{s_t}} \tilde{\mathbf{r}}_{s_t} \pi'_{s_t} \quad (4.18)$$

subject to

constraints (4.11) and (4.12),

and $\tilde{r}_{s_T}^* = 0$. With regret function $\tilde{r}_{s_t, u_{s_t}} - \tilde{r}_{s_t}^*$, the regret is calculated as $\mathcal{R}(\pi) = v(\mathbf{p}, \tilde{\mathbf{r}}, \pi, s_1) - v_1^*(\pi_{s_1}, s_1)$, where for all $s_t \in \mathcal{S}$, $v_T^*(\pi_{s_T}, s_T) = 0$, and for all $t < T$,

$$v_t^*(\pi_{s_t}, s_t) = \sum_u \pi_{s_t, u} [\tilde{r}_{s_t}^* + \sum_{s_{t+1}} p_{s_{t+1}, s_t, u} v_{t+1}^*], \quad (4.19)$$

where $p_{s_{t+1}, s_t, u}$ depends on policy π being evaluated. The difference between these two regrets can be $\Delta\mathcal{R}(\pi) = v_1^*(\pi_{s_1}, s_1) - v(\mathbf{p}, \tilde{\mathbf{r}}, \hat{\pi}^*, s_1)$, where $v_1^*(\pi_{s_1}, s_1)$ is an MDP with state-dependent immediate cost. Then, $\Delta\mathcal{R}(\pi)$ can be seen as the distance between $v_1^*(\pi_{s_1}, s_1)$ with policy π and $v(\mathbf{p}, \tilde{\mathbf{r}}, \hat{\pi}^*, s_1)$ with policy $\hat{\pi}^*$, i.e., it evaluates how similar these two MDPs are for *minimax-regret* criterion. By considering the Hausdorff metric [215], $\Delta\mathcal{R}(\pi)$ can be evaluated as

$$\Delta\mathcal{R}(\pi) = \max_t \max \{ \max_{s_t} \min_{s_t'} (|\tilde{r}_{s_t}^* - \tilde{r}_{s_t', u_t^*}^*| + T_K(\pi, \hat{\pi}^*)), \max_{s_t'} \min_{s_t} (|\tilde{r}_{s_t}^* - \tilde{r}_{s_t', u_t^*}^*| + T_K(\pi, \hat{\pi}^*)) \}, \quad (4.20)$$

where $T_K(\pi, \hat{\pi}^*)$ is Kantorovich distance between transition probabilities under π and $\hat{\pi}^*$ [215]. The worst $\Delta\mathcal{R}(\pi)$ is at t , when $v_1^*(\pi_{s_1}, s_1)$ visits the state with lowest immediate cost and $v(\mathbf{p}, \tilde{\mathbf{r}}, \hat{\pi}^*, s_1)$ visits the state with highest immediate cost with transition and

corresponding action probabilities both equal one. Since the immediate cost is lower and upper bounded, the worst $\Delta\mathcal{R}(\boldsymbol{\pi})$ is bounded. Then, $\tilde{r}_{s_t, u_{s_t}} - \tilde{r}_{s_t}^*$ can estimate actual regret with error bounded by (4.20).

By using the defined state-wise heuristic regret function, the Bellman equation of (4.10) can be expressed as

$$\tilde{v}_t(s_t) = \min_{\boldsymbol{\pi}_{s_t}} \max_{\mathbb{P} \in \mathcal{M}_{s_t}^E} \mathbb{E}_{\mathbb{P}}[\tilde{r}_{s_t} - \tilde{r}_{s_t}^* + \tilde{\mathbf{v}}_{s_{t+1}} \mathbf{p}_{s_t}]^{\top} \boldsymbol{\pi}_{s_t}, \quad (4.21)$$

where $\tilde{v}_T(s_T)$ is zero for all s_T . $\tilde{\mathbf{v}}_{s_{t+1}} \in \mathbb{R}^{|\mathcal{S}| \times |\mathcal{S}|^{U_{s_{t+1}}}}$ is a diagonal matrix with $(\tilde{v}_{t+1}(s_{t+1}))_{s_{t+1} \in \mathcal{S}}^{\top}$ on main diagonal. With auxiliary variable Z , (4.21) can be reformed as

$$\min -Z \quad (4.22)$$

subject to

$$\min_{\mathbb{P} \in \mathcal{M}_{s_t}^E} \mathbb{E}_{\mathbb{P}}[-\tilde{r}_{s_t} + \tilde{r}_{s_t}^* - \tilde{\mathbf{v}}_{s_{t+1}} \mathbf{p}_{s_t}]^{\top} \boldsymbol{\pi}_{s_t} \geq Z \quad (4.23)$$

constraints (4.11) and (4.12).

For ambiguity set (4.13), the joint distribution of $(\mathbf{p}_s, \tilde{\mathbf{r}}_s)$ and \tilde{n}_s is the marginal distribution of \tilde{n}_s , i.e., $\mathbb{P}[\tilde{n}_s] = \varpi_{n_s}$, and conditional distribution \mathbb{P}_{n_s} of $(\mathbf{p}_s, \tilde{\mathbf{r}}_s)$. Then, the minimization term in constraint (4.23) can be expressed as

$$\min \sum_{n \in \langle N_s \rangle} \varpi_n \mathbb{E}_{\mathbb{P}_n}[-\tilde{r}_{s_t} + \tilde{r}_{s_t}^* - \tilde{\mathbf{v}}_{s_{t+1}} \mathbf{p}_{s_t}]^{\top} \boldsymbol{\pi}_{s_t} \quad (4.24)$$

subject to

$$\mathbb{P}_n[(\mathbf{p}_{s_t}, \tilde{\mathbf{r}}_{s_t}^1) \in \mathcal{D}_n] = 1, \quad \forall n \in \langle N_{s_t} \rangle \quad (4.25)$$

$$\mathbb{E}_{\mathbb{P}_n}[(\mathbf{p}_{s_t}, \tilde{\mathbf{r}}_{s_t}^1)] = \boldsymbol{\mu}_n, \quad \forall n \in \langle N_{s_t} \rangle \quad (4.26)$$

$$\mathbb{E}_{\mathbb{P}_n}[\|\mathbf{1}^{\top}((\mathbf{p}_{s_t}, \tilde{\mathbf{r}}_{s_t}^1) - \boldsymbol{\mu})\|] \leq \varphi_n, \quad \forall n \in \langle N_{s_t} \rangle \quad (4.27)$$

$$\mathbb{E}_{\mathbb{P}_n}[\|(\mathbf{p}_{s_t}, \tilde{\mathbf{r}}_{s_t}), (\mathbf{p}_{s_t}, \tilde{\mathbf{r}}_{s_t})_n^{\dagger}\|_2] \leq \varrho_n, \quad \forall n \in \langle N_{s_t} \rangle, \quad (4.28)$$

Based on the infinite-dimensional duality theory [216] and the strong duality of (4.24) under Slater's conditions [267]. By substituting dual problem of (4.24) with minimization term in constraint (4.23), the (4.22) can be reformed as

$$\min \sum_{n \in \langle N_{s_t} \rangle} -\varpi_n(\eta_n + \boldsymbol{\mu}_n^{\top} \boldsymbol{\chi}_n + \boldsymbol{\varphi}_n^{\top} \boldsymbol{\xi}_n + \varrho_n \zeta_n) \quad (4.29)$$

subject to

$$\begin{aligned} & \eta_n + (\mathbf{p}_{s_t}, \tilde{\mathbf{r}}_{s_t})^{\top} \boldsymbol{\chi}_n + \|\mathbf{1}^{\top}((\mathbf{p}_{s_t}, \tilde{\mathbf{r}}_{s_t}) - \boldsymbol{\mu}^0)\|^{\top} \boldsymbol{\xi}_n + \\ & \|(\mathbf{p}_{s_t}, \tilde{\mathbf{r}}_{s_t}), (\mathbf{p}_{s_t}, \tilde{\mathbf{r}}_{s_t})_n^{\dagger}\|_2 \zeta_n + (\tilde{\mathbf{r}}_{s_t} + \tilde{\mathbf{v}}_{s_{t+1}} \mathbf{p}_{s_t})^{\top} \boldsymbol{\pi}_{s_t} \\ & \leq \tilde{r}_{s_t}^*, \quad \forall (\mathbf{p}_{s_t}, \tilde{\mathbf{r}}_{s_t}) \in \mathcal{D}_n \quad \forall n \in \langle N_{s_t} \rangle \end{aligned} \quad (4.30)$$

$$\boldsymbol{\xi}_n \geq \mathbf{0}, \zeta_n \geq 0, \quad \forall n \in \langle N_{s_t} \rangle \quad (4.31)$$

constraints (4.11) and (4.12),

where η , χ , ξ , and ζ are dual variables. Since the same \mathcal{M}_S is used for (4.10) and (4.14). The optimization problem (4.14) for state s_t can also be formulated similarly as

$$\min \sum_{n \in \langle N_{s_t} \rangle} -\varpi_n (\eta_n + \boldsymbol{\mu}_n^\top \boldsymbol{\chi}_n + \boldsymbol{\varphi}_n^\top \boldsymbol{\xi}_n + \varrho_n \zeta_n) \quad (4.32)$$

subject to

$$(4.30) \text{ with } \tilde{r}_{s_t}^* \text{ being replaced by } \hat{r}_{s_t}^* \quad (4.33)$$

constraints (4.11), (4.12), (4.15)-(4.17), and 4.31.

Then, for each state $s_t \in \mathcal{S}$ with $t < T$, the optimal policies can be solved through MILP (4.29) and (4.32) for problems (4.10) and (4.14), respectively. By using backward induction, the optimal policies for entire horizon can be obtained efficiently.

4.3.2 Derivations of State-Wise Dynamic Prices

In this section, the derivation of state-wise dynamic prices will be presented. $\hat{r}_{s,u}$ can be reformatted as $\hat{r}_{s,u} = \tilde{r}_{s,u}^1 + \hat{r}_{s,u}^2$, where $\tilde{r}_{s,u}^1 = C_t^b(\theta_t^i, \sigma_t^{i,x} P_t^{b,i,x}, P_t^{b,i}, \theta_t^x, P_t^{b,x})$ is uncertain under \mathcal{M}_s^E and $\hat{r}_{s,u}^2 = (\sigma_t^{i,x} P_t^{b,i,x} + P_t^{b,x} + P_t^{pv,x}) h_t^{p,h}$ is independent on \mathcal{M}_s^E . By considering branch & bound method, the relaxed LP for MILP (4.32) is defined as

$$\min \sum_{n \in \langle N_{s_t} \rangle} -\varpi_n (\eta_n + \boldsymbol{\mu}_n^\top \boldsymbol{\chi}_n + \boldsymbol{\varphi}_n^\top \boldsymbol{\xi}_n + \varrho_n \zeta_n) \quad (4.34)$$

subject to

$$\underline{\pi}_{s_t, u_k} \leq \pi_{s_t, u_k} \leq \bar{\pi}_{s_t, u_k}, \quad \forall k \quad (4.35)$$

constraints (4.15)-(4.17), and (4.30), (4.31),

where $\underline{\pi}_{s_t, u_k}$ and $\bar{\pi}_{s_t, u_k}$ are, respectively, the lower and upper bounds for integer variable π_{s_t, u_k} , which are obtained from the last iteration in branch & bound method. By solving LP (4.34), the solutions of (4.32) can be obtained [217]. The necessary and sufficient optimality conditions for LP (4.34) with the expressions of primal feasibility and complementary slackness being omitted is [218]

$$\begin{aligned} \hat{\varepsilon}_0^+ - \hat{\varepsilon}_0^- + \hat{\varepsilon}_1 + \sum_{i, \ell, x, n, j} \{ [(\hat{\varepsilon}_2^- - \hat{\varepsilon}_2^+) D_{vp}^{ix} - \hat{\varepsilon}_3^\ell \alpha_c^0 D_{lp}^{\ell x} - \hat{\varepsilon}_4 \beta_c^0] \mathbf{P}_{s_t}^{x\top} - \hat{\varepsilon}_5^{n,j} (\tilde{\mathbf{r}}_{s_t}^1 + \hat{\mathbf{r}}_{s_t}^2 \\ + \tilde{\mathbf{v}}_{s_{t+1}} \mathbf{p}_{s_t})^\top \} = \mathbf{0} \end{aligned} \quad (4.36)$$

$$\begin{aligned} \sum_j \hat{\varepsilon}_5^{n,j} = \varpi_n, \quad \sum_j \hat{\varepsilon}_5^{n,j} (\mathbf{p}_{s_t}, \tilde{\mathbf{r}}_{s_t}) = \varpi_n \boldsymbol{\mu}_n, \quad \sum_j \hat{\varepsilon}_5^{n,j} |\mathbf{1}^\top ((\mathbf{p}_{s_t}, \tilde{\mathbf{r}}_{s_t}) - \boldsymbol{\mu}^0)| + \hat{\varepsilon}_6^n = \varpi_n \varphi_n \\ , \quad \sum_j \hat{\varepsilon}_5^{n,j} \|(\mathbf{p}_{s_t}, \tilde{\mathbf{r}}_{s_t}), (\mathbf{p}_{s_t}, \tilde{\mathbf{r}}_{s_t})_n^\dagger\|_2 + \hat{\varepsilon}_7^n = \varpi_n \varrho_n, \quad \forall n \in \langle N_{s_t} \rangle, \end{aligned} \quad (4.37)$$

where $\hat{\varepsilon}_1 = \sum_{k \in \langle U_{s_t} \rangle} \hat{\varepsilon}_1^{k+} - \sum_{k \in \langle U_{s_t} \rangle} \hat{\varepsilon}_1^{k-}$, and $j \in \langle |D_n| \rangle$. Multipliers $\hat{\varepsilon}_0^- \hat{\varepsilon}_7$ are for constraints of (4.34). The optimality conditions of relaxed LP with constraints (4.11) and (4.12)

being removed for (4.29) with multipliers $\tilde{\varepsilon}_0$ - $\tilde{\varepsilon}_7$ are expressed as

$$\tilde{\varepsilon}_0^+ - \tilde{\varepsilon}_0^- - \sum_{n,j} \tilde{\varepsilon}_5^{n,j} (\tilde{\mathbf{r}}_{s_t}^1 + \tilde{\mathbf{r}}_{s_t}^2 + \tilde{\mathbf{v}}_{s_{t+1}} \mathbf{p}_{s_t})^\top = \mathbf{0} \quad (4.38)$$

$$(4.37) \text{ with } \hat{\varepsilon}_5 - \hat{\varepsilon}_7 \text{ replaced by } \tilde{\varepsilon}_5 - \tilde{\varepsilon}_7. \quad (4.39)$$

From (4.37) and (4.39), it can be observed that $\sum_{j \in \mathcal{D}_n} \hat{\varepsilon}_5^{n,j}$ and $\tilde{\varepsilon}_5^{n,j}$ are probability measures on $\mathcal{M}_{s_t}^E$. Due to the independence of $\tilde{\mathbf{r}}^2$ and $\hat{\mathbf{r}}^2$ on \mathcal{M}_s^E , conditions (4.36) and (4.38) can be reformatted, respectively, as

$$\begin{aligned} \hat{\varepsilon}_0^+ - \hat{\varepsilon}_0^- + \hat{\varepsilon}_1 + \sum_{i,\ell,x,n,j} [(\pm \hat{\varepsilon}_2^{i\pm} D_{vp}^{ix} - \hat{\varepsilon}_3^\ell \alpha_c^0 D_{lp}^{\ell x} - \hat{\varepsilon}_4 \beta_c^0) \mathbf{P}_{s_t}^{x\top} - \hat{\varepsilon}_5^{n,j} (\tilde{\mathbf{r}}_{s_t}^1 + \tilde{\mathbf{v}}_{s_{t+1}} \mathbf{p}_{s_t})^\top] \\ - \hat{\mathbf{r}}_{s_t}^2 = \mathbf{0} \end{aligned} \quad (4.40)$$

$$\tilde{\varepsilon}_0^+ - \tilde{\varepsilon}_0^- - \sum_{n,j} \tilde{\varepsilon}_5^{n,j} (\tilde{\mathbf{r}}_{s_t}^1 + \tilde{\mathbf{v}}_{s_{t+1}} \mathbf{p}_{s_t})^\top - \tilde{\mathbf{r}}_{s_t}^2 = \mathbf{0}. \quad (4.41)$$

Since, $\hat{\mathbf{r}}_{s_t}^2 = \sum_x h_t^{p,h} \mathbf{P}_{s_t}^{x\top}$, let $\tilde{\mathbf{r}}_{s_t}^2$ is expressed as

$$\sum_{x,i,\ell} [h_t^{p,h} \mp (\hat{\varepsilon}_2^{i\pm} D_{vp}^{ix} \mp \hat{\varepsilon}_3^\ell \alpha_c^0 D_{lp}^{\ell x} \mp \hat{\varepsilon}_4 \beta_c^0)] \mathbf{P}_{s_t}^{x\top} - \hat{\varepsilon}_1. \quad (4.42)$$

Then, if $\hat{\varepsilon}_5^{n,j} = \tilde{\varepsilon}_5^{n,j}$ for all n and j , the solutions satisfying (4.41), with $\tilde{\mathbf{r}}_{s_t}^2$ in the form of (4.42), will also satisfy (4.40). This requires that the complementary slackness conditions of constraint (4.30) for (4.10) and (4.14) are the same, i.e., $\tilde{r}_{s_t}^* = \hat{r}_{s_t}^*$. For $\hat{r}_{s_t}^*$ and $\tilde{r}_{s_t}^*$, the optimality conditions are, respectively, similar to conditions (4.36) and (4.38) without ε_5 . Then, similar to (4.40) and (4.41), by using (4.42) for $\tilde{\mathbf{r}}_{s_t}^2$, the optimality conditions of $\hat{r}_{s_t}^*$ and $\tilde{r}_{s_t}^*$ will be equivalent. So, with $\tilde{\mathbf{r}}_{s_t}^2$ in (4.42), the solutions of relaxed LP for (4.10) is the integer solutions of (4.14). In (4.42), $\tilde{\mathbf{r}}_{s_t}^2$ consists of a term for power injections, i.e., $h_t^{p,h} - \sum_{i,\ell} (\pm \hat{\varepsilon}_2^{i\pm} D_{vp}^{ix} - \hat{\varepsilon}_3^\ell \alpha_c^0 D_{lp}^{\ell x} - \hat{\varepsilon}_4 \beta_c^0)$. Then, the DSO can choose the state-wise dynamic price as $h_{t,s_t}^{p,x} = \sum_{i,\ell} (\pm \hat{\varepsilon}_2^{i\pm} D_{vp}^{ix} - \hat{\varepsilon}_3^\ell \alpha_c^0 D_{lp}^{\ell x} - \hat{\varepsilon}_4 \beta_c^0)$, which corresponds to the electricity price for system constraints. $\hat{\varepsilon}_1$ is the cost to guarantee that the system constraints are satisfied certainly.

4.4 Case Studies

The case studies are performed using Matlab with YAMILP and OpenDSS on PC with Intel Core i7-4770. An illustration of the St. Albert transit systems [219] studied in this research is shown in Fig. 4.2, from which a total of 7 routes and 6 EBs with data are selected. These data include drivers' IDs, schedules, velocities, accelerations, locations, and passengers' boarding and alighting. The solar irradiation data for Colorado park mountain are used [220]. The IEEE 123-node test feeder [221] is used. The single-line diagram of the modified test feeder with integrated EBCSs is shown in 4.3. The configurations of EB, BESS, and PV are listed in Table 4.1, where the battery round trip efficiency is 0.91. The day-ahead



Figure 4.2: St. Albert transit systems.

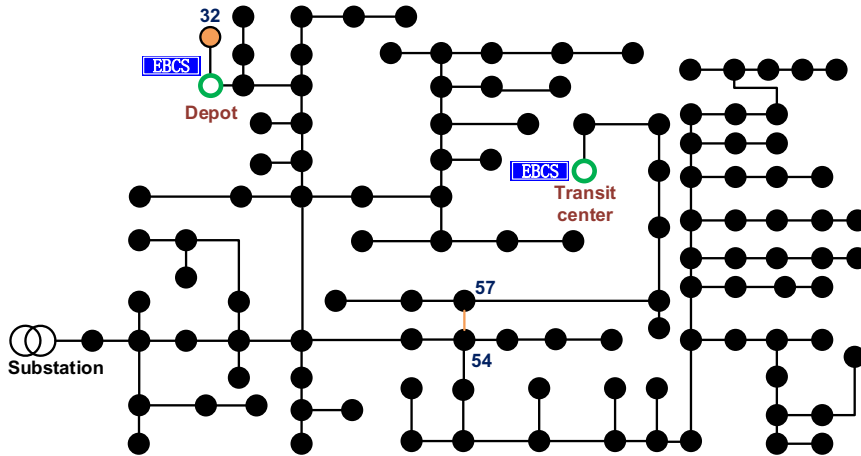


Figure 4.3: Modified IEEE 123-node test feeder with integrated EBCCs.

spot prices of the reference node are obtained from IESO Canada [224] and are shown in Fig. 4.4. The data of 360 days in spring and summer are used. The data of the first 300 days are used to generate optimal policies, while the data of the last 60 days are used for performance evaluations. The k-MLE [225] is used to cluster the empirical data of (p, \tilde{r}) into different events. The probability distribution of events is assumed to follow uniform distribution [43]. The φ_{n_s} is set to be $0.3\mu_{n_s}$ for all events.

Firstly, the impacts of EB charging on power distribution systems are analyzed, in which the number of events and the radius of Wasserstein metric are selected as 3 and 1.2, respectively. From Fig. 4.5, it can be observed that without using dynamic prices, the EBCC demand at the depot is extreme high for time slots with low spot prices, and the

Table 4.1
CONFIGURATION PARAMETERS FOR EB, BESS, AND PV

EB (BYD) [222]	BESS [223]	PV
Battery capacity 280kWh Charging power 60kW Unit cost 145\$/kWh Passenger capacity 58 $c_m, c_d, c_r, c_{tr}, c_{con}$ [204] EB weight 13,800kg Passenger weight 62kg	Capacity 360kWh/unit Max. power 120/kW Unit cost 145\$/kWh Quantity: 2 for depot, 1 for transit center	Area: 2000m ² for depot, 800m ² for transit center Efficiency 0.82 [220]

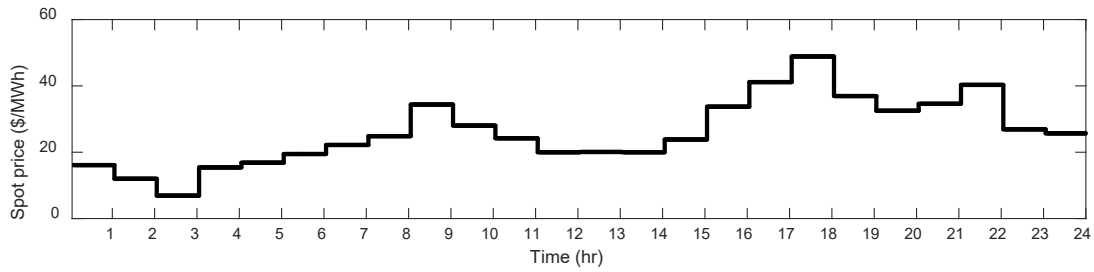


Figure 4.4: Spot prices for reference node h .

voltage level at node 32 drops below 0.95 p.u. Between 11 am and 3 pm, most of the EBs require recharging at the transit center, which increases the demand and causes congestion in line 54-57. Unlike EVs whose charging demand can be shifted, the BESS is supposed to reduce demand by discharging; however, the BESS discharges between 4 pm and 7 pm when the spot prices are high. As shown in Fig. 4.6, with dynamic prices that increase the spot prices of node at the depot for 1-4 am to the spot price for 5 am, partial charging demand is shifted to 1 am and 5 am for voltage level supporting. For time slots with line congestion, the spot prices of node at the transit center are increased to the spot price for 4 pm, which shifted partial BESS discharging power between 6 pm and 7 pm for line congestion relief. From Fig. 4.7, it can be observed that, to mitigate charging impacts, the charging cost under dynamic prices increases slightly by 9.2%. By comparing with the stochastic policies obtained based on violation risk constraints in [257] with 95% risk, the cost $\hat{\epsilon}_1$ for guaranteed satisfaction of constraints increases the cost slightly by 1.9327%.

To evaluate the performance regarding to robustness and conservatism of proposed approach, the out-of-sample performance [99] for last 60 days is considered for following cases:

- Case 1: Proposed approach with *minimax-regret* criterion, event-based ambiguity set with moment and statistical distance information, and heuristic regret function;
- Case 2: Case 1 with *min-max* criterion.
- Case 3: Case 1 without statistical distance information.

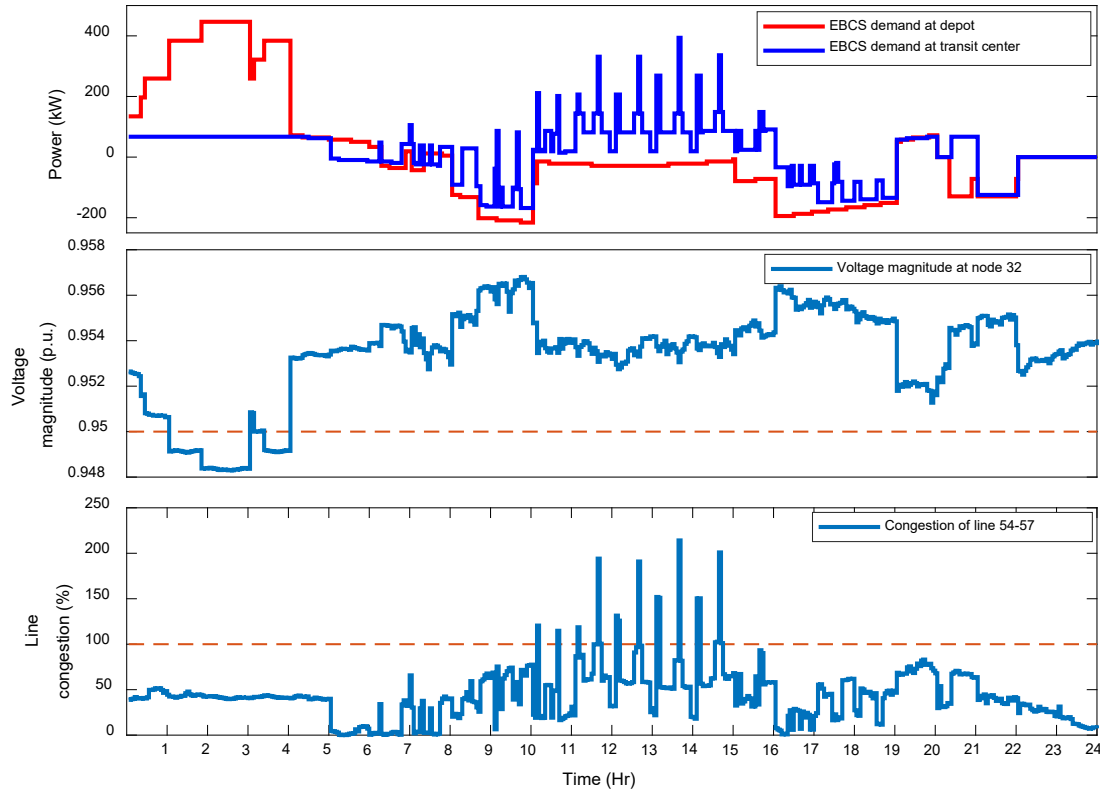


Figure 4.5: EBCS demand without using dynamic prices.

- Case 4: Robust approach in [87] with system constraints.

The event-based ambiguity set is used to address the uncertainties of reference distribution and moment information obtained from empirical data. It can be observed from Fig. 4.8 that, as the number of events increases, the standard deviation reduces. This indicates that the robustness is improved. However, the mean increases significantly, which gives overly conservative solutions. As shown in Fig. 4.8, in our problem, when the number of events is 3, the solutions have acceptable robustness and are less conservative. As shown in Fig. 4.9, as the radius of Wasserstein metric increases, the robustness can be improved. However, a larger radius gives overly conservative solutions with a significantly increased mean of charging cost. When the radius reaches 1.2, the mean has not increased significantly, after which the mean increases significantly, and the robustness improves slightly. Also, from Fig. 4.9, it can be observed that without considering the moment information, the robustness for all radius is improved slightly; however, it results in solutions with a significantly high mean and are overly conservative. The DRMDP reduces to empirical-based MDP when the radius is 0 [226], and the random bus loads are assumed to follow the empirical distribution. As shown in Fig. 4.9, the empirical-based MDP has low robustness, which indicates that inaccurate PDF estimation of random bus loads has significant impacts on stochastic energy management of EBCSs.

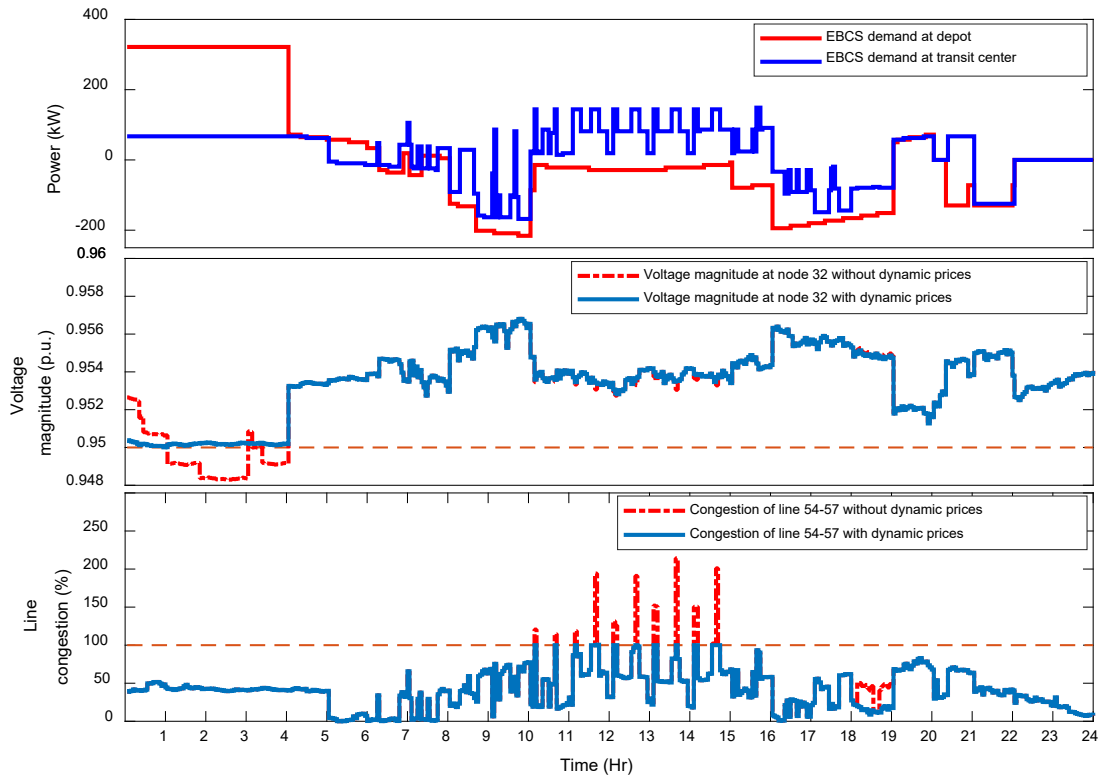


Figure 4.6: EBCS demand with dynamic prices.

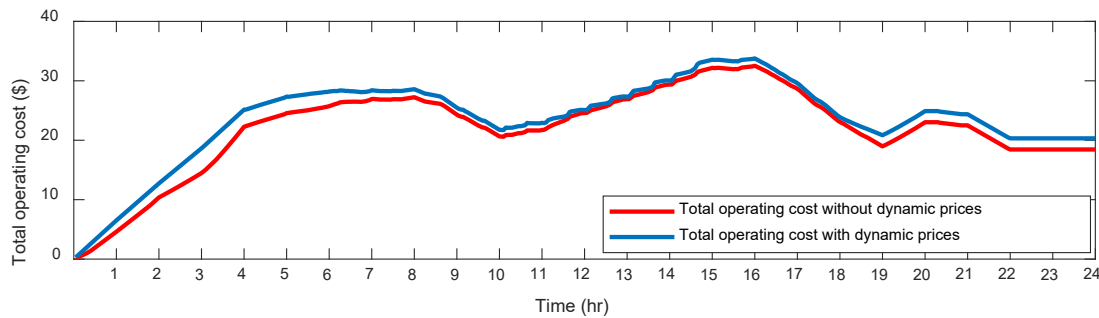


Figure 4.7: Charging cost for one day.

As shown in Fig. 4.10, by considering different cases, it can be observed that, for EBCS energy management under uncertainties, the usage of *min-max* criterion in Case 2 gives a higher mean than using *minimax-regret* criterion, and the robustness has not been improved significantly. Also, for the ambiguity set with only moment information in Case 3, the robustness has been improved significantly, but the mean also increases, which indicates that only considering moment information results in conservative solutions in our problem. Moreover, for Case 4, the usage of a robust approach can give high robustness; however, the solutions are overly conservative. Also, it can be observed in Fig. 4.9 and 4.10 that when the radius is 2, the solutions obtained without considering moment information are almost the same as Case 4 and the solutions obtained with moment information are

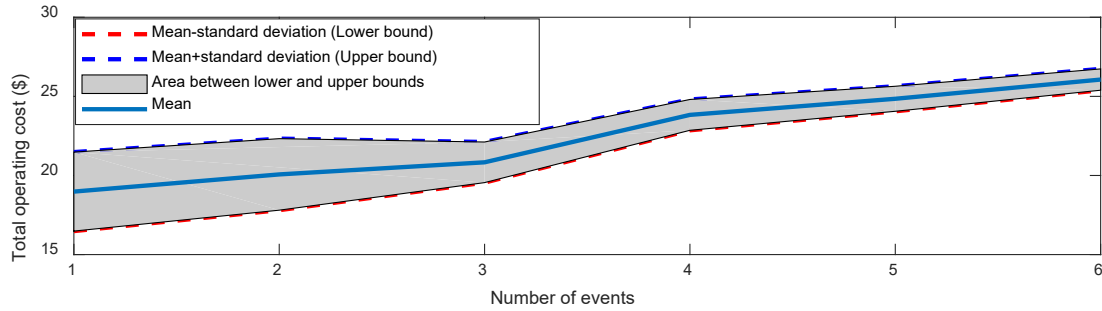


Figure 4.8: Ou-of-sample performance for different number of events.

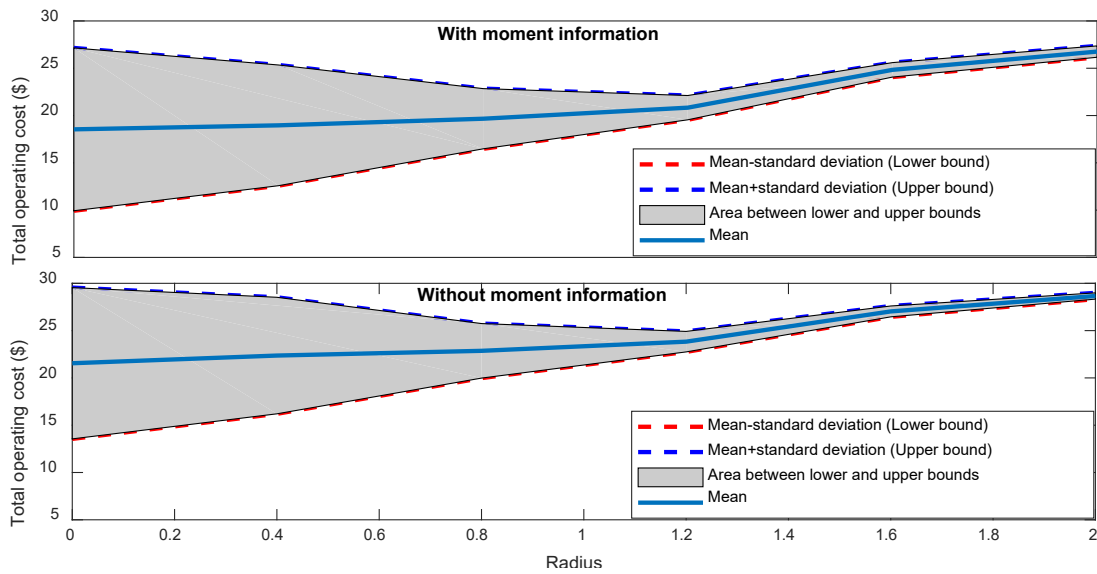


Figure 4.9: Out-of-sample performance for different radius.

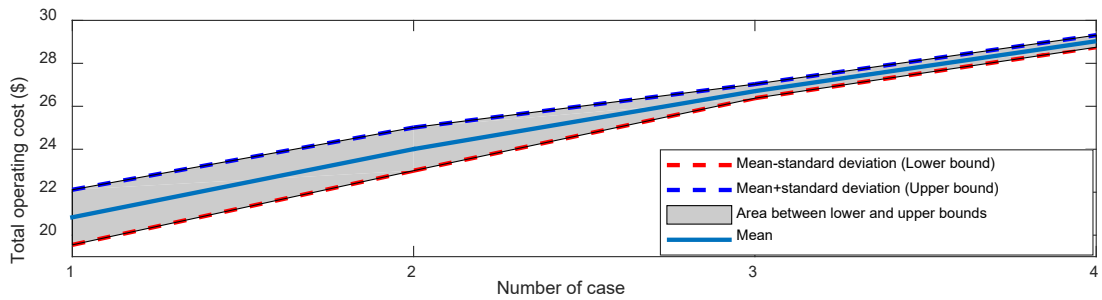


Figure 4.10: Out-of-sample performance for different cases.

close to Case 3, which indicates that when the radius is larger than 2 the DRMDP becomes robust MDP, which is consistent with the conclusion in [226]. Further, it can be observed from Table 4.2 that the out-of-sample performance of solutions obtained by using heuristic regret function is comparable to the of solutions obtained by using original regret function, especially for the standard deviation. Also, the usage of heuristic regret function can reduce computational complexity.

Table 4.2
PERFORMANCE OF PROPOSED HEURISTIC REGRET FUNCTION

	Mean (\$)	Standard deviation (\$)	Time (hr)
Case 1	20.832	1.282	2.2
Case 1 with conventional regret function	18.913	1.114	14.5

4.5 Summary

In this chapter, a stochastic energy management scheme for EBCSs with B2G capabilities is proposed. To address the errors in PDF estimations, the energy management problem is formulated as a DRMDP with uncertain transition probabilities and costs using event-based ambiguity set is formulated. The ambiguity with combined statistical distance and moment information is used with *minimax-regret* criterion for robust solutions that are less conservative. A heuristic *minimax-regret* function is proposed to express the formulated DRMDP problem dynamically and allow for the usage of backward induction manner. The dynamic prices for EBCS operation with mitigated impacts on SDSs are derived based on the unique structure of immediate cost in the formulated problem.

5

Cyber-Physical Security Analysis of BESSs in SDSs

In this chapter, the cyber-physical security of BESSs in SDSs is analyzed with specific attention to cyber-physical attacks against system information integrity in SDSs, i.e., the FDIAs. As defined by National Institute of Standards and Technology (NIST) [227], the future smart distribution system consists of the physical power system and cyber system. The cyber system collects, transmits, and processes the physical power system data, and enhances the optimization and automatic control of the physical power system. This constitutes one of the most complicated CPS in the history. However, the CPS exposes the future smart distribution system to severe cyber-physical attacks [228]. As a confirmed cyber-physical attack targeting on the distribution system, the Ukraine power grid cyber-physical attack took place in 2015 left about 230,000 people without electricity [229]. The FDIAs, as one of the most severe cyber-physical attacks, can result in energy theft on the customers, false dispatch on the power distribution, and power generation breakdown [103]. For example, the results in [104] show that the FDIA on local energy trading in residential distribution system can cause a benefit reduction up to 94%.

Also, BESSs are becoming vital for improving sustainability, efficiency, and resiliency of SDSs [230]. To fully exploit these benefits, the accurate SoC estimation of BESSs is important [50]. With the advancement of BMSs and the emerging IoT technology, the BESSs are becoming CPSs and the SoC can be estimated accurately using real-time battery pack terminal voltage and current measurements [12]. However, this also exposes SoC estimation to severe cyber-physical attacks [7, 13–15]. Promoting countermeasures is vital for the security protection of SoC estimation of BESSs, where the study on the mechanism of cyber-physical attacks against SoC estimation is essential. In this chapter, the mechanism of FDIAs against SoC estimation of BESSs in SDSs is investigated. This chapter consists

of two parts for the cyber-physical security analysis of BESSs in SDSs, where the first part is focused on the general construction principle of practical FDIAs in SDSs. The second part is more about the investigation of the mechanism of FDIAs against SoC estimation of BESSs in SDSs.

In power transmission systems, the FDIAs against SSE have been well studied. However, due to the unique features of power distribution systems including the low x/r ratio, existence of one- and/or two-phase branches, unbalanced load distributions, and unsymmetrical line parameters, the research on FDIAs in SDSs is still open. Although, the vulnerability of terminal devices in BESSs to cyber-physical attacks have been revealed in literature. However, the analysis of cyber-physical threat to CPS-based BESSs that focuses on the mechanism of the penetration of the cyber-physical attacks launches at terminal devices into the physical operation of BESSs has not been well studied. In this chapter, the construction principle of FDIAs in practical SDSs that are characterized by low x/r ratio, multiphase branches/laterals, unbalanced load distributions, and unsymmetrical line parameters is firstly investigated. Then, based on the construction of FDIAs in practical SDSs, different mechanisms of FDIAs against SoC estimation of BESSs are studied and evaluated.

5.1 The Construction Principle of False Data Injection Attacks in SDSs

In this section, the construction principle of practical FDIAs in multiphase and unbalanced SDSs will be studied. Also, the feasibility and limitations of performing FDIAs based on equivalent measurements in practice will be discussed with insights being provided.

5.1.1 Local State-Based Linear DSSE for Multiphase and Unbalanced Smart Distribution Systems

In order to construct the FDIAs numerically, the linear expression of DSSE is required. And the linear DSSE should base on the local state only, so that the FDIAs can be constructed with the least information of system states. In this section, the modeling of three-phase and unbalanced distribution systems is presented first. Then, the DSSE for three-phase and unbalanced distribution systems based on the method in [231] is introduced. Finally, the local state-based linear DSSE for multiphase and unbalanced distributions systems will be presented.

The Modeling of Three-Phase and Unbalanced Distribution Systems

Due to the unbalanced loads and unsymmetrical line parameters in three-phase distributions systems, a 3×3 matrix is required to represent the line admittance \mathbf{Y}_{kl} [232]. The transformers in distribution systems can be modeled as distribution lines, and the details

can be referred in [232] and [233]. The Δ -connected loads are modeled as equivalent Y -connected current sources as in [234]. Based on KVL and KCL, in rectangular form, we have

$$[I_{kl.re}^a, \dots, I_{kl.im}^c]^T = \mathbf{Y}_{kl}[V_{k.re}^a - V_{l.re}^a, \dots, V_{k.im}^c - V_{l.im}^c]^T, \quad (5.1)$$

where $I_{kl} = I_{kl.re} + jI_{kl.im}$ and $V_k = V_{k.re} + jV_{k.im}$. For bus k , the bus current injections can be expressed as

$$[I_{k.re}^a, \dots, I_{k.im}^c]^T = \mathbf{Y}_k[\mathbf{V}_{k1}, \dots, \mathbf{V}_{k(N-1)}, \mathbf{V}_{kN}]^T, \quad (5.2)$$

where \mathbf{Y}_k is the equivalent bus primitive admittance matrix in rectangular form, and \mathbf{V}_{kl} , for $l = 1 \dots N$, is the voltage drop.

Smart Distribution System Measurements

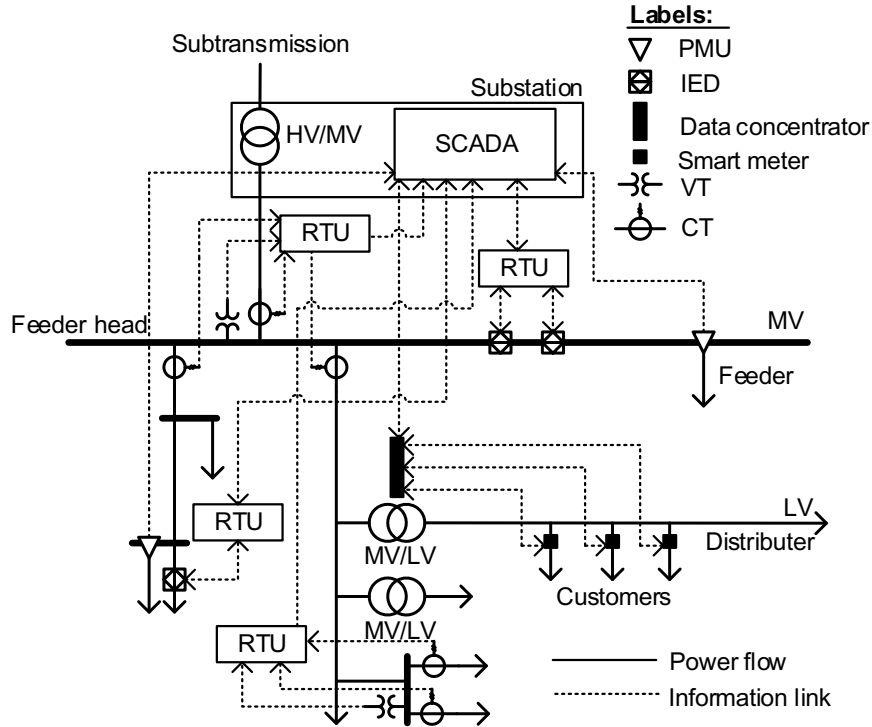


Figure 5.1: A single-line diagram of smart distribution system with different types of measurements.

Different from power transmission systems, which are covered by a large amount of real-time measurements, the conventional distribution system monitoring relies mainly on the distribution SCADA system with most real-time measurements originated at the high-to-medium voltage (HV/MV) substations and limited real-time measurements at lines and nodes along the medium-voltage (MV) feeders. This causes the measurements paucity of

DSSE, and the power distribution systems are typically underdetermined. To address this issue, in both industry and academia, the pseudo measurements, which are the estimations of load profiles based on historical data, are involved to increase the redundancy of distribution system measurements [235] [110]. Further, with the development of smart distribution systems, new sources of data have been created at remarkable volumes [236]. By leveraging IEDs such as automated feeder switches, circuit breakers, digital relays, and smart inverters of DER, more real-time system topology information and power, current, and voltage measurements of MV distribution systems can be obtained [118]. Also, the deployment of PMU, especially the μ PMU with low capital cost, is rolling out in most power distribution systems [237] [238]. All these sources of data can be utilized to improve the power distribution system observability. Recently, the utilization of AMI systems installed at medium-to-low voltage (MV/LV) transformers and smart meters employed in LV distribution systems has been investigated to provide near real-time measurements for the quality improvement of pseudo measurements [239].

The measurements of a typical smart distribution system are illustrated in Fig. 5.1. At the HV/MV substation, the distribution SCADA collects data from the system and uses the collected data for substation, feeder, and end user load controls. At the feeder head, the current transformer (CT) and voltage transformer (VT) are used to measure the current of each feeder and the voltage at the substation. These measurements are firstly collected by the RTU, in which the local vector quantities of current and voltage are computed. Then, the local vector quantities are converted to the magnitudes of voltage and real and reactive power [240], which are transmitted by the RTU through local area network (LAN) to the SCADA. Also, in the MV distribution system, the CT and VT are used to measure feeder current flow and feeder-end or DER voltage [239], respectively, and the IED with PQ features can provide the feeder real and reactive power flow measurements [241]. Similar to CT and VT, the IEDs communicate with RTU to transmit measurements, through FAN, to the SCADA. The PMU/ μ PMU installed at some critical points in MV distribution system can provide the synchronized voltage, current, and power phasor measurements, which are transmitted to the SCADA through FAN. Also, nowadays, many IED and RTU have been upgraded to provide synchronous phasor measurements [242]. Based on the AMI system, the real and reactive power consumption data, collected by the individual smart meters in LV distribution systems, can be aggregated, through the NAN, by data concentrator to provide the near real-time bus power injection measurements of the MV distribution systems. These measurements are transmitted to the SCADA through FAN. For large-scale power distribution systems with a large number of measurement points, it is impractical to telemeter all points through real-time measurement devices. To guarantee the observability, the pseudo measurements generated at the SCADA, based on historical customer load profiles, can be used as bus power injection measurements.

The DSSE for Three-Phase and Unbalanced Distribution Systems

Consider a general linear weighted least square (WLS)-based state estimation in the form of $\mathbf{z} = \mathbf{H}\mathbf{x} + \mathbf{e}$, where \mathbf{z} is the set of measurements, \mathbf{H} is the measurement function matrix, which is determined based on the power flow equations and the j th element relates the j th measurement to states, and \mathbf{x} is the set of system states. The vector \mathbf{e} is the set of measurement errors. If the measurement errors are normally distributed with zero mean, there is a closed-form solution in the form of

$$\hat{\mathbf{x}} = (\mathbf{H}^T \mathbf{W} \mathbf{H})^{-1} \mathbf{H}^T \mathbf{W} \mathbf{z}, \quad (5.3)$$

where $\hat{\mathbf{x}}$ are estimated states. The weight matrix $\mathbf{W} = \mathbf{R}^{-1}$ with \mathbf{R} denoting the covariance matrix of measurement errors.

In this research, in order for the power distribution systems to be fully observable, we choose the measurements in a way such that the number of measurements is sufficiently larger than the number of states to formulate an overdetermined DSSE problem. More specifically, the real-time voltage, current, and power measurements obtained from RTU, IED, PMU/ μ PMU, and AMI are assumed to be available in a power distribution system, and the optimal placement of these real-time measurement devices is left for our future work. The pseudo measurements obtained from historical load data, by using the method in [110], are leveraged to improve measurement redundancy. In general, the DSSE considers three-phase measurements in rectangular forms of complex branch current flows \mathbf{I}_{br_mea} , complex branch power flows \mathbf{S}_{br_mea} , complex bus power injections \mathbf{S}_{bus_mea} obtained from the real-time measurements and pseudo measurements, complex bus voltage measurements \mathbf{V}_{bus_mea} , and bus voltage magnitude measurements $|\mathbf{V}|_{bus_mea}$. For the current measurements, i.e., \mathbf{I}_{br_mea} and \mathbf{I}_{bus_mea} , the measurement functions can be represented by (5.1) and (5.2), respectively. The measurement functions of \mathbf{V}_{bus_mea} can be expressed as $[\mathbf{V}_{k_mea}^{a,b,c}]^T = \mathbf{U}[\mathbf{V}_k^{a,b,c}]^T$, where \mathbf{U} is an identity matrix. Traditionally, the bus voltage magnitude measurements $|\mathbf{V}|_{bus_mea}$ are converted to equivalent complex bus voltage measurements \mathbf{V}_{bus_equ} based on the phase angle of the nearest bus with phasor measurements. The complex power measurements \mathbf{S}_{br_mea} and \mathbf{S}_{bus_mea} are converted to equivalent currents as

$$\mathbf{I}_{kl_equ} = (\mathbf{S}_{kl_mea} / \tilde{V}_k)^*, \quad \mathbf{I}_{k_equ} = (\mathbf{S}_{k_mea} / \tilde{V}_k)^*, \quad (5.4)$$

where \tilde{V}_{bus} is the estimated bus voltage. And the system-based measurement functions for the power measurements can be expressed by using (5.1) and (5.2). Then, the DSSE for a three-phase and unbalanced distribution system is expressed as

$$[\mathbf{V}_{bus_equ}, \mathbf{V}_{bus_mea}, \mathbf{I}_{br_mea}, \mathbf{I}_{br_equ}, \mathbf{I}_{bus_equ}]^T = [\mathbf{U}, \mathbf{U}, \mathbf{Y}_{br}, \mathbf{Y}_{br}, \mathbf{Y}_{bus}]^T \mathbf{V} + \mathbf{e}, \quad (5.5)$$

where the matrices \mathbf{Y}_{br} and \mathbf{Y}_{bus} are the constant measurement functions of the branch current flow and bus current injection measurements. The vector \mathbf{V} is the set of system

states, which are typically selected as the bus voltages in rectangular form to handle distribution systems with different topology [243]. As discussed in [244–247], the variances of the equivalent current measurements follow the same distributions of that of power measurements, and the matrix \mathbf{R} stays the same. Then, the DSSE is solved iteratively. During each iteration, the values of \mathbf{V}_{bus_equ} , \mathbf{I}_{br_equ} , and \mathbf{I}_{bus_equ} are updated based on the state estimation solution calculated from previous iteration by using (5.3). The DSSE discussed above is designed for three-phase and unbalanced distribution systems. And, in order to calculate \mathbf{V}_{bus_equ} for a bus with voltage magnitude measurement, the states of the nearby buses are required. This increases the efforts of the attackers.

The Local State-Based Linear DSSE for Multiphase and Unbalanced Distribution Systems

For the one-line and two-line feeders in practical distributions systems, the virtual line(s) is(are) added to the missing phase(s). In the admittance matrix, the corresponding diagonal element(s) of missing phase(s) is(are) assigned with arbitrary number(s) y^{vv} to avoid the singularity of constant matrix \mathbf{H} of DSSE. Consider line kl with phase b and c as an example. By adding a virtual line, we have

$$\mathbf{Y}_{kl} = \begin{bmatrix} y_{kl}^{vv} & 0 & 0 \\ 0 & y_{kl}^{bb} & y_{kl}^{bc} \\ 0 & y_{kl}^{cb} & y_{kl}^{cc} \end{bmatrix}, \quad (5.6)$$

where the mutual admittance between an existing phase and a missing phase is set to zero for the validity of Ohm's law. For the missing phases, the corresponding current and power measurements are set to zero, while the corresponding voltage measurements are set to the estimated bus voltages of the nearest upstream bus with the missing phases.

Different from power transmission systems, the synchronous phasor measurements are limited in power distribution systems, and most of the buses have only voltage magnitude measurements. The voltage magnitude measurements introduce nonlinearity to the measurement functions. In conventional DSSE, for a bus with voltage magnitude, the voltage magnitude measurement function is linearized by approximating the phase angles of this bus with phase angles of a nearby bus that has phasor measurements, or the phase angles are assumed to be the same as that of the voltages at substation. However, from the perspectives of attackers, this increases the number of required measurements that attackers need access to. To reduce the efforts of the attackers, the linearization of the voltage magnitude measurement function of a bus with voltage magnitude measurement should rely solely on the complex bus voltage states of this bus, i.e., the local information. In order to allow the attackers to use the local information only to reduce the number of required measurements, the Alpha Max and Beta Min [248] method is used. This method approximates the magnitude of the complex voltage based on the local states only. And the approximation can be expressed as $|V|_{l_mea} \approx \alpha \max\{|V|_{l_re}, |V|_{l_im}\} + \beta \min\{|V|_{l_re}, |V|_{l_im}\}$, where

the parameters α and β depend on the value of $\arctan(V_{im}/V_{re})$. For distribution system, at the slack bus, the bus voltage phase angles are 0° , -120° , and 120° for phases a, b, and c, respectively. And the deviations of bus voltage phase angles are typically small [234]. So, for any buses at the downstream, the real and imaginary parts of voltages satisfy

- $V_{re}^a > 0$, $V_{im}^a < 0$, and $|V_{re}^a| > |V_{im}^a|$,
- $V_{re}^b < 0$, $V_{im}^b < 0$, and $|V_{re}^b| < |V_{im}^b|$,
- $V_{re}^c < 0$, $V_{im}^c > 0$, and $|V_{re}^c| < |V_{im}^c|$.

Then, the measurement function of $|\mathbf{V}|_{bus_mea}$ can be expressed as

$$[|\mathbf{V}|_{l_mea}^{a,b,c}]^T = \mathbf{M}[V_{l_re}^a, V_{l_im}^a, \dots, V_{l_re}^c, V_{l_im}^c]^T, \quad (5.7)$$

where the matrix \mathbf{M} is a constant matrix in the form of

$$\mathbf{M} = \begin{bmatrix} \alpha & -\beta & 0 & 0 & 0 & 0 \\ 0 & 0 & -\beta & -\alpha & 0 & 0 \\ 0 & 0 & 0 & 0 & -\beta & \alpha \end{bmatrix}. \quad (5.8)$$

The local state-based DSSE for a multiphase and unbalanced distribution system can be expressed as

$$[|\mathbf{V}|_{bus_mea}, \mathbf{V}_{bus_mea}, \mathbf{I}_{br_mea}, \mathbf{I}_{br_equ}, \mathbf{I}_{bus_equ}]^T = [\mathbf{M}, \mathbf{U}, \mathbf{Y}_{br}, \mathbf{Y}_{br}, \mathbf{Y}_{bus}]^T \mathbf{V} + \mathbf{e}. \quad (5.9)$$

After the convergence of iteration, the DSSE is in the form of $\tilde{\mathbf{z}} = \mathbf{H}\mathbf{x} + \mathbf{e}$, where $\tilde{\mathbf{z}}$ is the set of equivalent measurements after convergence. If the attackers have access to or can approximate the vector $\tilde{\mathbf{z}}$, the attackers can construct FDIAs numerically based on the linear DSSE in the form of (5.9). In the next section, the principles of practical FDIAs against DSSE, without knowing the entire system states, by using the linear DSSE $\tilde{\mathbf{z}} = \mathbf{H}\mathbf{x} + \mathbf{e}$ will be discussed.

5.1.2 The Principles of FDIAs Against DSSE

In order to conduct cyber-physical attacks in power distribution systems, the attackers need to know the strategies of the distribution system automation controls and determine which and how the measurements are to be compromised. For example, if the attackers wish to attack on the LTC transformers to reduce the energy efficiency by increasing the system operating voltage level, the attackers need to know the total number of taps and the voltage change caused by one tap change of the LTC transformers. If the attackers aim at disrupting the power distribution systems stability by manipulating the voltage controlled distributed generators (VC DG) to inject excessive power, the attackers are required to know the control schemes of the VC DG, to determine the change on the bus voltages where the VC DG is connected. In this research, without loss of generality, the attackers are

assumed to have the full knowledge on the strategies of the system controls and are able to identify the targeting measurements and determine how the targeting measurements should be compromised, in order to affect the outcome of system controls. We focus mainly on the methodology for constructing a vector of compromised measurements, including the targeting measurements, for the FDIAs against DSSE, to fundamentally analyze the vulnerability of smart distribution systems to the FDIAs. In particular, an FDIA injects malicious data into the measurements by constructing an attack vector \mathbf{a} , where $a_i \neq 0$ for i belonging to the targeting measurement set. The targeting measurement set contains the measurements that are predetermined by the attackers based on the strategies for different attacking scenarios. Also, the targeting measurement set contains the measurements that are determined based on the proposed FDIA, in such a way that the compromises on the attacks' predetermined measurements can bypass the BDD mechanism, i.e., without being detected.

Generally, in TSSE and DSSE, the BDD is based on the measurement residual $\mathbf{r} = \mathbf{z} - \mathbf{H}\hat{\mathbf{x}}$. One of the methods used for the BDD is the Chi-square (χ^2) test. The χ^2 test is performed based on the assumption that the measurement errors are uncorrelated, and the measurement residuals $\frac{\mathbf{r}}{\text{diag}(\mathbf{R})}$ are all in standard normal distributions. And the distribution of the l^2 -norm of the measurement residuals $\frac{\mathbf{r}}{\text{diag}(\mathbf{R})}$ is in a χ^2 distribution. However, in power distribution systems, due to the usage of pseudo measurements, the assumption of measurement residuals determined by $\frac{\mathbf{r}}{\text{diag}(\mathbf{R})}$ makes the χ^2 test inaccurate [250]. Then, the normalized residual test which considers the residual covariance matrix is adopted. The normalized measurement residual vector $\mathbf{r}^N = \frac{|\mathbf{r}|}{\sqrt{\text{diag}(\mathbf{S}\mathbf{R})}}$ is used to test the existence of bad measurements, where \mathbf{S} is the measurement sensitivity vector, and $\mathbf{S} = \mathbf{I} - \mathbf{K}$ with hat matrix $\mathbf{K} = \mathbf{H}(\mathbf{H}^T\mathbf{W}\mathbf{H})^{-1}\mathbf{H}^T\mathbf{W}$. And if $\max \mathbf{r}^N > \lambda$, there exists at least one bad measurement.

In this research, the proposed local state-based linear DSSE is adopted by the attackers to construct FDIAs numerically with least information of system states. For the system operators, different types of nonlinear WLS-based DSSE methods, such as node voltage based DSSE methods and branch current based DSSE methods, can be used. In order to use the proposed local state-based linear DSSE for the construction of FDIAs against the original nonlinear DSSE, the following condition needs to be satisfied.

Remark 1. *The linear DSSE $\tilde{\mathbf{z}} = \mathbf{H}\mathbf{x} + \mathbf{e}$ with equivalent measurement set $\tilde{\mathbf{z}}$ can be used to construct an FDIA against the original nonlinear DSSE with original measurement set \mathbf{z} , if $(\mathbf{z} + \Delta\mathbf{z})|_{\mathbf{x}_a} = \tilde{\mathbf{z}} + \mathbf{a}$, where $\Delta\mathbf{z}$ is a constant vector and \mathbf{x}_a is the system state set after the FDIA \mathbf{a} .*

For different WLS-based DSSE methods, if all the measurements with nonlinear measurement functions can be converted to the equivalent measurements with linear measurement functions. The WLS-based DSSE estimators can be expressed in a linear form of $\tilde{\mathbf{z}} = \mathbf{H}\tilde{\mathbf{x}} + \mathbf{e}$ [110], where $\tilde{\mathbf{z}}$ is the equivalent measurement set with all the measurements with nonlinear measurement functions replaced by the equivalent measurements with lin-

ear measurement functions under the estimated system state set \tilde{x} . Then, by injecting an FDIA \mathbf{a} against the linear DSSE $\tilde{z} = \mathbf{H}\tilde{x} + \mathbf{e}$, we have $\tilde{z} + \mathbf{a} = \mathbf{H}\mathbf{x}_a + \mathbf{e}$, where \mathbf{x}_a is the new system state set after the FDIA \mathbf{a} . If the attackers can guarantee that, after the injection of FDIA \mathbf{a} , the attacked original measurement set \mathbf{z} can be converted to the equivalent measurement set $\tilde{z} + \mathbf{a}$ with the new system state set \mathbf{x}_a , and the proposed FDIAs based on the local state-based linear DSSE can be conducted on different types of original nonlinear WLS-based DSSE. After the FDIA, in general, for the original nonlinear DSSE with original measurement set \mathbf{z} , $\mathbf{z} + \mathbf{a} \neq \mathbf{h}(\mathbf{x}_a) + \mathbf{e}$, due to the difference between the linear measurement functions \mathbf{H} and the nonlinear measurement functions $\mathbf{h}(\cdot)$. However, if for the new system state set \mathbf{x}_a , there exists a constant set $\Delta\mathbf{z}$ that gives $(\mathbf{z} + \Delta\mathbf{z})|_{\mathbf{x}_a} = \tilde{z} + \mathbf{a}$, and the original measurements are compromised based on $\Delta\mathbf{z}$, instead of \mathbf{a} . Then, after the convergence of original nonlinear DSSE to the new system state set \mathbf{x}_a , the original nonlinear DSSE becomes $\tilde{z} + \mathbf{a} = \mathbf{H}\mathbf{x}_a + \mathbf{e}$. Thus, if the FDIA \mathbf{a} can bypass the LNR test based on linear DSSE, the attack vector $\Delta\mathbf{z}$ is an FDIA for the original nonlinear DSSE.

In the rest of this section, we will present the principles of three-phase coupled FDIAs against the proposed local state-based linear DSSE with equivalent measurement set \tilde{z} in details. In order to decouple the multiple phases into independent single phases to reduce the number of required measurements, the method used to construct three-phase decoupled FDIAs will also be introduced. Then, the modifications on original measurements, i.e., $\Delta\mathbf{z}$, for the FDIAs against the original nonlinear DSSE will be discussed.

FDIAs Against the Linear DSSE

In this subsection, the principles of the proposed three-phase coupled and decoupled FDIAs against the proposed local state-based linear DSSE will be presented.

A Three-phase Coupled FDIA Based on the linear DSSE in the form of $\tilde{z} = \mathbf{H}\mathbf{x} + \mathbf{e}$, after the injection of FDIA \mathbf{a} , the compromised measurement residual \mathbf{r}_a can be expressed as

$$\begin{aligned} \mathbf{r}_a &= \tilde{z}_a - \mathbf{H}\hat{\mathbf{x}}_a = \tilde{z} + \mathbf{a} - \mathbf{H}[\hat{\mathbf{x}} + (\mathbf{H}^T\mathbf{W}\mathbf{H})^{-1}\mathbf{H}^T\mathbf{W}\mathbf{a}] \\ &= \tilde{z} - \mathbf{H}\hat{\mathbf{x}} + \mathbf{a} - \mathbf{H}(\mathbf{H}^T\mathbf{W}\mathbf{H})^{-1}\mathbf{H}^T\mathbf{W}\mathbf{a}. \end{aligned} \quad (5.10)$$

If we let $\mathbf{a} = \mathbf{H}\mathbf{c}$, where \mathbf{H} is the measurement function set with the consideration of coupling among phases and \mathbf{c} is an arbitrary constant vector. The compromised measurements residual \mathbf{r}_a can be rewritten as

$$\begin{aligned} \mathbf{r}_a &= \tilde{z} - \mathbf{H}\hat{\mathbf{x}} + \mathbf{H}\mathbf{c} - \mathbf{H}(\mathbf{H}^T\mathbf{W}\mathbf{H})^{-1}(\mathbf{H}^T\mathbf{W}\mathbf{H})\mathbf{c} \\ &= \tilde{z} - \mathbf{H}\hat{\mathbf{x}} + \mathbf{H}\mathbf{c} - \mathbf{H}\mathbf{c} = \tilde{z} - \mathbf{H}\hat{\mathbf{x}} = \mathbf{r}. \end{aligned} \quad (5.11)$$

So, the compromised measurement residual \mathbf{r}_a after FDIA $\mathbf{a} = \mathbf{H}\mathbf{c}$ is the same as the measurement residual \mathbf{r} before FDIAs. Since the measurement residual \mathbf{r} can bypass the LNR test, the compromised measurement residual \mathbf{r}_a with malicious data can also bypass

the LNR test for the linear DSSE. By considering the three-phase coupling in the attack vector, the FDIA $\mathbf{a} = \mathbf{H}\mathbf{c}$ can always bypass the LNR test successfully. However, due to the coupling among phases, the modification on one phase will affect the other phases, which increase the number of required measurements to be compromised by the attackers.

A Three-phase Decoupled FDIA In order to reduce the number of required measurements, the three-phase modeling of the distribution system is decoupled into three independent single-phase models, by using the current compensation method, as follows:

$$\begin{aligned} [I_{kl}^a, I_{kl}^b, I_{kl}^c]^T &= \mathbf{Y}_{kl}[V_k^a - V_l^a, V_k^b - V_l^b, V_k^c - V_l^c]^T = (\mathbf{Y}_{kl}^d + \mathbf{Y}_{kl}^c)[V_k^a - V_l^a, V_k^b - V_l^b, \\ &V_k^c - V_l^c]^T, \end{aligned} \quad (5.12)$$

where the decoupled admittance matrix \mathbf{Y}_{kl}^d contains only the diagonal elements of matrix \mathbf{Y}_{kl} , while the compensation admittance matrix \mathbf{Y}_{kl}^c contains only the off-diagonal elements of matrix \mathbf{Y}_{kl} . Consider branch kl phase a as an example. For the measurement errors in the three-phase decoupling process, we have

$$\sigma^2(I_{kl}^{dec.a}) = \sigma^2(I_{kl.equ}^a - y_{kl}^{ab}(\tilde{V}_k^b - \tilde{V}_l^b) - y_{kl}^{ac}(\tilde{V}_k^c - \tilde{V}_l^c)) = \sigma^2(I_{kl.equ}^a). \quad (5.13)$$

This indicates that the consideration of the three-phase decoupling by the attacker will not affect the measurement error covariance matrix \mathbf{R} . Then, for the three-phase decoupling, the measurement function vector is decomposed into $\mathbf{H} = \mathbf{H}_d + \mathbf{H}'_d$, where \mathbf{H}_d is the measurement function set with \mathbf{Y} being replaced by \mathbf{Y}^d . The attack vector \mathbf{a} is set to $\mathbf{a} = \mathbf{H}_d\mathbf{c}$, such that the number of required measurements can be reduced. Let $\mathbf{E} = (\mathbf{H}^T\mathbf{W}\mathbf{H})^{-1}\mathbf{H}^T\mathbf{W}$, which is the pseudo inverse of the matrix \mathbf{H} , and $\mathbf{E}\mathbf{H} = \mathbf{I}$, where \mathbf{I} is an identity matrix, then

$$\mathbf{r}_a = \tilde{\mathbf{z}}_a - (\mathbf{H}_d + \mathbf{H}'_d)\hat{\mathbf{x}}_a = \mathbf{r} + (\mathbf{K} - \mathbf{I})\mathbf{H}'_d\mathbf{c}, \quad (5.14)$$

where the matrix \mathbf{K} is the hat matrix in the form of $\mathbf{K} = \mathbf{H}(\mathbf{H}^T\mathbf{W}\mathbf{H})^{-1}\mathbf{H}^T\mathbf{W}$. It can be observed that in order to reduce the total number of required measurements, the measurement residual \mathbf{r}_a after attack increases by $\Delta\mathbf{r}_a = (\mathbf{K} - \mathbf{I})\mathbf{H}'_d\mathbf{c}$. For different constructions of FDIAs, the increment in the measurement residual can be different, and this will be discussed in Subsection 5.1.3.

The Modifications on Original Measurements

For now, we have discussed the principles of three-phase coupled and three-phase decoupled FDIAs against linear DSSE. In the linear DSSE, the attack vector \mathbf{a} compromises the measurements in the equivalent measurement set $\tilde{\mathbf{z}}$, which includes the bus voltage measurements and equivalent current measurements $\mathbf{I}_{br.equ}$ and $\mathbf{I}_{bus.equ}$. However, as discussed in **Remark 1**, in order for the FDIAs constructed based on the linear DSSE to be

able to launch on the original nonlinear DSSE, the attackers need to know the required modifications on the original measurement set, i.e., the Δz .

In this subsection, the method to obtain Δz based only information of compromised measurements will be discussed. For the original complex power measurements $P + jQ$, we need to find the required changes Δz (i.e., the ΔP and ΔQ) for the corresponding attack vector \mathbf{a} . Accordingly, for the system complex bus voltage states after attack $\hat{V}_a = \hat{V} + \Delta V$, where \hat{V} is the estimated system state set before FDIA, and ΔV is the set of modifications on the system states introduced by the FDIA, we have $(z + \Delta z)|_{\hat{V}_a} = \tilde{z} + \mathbf{a}$, as discussed in **Remark 1**. Then, we have

$$\left(\frac{P + jQ + \Delta P + j\Delta Q}{\hat{V}_{a,re} + j\hat{V}_{a,im}} \right)^* = \tilde{z} + \mathbf{a} = (I_{equ,re} + jI_{equ,im}) + (I_{a,re} + jI_{a,im}), \quad (5.15)$$

where $\hat{V}_{a,re}$ and $\hat{V}_{a,im}$ are, respectively, the real and imaginary parts of the local voltage state of the bus with the compromised measurement. And $I_{equ,re}$ and $I_{equ,im}$ are the real and imaginary parts of the equivalent current measurements before the FDIA, respectively. While $I_{a,re}$ and $I_{a,im}$ are, respectively, the real and imaginary parts of malicious data injected by the attackers on the equivalent current measurements. Since the bus voltage magnitude in distribution system is close to 1 p.u., for the real part of this complex number, we have

$$(P + \Delta P)(\hat{V}_{re} + \Delta V_{re}) + (Q + \Delta Q)(\hat{V}_{im} + \Delta V_{im}) \approx I_{equ,re} + I_{a,re}, \quad (5.16)$$

where $\hat{V}_{a,re} = \hat{V}_{re} + \Delta V_{re}$ is the real part of the local voltage state after FDIA, and $I_{a,re}$ belongs to the attack vector \mathbf{a} . Similarly, for the imaginary part, we have

$$(P + \Delta P)(\hat{V}_{im} + \Delta V_{im}) - (Q + \Delta Q)(\hat{V}_{re} + \Delta V_{re}) \approx I_{equ,im} + I_{a,im}. \quad (5.17)$$

Since $(P\hat{V}_{re} + Q\hat{V}_{im}) \approx I_{equ,re}$ and $(P\hat{V}_{im} - Q\hat{V}_{re}) \approx I_{equ,im}$, we can derive

$$P\Delta V_{re} + \Delta P\hat{V}_{re} + \Delta P\Delta V_{re} + Q\Delta V_{im} + \Delta Q\hat{V}_{im} + \Delta Q\Delta V_{im} \approx I_{a,re} \quad (5.18)$$

$$P\Delta V_{im} + \Delta P\hat{V}_{im} + \Delta P\Delta V_{im} - Q\Delta V_{re} - \Delta Q\hat{V}_{re} - \Delta Q\Delta V_{re} \approx I_{a,im}. \quad (5.19)$$

By solving (5.18) and (5.19), ΔP and ΔQ can be determined as

$$\Delta P = \frac{ce + df}{c^2 + d^2}, \quad \Delta Q = \frac{de - cf}{c^2 + d^2}, \quad (5.20)$$

where $c = (\hat{V}_{re} + \Delta V_{re})$, $d = (\hat{V}_{im} + \Delta V_{im})$, $e = I_{a,re} - (P\Delta V_{re} + Q\Delta V_{im})$, and $f = I_{a,im} - (P\Delta V_{im} - Q\Delta V_{re})$. In order to determine the values of ΔP and ΔQ , the local information of the corresponding bus (i.e., $I_{a,re}$, $I_{a,im}$, V_{re} , V_{im} , ΔV_{re} , ΔV_{im} , P , and Q) is required. The methods to obtain these values are summarized as follows:

- The values of $I_{a,real}$ and $I_{a,imag}$ are based on the attack vector \mathbf{a} .

- The values of V_{re} , V_{im} , P , and Q can be obtained through the methods in [33], or measured directly.
- The values of ΔV_{re} and ΔV_{im} can be determined from $\mathbf{E}\mathbf{a}$, which does not require the estimated system states.

So, in order to construct an FDIA against the original nonlinear DSSE by using the proposed linear DSSE, only the local information about V_{re} , V_{im} , P , and Q are required.

Remark 2. *If the attacker changes some states by using $\mathbf{a} = \mathbf{H}\mathbf{c}$ (for three-phase coupled FDIA), or $\mathbf{a} = \mathbf{H}_d\mathbf{c}$ (for three-phase decoupled FDIA), the number of measurements required by the original nonlinear DSSE is the same as that required by the linear DSSE.*

For the FDIAs, in order to change the targeted states stealthily, the measurements have to be compromised coordinately. In three-phase coupled case, the modifications $\Delta\mathbf{V}$ on the system states can be determined as $\Delta\mathbf{V} = \mathbf{E}\mathbf{a} = (\mathbf{H}^T\mathbf{W}\mathbf{H})^{-1}\mathbf{H}^T\mathbf{W}\mathbf{a}$, and the attack vector $\mathbf{a} = \mathbf{H}\mathbf{c}$. Then, we have $\Delta\mathbf{V} = \mathbf{c}$. For the three-phase decoupled case, the attacker assumes that $\mathbf{H} = \mathbf{H}_d$ and uses the attack vector $\mathbf{a} = \mathbf{H}_d\mathbf{c}$, we have $\Delta\mathbf{V} = \mathbf{c}$. However, this introduces $\Delta\mathbf{r}_a$ to the measurements residual, as discussed in Subsection 5.1.2. Without considering the $\Delta\mathbf{r}_a$, the FDIA only changes the targeted states. So, for the buses, excluding the ones with the targeted states, $\Delta\mathbf{V} = \mathbf{0}$. Therefore, if $\mathbf{I}_a = \mathbf{0}$, the corresponding original power measurements are not required to be compromised. For the targeting buses without power measurements, there is no need to compromise any power measurements on these buses. So, the only original power measurements need to be compromised are the equivalent current measurements in \mathbf{a} with non-zero values. In other words, the FDIAs based on the proposed linear DSSE only need the corresponding local states of the compromised power measurements to be able to launch successfully against the original nonlinear DSSE. However, the FDIAs based directly on the original nonlinear DSSE require the information of the entire system states, which is extremely difficult for the attackers to obtain in practice.

5.1.3 The Construction of Attack Vectors

As discussed above, the attackers can firstly construct an FDIA vector \mathbf{a} based on the proposed local state-based linear DSSE. Then, the required modification $\Delta\mathbf{z}$, i.e., the FDIA vector on the original nonlinear DSSE can be derived using the methods in Subsection 5.1.2. In this section, the construction of attack vectors for the proposed three-phase coupled and decoupled FDIAs against the proposed local state-based linear DSSE are presented in detail.

Three-Phase Coupled Random FDIA

If the attacker wishes to construct random FDIAs with the consideration of three-phase coupling, the attack vector is given by $\mathbf{a} = \mathbf{H}\mathbf{c}$, as discussed in Subsection 5.1.2. Let $\mathbf{A} =$

$\mathbf{H}(\mathbf{H}^T \mathbf{H})^{-1} \mathbf{H}^T$, which is a square matrix. The equation $\mathbf{a} = \mathbf{H}\mathbf{c}$ for arbitrary constant \mathbf{c} can be rewritten as

$$\mathbf{A}\mathbf{a} = \mathbf{A}\mathbf{H}\mathbf{c} \Leftrightarrow \mathbf{A}\mathbf{a} = \mathbf{H}\mathbf{c} \Leftrightarrow \mathbf{A}\mathbf{a} = \mathbf{a} \Leftrightarrow (\mathbf{A} - \mathbf{I})\mathbf{a} = \mathbf{0}, \quad (5.21)$$

which means that the random attack vector \mathbf{a} has to satisfy $\mathbf{B}\mathbf{a} = \mathbf{0}$, where $\mathbf{B} = (\mathbf{A} - \mathbf{I})$, in order to bypass the LNR test. Let $\mathbf{a} = [\cdots, a_i, \cdots, a_j, \cdots, 0, \cdots, a_k, \cdots]^T$, where a_i, \cdots, a_k are the non-zero variables that the attacker wishes to inject on the corresponding meters and k is the total number of measurements that the attacker can compromise. Then, $\mathbf{B}\mathbf{a} = \mathbf{0}$ is equivalent to $\mathbf{B}'\mathbf{a}' = \mathbf{0}$, where \mathbf{B}' contains only the $i - k^{\text{th}}$ column vector of matrix \mathbf{B} and \mathbf{a}' contains only the $i - k^{\text{th}}$ elements of vector \mathbf{a} . So, the random attack vector can be constructed by solving $\mathbf{B}'\mathbf{a}' = \mathbf{0}$, and there is at least one non-zero solution, if and only if the rank of \mathbf{B}' is less than k . Also, \mathbf{a}' can be solved as $\mathbf{a}' = (\mathbf{I} - \mathbf{B}'^+ \mathbf{B}')\mathbf{d}$, where \mathbf{B}'^+ is the Moore-Penrose matrix inverse of matrix \mathbf{B}' , and \mathbf{d} is an arbitrary non-zero vector.

Three-Phase Decoupled Random FDIA

Perfect Three-Phase Decoupled Random FDIA

Remark 3. A perfect attack vector for three-phase decoupling is a attack vector $\mathbf{a} = \mathbf{H}_d \mathbf{c}$, with the constant vector \mathbf{c} that satisfies $\mathbf{H}'_d \mathbf{c} = \mathbf{H}\mathbf{b}$, where the vector \mathbf{b} is an arbitrary constant vector. The perfect three-phase decoupled attack does not change the measurement residual after FDIAs.

From (5.14), if we let $\mathbf{H}'_d \mathbf{c} = \mathbf{H}\mathbf{b}$, where \mathbf{b} is an arbitrary constant vector, then

$$\Delta r_a = (\mathbf{K} - \mathbf{I})\mathbf{H}\mathbf{b} = \mathbf{H}\mathbf{E}\mathbf{H}\mathbf{b} - \mathbf{H}\mathbf{b} = \mathbf{0}, \quad (5.22)$$

which means that, if $\mathbf{H}'_d \mathbf{c} = \mathbf{H}\mathbf{b}$, then the attack vector $\mathbf{a} = \mathbf{H}_d \mathbf{c}$ does not change the measurement residual and the compromised measurement residual r_a is the same as the measurement residual before FDIA. And the three-phase decoupled FDIA $\mathbf{a} = \mathbf{H}_d \mathbf{c}$ with $\mathbf{H}'_d \mathbf{c} = \mathbf{H}\mathbf{b}$ can always bypass the LNR test, which is a perfect three-phase decoupled FDIA. To remove the arbitrary constant vector \mathbf{b} , we rewrite $\mathbf{H}'_d \mathbf{c} = \mathbf{H}\mathbf{b}$ as

$$\mathbf{H}'_d \mathbf{c} = \mathbf{H}\mathbf{b} \Leftrightarrow \mathbf{A}\mathbf{H}'_d \mathbf{c} = \mathbf{A}\mathbf{H}\mathbf{b} \Leftrightarrow \mathbf{A}\mathbf{H}'_d \mathbf{c} = \mathbf{H}'_d \mathbf{c}. \quad (5.23)$$

Let $\mathbf{C} = (\mathbf{H}'_d \mathbf{H}_d)^{-1} \mathbf{H}'_d$. We have

$$\mathbf{a} = \mathbf{H}_d \mathbf{c} \Leftrightarrow \mathbf{C}\mathbf{a} = \mathbf{C}\mathbf{H}_d \mathbf{c} \Leftrightarrow \mathbf{C}\mathbf{a} = \mathbf{c}. \quad (5.24)$$

By substituting (5.24) into (5.23), we can obtain that the attack vector \mathbf{a} has to satisfy

$$\mathbf{A}\mathbf{H}'_d \mathbf{C}\mathbf{a} = \mathbf{H}'_d \mathbf{C}\mathbf{a} \Leftrightarrow (\mathbf{A}\mathbf{H}'_d \mathbf{C} - \mathbf{H}'_d \mathbf{C})\mathbf{a} = \mathbf{0}, \quad (5.25)$$

to construct a perfect three-phase decoupled FDIA. Similarly, with the three-phase coupled random attack, we define $\mathbf{a} = [\cdots, a_i, \cdots, a_j, \cdots, 0, \cdots, a_k, \cdots]^T$, and \mathbf{a}' contains only the

$i - k^{\text{th}}$ elements of vector \mathbf{a} . Let matrix $\mathbf{D} = (\mathbf{A}\mathbf{H}'_d\mathbf{C} - \mathbf{H}'_d\mathbf{C})$, and matrix \mathbf{D}' contains only the $i - k^{\text{th}}$ column vectors of matrix \mathbf{D} . The perfect three-phase decoupled random FDIA is obtained by solving $\mathbf{D}'\mathbf{a}' = \mathbf{0}$. In order to have non-zero solutions, the rank of \mathbf{D}' has to be less than k .

The perfect three-phase decoupled random FDIA has advantages than the three-phase coupled random FDIA, if and only if, for a given value of k which represents the number of measurements that can be compromised by the attackers, the smallest rank of \mathbf{D}' for all the possible attack vector \mathbf{a} is less than k , while the smallest rank of \mathbf{A}' for all the possible attack vector \mathbf{a} is larger than or equal to k . This means that the attackers can construct an FDIA with a smaller number of required measurements by using perfect three-phase decoupled random FDIA than using three-phase coupled random FDIA. This depends on the topology and the locations and types of measurements in a specific distribution system. Indeed, the equation $\mathbf{H}'_d\mathbf{c} = \mathbf{H}\mathbf{b}$ indicates how strong the coupling among the three phases in a specific distribution system is. If in some distribution systems the equation $\mathbf{H}'_d\mathbf{c} = \mathbf{H}\mathbf{b}$ cannot be satisfied strictly, the attacker can approximate it by using $\mathbf{H}'_d\mathbf{c} = \mathbf{H}\mathbf{b} + \boldsymbol{\delta}$, where $\boldsymbol{\delta}$ is a vector containing the measurement residual increments caused by approximating the multiphase and unbalanced distribution systems with three-phase decoupled model. Then the measurement residual changes $\Delta\mathbf{r}_a = (\mathbf{K} - \mathbf{I})\boldsymbol{\delta}$. If the largest value of vector $\boldsymbol{\delta}$ is very small, e.g., in the order of 10^{-11} , the measurement residual changes will be negligible comparing to the nominal measurement errors, which are typically $10^{-2} - 10^{-3}$ [246]. In other words, an attacker still has the confidence to launch the attack $\mathbf{a} = \mathbf{H}_d\mathbf{c}$, in order to reduce the number of measurements required.

Imperfect Three-Phase Decoupled Random Attack If there is no solution for $\mathbf{D}'\mathbf{a}' = \mathbf{0}$, and the largest value of $\boldsymbol{\delta}$ is significantly large, the measurement residual increases significantly, and no perfect three-phase decoupled FDIAs can be constructed.

Remark 4. *If the attacker uses the three-phase decoupled attack with significantly large value of $\max \boldsymbol{\delta}$, to reduce the number of required measurements, the measurement residual changes significantly. This is an imperfect three-phase decoupled FDIA, for which the probabilities of successful attacks can be derived numerically.*

The measurement residual after the injection of an imperfect attack vector $\mathbf{a} = \mathbf{H}_d\mathbf{c}$ is

$$\mathbf{r}_a = \mathbf{r} + (\mathbf{K} - \mathbf{I})\mathbf{H}'_d\mathbf{c} = (\mathbf{I} - \mathbf{K})\mathbf{e} + (\mathbf{K} - \mathbf{I})\mathbf{H}'_d\mathbf{c}. \quad (5.26)$$

Since the measurement errors are $\mathbf{e}_i \sim \mathcal{N}(0, \mathbf{R}_{ii})$ for all i , the mean of \mathbf{r}_a can be derived as

$$\boldsymbol{\mu}_{\mathbf{r}_a} = (\mathbf{K} - \mathbf{I})\mathbf{H}'_d\mathbf{c} = -\mathbf{S}\mathbf{H}'_d\mathbf{c}, \quad (5.27)$$

where $\mathbf{S} = (\mathbf{I} - \mathbf{K})$. The covariance of \mathbf{r}_a can be derived as

$$\boldsymbol{\Omega}_{\mathbf{r}_a} = \mathbf{E}(\mathbf{r}_a\mathbf{r}_a^T) = \mathbf{E}((\mathbf{r} + (\mathbf{K} - \mathbf{I})\mathbf{H}'_d\mathbf{c})(\mathbf{r} + (\mathbf{K} - \mathbf{I})\mathbf{H}'_d\mathbf{c})^T) = \mathbf{E}(\mathbf{r}\mathbf{r}^T), \quad (5.28)$$

where E donates the operation of expectation. Without the injection of attack vector, the distributions of measurement residuals are $\mathbf{r} \sim \mathcal{N}(\mathbf{0}, \mathbf{SR})$ [251]. After the injection of an imperfect attack vector $\mathbf{a} = \mathbf{H}_d \mathbf{c}$, the distributions of measurement residuals are $\mathbf{r}_a \sim \mathcal{N}(-\mathbf{S}\mathbf{H}'_d \mathbf{c}, \mathbf{SR})$, and $\frac{\mathbf{r}_a}{\sqrt{\text{diag}(\mathbf{SR})}} \sim \mathcal{N}(\frac{-\mathbf{S}\mathbf{H}'_d \mathbf{c}}{\sqrt{\text{diag}(\mathbf{SR})}}, \mathbf{1})$. Then, the normalized measurement residuals with bad data injection (i.e., the \mathbf{r}_a^N) are folded normal distributions with the cumulative distribution function (CDF) of the measurement residual, $F_i(y)$, for measurement i , expressed as

$$F_i(y) = Pr(r_{a,i}^N \leq y) = \begin{cases} \frac{1}{2} [erf(\frac{y+\mu_{r_{a,i}}}{\sqrt{2}}) + erf(\frac{y-\mu_{r_{a,i}}}{\sqrt{2}})], & \text{for } \mu_{r_{a,i}} \neq 0 \\ erf(\frac{y}{\sqrt{2}}), & \text{for } \mu_{r_{a,i}} = 0, \end{cases} \quad (5.29)$$

where $erf()$ represents the error function. The probability $Pr(\text{success})$ that the imperfect attack vector $\mathbf{a} = \mathbf{H}_d \mathbf{c}$ can bypass the LNR test, i.e., the $\max \mathbf{r}_a^N \leq \lambda$, can be expressed as

$$Pr(\text{success}) = Pr(\max \mathbf{r}_a^N \leq \lambda) = \prod_{i=1}^M F_i(y \leq \lambda), \quad (30)$$

where M is the total number of measurements. For an imperfect three-phase decoupled attack, the attacker needs to find a constant vector \mathbf{c} that compromises the desired number of measurements while having the largest probability of success, i.e., maximizing the probability $Pr(\text{success})$.

In order to derive the successful probability for imperfect three-phase decoupled FDIA, as discussed above, and calculate the modifications on original measurements, as discussed in Subsection 5.1.2, the attacker is required to have knowledge about the matrix \mathbf{R} . A potential solution to this problem is to approximate this matrix by using the nameplates of the measurement devices.

5.1.4 Case Study

To evaluate the performances of proposed FDIAs, the case studies are conducted using IEEE 13 Bus Test Feeder (Case I) and IEEE 37 Bus Test Feeder (Case II). In the case studies, the standard deviations of real-time measurements are considered to be 0.5% for phasor measurements and 1% for magnitude measurements. The pseudo measurements are considered to have 30% standard deviations [249]. The standard deviations of measurements of missing phases are set to be 1×10^{-6} . The threshold for the iteration process of the proposed linear DSSE is set to be $\epsilon = 1 \times 10^{-5}$. The LNR test threshold is $\lambda = 3$ [250]. For the voltage magnitude approximation, the value of parameters α and β for each phase, are given as $\alpha = 0.9992$ and $\beta = 0.0561$ for phase a, $\alpha = 0.8160$ and $\beta = 0.5791$ for phase b, and $\alpha = 0.8759$ and $\beta = 0.4841$ for phase c [248]. The systems topology and measurements of Cases I and II are shown in Fig. 5.2 and 5.3, respectively. For the IEEE 13 Bus Test Feeder, the buses 671 and 692, with the switch closed, are combined to bus 671. Bus 632 is selected as the slack bus. For the IEEE 37 Bus Test Feeder, bus 701 is selected as the slack bus. In

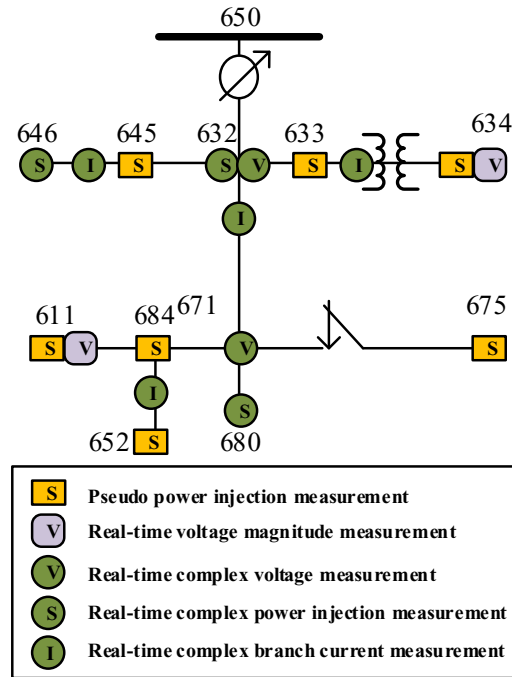


Figure 5.2: IEEE 13 Bus Test Feeder (Case I)

this research, without loss of generality for the investigation on vulnerability of DSSE to FDIAs, the optimal placement of real-time measurement devices is not considered. It is assumed that for all the buses without real-time complex power injection measurements, the pseudo measurements based on AMI data and/or historical data are always available. Thus, the systems are considered to be fully observable with enough measurements.

The estimation errors of proposed linear DSSE for Case I, under no attacks, are shown in Fig. 5.4. It can be observed that the mean estimation error is 0.16148%. For Case II, the mean estimation error is 0.2832%. The mean estimation errors for traditional nonlinear DSSE proposed in [252], with the same measurements, of these two cases, are 0.160025% and 0.2805%, respectively. The differences are small for both cases and are caused by the assumptions of 1 p.u. voltage magnitudes and the approximations of bus voltage magnitude measurements. To evaluate the performance of the proposed FDIAs in real application, different FDIAs are constructed based on the proposed method with the adoption of local state-based linear DSSE. And the constructed FDIAs are conducted in the WLS-based nonlinear DSSE in [252] to perform the LNR test. The LNRs of DSSE under no attacks, for Cases I and II, are shown in Fig. 5.5 and Fig. 5.6, respectively. It can be observed that the LNRs of 100 Monte Carlo (MC) simulations are all below the LNR test threshold for both cases. Then, for Cases I and II, we test simple attacks on phase c voltage magnitude of bus 611 and phase b voltage magnitude of bus 728, respectively. The results are shown in Fig. 5.5 and Fig. 5.6 for Cases I and II, respectively. It can be observed that simple attacks can always be detected in both cases. For Case I, we construct a three-phase coupled FDIA,

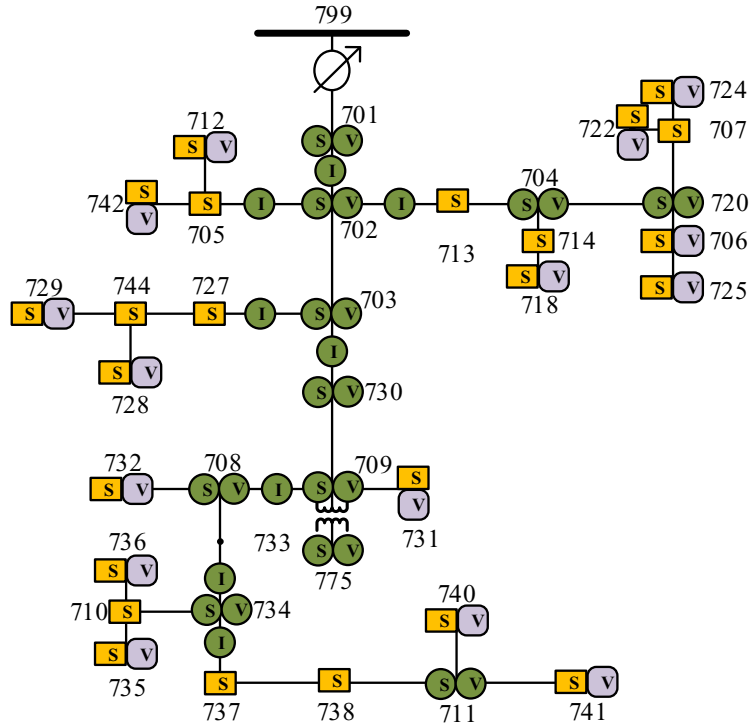


Figure 5.3: IEEE 37 Bus Test Feeder (Case II)

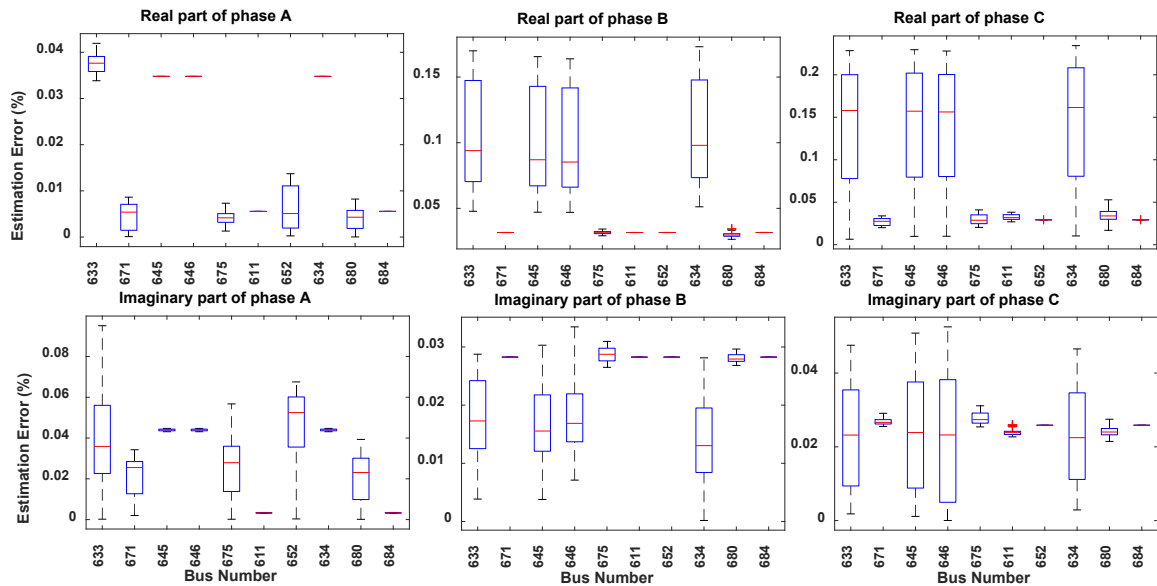


Figure 5.4: The estimation results under no attacks.

based on the method proposed in Subsection 5.1.3, targeting the phase c state of bus 611. The voltage profile after this FDIA is shown in Fig. 5.7, from which it can be observed that only the voltage at bus 611 has been changed. The LNR results are shown in Fig. 5.5. It can be observed that the LNRs for all MC simulations of this FDIA are all below 3. And it is almost the same as the LNR results for DSSE under no attacks. For Case II, a three-phase

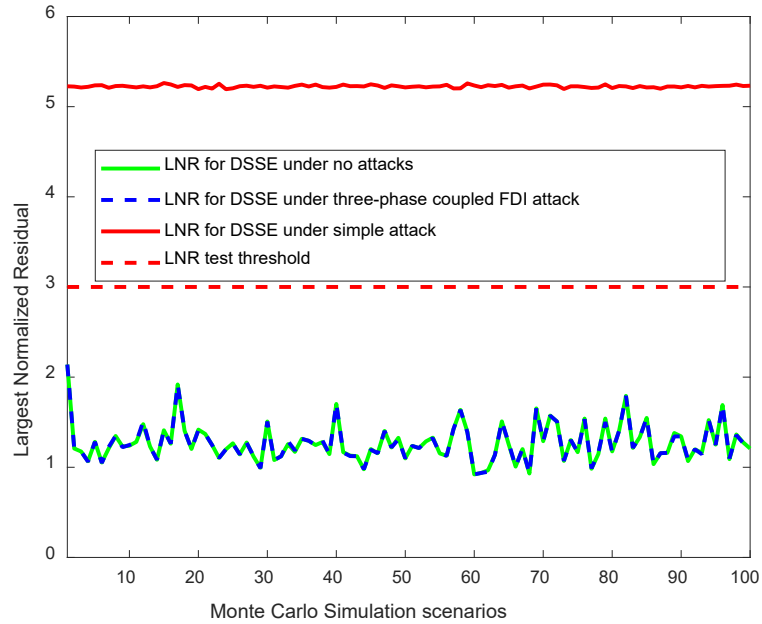


Figure 5.5: The LNR results for 100 MC simulations (Case I).

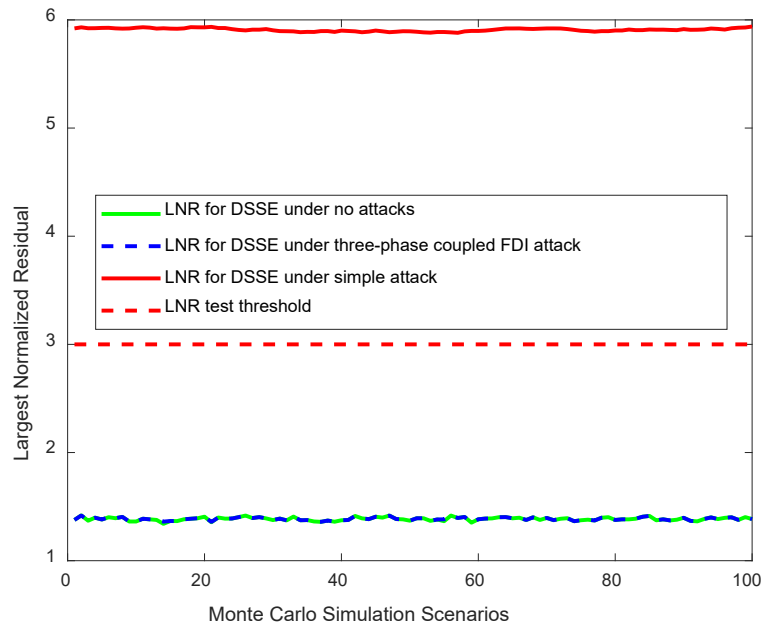


Figure 5.6: The LNR results for 100 MC simulations (Case II).

coupled FDIA on phase b state of bus 728 is constructed. As shown in Fig. 5.6, similar to Case I, the proposed three-phase coupled FDIA can also bypass the LNR test for all MC simulations in Case II.

Further, more attack scenarios are performed on both Case I and II to show the performance of the proposed FDIAs. In Case I, we conduct four more different FDIAs on the states of bus 633 phase a, bus 646 phase b, bus 652 phase a, and bus 675 phase c. The

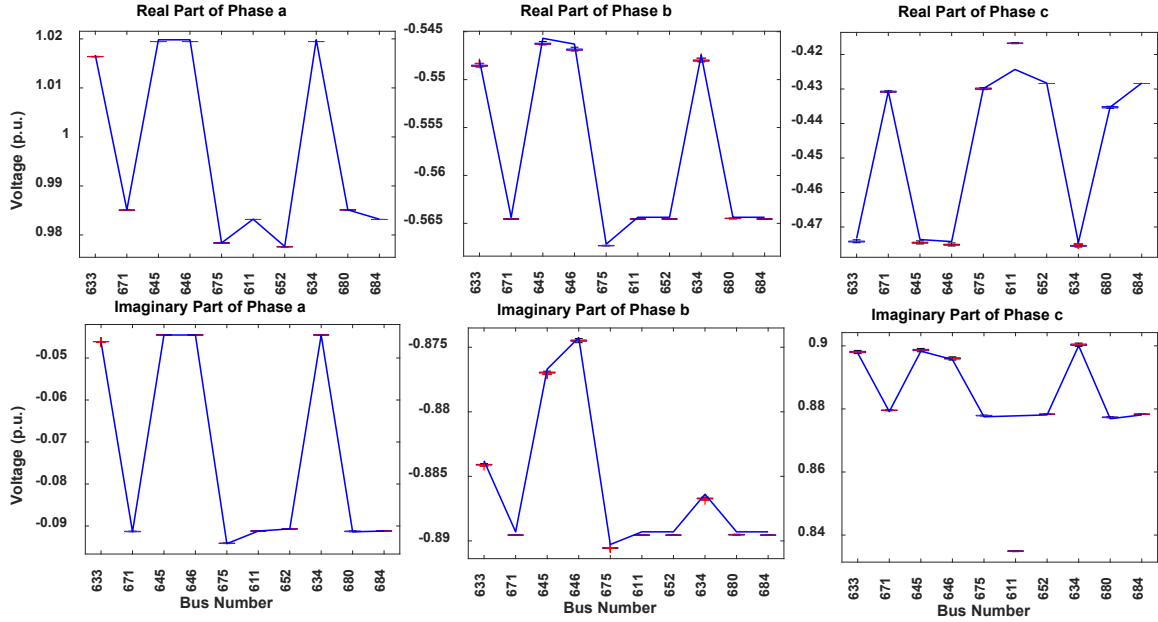


Figure 5.7: The bus voltage profile under attacks for Case I (The lines in blue are for the voltage profile under no attacks, and the boxplots in red are for the voltage profile under attacks).

corresponding results of these four FDIAs for Case I are shown in Fig. 5.8. For the Case II, the four more FDIAs conducted are on the states of bus 741 phase a, bus 731 phase c, bus 725 phase b, and bus 729 phase b. And the results of these four FDIAs for Case II are shown in Fig. 5.9. It can be observed from Fig. 5.8 and Fig. 5.9 that for both cases, the LNR test results of simple FDIA are always above the LNR test threshold, which means that the simple FDIA can always be detected. For the proposed three-phase coupled FDIAs, for both cases, the LNR test results of these four FDI scenarios are always below the LNR test threshold, and they are similar to the LNR test results under no attacks.

To compare the proposed three-phase coupled and perfect three-phase decoupled FDIAs, the phase b state of bus 645 and phase b state of bus 720 are selected as targeting states for Cases I and II, respectively. Firstly, the $\max \delta$ is set to be zero, which corresponds to the perfect three-phase decoupled FDIAs that give no measurement residual changes. The number of required measurements by the three-phase coupled and three-phase decoupled FDIAs, for both cases, are the same. This means that for the IEEE 13 and 37 Bus Test Feeders, the three phases cannot be decoupled completely with current measurements. Next, we set $\max \delta = 10^{-11}$, which gives negligible measurement residual changes comparing with the nominal measurement errors. For Case I, the number of required measurements by the three-phase coupled FDIA is 20, while that of the perfect three-phase decoupled FDIA is 10. Moreover, for Case II, the number of required measurements for three-phase coupled and perfect three-phase decoupled FDIAs are 24 and 19, respectively. For both cases, the number of required measurements has been reduced by using the proposed per-

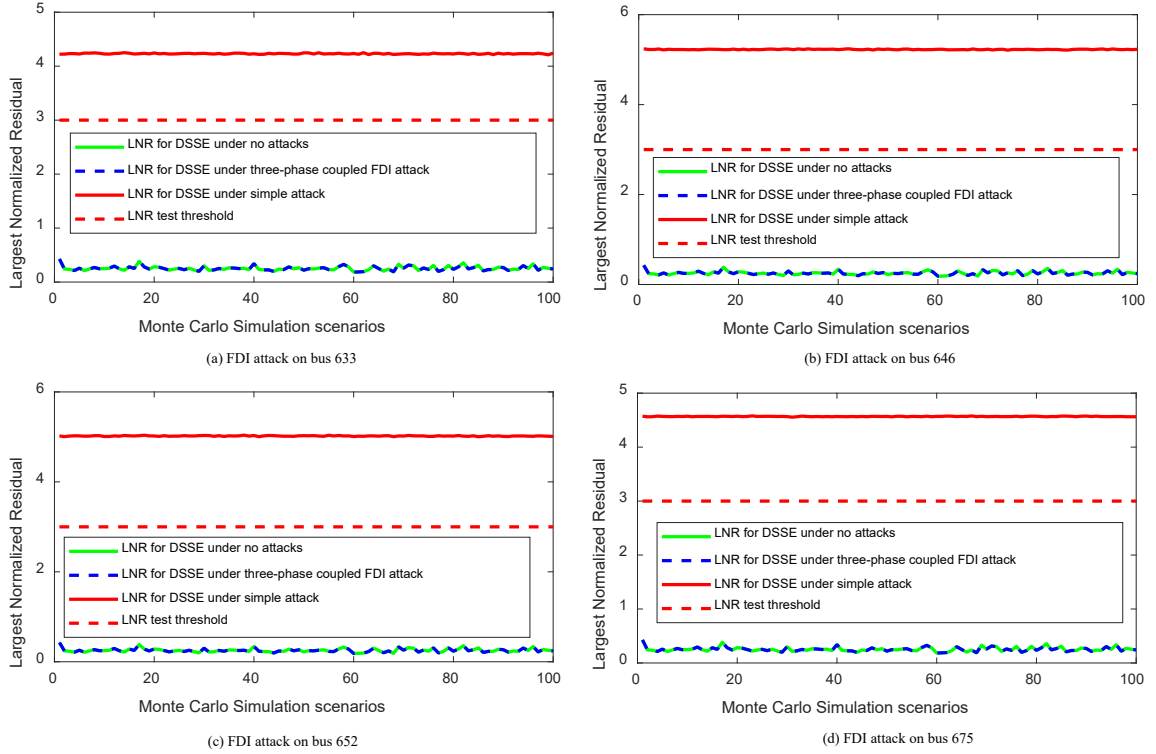


Figure 5.8: The LNR results for 100 MC simulations of Case I.

fect three-phase decoupled FDIAs. The corresponding LNR results for Cases I and II are shown in Fig. 5.10 and Fig. 5.11, respectively. It can be observed that, for both cases, the proposed three-phase decoupled FDIAs give almost the same LNR results as the three-phase coupled attacks, and they are all below the LNR test threshold. Also, we perform a brute search for the measurements of Case I and find out that the largest rank of matrix A , for three-phase coupled FDIAs, is 66, which is the total number of states. If all the three phases are completely decoupled, the theoretical value of the largest rank of matrix D , for perfect three-phase decoupled FDIAs, should be 33, which is one-third of the completely coupled three phases. However, in the case study, the largest rank of the matrix D is 42, which means that for the IEEE 13 Bus Test Feeder, only partial measurements are weakly three-phase coupled.

The imperfect three-phase decoupled FDIAs are compared with the three-phase coupled FDIAs by selecting different number of randomly attacked states. The numbers of required measurements, for Cases I and II, are shown in Fig. 5.12 and Fig. 5.13, respectively. It can be observed that, for both cases, the numbers of required measurements of the imperfect three-phase decoupled FDIAs are always smaller than that of three-phase coupled FDIAs. For both cases, the number of required measurements are converged to specific values as the number of randomly attacked states increases. This is due to the limits of real-time measurements that can be compromised. The probabilities of successful imperfect three-

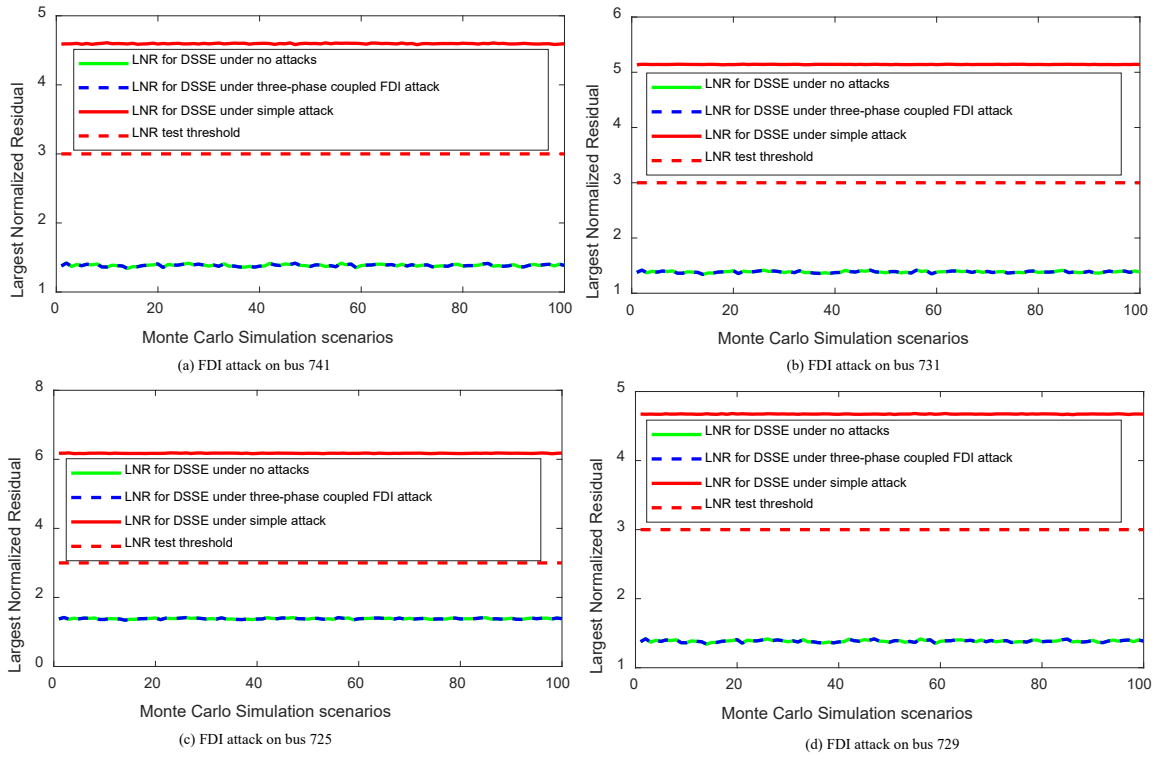


Figure 5.9: The LNR results for 100 MC simulations of Case II.

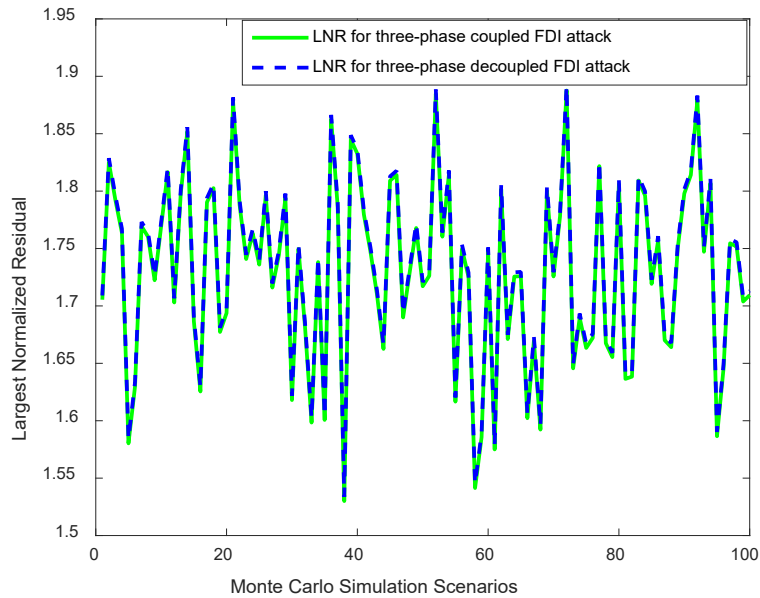


Figure 5.10: The LNR results for 100 MC simulations under attacks (Case I).

phase decoupled random attacks, for both cases, are calculated, based on exact matrix \mathbf{R} and approximated matrix $\hat{\mathbf{R}}$. The results are shown in Fig. 5.14 and Fig. 5.15, respectively. It can be observed that the calculated probabilities are close to the obtained through the MC simulations for both cases. And the errors introduced by approximating the matrix \mathbf{R}

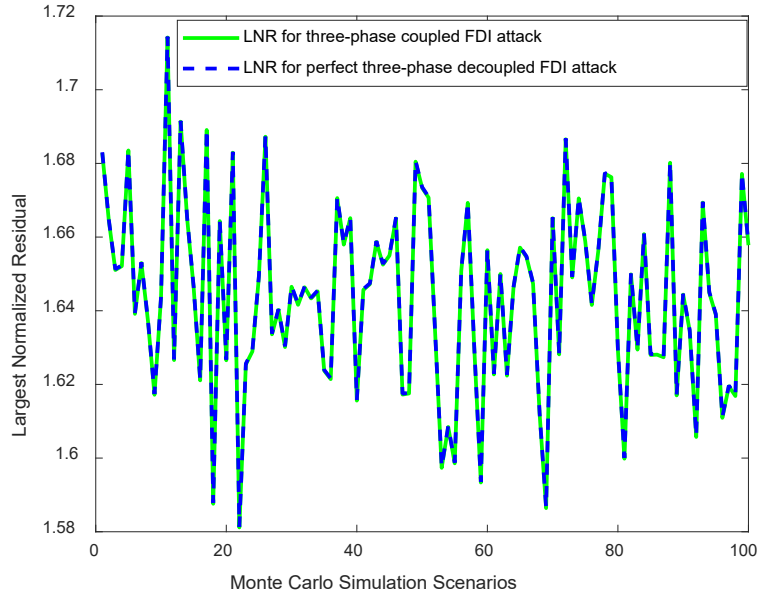


Figure 5.11: The LNR results for 100 MC simulations under attacks (Case II).

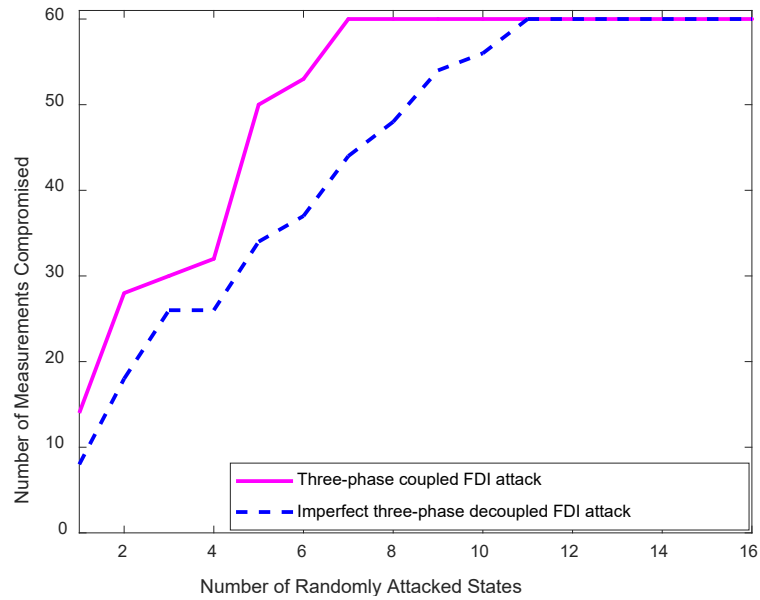


Figure 5.12: The required number of measurements to be compromised (Case I).

using nameplates are small.

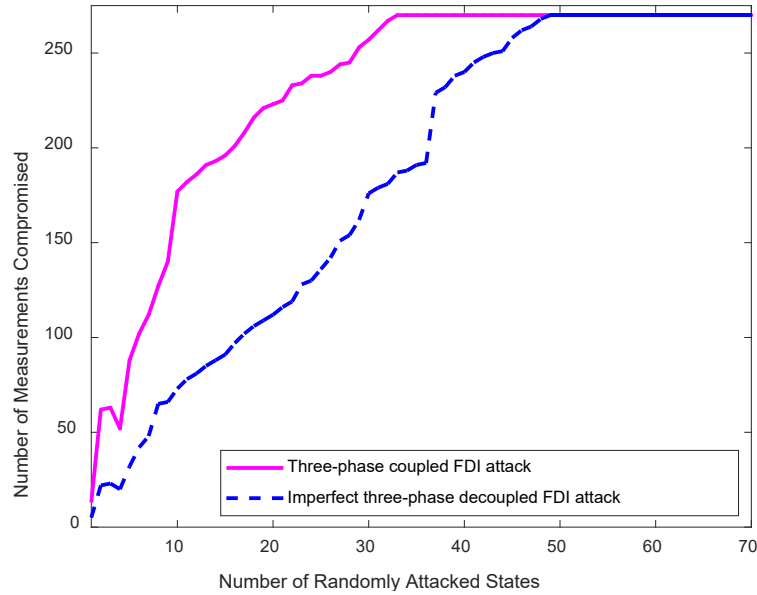


Figure 5.13: The required number of measurements to be compromised (Case II).

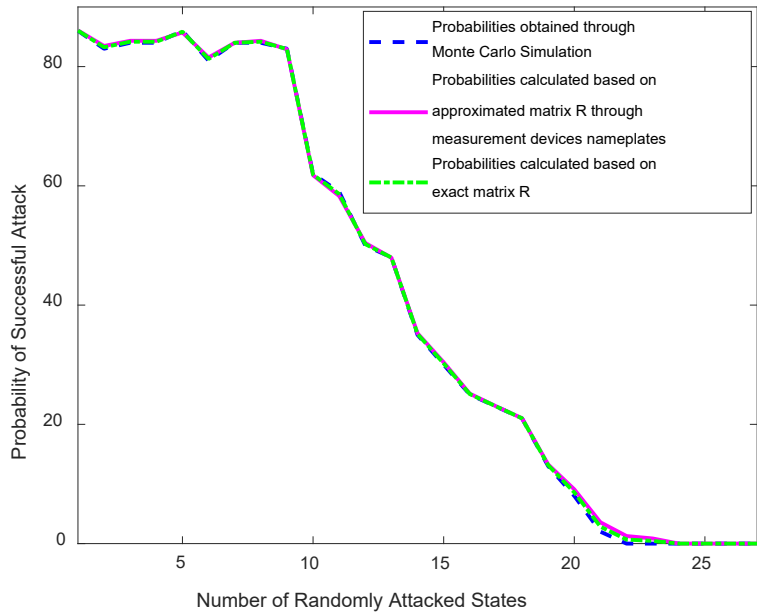


Figure 5.14: The probabilities of successful imperfect three-phase decoupled random attack (Case I).

5.2 False Data Injection Attacks Against State of Charge Estimation of BESSs in SDSs

In Section 5.1, the construction principle of FDIAs in SDSs has been studied, where the feasibility of practical FDIAs in the future SDSs has been discussed with insights. From the results in Section 5.1, it can be concluded that an adversary with limited capabilities is able

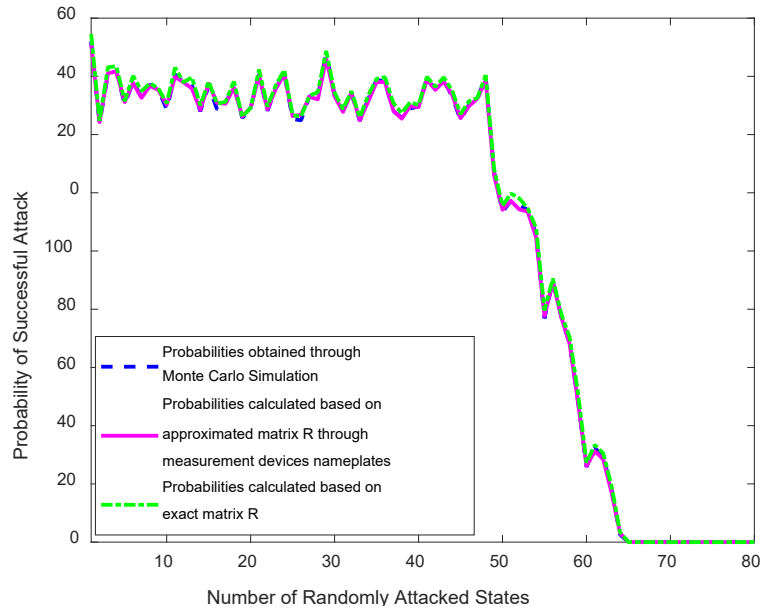


Figure 5.15: The probabilities of successful imperfect three-phase decoupled random attack (Case II).

to launch FDIAs against system information integrity of SDSs. As important system information of the stochastic energy management of BESSs in SDSs, the SoC of battery packs may also be prone to this kind of attack. In this section, the mechanisms of FDIAs against SoC estimation of BESSs in SDSs will be studied to provide guidelines for the development of countermeasures and stochastic energy management of BESSs that is resilient to this kind of attacks.

5.2.1 System Model

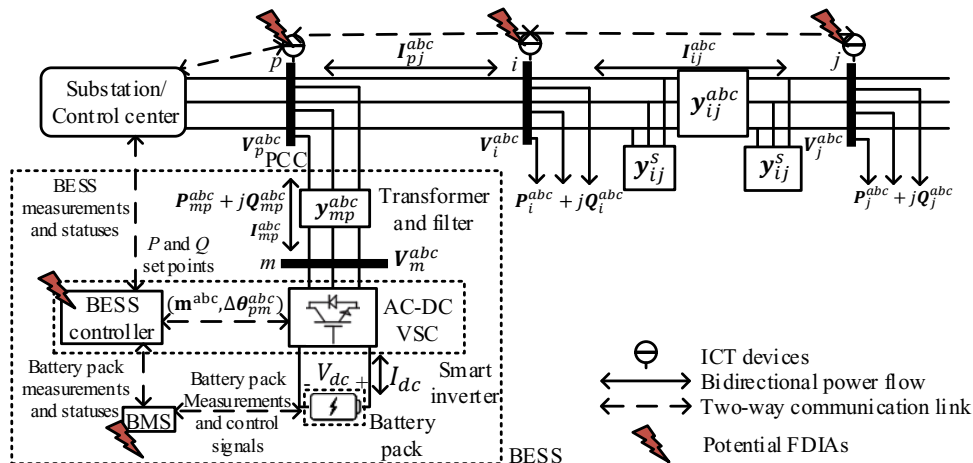


Figure 5.16: A typical architecture of SDSs with BESSs.

As shown in Fig. 5.16 [230], for an SDS with BESSs, the ICT devices collect measure-

ments, control electronic devices, and communicate with the control center located at substation through two-way communication links. The BESS connects at point of common coupling (PCC) through three-phase AC-DC voltage source converter (VSC), transformer, and filter with bidirectional power flows. The BESS controller determines the three-phase control variables of magnitude modulations m^{abc} and phase-displacement angles $\Delta\theta_{pm}^{abc}$, based on active and reactive power setpoints given by the control center. The BMS collects battery pack measurements, e.g., temperature, terminal voltage, and current, and estimates battery pack statuses, e.g., SoC and state of health (SoH), for battery pack monitoring and control [253]. The BESS measurements and statuses are transmitted to the control center by smart inverter for energy management. The potential FDIAs can be launched at ICT devices and smart inverter/BMS. In this research, the system steady states for discrete-time slots with equal length of Δt are considered. The model errors of DSSE and SoC estimation are not considered [25,29]. The complex variables are in polar coordinates, while \bar{x} , \hat{x} , and \tilde{x} denote the measurement, estimation and prediction of variable x , respectively.

Modeling for SDSs with BESSs

SDSs have phase imbalances and require for three-phase models. As shown in Fig. 5.16, the π model of feeder section ij of a solidly grounded SDS consists of 3×3 series admittance matrix \mathbf{y}_{ij}^{abc} and shunt admittance matrix \mathbf{y}_{ij}^s [254]. The current injections $\mathbf{I}^{abc} = [\mathbf{I}_1^{abc}, \dots, \mathbf{I}_i^{abc}, \dots, \mathbf{I}_N^{abc}]^T$, where N is the total number of buses and $\mathbf{I}_i^{abc} = [I_i^a, I_i^b, I_i^c]$, is calculated as

$$\mathbf{I}^{abc} = \mathbf{Y}^{abc} \mathbf{V}^{abc}, \quad (5.30)$$

where $\mathbf{V}^{abc} = [\mathbf{V}_1^{abc}, \dots, \mathbf{V}_i^{abc}, \dots, \mathbf{V}_N^{abc}]^T$ and $\mathbf{V}_i^{abc} = [V_i^a, V_i^b, V_i^c]$. \mathbf{Y}^{abc} is the nodal admittance matrix with diagonal entry \mathbf{Y}_{ii}^{abc} and off-diagonal entry \mathbf{Y}_{ij}^{abc} , for $i \neq j$, being calculated, respectively, as $\mathbf{Y}_{ii}^{abc} = \sum_{j \in \mathcal{A}_i} (\mathbf{y}_{ij}^{abc} + \mathbf{y}_{ij}^s)$ and $\mathbf{Y}_{ij}^{abc} = \mathbf{Y}_{ji}^{abc} = -\mathbf{y}_{ij}^{abc}$, where \mathcal{A}_i is the set of buses adjacent to bus i . As shown in Fig. 5.16, for each BESS, the transformer and filter are modeled as admittance matrix \mathbf{y}_{mp}^{abc} . The VSC is modeled using control variables m^{abc} and $\Delta\theta^{abc}$, AC-side resistor R_{ac} , and DC-side resistor R_{dc} [102]. Also, for m^α and $\Delta\theta^\alpha$ in phase α , the following equations hold for VSC:

$$m^\alpha = \sqrt{2}|V|_m^\alpha V_{dc}; \quad \Delta\theta_{pm}^\alpha = \theta_m^\alpha - \theta_p^\alpha, \quad (5.31)$$

where $|V|_m^\alpha$ is the voltage magnitude in phase α of AC-side bus, i.e., bus m in Fig. 5.16, and V_{dc} is the DC-side voltage. θ_m and θ_p are the corresponding phase angles. The following power balance equation holds for BESS with VSC losses:

$$\sum_{\alpha=\{a,b,c\}} P_{mp}^\alpha + (|I|_{mp}^\alpha)^2 R_{ac} + V_{dc} I_{dc} + V_{dc}^2 R_{dc} = 0, \quad (5.32)$$

where P_{mp}^{abc} and I_{mp}^{abc} relate to \mathbf{V}_m^{abc} and \mathbf{V}_p^{abc} through \mathbf{Y}_{mp}^{abc} . The DC-side voltage and current are assumed to be equivalent to battery pack terminal voltage and current, as in [255].

Measurements in SDSs with BESSs

The typical real-time measurements for SDSs are magnitudes of bus voltage $|\bar{V}|$ and branch current $|\bar{I}|$ measured by IEDs and other RTUs of SCADA systems and voltage phasor measurement $\bar{\theta}$ from μ PMUs [257]. Also, pseudo measurements for bus active \bar{P} and reactive \bar{Q} power injections are widely used [27]. For each BESS, the battery pack terminal voltage \bar{V}_{dc} and current \bar{I}_{dc} , and AC-side voltage magnitude $|\bar{V}|_{ac}$, active \bar{P}_{ac} and reactive \bar{Q}_{ac} power, and current flow magnitude $|\bar{I}|_{ac}$ are measured [102]. The control variables \bar{m} and $\Delta\bar{\theta}$ are also considered as real-time measurements. By inserting virtual admittance with arbitrary nonzero values for missing phases, the missing phases are analogous to zero-injection phases [256]. Then, for both missing and zero-injection phases, the corresponding voltage variables are eliminated [257].

DSSE for SDSs with BESSs

For SDSs with BESSs, the system state vector \mathbf{x} is defined as $\mathbf{x} = [|\mathbf{V}|_1^{abc}, \boldsymbol{\theta}_1^{abc}]^T$, where $|\mathbf{V}|_1^{abc}$ and $\boldsymbol{\theta}_1^{abc}$ are the magnitudes and phase angles of all bus voltages including the VSC AC-side bus voltages [102], except for missing and zero-injection phases. The phase angle of slack bus is selected as reference. The measurement vector $\mathbf{z} = [|\bar{V}|, |\bar{I}|, \bar{\theta}, \bar{P}, \bar{Q}, \bar{V}_{dc}, \bar{I}_{dc}, |\bar{V}|_{ac}, |\bar{I}|_{ac}, \bar{P}_{ac}, \bar{Q}_{ac}, \bar{m}, \Delta\bar{\theta}]^T$ relate to \mathbf{x} through measurement functions $\mathbf{h}(\cdot)$ as $\mathbf{z} = \mathbf{h}(\mathbf{x}) + \boldsymbol{\delta}$, where $\mathbf{h}(\cdot)$ are derived based on (5.30), (5.31), and (5.32) using the formations in [258]. $\boldsymbol{\delta}$ are independent random measurement noises following normal distributions with zero means. The corresponding weighted least square (WLS)-based DSSE is formulated as an optimization problem as below:

$$\hat{\mathbf{x}} = \arg \min_{\mathbf{x}} (\mathbf{z} - \mathbf{h}(\mathbf{x}))^T \mathbf{W} (\mathbf{z} - \mathbf{h}(\mathbf{x})), \quad (5.33)$$

where $\hat{\mathbf{x}}$ are the estimated system states and \mathbf{W} is the weight matrix for measurements. In this research, the wide choice for $\mathbf{W} = \text{diag}\{\sigma_1^{-2}, \dots, \sigma_k^{-2}, \dots, \sigma_M^{-2}\}$, where σ_k^2 is the variance of k^{th} measurement noise and M is the total number of measurements, in [27] is considered. Optimization problem (5.33) is solved iteratively using Gauss-Newton method.

Measurement Residual-based BDD in DSSE

In DSSE, bad measurements may be introduced from various sources e.g., meter reading failures or cyber-physical attacks. As an important function of DSSE, the system operators consider the geographical correlations and statistics of measurement noises for BDD based on measurement residual $\|\Delta\hat{\mathbf{z}}\|_2 = \|\mathbf{z} - \hat{\mathbf{z}}\|_2$, where $\hat{\mathbf{z}}$ is the estimated measurements calculated from $\mathbf{h}(\hat{\mathbf{x}})$ using estimated system states $\hat{\mathbf{x}}$. For normally distributed measurement noises $\boldsymbol{\delta}$, the squared measurement residual $\|\Delta\hat{\mathbf{z}}\|_2^2$ follows chi-square (χ^2) distribution with $(|\mathbf{z}| - |\mathbf{x}|)$ degrees of freedom, where $|\mathbf{z}|$ and $|\mathbf{x}|$ represent the cardinalities of \mathbf{z} and \mathbf{x} , respectively. The hypothesis test is used to determine threshold τ with significance level λ , such that $\|\Delta\hat{\mathbf{z}}\|_2 > \tau$ indicates bad data with false alarm probability of λ [102].

Extended Kalman Filter for SoC Estimation of BESSs

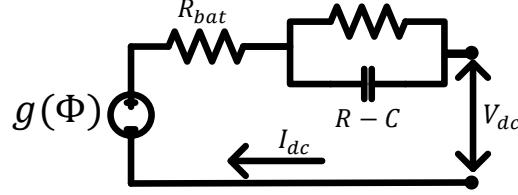


Figure 5.17: Unit model of battery pack.

The battery pack of a BESS typically consists of multiple cells for voltage and power requirements [259]. The consideration of estimated SoCs of all cells for precise SoC estimation of BESSs usually results in high computational complexities and implementation costs [260]. In practice, the unit model of battery pack is generally adopted for SoC estimation [53], where the cell screening is used for improved cell balancing [53]. Then, the unit model as shown in Fig. 5.17 consists of lumped parameters of battery resistor R_b , R-C pair for first-order dynamics, terminal voltage V_{dc} , current I_{dc} , and OCV $g(\Phi)$ as a nonlinear function of battery pack SoC Φ . These parameters are estimated by recursive least-square (RLS) filter as in [53]. Based on the unit model, the extended Kalman filter (EKF) has been widely used for SoC estimation [52]. Based on this, SoC is estimated with predict and update. The predicted SoC $\tilde{\Phi}_t$ is obtained with estimated SoC $\hat{\Phi}_{t-1}$ and current measurement \bar{I}_{dc}^{t-1} using Coulomb counting method as

$$\tilde{\Phi}_t = \hat{\Phi}_{t-1} + \frac{\Delta t}{C_{bat}} \bar{I}_{dc}^{t-1}, \quad (5.34)$$

where C is the battery pack nominal capacity. The predicted variance $\tilde{\mathcal{P}}_t$ of estimation error is calculated as $\tilde{\mathcal{P}}_t = \hat{\mathcal{P}}_{t-1} + Q$, where Q is the variance of Gaussian white process noise with zero mean. Then, $\tilde{\Phi}_t$ is updated based on terminal voltage measurement \bar{V}_{dc}^t for time slot t as follows:

$$\hat{\Phi}_t = \tilde{\Phi}_t + K_t(\bar{V}_{dc}^t - \tilde{V}_{dc}^t), \quad (5.35)$$

where \tilde{V}_{dc}^t is the predicted terminal voltage and is calculated based on $\tilde{\Phi}_t$, and K_t is the Kalman gain given by $K_t = \frac{\partial g(\Phi)}{\partial \Phi} \big|_{\tilde{\Phi}_t} \tilde{\mathcal{P}}_t [(\frac{\partial g(\Phi)}{\partial \Phi} \big|_{\tilde{\Phi}_t})^2 \tilde{\mathcal{P}}_t + \mathcal{R}]^{-1}$, where \mathcal{R} is the assumed measurement noise variance. Also, the variance of estimation error is updated as $\hat{\mathcal{P}}_t = (1 - K_t \frac{\partial g(\Phi)}{\partial \Phi} \big|_{\tilde{\Phi}_t}) \tilde{\mathcal{P}}_t$. In practice, the initial SoC estimation, i.e., $\hat{\Phi}_0$, is obtained when the battery pack has been staying in open circuit for a few hours [12].

Construction Principle of FDIAs against SoC Estimation of BESSs in SDSs

The vulnerability of BESSs to FDIAs has been widely studied by exploiting the security of communication networks [28]. However, there is a lack of analytical analysis of the vulnerability of BESSs to FDIAs. In this section, the construction principle of FDIAs against SoC

estimation is analyzed through the construction of static FDIAs targeting on one snapshot of SoC estimation. Based on this, the vulnerability of SoC estimation of BESSs to FDIAs is investigated analytically through the theoretical derivation of SoC estimation errors caused by FDIAs. Also, a detection method based on an innovation test is proposed to analyze the temporal correlation characteristics of measurements in SoC estimations of BESSs.

Construction of Static FDIAs against SoC Estimation

The construction principle of static FDIAs targeting on one snapshot of DSSE in [256] is considered. The attack vector ε on measurement data that can bypass measurement residual-based BDD in Subsection 5.2.1 is determined strategically as

$$\varepsilon = \mathbf{h}(\hat{\mathbf{x}} + \boldsymbol{\vartheta}) - \mathbf{h}(\hat{\mathbf{x}}), \quad (5.36)$$

where $\boldsymbol{\vartheta}$ are manipulations on estimated states introduced by ε . Intuitively, the objective of a FDIA against SoC estimation is to maximize the absolute difference between the actual and estimated SoC. Based on (5.34) and (5.35), the estimated SoC $\hat{\Phi}_t$ is determined recursively with measurements \bar{V}_{dc}^t and \bar{I}_{dc}^t as

$$\hat{\Phi}_t = \hat{\Phi}_{t-1} + \frac{\Delta t}{C_{bat}} \bar{I}_{dc}^{t-1} + K_t(\bar{V}_{dc}^t - \tilde{V}_{dc}^t), \quad (5.37)$$

where the measurement value \bar{V}_{dc}^t and predicted value \tilde{V}_{dc}^t of battery pack terminal voltage are expressed, respectively, as

$$\bar{V}_{dc}^t = g(\Phi_t) + V_{rc}^t + I_{dc}^t R_{bat} + \delta_{\bar{V}_{dc}}^t \quad (5.38)$$

$$\tilde{V}_{dc}^t = g(\tilde{\Phi}_t) + \hat{V}_{rc}^t + (I_{dc}^t + \delta_{\bar{I}_{dc}}^t) R_{bat}, \quad (5.39)$$

where $\delta_{\bar{V}_{dc}}^t$ and $\delta_{\bar{I}_{dc}}^t$ are measurement noises of battery pack terminal voltage and current, respectively. Since the variance of R-C pair voltage for measurement noise is minimal, $V_{rc}^t = \hat{V}_{rc}^t$ [263]. Then, the term $\bar{V}_{dc}^t - \tilde{V}_{dc}^t$ in (5.37) can be expressed based on (5.38) and (5.39) as

$$\bar{V}_{dc}^t - \tilde{V}_{dc}^t = g(\Phi_t) - g(\tilde{\Phi}_t) - R_{bat} \delta_{\bar{I}_{dc}}^t + \delta_{\bar{V}_{dc}}^t, \quad (5.40)$$

where, based on (5.34), $g(\Phi_t) - g(\tilde{\Phi}_t)$ can be determined as

$$\begin{aligned} g(\Phi_t) - g(\tilde{\Phi}_t) &= g\left(\Phi_{t-1} + \frac{\Delta t}{C_{bat}} I_{dc}^{t-1}\right) - g\left(\hat{\Phi}_{t-1} + \frac{\Delta t}{C_{bat}} (I_{dc}^{t-1} + \delta_{\bar{I}_{dc}}^{t-1})\right) \\ &= \beta \left(\Delta \Phi_{t-1} - \frac{\Delta t}{C_{bat}} \delta_{\bar{I}_{dc}}^{t-1}\right), \end{aligned} \quad (5.41)$$

where $\Delta \Phi_{t-1} = \Phi_{t-1} - \hat{\Phi}_{t-1}$ is the SoC estimation error for time slot $t - 1$ caused by measurement noises. The second equality holds due to that, for proper range of SoC estimation, $g(\Phi)$ can be linearized with constant slope $\beta > 0$ [264]. Then, by combining (5.37),

(5.40), and (5.41), $\Delta\Phi_t$ can be evaluated as

$$\Delta\Phi_t = \Phi_t - \hat{\Phi}_t = (1 - \beta K_t)\Delta\Phi_{t-1} - (1 - \beta K_t)\frac{\Delta t}{C_{bat}}\delta_{\bar{I}_{dc}}^{t-1} + K_t(R_{bat}\delta_{\bar{I}_{dc}}^t - \delta_{\bar{V}_{dc}}^t). \quad (5.42)$$

By injecting attack vector ε_t on measurements for time slot t , the difference between actual and estimated SoC becomes $\Delta\Phi_t^\varepsilon$ which can be expressed as

$$\begin{aligned} \Delta\Phi_t^\varepsilon &= (1 - \beta K_t)\Delta\Phi_{t-1} - (1 - \beta K_t)\frac{\Delta t}{C_{bat}}\delta_{\bar{I}_{dc}}^{t-1} + K_t(R_{bat}\delta_{\bar{I}_{dc}}^t - \delta_{\bar{V}_{dc}}^t + R_{bat}\varepsilon_{\bar{I}_{dc}}^t - \varepsilon_{\bar{V}_{dc}}^t) \\ &= K_t(R_{bat}\varepsilon_{\bar{I}_{dc}}^t - \varepsilon_{\bar{V}_{dc}}^t) + \Delta\Phi_t, \end{aligned} \quad (5.43)$$

where $\varepsilon_{\bar{V}_{dc}}^t$ and $\varepsilon_{\bar{I}_{dc}}^t$ are tampers on measurements \bar{V}_{dc} and \bar{I}_{dc} , respectively. From (5.43), it can be observed that by injecting ε_t , $\Delta\Phi_t^\varepsilon$ will deviate from $\Delta\Phi_t$. Then, the optimization problem of an adversary for maximizing the absolute difference between actual and estimated SoC can be expressed as

$$\max_{\varepsilon_t} |\Delta\Phi_t^\varepsilon| \quad (5.44)$$

subject to

$$\varepsilon_t = \mathbf{h}(\hat{\mathbf{x}}_t + \boldsymbol{\vartheta}_t) - \mathbf{h}(\hat{\mathbf{x}}_t) \quad (5.45)$$

$$\mathbf{e}_{\bar{m}\alpha}^T(\mathbf{z}_t + \varepsilon_t) \leq \bar{m}, \quad \forall \alpha \in \{a, b, c\} \quad (5.46)$$

$$-\bar{I}_{dc} \leq \mathbf{e}_{\bar{I}_{dc}}^T(\mathbf{z}_t + \varepsilon_t) \leq \bar{I}_{dc} \quad (5.47)$$

$$\underline{V}_{dc} \leq \mathbf{e}_{\bar{V}_{dc}}^T(\mathbf{z}_t + \varepsilon_t) \leq \bar{V}_{dc} \quad (5.48)$$

$$\mathbf{e}_{\bar{P}_{ac}}^T(\mathbf{z}_t + \varepsilon_t) = P_{ac}^{set}; \quad \mathbf{e}_{\bar{Q}_{ac}}^T(\mathbf{z}_t + \varepsilon_t) = Q_{ac}^{set}, \quad (5.49)$$

where $\mathbf{e}_{\{\cdot\}}$ is standard basis vector and \bar{m} is the upper limit of magnitude modulation for stable operation. Also, \bar{I}_{dc} is battery pack current limit, while \underline{V}_{dc} and \bar{V}_{dc} are battery pack voltage limits. Constraint (5.49) is for the active and reactive power setpoints. After the compensation of initial SoC variation that is typically achieved in a few steps [265], the EKF becomes time-invariant and asymptotically stable. The EKF estimation error variance \hat{P} reaches a steady-state value with a constant $K \in (0, 1/\beta)$ [267]. It is assumed that, before the attack, the EKF is already in a steady state with constant gain. The objective function $\max_{\boldsymbol{\vartheta}_t} |\Delta\Phi_t^\varepsilon|$ can be relaxed to $\max_{\boldsymbol{\vartheta}_t} \Delta\Phi_t^\varepsilon$ for underestimation or $\min_{\boldsymbol{\vartheta}_t} \Delta\Phi_t^\varepsilon$ for overestimation. Without loss of generality, in the rest of this thesis, only the case of underestimation is considered, and the results of which can be easily applied to the case of overestimation.

Detection of Static FDIAs against SoC Estimation

Due to constraint (5.45), the attack vector obtained from (5.44) can bypass the BDD in Subsection 5.2.1. In this section, the detection of this kind of static FDIA against SoC estimation using EKF innovation test on measurement \bar{V}_{dc}^t will be discussed. The innovation $\Delta\tilde{V}_{dc}^t$ of EKF-based SoC estimation is the difference between measurement and predicted values of

terminal voltage [14] and is expressed as $\Delta\tilde{V}_{dc}^t = \bar{V}_{dc}^t - \tilde{V}_{dc}^t$. Based on (5.40) and (5.41), $\Delta\tilde{V}_{dc}^t$ can be derived as

$$\Delta\tilde{V}_{dc}^t = \beta(\Delta\Phi_{t-1} - \frac{\Delta t}{C_{bat}}\delta_{\bar{I}_{dc}}^{t-1}) - R_{bat}\delta_{\bar{I}_{dc}}^t + \delta_{\bar{V}_{dc}}^t, \quad (5.50)$$

where, based on (5.42), $\Delta\Phi_{t-1}$ is determined recursively as

$$\Delta\Phi_{t-1} = \prod_{l=1}^{t-1} (1 - \beta K_l) \Delta\Phi_0 - \sum_{l=1}^{t-1} \left\{ \prod_{l'=l+1}^{t-1} (1 - \beta K_{l'}) [(1 - \beta K_l) \frac{\Delta t}{C_{bat}} \delta_{\bar{I}_{dc}}^{l-1} + K_l (R_{bat} \delta_{\bar{I}_{dc}}^l - \delta_{\bar{V}_{dc}}^l)] \right\}, \quad (5.51)$$

where $\Delta\Phi_0$ follows normal distribution with zero mean and variance \mathcal{P}_0 [268]. Then, the mean of $\Delta\Phi_{t-1}$ is zero. As $t \rightarrow \infty$, the steady-state variance $\sigma^2[\Delta\Phi_{t-1}]$, by considering the constant Kalman gain K in Subsection 5.2.1, converges to

$$\sigma^2[\Delta\Phi_{t-1}] = \frac{[(\frac{1}{K} - \beta) \frac{\Delta t}{C_{bat}}]^2 + R_{bat}^2 \sigma_{\delta_{\bar{I}_{dc}}}^2 + \sigma_{\delta_{\bar{V}_{dc}}}^2}{2\beta/K - \beta^2}. \quad (5.52)$$

Since the i.i.d. random variables $\Delta\Phi_0$, $\delta_{\bar{I}_{dc}}$, and $\delta_{\bar{V}_{dc}}$ follow normal distributions, $\Delta\Phi_{t-1}$ also follows normal distribution with zero mean and variance (5.52). Then, $\Delta\tilde{V}_{dc}^t$ follows normal distribution with zero mean and variance expressed as

$$\sigma^2[\Delta\tilde{V}_{dc}^t] = \frac{[(\frac{1}{K} - \beta) \frac{\Delta t}{C_{bat}}]^2 + R_{bat}^2 \sigma_{\delta_{\bar{I}_{dc}}}^2 + \sigma_{\delta_{\bar{V}_{dc}}}^2}{2/\beta K - 1} - [(\beta \frac{\Delta t}{C_{bat}})^2 + R_{bat}^2 \sigma_{\delta_{\bar{I}_{dc}}}^2 + \sigma_{\delta_{\bar{V}_{dc}}}^2]. \quad (5.53)$$

By injecting attacks $\varepsilon_{\bar{V}_{dc}}$ and $\varepsilon_{\bar{I}_{dc}}$, the deviation of innovation is $-(R_{bat}\varepsilon_{\bar{I}_{dc}} - \varepsilon_{\bar{V}_{dc}})$. Based on (5.43), for any successful static FDIA against SoC estimation, i.e., $\Delta\Phi_t^\varepsilon \neq \Delta\Phi_t$, the term $R_{bat}\varepsilon_{\bar{I}_{dc}} - \varepsilon_{\bar{V}_{dc}} \neq 0$, which modifies the value of innovation $\Delta\tilde{V}_{dc}^t$. Based on innovation squared test statistic [269], the square of attack-free $\Delta\tilde{V}_{dc}^t$ follows central χ^2 distribution with a freedom of 1. With a specified false alarm probability λ^{ekf} , a threshold τ^{ekf} can be defined as in [102]. Then, a static FDIA against BESS SoC estimation will be detected if $\|\Delta\tilde{V}_{dc}^t\|_2 > \tau^{ekf}$ with false alarm probability of λ^{ekf} .

5.2.2 Sequential FDIAs against SoC Estimation of BESSs within SDSs

In Subsection 5.2.1, the innovation test-based detection for static FDIAs against SoC estimation is discussed. In [36], the construction of FDIAs against innovation test is studied, where a FDIA that can bypass the innovation test is constructed as

$$-\sqrt{\tau^{ekf}} \leq \bar{V}_{dc}^t - \tilde{V}_{dc}^t + \varepsilon_{\bar{V}_{dc}}^t - R_{bat}\varepsilon_{\bar{I}_{dc}}^t \leq \sqrt{\tau^{ekf}}. \quad (5.54)$$

However, the feasible solutions of $\varepsilon_{\bar{V}_{dc}}^t$ and $\varepsilon_{\bar{I}_{dc}}^t$ for (5.54) are relatively small, which results in insignificant impacts of static FDIAs against SoC estimation constructed based on (5.54) [39]. It can be observed from (5.37) that, besides tampering \bar{V}_{dc}^t and \bar{I}_{dc}^t , the tamperers on

measurements for time slot $t - 1$ also misleads the SoC estimation for time slot t . Then, a sequential FDIA against SoC estimation is proposed, where the adversary at current time slot $t - L + 1$ constructs a sequence of attack vectors $\bar{\varepsilon}_t^L = [\varepsilon_{t-L+1}, \dots, \varepsilon_t, \dots, \varepsilon_t]$ targeting on SoC estimation for future time slot t .

Mechanism of Sequential FDIA with Post-Attack Compromising against SoC Estimation

With the moderate temperature and estimation horizon, the R-C pair dynamics and battery degradation do not vary significantly [35]. Then, with a moderate attacking horizon \mathcal{L} , i.e., from $t - L + 1$ to t , there are no significant changes on lumped parameters, and the EKF-based SoC estimation is approximated as an RLS filter [270]. Then, with L time-series measurements $\bar{V}_{dc}^{L,t}$ and $\bar{I}_{dc}^{L,t}$ from time slot $t - L + 1$ to t , $\hat{\Phi}_t$ is obtained from the following optimization problem [271]:

$$\hat{\Phi}_t = \arg \min_{\Phi_t} \frac{1}{2} \sum_{l \in \mathcal{L}} (\bar{V}_{dc}^l - f_l(\Phi_t))^2, \quad (5.55)$$

where $f_l(\Phi_t)$ recursively relates Φ_t to V_{dc}^l for time slot l using Coulomb counting method and is expressed as

$$V_{dc}^l = f_l(\Phi_t) = g(\Phi_t) - \sum_{l'=l}^{t-1} \frac{\beta \Delta t}{C_{bat}} I_{dc}^{l'} + V_{rc}^l + I_{dc}^l R_{bat}, \quad (5.56)$$

where β is the constant slope defined in Subsection 5.2.1. Similarly, considering the minimal variance of V_{rc} as in (5.40), the measurement residual $\Delta \hat{V}_{dc}^l$ is calculated based on (5.56) as

$$\Delta \hat{V}_{dc}^l = \bar{V}_{dc}^l - \hat{V}_{dc}^l = f_l(\Phi_t) - f_l(\hat{\Phi}_t) = \beta \Delta \Phi_t + \sum_{l'=l}^{t-1} \frac{\beta \Delta t}{C_{bat}} \delta_{I_{dc}}^{l'} - R_{bat} \delta_{I_{dc}}^l + \delta_{V_{dc}}^l. \quad (5.57)$$

By substituting (5.57) into (5.55), $\Delta \Phi_t$ is determined from optimality condition $\sum_l \Delta \hat{V}_{dc}^l \partial \Delta \hat{V}_{dc}^l / \partial \Phi_t = 0$ for $\Phi_t = \hat{\Phi}_t$ as

$$\Delta \Phi_t = \frac{1}{\beta L} \sum_{l \in \mathcal{L}} (R_{bat} \delta_{I_{dc}}^l - \delta_{V_{dc}}^l - \sum_{l'=l}^{t-1} \frac{\beta \Delta t}{C_{bat}} \delta_{I_{dc}}^{l'}). \quad (5.58)$$

By introducing sequential FDIA $\bar{\varepsilon}_t^L$, the difference between actual and estimated SoC $\Delta \Phi_t^{\bar{\varepsilon}_t^L}$ is expressed as

$$\Delta \Phi_t^{\bar{\varepsilon}_t^L} = \frac{1}{\beta L} \sum_{l \in \mathcal{L}} (R_{bat} \varepsilon_{I_{dc}}^l - \varepsilon_{V_{dc}}^l - \sum_{l'=l}^{t-1} \frac{\beta \Delta t}{C_{bat}} \varepsilon_{I_{dc}}^{l'}) + \Delta \Phi_t. \quad (5.59)$$

The optimization problem of an adversary with sequential FDIA $\bar{\varepsilon}_t^L$ over SoC estimation horizon \mathcal{L} is expressed as

$$\max_{\bar{\varepsilon}_t^L} \Delta\Phi_t^{\bar{\varepsilon}_t^L} \quad (5.60)$$

subject to

$$|\bar{V}_{dc}^l - \tilde{V}_{dc}^l - R_b e_{I_{dc}}^T \varepsilon_l + e_{V_{dc}}^T \varepsilon_l| \leq \sqrt{\tau^{ekf}}, \quad \forall l \in \mathcal{L} \quad (5.61)$$

constraints (5.45)-(5.49), $\forall l \in [t - L + 1, t]$,

where constraint (5.61) is for FDIA to bypass the innovation test following (5.54).

By injecting FDIA $\bar{\varepsilon}_t^{L*}$ obtained from (5.60) over the attacking horizon \mathcal{L} , the estimated SoC for time slot t deviates from the actual SoC by a large value. However, the inaccurately estimated SoC for t results in a large innovation for $t + 1$, which alters the suspicious SoC estimation. Therefore, the adversary needs to continue injecting attack vectors for post-attack compromising of sequential FDIAs. More specifically, the post-attack compromising of a sequential FDIA targeting on time slot t can be achieved by following the steps below:

1. Set $l = t + 1$,
2. If $|\bar{V}_{dc}^l - \tilde{V}_{dc}^l| \leq \sqrt{\tau^{ekf}}$, go to 5); else, go to 3),
3. Solve the following problem for ε_l^* and go to 4)

$$\max_{\varepsilon_l} |\bar{V}_{dc}^l - \tilde{V}_{dc}^l + e_{V_{dc}}^T \varepsilon_l - R_b e_{I_{dc}}^T \varepsilon_l|$$

subject to

constraints (5.45)-(5.49) and (5.61),

4. Inject ε_l^* to compromise sequential FDIA $\bar{\varepsilon}_t^L$ for time slot l , and repeat 2) - 4) with $l = l + 1$,
5. End for post-attack compromising.

An Online Approach for Practical Construction of Sequential FDIAs

Since each ε of $\bar{\varepsilon}_t^L$ modifies \bar{V}_{dc} and \bar{I}_{dc} with small values and V_{dc} and I_{dc} are within their limits during normal operation [35], the range of ε_l under constraints (5.45)-(5.49) is not affected by $\varepsilon_{l' \neq l}$. Then, under constraints (5.45)-(5.49), the attack vectors of a sequential FDIA are independent. However, according to (5.40), for any $k + 1 \in \mathcal{L}$, constraint (5.61) can be revised as

$$|\Delta\Phi_{k+1} + \beta(\Delta\Phi_k^{\bar{\varepsilon}_k} - \frac{\Delta t}{C} \varepsilon_{I_{dc}}^k) - R_b \varepsilon_{I_{dc}}^{k+1} + \varepsilon_{V_{dc}}^{k+1}| \leq \sqrt{\tau^{ekf}}, \quad (5.62)$$

where $\Delta\Phi_{k+1} = \beta(\Delta\Phi_k - \frac{\Delta t}{C}\delta_{I_{dc}}^k) - \delta_{I_{dc}}^{k+1}R_b + \delta_{V_{dc}}^{k+1}$ is the SoC estimation error for time slot $k+1$ caused by measurement noises, and $\Delta\Phi_k^{\vec{\varepsilon}^k}$ is the SoC estimation error caused by attack vectors up to k of a sequential FDIA, which is expressed as

$$\Delta\Phi_k^{\vec{\varepsilon}^k} = \sum_{l=t-L+1}^k \left(\frac{R_b\varepsilon_{I_{dc}}^l - \varepsilon_{V_{dc}}^l}{\beta L'} - \sum_{l'=l}^{k-1} \frac{\beta\Delta t}{CL'}\varepsilon_{I_{dc}}^{l'} \right), \quad (5.63)$$

where $L' = k-t+L$. According to (5.62) and (5.63), the range of ε_{k+1} under constraint (5.61) depends on attack vectors up to k . Since $\vec{\varepsilon}_t^L$ is determined at time slot $t-L+1$, the system states, active and reactive power setpoints, and measurements for time slot $l > t-L+1$ are unknown. This results in great challenges on the construction of practical sequential FDIAs. In this section, an online approach for practical construction of sequential FDIAs is proposed. For any time slot $k+1$, $\Delta\Phi_t^{\vec{\varepsilon}_t^L}$ can be reformulated using the expression of $\Delta\Phi_k^{\vec{\varepsilon}^k}$ in (5.63) as

$$\begin{aligned} \Delta\Phi_t^{\vec{\varepsilon}_t^L} &= \frac{1}{\beta L} \{ (\beta(k-t+L)(\Delta\Phi_k^{\vec{\varepsilon}^k} - \frac{\Delta t}{C}\varepsilon_{I_{dc}}^k) + [R_b - (k-t+L+1)]\frac{\beta\Delta t}{C})\varepsilon_{I_{dc}}^{k+1} - \varepsilon_{V_{dc}}^{k+1} \\ &\quad + \Delta\Phi_t^{\vec{\varepsilon}^{k+2}} \} + \Delta\Phi_t, \end{aligned} \quad (5.64)$$

where $\Delta\Phi_t^{\vec{\varepsilon}^{k+2}}$ depends only on attack vectors after time slot $k+1$. The optimal sequential FDIA can be denoted as $\vec{\varepsilon}_t^{L*} = [\vec{\varepsilon}_{-k}^*, \varepsilon_{k+1}^*, \vec{\varepsilon}_{k+2}^*]$, where $\vec{\varepsilon}_{-k}^*$ and $\vec{\varepsilon}_{k+2}^*$ are the components of optimal sequential FDIA $\vec{\varepsilon}_t^{L*}$ for time slots $[t-L+1, k]$ and $[k+2, t]$, respectively. By considering $\varepsilon_{V_{dc}}^{k+1*} = \Delta\varepsilon_{V_{dc}}^{k+1*} - \beta(\Delta\Phi_k^{\vec{\varepsilon}^k} - \frac{\Delta t}{C}\varepsilon_{I_{dc}}^{k*})$, $\Delta\Phi_t^{\vec{\varepsilon}_t^{L*}}$ is determined following (5.64) as

$$\begin{aligned} \Delta\Phi_t^{\vec{\varepsilon}_t^{L*}} &= \Delta\Phi_t + \frac{1}{\beta L} [(\beta(k-t+L+1)(\Delta\Phi_k^{\vec{\varepsilon}^k} - \frac{\Delta t}{C}\varepsilon_{I_{dc}}^{k*}) + \Delta\Phi_t^{\vec{\varepsilon}^{k+2}}) + \max_{\Delta\varepsilon_{V_{dc}}^{k+1}, \varepsilon_{I_{dc}}^{k+1}} \frac{1}{\beta L} \\ &\quad \{ [R_b - (k-t+L+1)]\frac{\beta\Delta t}{C}\varepsilon_{I_{dc}}^{k+1} - [\Delta\varepsilon_{V_{dc}}^{k+1} - \beta(\Delta\Phi_k^{\vec{\varepsilon}^k} - \frac{\Delta t}{C}\varepsilon_{I_{dc}}^{k*})] \}], \end{aligned} \quad (5.65)$$

and the constraint (5.61) can be reformulated following (5.62) with $\varepsilon_{V_{dc}}^{k+1} = \Delta\varepsilon_{V_{dc}}^{k+1} - \beta(\Delta\Phi_k^{\vec{\varepsilon}^k} - \frac{\Delta t}{C}\varepsilon_{I_{dc}}^{k*})$ as

$$\begin{aligned} |\Delta\Phi_{k+1} + \beta(\Delta\Phi_k^{\vec{\varepsilon}^k} - \frac{\Delta t}{C}\varepsilon_{I_{dc}}^{k*}) - R_b\varepsilon_{I_{dc}}^{k+1} + \Delta\varepsilon_{V_{dc}}^{k+1} - \beta(\Delta\Phi_k^{\vec{\varepsilon}^k} - \frac{\Delta t}{C}\varepsilon_{I_{dc}}^{k*})| &\leq \sqrt{\tau^{ekf}} \\ \iff |\Delta\Phi_{k+1} - R_b\varepsilon_{I_{dc}}^{k+1} + \Delta\varepsilon_{V_{dc}}^{k+1}| &\leq \sqrt{\tau^{ekf}}. \end{aligned} \quad (5.66)$$

From the above equation, it can be observed that the ranges of variables $\varepsilon_{I_{dc}}^{k+1}$ and $\Delta\varepsilon_{V_{dc}}^{k+1}$ depend only on $\Delta\Phi_{k+1}$ which is not affected by the attack vectors of other time slots. This indicates that, for each time slot $l \in \mathcal{L}$, the adversary only needs solve the optimization

problem expressed as follows:

$$\max_{\Delta \varepsilon_{V_{dc}}^l, \varepsilon_{I_{dc}}^l} \frac{1}{\beta L} [R_b \varepsilon_{I_{dc}}^l - (\Delta \varepsilon_{V_{dc}}^l - \beta (\Delta \Phi_{l-1}^{\varepsilon_{I_{dc}}^*} - \frac{\Delta t}{C} \varepsilon_{I_{dc}}^{l-1*})) - (l - t + L) \frac{\beta \Delta t}{C} \varepsilon_{I_{dc}}^l] \quad (5.67)$$

subject to

$$e_{V_{dc}}^T \varepsilon_l = \Delta \varepsilon_{V_{dc}}^l - \beta (\Delta \Phi_{l-1}^{\varepsilon_{I_{dc}}^*} - \frac{\Delta t}{C} \varepsilon_{I_{dc}}^{l-1*}) \quad (5.68)$$

$$e_{I_{dc}}^T \varepsilon_l = \varepsilon_{I_{dc}}^l \quad (5.69)$$

constraints (5.45)-(5.49) and (5.66).

For the current time slot l , the adversary determines the optimal attack vector ε_l^* by solving (5.67), which only requires the information of system states, active and reactive power setpoints, and measurements for l and the value of $\beta (\Delta \Phi_{l-1}^{\varepsilon_{I_{dc}}^*} - \frac{\Delta t}{C} \varepsilon_{I_{dc}}^{l-1*})$ depending on the attack vectors for time slots preceding l . Then, the attack vector for each time slot within the attacking horizon \mathcal{L} can be determined dynamically.

For practical sequential FDIAs, the assumption about the insignificant changes of the lumped parameters, which is feasible for regular BESS operation with a moderate estimation horizon [35], is required. Thus, one of the possible directions for countermeasures against sequential FDIAs is to leverage the concept of CPVD. In power systems, the application of CPVD for the detection of FDIAs has been widely studied based on distributed flexible AC transmission system (D-FACTS) [272]. For the BESSs that lack capability for system typologies or parameters alternating, the inserting of watermarks [273] on the dynamics of R-C pairs can significantly alternate lumped parameters dynamically. However, there still requires great challenges in designing optimal watermarks that can cause significant variations of the dynamics of R-C pairs while imposing the least impacts on the performance of SoC estimation.

5.2.3 Case Studies

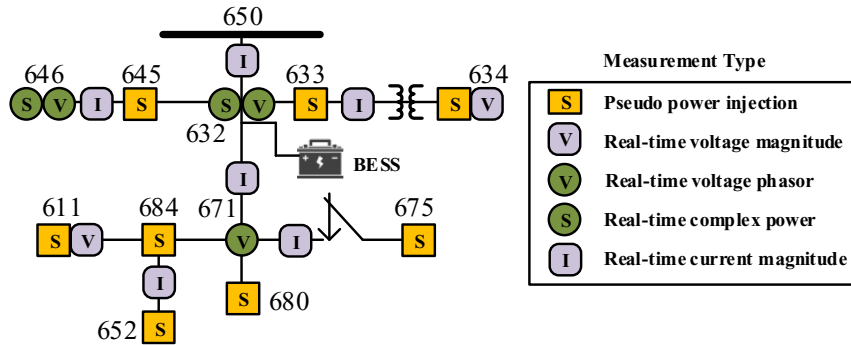


Figure 5.18: Modified IEEE 13 bus test feeder with BESS at bus 632.

In this section, the case studies based on the modified IEEE 13 bus test feeder in [256] are performed to investigate the vulnerability of BESS SoC estimation to FDIAs in SDSs.

Table 5.1
BATTERY PACK RATINGS

Nominal Capacity	571.9kWh/816Ah
Nominal Power	250kW
Nominal DC Voltage	700.8V
DC Voltage Range	595.2 – 787.2V
Nominal DC Current	357A
DC Current Range	–400 – 400A

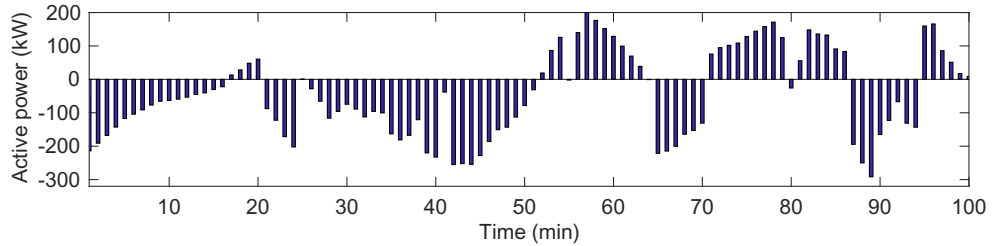


Figure 5.19: Active power setpoints for BESS.

The system topology and measurement deployments are illustrated in Fig. 5.18, where the bus 650 is selected as the slack bus. For all buses, the pseudo measurements for active and reactive power injections are always available to have a fully observable SDS. Considering the statistics of measurement noises, the case studies are performed under Monte Carlo simulations with 100 scenarios. For real-time measurements, the standard deviations are 1% and 0.5% for magnitude and phasor measurements. The standard deviations of pseudo measurements are 30% [274]. For measurement residual-based BDD and innovation test, the measurement residuals and innovations are normalized using standard deviations. The thresholds τ and τ^{ekf} are selected, respectively, as 4.5854 and 1.960 for a confidence level of 95%.

For BESS connecting at bus 632, the Lithium-ion battery pack with well-balanced cells in [275] is considered, and the ratings are listed in Table 5.1. This battery pack consists of 12 parallel racks, where each rack is formed by 12 modules connecting in series. For each module, the 16 cells rating at 68Ah and 3.1 – 4.1V for each cell are connected in series. The BESS active power setpoints considered are shown in Fig. 5.19, and the reactive power setpoints are assumed to be all zeros. The initial SoC of BESS is set to be 84%. The experimental OCV data for Lithium-ion battery is obtained from [276] for ambient temperature at 25°C and SoC range of 14% – 100%. The operational SoC range is considered as 20% – 95%, within which the battery resistor is $R_{bat} = 0.2816\Omega$ for each rack and the slope of OCV function is $\beta \approx 1.75V/1\%SoC$. Considering the impacts of dynamic R-C pair, the battery pack model of Matlab/Simulink [277] is used for SoC estimation based on EKF, in which the ambient temperature is 23°C and the temperature characteristics of all cells are well balanced. It should be noted that, as discussed in Subsection 5.2.1 and 5.2.2, for the construction of static and sequential FDIAs and detection of static FDIAs, the explicit

R-C pair model is not required, due to the minimal V_{rc} variance caused by measurement noises. For the EKF process, $Q = 0.1$ and $\mathcal{R} = 10$. The attacking horizon in sequential FDIAs is $L = 60$ with $\Delta t = 60s$.

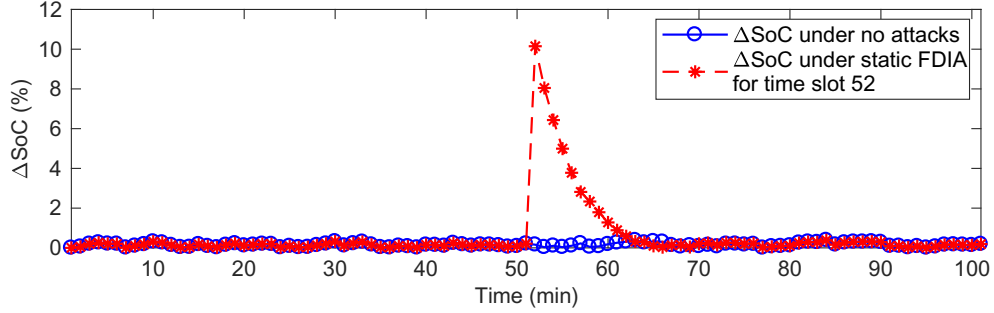


Figure 5.20: Static FDIA against SoC estimation.

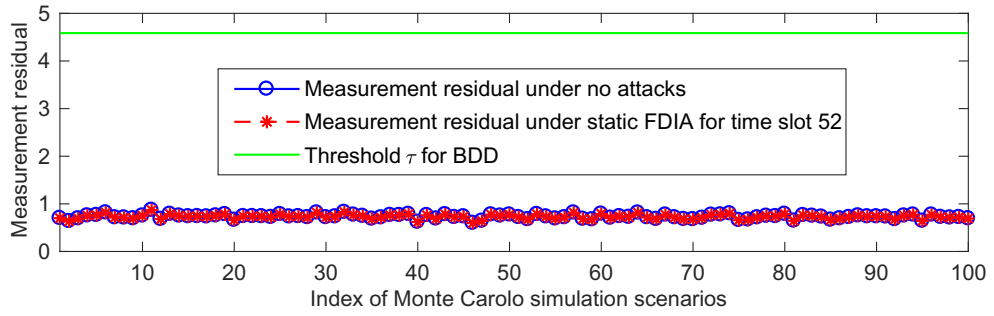


Figure 5.21: Measurement residual under static FDIA.

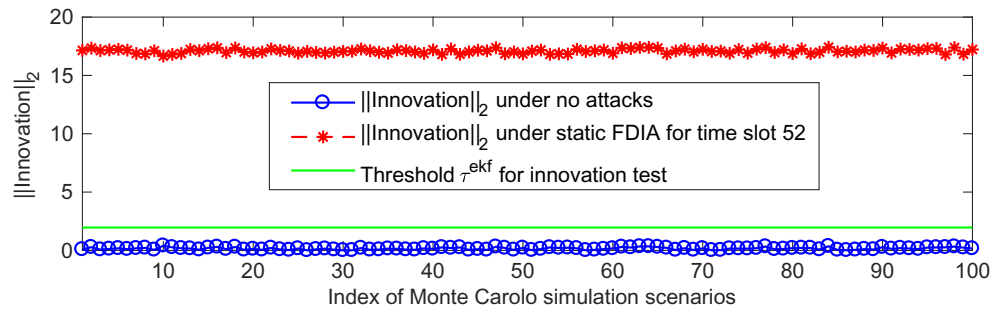


Figure 5.22: Innovation under static FDIA.

Firstly, a static FDIA against BESS SoC estimation for time slot 52 is constructed based on the method in Subsection 5.2.1. The impact of this static FDIA against SoC estimation is shown in Fig. 5.20, from which it can be observed that the static FDIA can cause a larger deviation of SoC estimation from actual SoC for time slot 52, compared with the SoC estimation under no attacks. After time slot 52, the impact of this static FDIA last for several time slots; however, the impact diminishes as time goes on, due to the existence of Kalman gain. Also, from Fig. 5.21, it can be observed that, for all the Monte Carlo simulation scenarios, the measurement residuals after static FDIA are the same with the measurement

residuals before static FDIA and are always below the threshold τ for BDD. This indicates that the constructed static FDIA can always bypass the BDD, if the measurements before FDIA are free of bad data, and will not be detected by the control center. It can be observed from Fig. 5.22 that the innovations of battery pack terminal voltage before and after static FDIA have the same patterns, since the variations of innovations are caused by random measurement noises. However, the innovations after static FDIA deviate from the innovations before static FDIA by a large value. This is caused by the static FDIA, and all the innovations after static FDIA exceed the threshold τ^{ekf} for the innovation test. This means that the detection method in Subsection 5.2.1 can always detect the static FDIA against BESS SoC estimation with large values.

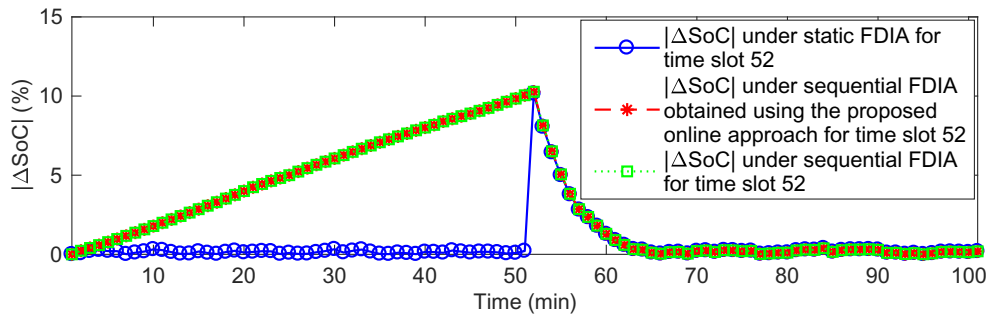


Figure 5.23: Sequential FDIA against SoC estimation.

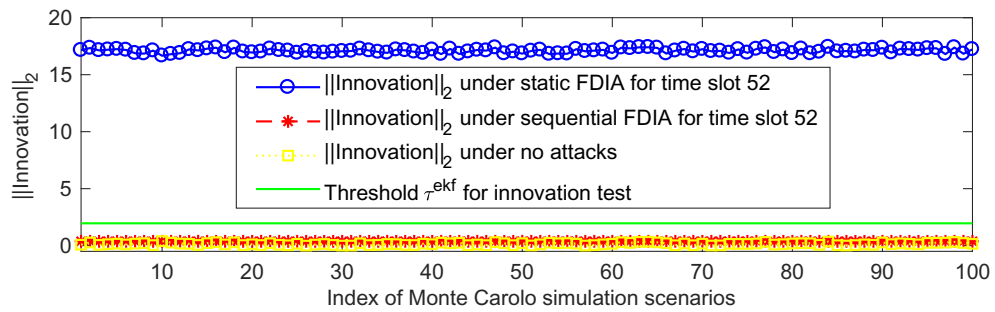


Figure 5.24: Innovation under sequential FDIA.

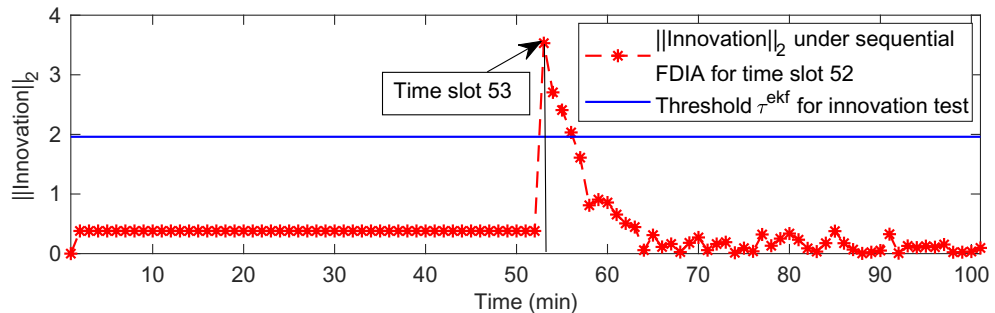


Figure 5.25: Innovations for different time slots under sequential FDIA.

From Fig. 5.23, it can be observed that the proposed online approach can obtain the same sequential FDIA as the one obtained using the method in Subsection 5.2.2, with the assumption that the system states, active and reactive power setpoints, and measurements for future time slots are available. Also, Fig. 5.23 indicates that different from static FDIA, which causes a sudden change of SoC estimation for time slot 52, the sequential FDIA gradually compromises the SoC estimation result for time slot 52, and it has the same impact as that of static FDIA on SoC estimation. Also, from Fig. 5.24, compared with the static FDIA, the sequential FDIA results in small innovations that are all below the threshold τ^{ekf} . So, from the results shown in Fig. 5.23 and 5.24, it can be concluded that the proposed sequential FDIA can achieve the same performance on compromising SoC estimation results as that of static FDIA, and it can always bypass the innovation test. However, it can be observed in Fig. 5.25 that, due to the large error of SoC estimation caused by sequential FDIA for time slot 52, the innovation for time slot 53 becomes significantly large, which will alter the existence of abnormal SoC estimation.

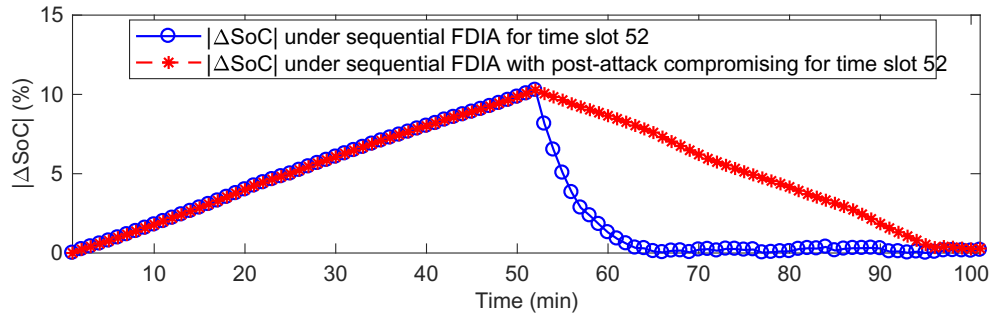


Figure 5.26: Sequential FDIA with post-attack compromising.

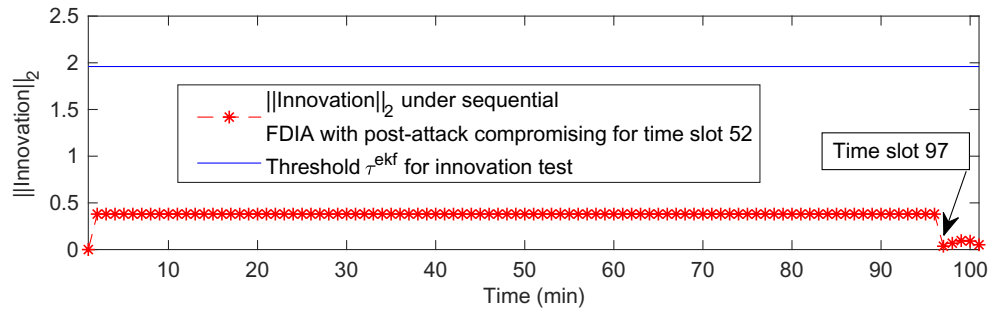


Figure 5.27: Innovations for different time slots under sequential FDIA with post-attack compromising.

Therefore, for a successful sequential FDIA against BESS SoC estimation, the adversary is required to perform post-attack compromising to avoid the large innovations for time slots after the sequential FDIA. By following the steps discussed in Subsection 5.2.2, the results for a sequential FDIA with the corresponding post-attack compromising are shown in Fig. 5.26. It can be observed that, compared with sequential FDIA, the sequential FDIA

with post-attack compromising still injects attack vectors after time slot 52, which is aimed at reducing the innovations of measurements after the sequential FDIA targeting on time slot 52. From Fig. 5.27, it can be observed that by considering the post-attack compromising, the attack vectors, constructed by following the steps in Subsection 5.2.2, are injected for time slots after sequential FDIA to avoid the innovations exceeding the threshold. Also, it can be observed from Fig. 5.27 that the post-attack compromising ended at time slot 96. So, in comparison with sequential FDIA, the sequential FDIA with post-attack compromising requires a longer attacking horizon.

5.3 Summary

In this chapter, the cyber-physical security vulnerability of BESSs in SDSs is investigated with a specific focus on the typical system information integrity attacks, i.e., FDIAs. For the cyber-physical security vulnerability, the construction principle of practical FDIAs in SDSs is first studied to show that the FDIAs in SDSs are practically applicable. Also, the feasibility and limitations of performing FDIAs in SDSs are discussed in detail. Based on the construction principle of FDIAs in SDSs, the mechanisms of FDIAs against SoC estimation of BESSs in SDSs are studied, which provide insights on the vulnerability of BESSs in SDSs to cyber-physical attacks.

6

Conclusions and Future Works

To better accommodate the ever-increasing load demands and environmental concerns, the conventional power distribution systems are undergoing massive shifts towards the more efficient, reliable, sustainable, and intelligent SDSs. In the development towards SDSs, the BESS has attracted a great amount of attention from researchers in both academia and industry. The BESS can support a wide range of applications in both demand-side and grid-scale services due to the flexible control and fast response of battery devices. In addition to the constant progress in battery technologies and power electronics, the development of reliable and intelligent battery energy storage management schemes has been in an urgent need in recent years. One of the most significant challenges in battery energy storage management is the randomness in SDSs. In future SDSs, the active energy management of BESSs relies heavily on efficient and reliable information transmission among different entities. However, information transmission may be prone to severe cyber-physical attacks. Thus, in this thesis, the stochastic energy management and cyber-physical security of BESSs in SDSs are investigated.

To reduce the computational complexity for stochastic energy management of BESSs that involve multiple energy pathways with distinct timescale characteristics, a novel stochastic multi-timescale energy management scheme is proposed with its application in commercial greenhouses with RES. Then, for SDSs with high BESSs penetration, a hierarchical and decentralized stochastic energy management scheme is proposed to effectively manage the BESSs within SDSs for joint cost minimization of both DSO and customers, while maintaining the voltage levels within the required range. Also, the proposed hierarchical and decentralized stochastic energy management scheme can significantly reduce the computational complexity, making it suitable for complex and large-scale SDSs. The stochastic energy management of EBCSs with EBs functioning as mobile BESSs is investi-

gated in this thesis, where the problem is formulated as a DRMDP for the highly statistical random RES and EBs with fixed routes and schedules while considering the impacts of random bus loads with inaccurate PDF estimation. With the formulated DRMDP for stochastic EBCSs energy management, the solutions are robust to errors of PDF estimations and are less conservative with better performance in minimizing the expected cost of EBCSs operation. Further, the cyber-physical security of BESSs in SDSs is investigated by analyzing the vulnerability of BESSs in practical multiphase and unbalanced SDSs to classical FDIAs, which provides helpful guidance in designing countermeasures against FDIAs targeting BESSs in SDSs. Also, a potential countermeasure using CPVD method is highlighted.

In this thesis, different heuristic or approximated solution methods, such as heuristic search and pruning, are proposed to reduce the proposed energy management schemes' computational complexity to facilitate practical applications. However, for successful applications, besides the concerns on computational complexity, the reliability of the proposed energy management schemes is also a major concern, which still requires extensive studies.

6.1 Contributions of Thesis

The main contributions of this thesis can be summarized as follows:

- A stochastic multi-timescale energy management problem is formulated with coupled STS thermal process and FTS electrical process. An approximation solution method is proposed by considering the monotonicity of daily MMDP problem and the homogeneity of optimal policy from day to day to facilitate practical applications with less computational complexity.
- A hierarchical and decentralized stochastic energy management scheme for SDSs with high BESS penetration is proposed for the joint optimization of DSO and customers while regulating the voltage levels within the required range. An energy management scheme based on exhaustive backups is proposed to solve the formulated energy management problem in a decentralized manner. To reduce the computational complexity of DSO, a heuristic search with pruning scheme is proposed.
- A method for stochastic energy management of EBCSs is proposed using DRMDP with an event-based ambiguity set with combined statistical distance and moment information to achieve *minimax-regret* criterion for robust solutions that are less conservative. The day-ahead dynamic prices are derived to mitigate the EB charging impacts on power distribution systems. A heuristic regret function is proposed to obtain tractable solutions with reduced computational complexity.

- A local state-based linear DSSE for multiphase and unbalanced distribution systems is proposed from the perspective of attackers. The constructions of three-phase coupled, perfect three-phase decoupled, and imperfect three-phase decoupled FDIAs are analyzed with the probabilities of successful FDIAs derived numerically. The mechanism of FDIAs against SoC estimation in SDSs that can bypass both measurement residual-based BDD and innovation test is proposed by considering the temporal correlations of BESS measurements.

6.2 Directions for Future Work

The stochastic energy management and cyber-physical security of BESSs in SDSs is a broad research area. Although several critical issues have been addressed in this thesis, there are still many research issues to be investigated. The following topics are proposed for future work:

- The applications of the proposed stochastic multi-timescale energy management scheme to other energy systems with more complex multi-timescale characteristics, such as the microgrids consisting of diversified energy carriers, i.e., multi-carrier microgrids, will be studied. Extensive research is still needed to reduce the computational complexity of large-scale systems. Also, the optimal selection of timescales for each energy pathway considering the requirements of different energy carriers and characteristics of different energy sources, demands, and storage units, are still open issues and require future research. A possible solution is to analyze the equivalence between the single-timescale problem and the transformed multi-timescale energy management problem. The equivalence should consider the lower bound of the ratio between the time slot duration of different energy pathways, which gives the longest time slot duration of the STS process, without violating the regulation requirements. Adaptive timescale durations for dynamic weather conditions can be studied further to reduce the computational complexity of the energy management problem.
- The energy management schemes for smart distribution systems with BESS based on game theory, where, instead of coordination, the DSO and customer will try to minimize their costs. Also, by adopting the concept of peer-to-peer (P2P) energy transactions, the utilization of local energy generation can be potentially improved. However, typical P2P energy transaction is mainly used for the profit maximization of a peer, based on an objective function different from the proposed energy management scheme. Involving such P2P energy transactions in the hierarchical and decentralized stochastic energy management architecture is a fascinating research topic and will be investigated in our future work.
- The extension of the MDP-based discrete stochastic control process model for BESS

energy management problems to MDPs with continuous action and state spaces. However, explicitly considering the continuous action and state spaces as impractical as solving an MDP requires computing all actions and states' value functions. One possible direction is to improve the existing nearest vertex of neighboring vertices methods to have a more accurate approximation of the action and state spaces using the discrete values. For example, the Kuhn triangulation could be a promising method to better approximate the true value functions using discrete values, as it allows efficient determination of the vertices in a point's barycentric coordinate system with the convex interpolation weights. Moreover, to overcome the high computational complexity issue of using MDP for large-scale systems, Q-learning implementation to interpolate the MDP model using data-driven approaches with expressing the reward and transition functions explicitly. However, the same as most machine learning applications in industry, the lack of training data set with a sufficient amount of data impedes machine learning's successful industrial applications. To overcome this issue, one possible solution is to leverage the synthetic data that are generated from experiments to train the real data-based MDP model through transfer learning, which can eliminate the divergences between the synthetic data domain and real data domain with different probability distributions.

- The PDF estimation errors of velocity and solar irradiation will also be considered for the stochastic energy management of EBCSs. By considering these estimation errors, the s-rectangularity may not be held. To address this issue, a possible solution is to consider factored transition probabilities and costs, where the uncertainties of transition probabilities and costs arising from several factors, such as bus loads, EB velocities, and solar irradiation, and each of these factors may be assumed to follow s-rectangularity. Currently, the mobility of EBs is treated as an exogenous random process, and there is no consideration for the interaction with the transportation network. In our future work, the development and usage of scenario-based and road-segmented transportation network models based on information from the incorporated intelligent transportation systems will be studied to improve the performance in modeling mobility of EBs.
- The countermeasures against cyber attacks targeting BESSs in SDSs will be investigated. Based on the discussions in this thesis, the difficulty of FDIAs in practical distribution systems depends heavily on how unbalanced the distribution systems are. More specifically, the more unbalanced the distribution systems are, the more measurements the attackers are required to compromise. Then the fewer efforts the DSOs need for the countermeasures. On the other hand, if the distribution systems are well balanced, the attackers can launch FDIAs with fewer efforts. This makes it difficult for the DSOs to perform countermeasures. The derived probabilities of successful FDIAs can guide the DSOs to secure buses more efficiently for counter-

measures. However, how to analyze it numerically still requires extensive research. Instead of physically protecting selected devices, the application of CPVD methods, specifically the watermarks for SoC estimation, is also a promising solution. However, extensive research is required to optimize the watermarks that will have the least impact on the performance of SoC estimation under no attacks. Moreover, from the standpoint of communication security, the leverage of encryption, authentication, and tamper-proof features of Blockchain technologies to protect the BESSs in SDSs against cyber-physical attacks will be investigated.

Bibliography

- [1] United States NIST (National Institute of Standards and Technology), *Framework and Roadmap for Smart Grid Interoperability Standards*. Accessed: Aug. 21, 2018. [Online]. Available: <http://www.nist.gov/smartgrid>.
- [2] M. Arif, A. Oo, and A. Ali, "Energy storage: applications and advantages," in *Smart Grids: Opportunities, Developments, and Trends*, New York, Springer, 2013, pp. 77-109.
- [3] M. Reuss, M. Beck, and J. P. Muller, "Design of a seasonal thermal energy storage in the ground," *Solar Energy*, vol. 59, pp. 247-257, Jun. 1997.
- [4] K. C. Divya and J. Ostergaard, "Battery energy storage technology for power systems-an overview," *Electr. Power Syst. Res.*, vol. 79, pp. 511-520, Apr. 2009.
- [5] H. S. Chen, "Progress in electrical energy storage system: a critical review," *Progr. Natural Sci.*, vol. 19, pp. 291-312, Mar. 2009.
- [6] W. Huang and J. A. A. Qahouq, "Distributed battery energy storage system architecture with energy sharing control for charge balancing," in *Proc. IEEE APEC'14*, June 2014.
- [7] S. Kumbhar et al., "Cybersecurity for battery management systems in cyber-physical environments," in *Proc. IEEE ITEC'18*, June 2018.
- [8] T. Kim et al., "An overview of cyber-physical security of battery management systems and adoption of blockchain technology," *IEEE Trans. Emerg. Sel. Topics Power Electron.*, vol. 1, no. 1, pp. 1-33, Jan. 2020.
- [9] A. B. Lopez et al., "A security perspective on battery systems of the Internet of Things," *J. Hardware and Systems Security*, vol. 1, no. 2, pp. 188-199, 2017.
- [10] N. Mhaisen, N. Fetais, and A. Massound, "Secure smart contract-enabled control of battery energy storage systems against cyber-attacks," *Alex. Eng. J.*, vol. 58, no. 4, pp. 1291-1300, Dec. 2019.
- [11] A. Adhikaree, T. Kim, J. Vagdoda, A. Ochoa, P. J. Hernandez, and Y. Lee, "Cloud-based battery condition monitoring platform for large-scale lithium-ion battery energy storage systems using Internet-of-Things (IoT)," in *Proc. 2017 IEEE ECCE'17*, Oct. 2017, pp. 1004-1009.

- [12] W. Y. Chang, "The state of charge estimation methods for battery: a review, *IRSN Appl. Math.*, vol. 2013, no. 1, pp. 186-192, Jul. 2013.
- [13] H. Zhang, W. Meng, J. Qi, X. Wang, and W. X. Zheng, "Distributed load sharing under false data injection attack in an inverter-based microgrid," *IEEE Trans. Ind. Electron.*, vol. 66, no. 2, pp. 1543-1551, Feb. 2019.
- [14] M. Zhang et al., "False data injection attacks against smart grid state estimation: construction, detection, and defense," *Sci. China Technol. SC.*, vol. 23, no. 216, pp. 1-11, Sep. 2019.
- [15] Q. Guo, S. Xin, L. Xu, and H. Sun, "EMS communication routings' optimisation to enhance power system security considering cyber-physical interdependence," *IET Cyber-Phys. Syst., Theory Appl.*, vol. 3, no. 1, pp. 44-53, Mar. 2018.
- [16] Electricity Information Sharing and Analysis Center. (2016) Analysis of the Cyber Attack on the Ukrainian Power Grid. Accessed: Aug. 21, 2018. [Online]. Available: https://ics.sans.org/media/E-ISAC_SANS_Ukraine_DUC_5.pdf.
- [17] Accuvant Labs. (2011) Battery Firmware Hacking Inside the Innards of a Smart Battery. Accessed: Aug. 21, 2018. [Online]. Available: https://media.blackhat.com/bh-us-11/Miller/BH.US.11_Miller_Battery_Firmware_Public_WP.pdf.
- [18] C. Sun, F. Sun, and S.J. Moura, "Nonlinear predictive energy management of residential buildings with photovoltaics & batteries," *J. Power Sources*, vol. 325, no.21, pp. 723-731, Sep. 2016.
- [19] R. Palma-Behnke, C. Benavides, F. Lanas, B. Severino, L. Reyes, J. Llanos, and D. Saez, "A microgrid energy management system based on the rolling horizon strategy," *IEEE Trans. Consumer Electron.*, vol. 4, no. 2, pp. 996-1006, Apr. 2013.
- [20] T. Kim and H. Poor, "Scheduling power consumption with price uncertainty," *IEEE Trans. Smart Grid*, vol. 2, no. 3, pp. 519-527, July 2011.
- [21] J. Donadee, M. Ilic, and O. Karabasoglu, "Optimal autonomous charging of electric vehicles with stochastic driver behavior," in *Proc. IEEE VPPC'14*, Oct. 2014.
- [22] J. Donadee and M. Ilic, "Stochastic optimization of grid to vehicle frequency regulation capacity bids," *IEEE Trans. Smart Grid*, vol. 5, no. 2, pp. 1061-1069, Mar. 2014.
- [23] Y. Liu, Y. Zhang, K. Chen, S. Z. Chen, and B. Tang, "Equivalence of multi-timescale optimization for home energy management considering user discomfort preference," *IEEE Trans. Smart Grid*, vol. 8, no. 4, pp. 1876-1887, July 2017.
- [24] T. Li and M. Dong, "Residential energy storage management with bidirectional energy control," *IEEE Trans. Smart Grid*, vol.1, no. 1, pp. 1-1, May 2018.

- [25] D. Rosewater et al., "Battery energy storage state-of-charge forecasting: models, optimization, and accuracy," *IEEE Trans. Smart Grid*, vol. 10, no. 3, pp. 2453-2462, May 2019.
- [26] F. Ahmad et al., "Distribution system state estimation a step towards smart grid," *Renew. Sustain. Energy Rev.*, vol. 81, pp. 2659-2671, Jan. 2017.
- [27] K. Dehghanpour, Z. Wang, J. Wang, Y. Yuan, and F. Bu, "A survey on state estimation techniques and challenges in smart distribution systems," *IEEE Trans. Smart Grid*, vol. 10, no. 2, pp. 2312-2322, March 2019.
- [28] N. Mhasisen, N. Fetais, and A. Massoud, "Secure smart contract-enabled control of battery energy storage systems against cyber-attacks," *Alex. Eng. J.*, vol. 58, no. 4, pp. 1291-1300, Dec. 2019.
- [29] L. Xie, Y. Mo, and B. Sinopoli, "Integrity data attacks in power market operations," *IEEE Trans. Smart Grid*, vol. 2, no. 4, pp. 659666, Dec. 2011.
- [30] Y. Yuan, Z. Li, and K. Ren, "Modeling load redistribution attacks in power systems," *IEEE Trans. Smart Grid*, vol. 2, no. 2, pp. 382390, Jun. 2011.
- [31] J. Lin et al., "On false data injection attacks against distributed energy routing in smart grid," in *Proc. IEEE/ACM ICCPS'12*, Apr. 2012.
- [32] L. Che, X. Liu and Z. Li, "Fast screening out high risk lines under false data injection attacks," *IEEE Trans. Smart Grid*, vol. 1, no. 1, pp. 1-1, June 2018.
- [33] R. Deng, P. Zhuang, and H. Liang, "False data injection attacks against state estimation in power distribution systems," *IEEE Trans. Smart Grid*, vol. 10, no. 3, pp. 2871-2881, May 2019.
- [34] L. Che, X. Liu, Z. Li, and Y. Wen, "False data injection attacks induced sequential outages in power systems," *IEEE Trans. Power Syst.*, vol. 34, no. 2, pp. 1513-1523, Mar. 2019.
- [35] C. Unterrieder, C. Zhang, M. Lunglmayr, R. Priewasser, S. Marsili, and M. Huemer, "Battery state-of-charge estimation using approximate least squares," *J. Power Sour.*, vol. 278, no. 1, pp. 274-286, Mar. 2015.
- [36] Q. Yang, L. Chang, and W. Yu, "On false data injection attacks against Kalman filtering in power system dynamic state estimation," *Security Commun. Netw.*, vol. 9, no. 9, pp. 833-849, Aug. 2016.
- [37] J. Zhao et al., "Power system dynamic state estimation: motivations, definitions, methodologies, and future work," *IEEE Trans. Power Syst.*, vol. 34, no. 4, pp. 3188-3198, July 2019.

- [38] J. Zhao, G. Zhang, Z. Y. Dong, and K. P. Wong, "Forecasting-aided imperfect false data injection attacks against power system nonlinear state estimation," *IEEE Trans. Smart Grid*, vol. 7, no. 1, pp. 6-8, Jan. 2016.
- [39] C. Liu, H. Liang, T. Chen, J. Wu, and C. Long, "Joint admittance perturbation and meter protection for mitigating stealthy FDI attacks against power system state estimation," *IEEE Trans. Power Syst.*, vol. 35, no. 2, pp. 1468-1478, Mar. 2020.
- [40] A. Bhattacharya, J. P. Kharoufeh, and B. Zeng, "Managing energy storage in microgrids: a multistage stochastic programming approach," *IEEE Trans. Smart Grid*, vol. 9, no. 1, pp. 483-496, Jan. 2018.
- [41] W. B. Powell, "Clearing the jungle of stochastic optimization clearing the jungle of stochastic optimization", *Inform's TutORials in Operations Research*, 2014, Oct. 2014.
- [42] R. Bellman, "The theory of dynamic programming," *RAND Corporation Proc. National Academy of Sciences*, pp. 503-715, 1952.
- [43] H. Xu and S. Mannor, "Distributionally robust Markov decision processes," in *NIPS'10*, Dec. 2010.
- [44] A. Nilim and L. El Ghaoui, "Robust control of Markov decision processes with uncertain transition matrices," *Operations Research*, vol. 53, no. 5, pp. 780798, Sept. 2005.
- [45] C. C. White III and H. K. El Deib, "Markov decision processes with imprecise transition probabilities," *Operations Research*, vol. 42, no. 4, pp. 739748, July 1992.
- [46] G. N. Iyengar, "Robust dynamic programming," *Mathematics of Operations Research*, vol. 30, no. 2, pp. 257280, Jan. 2005.
- [47] P. Yu and H. Xu, "Distributionally robust counterpart in Markov decision processes," *IEEE Trans. Automat. Control*, vol. 61, no. 9, pp. 25382543, Sep. 2016.
- [48] G. A. Hanasusanto, D. Kuhn, S. W. Wallace, and S. Zymmler, "Distributionally robust multi-item newsvendor problems with multimodal demand distributions," *Mathematical Programming*, vol. 152, pp. 1-32, 2015.
- [49] F. Schweppe, J. Wildes, and D. Rom, Power system static state estimation: Parts I, II, and III, in *Proc. PICA*, June 1969.
- [50] S. Peng, C. Chen, H. Shi, and Z. Yao, "State of charge estimation of battery energy storage systems based on adaptive unscented Kalman filter with a noise statistics estimator," *IEEE Access*, vol. 5, pp. 13202-13212, July 2017.
- [51] V. Sangwan, R. Kumar, and A. K. Rathore, "State-of-charge estimation for li-ion battery using extended Kalman filter (EKF) and central difference Kalman filter (CDKF)," in *IEEE IAS'17*, Oct. 2017.

- [52] M. Cacciato, G. Nobile, G. Scarcella, and G. Scelba, "Real-time model-based estimation of SOC and SOH for energy storage systems," *IEEE Trans. Power Electron.*, vol. 32, no. 1, pp. 794-803, Jan. 2017.
- [53] R. Xiong, F. Sun, X. Gong, and H. He, "Adaptive state of charge estimator for lithium-ion cells series battery pack in electric vehicles," *J. Power Sources*, vol. 242, no. 1, pp. 699-713, Nov. 2013.
- [54] U.S. EPA, "Inventory of U.S. GHG emissions and sinks," Apr. 2016.
- [55] M. Djevic and A. Dimitrijevic, "Energy consumption for different greenhouse constructions," *Energy*, vol. 34, no. 9, pp. 1325-1331, Sept. 2009.
- [56] A. Vadiie and V. Martin, "Energy management strategies for commercial greenhouses," *Appl. Energy*, vol. 114, pp. 880-888, Feb. 2014.
- [57] G. Straten, *Optimal control of greenhouse cultivation*, Boca Raton, CRC Press, Nov. 2011.
- [58] J. G. Hare, B. Norton, and S.D. Probert, "Design of greenhouses: thermal aspects," *Appl. Energy*, vol. 18, pp. 49-82, Apr. 1984.
- [59] J. Oliveira, J. Boaventura, and P.M. Oliveira, "Automation and control in greenhouses: state-of-the-art and future trends," *CONTROL 2016 Springer*, pp. 597-606, Sept. 2016.
- [60] D. Harrison, "An energy-producing greenhouse", *Greenhouse Canada*, 2018. Accessed: July 17, 2017. [Online]. Available: <https://www.uniongas.com/business/your-business/greenhouse>.
- [61] Y. Tong, T. Kozai, N. Nishioka, and K. Ohyama, "Reductions in energy consumption and CO₂ emissions for greenhouses heated with heat pumps," *Trans. ASABE*, vol. 28, pp. 401-406, Mar. 2012.
- [62] M. C. Bozchalui, C. A. Canizares, and K. Bhattacharya, "Optimal energy management of greenhouses in smart grids," *IEEE Trans. Smart Grid*, vol. 6, no. 2, pp. 827-835, Mar. 2015.
- [63] M. O. Neamtu and N. D. Trip, "A geothermal generator for grid greenhouse electrical power generator for supplying microgrid," in *Proc. IEEE EDPE'15*, Nov. 2015.
- [64] M. Cossu, L. Murgia, L. Ledda, P. A. Deligios, and A. Sirigu, "Solar radiation distribution inside a greenhouse with south-oriented photovoltaic roofs and effects on crop productivity," *Appl. Energy*, vol. 133, pp. 89-100, Nov. 2014.
- [65] R. Hassanien, E. Hassanien, M. Li, and W. D. Lin, "Advanced applications of solar energy in agricultural greenhouses," *Renew. Sustain. Energy Rev.*, vol.54, pp. 989-1001, Feb. 2016.

- [66] E. Byon, L. Ntaimo and Y. Ding, "Optimal maintenance strategies for wind turbine systems under stochastic weather conditions," *IEEE Trans. Rel.*, vol. 59, no. 2, pp. 393-404, June 2010.
- [67] L. Zhang and Y. Li, "Optimal energy management of wind-battery hybrid power system with two-scale dynamic programming," *IEEE Trans. Sustain. Energy*, vol. 4, no. 3, pp. 765-773, July 2013.
- [68] Y. Guo, M. Pan, Y. Fang, and P. P. Khargonekar, "Decentralized coordination of energy utilization for residential households in the smart grid," *IEEE Trans. Smart Grid*, vol. 4, no. 3, pp. 1341-1350, Sept. 2013.
- [69] J. Wu and X. Guan, "Coordinated multi-microgrids optimal control algorithm for smart distribution management system," *IEEE Trans. Smart Grid*, vol. 4, no. 4, pp. 2174-2181, Dec. 2013.
- [70] Z. Wang, B. Chen, J. Wang, M. M. Begovic, and C. Chen, "Coordinated energy management of networked microgrids in distribution systems," *IEEE Trans. Smart Grid*, vol. 6, no. 1, pp. 45-53, Jan. 2015.
- [71] V. Bui, A. Hussain, and H. Kim, "A multiagent-based hierarchical energy management strategy for multi-microgrids considering adjustable power and demand response," *IEEE Trans. Smart Grid*, vol. 9, no. 2, pp. 1323-1333, March 2018.
- [72] M. Zipf and D. Mst, "Cooperation of TSO and DSO to provide ancillary services," in *Proc. IEEE EEM'16*, Aug. 2016.
- [73] J. Morin, F. Colas, X. Guillard, J. Dieulot, and S. Grenard, "Joint DSOTSO reactive power management for an HV system considering MV systems support," *IEEE CIREN*, vol. 2, no. 1, pp. 1269-1273, Oct. 2017.
- [74] S. Uemura, "Coordinated operation of TSO, DSO and consumers in voltage management in case of interconnecting large amount of PV," in *Proc. CIREN Workshop'16*, Nov. 2016.
- [75] W. Su, J. Wang, and J. Roh, "Stochastic energy scheduling in microgrids with intermittent renewable energy resources," *IEEE Trans. Smart Grid*, vol. 5, no. 4, pp. 1876-1883, July 2014.
- [76] M. Fathi and H. Bevrani, "Adaptive energy consumption scheduling for connected microgrids under demand uncertainty," *IEEE Trans. Power Del.*, vol. 28, no. 3, pp. 1576-1583, July 2013.
- [77] A. F. Raab, E. Lauth, K. Strunz, and D. Gohlich, "Implementation schemes for electric bus fleets at depots with optimized energy procurements in virtual power plant operations," *World Electr. Veh. J.*, vol. 10, no. 1, pp. 5, Jan. 2019.

- [78] Bus2Grid. <https://gtr.ukri.org/projects?ref=104230>.
- [79] First Priority GreenFleet. <https://www.1fpg.com/first-priority-greenfleet-vehicle-to-grid>.
- [80] M. Moataz, F. Hany, E. T. Nader, and F. Mark, "Simulation of electric buses on a full transit network: operational feasibility and grid impact analysis," *Electr. Pow. Syst. Res.*, vol. 142, pp. 163-175, Jan. 2017.
- [81] H. Ding, Z. Hu, and Y. Song, "Value of the energy storage system in an electric bus fast charging station," *Appl. Energy*, vol. 157, no. 1, pp. 630-639, Nov. 2015.
- [82] P. Dicke, B. Meyer, and M. Pruckner. "Electrification of public bus transport under the usage of electricity generated by renewables," in *Proc. IEEE ICITE'17*, Sept. 2017.
- [83] Y. Cheng, W. Wang, Z. Ding, and Z. He, "Electric bus fast charging station resource planning considering load aggregation and renewable integration," *IET Renew. Power Gener.*, vol. 13, no. 7, pp. 1132-1141, May 2019.
- [84] E. Iversen, J. Morales, and H. Madsen, "Optimal charging of an electric vehicle using a Markov decision process," *Appl. Energy*, vol. 123, pp. 112, Jun. 2014.
- [85] M. Shin, D. Choi, and J. Kim, "Cooperative management for PV/ESS-enabled electric-vehicle charging stations," *IEEE Trans. Ind. Informat.*, vol. 1, no. 1, pp. 1-1, Sept. 2019.
- [86] C. Luo, Y. Huang, and V. Gupta, "Stochastic dynamic pricing for EV charging stations with renewable integration and energy storage," *IEEE Trans. Smart Grid*, vol. 9, no. 2, pp. 1494-1505, March 2018.
- [87] Q. Huang, Q. Jia, and X. Guan, "Robust scheduling of EV charging load with uncertain wind power integration," *IEEE Trans. Smart Grid*, vol. 9, no. 2, pp. 1043-1054, March 2018.
- [88] R. Deng, Y. Liu, W. Chen, and H. Liang, "A survey on electric buses - energy storage, power management, and charging scheduling," *IEEE Trans. Intell. Transp. Syst.*, vol. 1, no. 1, pp. 1-14, Dec. 2019.
- [89] P. Martinex, P. Sorba, and A. Ivan, "Energy consumption of passenger land transport modes," *Energy Environ. Sci.*, vol. 21, no. 6, pp. 577-600, 2010.
- [90] Y. Ji, J. Zhao, Z. Zhang, and Y. Du, "Estimating bus loads and OD flows using location-stamped farebox and Wi-Fi signal data," *J. of Advanced Trans.*, vol. 20, no. 7, pp. 10-16, May 2017.

- [91] W. Sun, T. Song, and H. Zhong, "Study on bus passenger capacity forecast based on regression analysis including time series," in *Proc. ICMTMA'09*, Apr. 2009.
- [92] Y. Tu and J. Yang, "Analysis and forecast of passenger flow based on public transportation IC card and GPS data," in *Proc. IEEE ICCSNT'16*, Dec. 2016.
- [93] X. Tang, X. Lin, and F. He, "Robust scheduling strategies of electric buses under stochastic traffic conditions," *Transp. Res.*, vol. 10, no. 1, pp. 163-182, Aug. 2019.
- [94] R. Xie, W. Wei, M. E. Khodayar, J. Wang, and S. Mei, "Planning fully renewable powered charging stations on highways: a data-driven robust optimization approach," *IEEE Trans. Transport. Electrification*, vol. 4, no. 3, pp. 817-830, Sept. 2018.
- [95] P. Xiong, P. Jirutitijaroen and C. Singh, "A Distributionally Robust Optimization Model for Unit Commitment Considering Uncertain Wind Power Generation," *IEEE Trans. Power Syst.*, vol. 32, no. 1, pp. 39-49, Jan. 2017.
- [96] Y. Zhang, S. Shen, B. Li and J. L. Mathieu, "Two-stage distributionally robust optimal power flow with flexible loads," in *proc. IEEE PowerTech*, June 2017.
- [97] A. Zare, C. Y. Chung, J. Zhan, and S. O. Faried, "A distributionally robust chance-constrained MILP model for multistage distribution system planning with uncertain renewables and loads," *IEEE Trans. Power Syst.*, vol. 33, no. 5, pp. 5248-5262, Sept. 2018.
- [98] K. Regan, C. Boutilier, "Regret-based reward elicitation for markov decision processes," in *Proc. UAI'09*, May 2009.
- [99] G. Perakis and G. Roels, "Regret in the newsvendor model with partial information," *Oper. Res.*, vol. 56, no. 1, pp. 188-203, Jan. 2008.
- [100] K. Natarajan, D. Shi, and K. C. Toh, "A probabilistic model for minmax regret in combinatorial optimization," *Oper. Res.*, vol. 62, no. 1, pp. 160-181, 2013.
- [101] W. Wiesemann, D. Kuhn, B. Rustem, "Robust Markov decision processes," *Math. Oper. Res.*, vol. 38, no. 1, pp. 153-183, Feb. 2013.
- [102] A. de la Villa Jaen, E. Acha, and A. G. Exposito, "Voltage source converter modeling for power system state estimation: STATCOM and VSC-HVDC," *IEEE Trans. Power Syst.*, vol. 23, no. 4, pp. 1552-1559, Nov. 2008.
- [103] S. Kar, G. Hug, J. Mohammadi, and J. M. F. Moura, "Distributed state estimation and energy management in smart grids: a consensus+ innovations approach," *IEEE J. Sel. Topics Signal Process.*, vol. 8, no. 6, pp. 1022-1038, Dec. 2014.

- [104] S. N. Islam, M. A. Mahmud, and A. M. T. Oo, "Impact of optimal false data injection attacks on local energy trading in a residential microgrid," *ICT Express*, vol. 4, no. 1, pp. 30-34, May 2018.
- [105] H. He and J. Yan, "Cyber-physical attacks and defences in the smart grid: a survey," *IET Cyber-Phys. Syst., Theory Appl.*, vol. 1, no. 1, pp. 13-27, June 2016.
- [106] T. T. Kim and H. V. Poor, "Strategic protection against data injection attacks on power grids," *IEEE Trans. Smart Grid*, vol.2, no. 2, pp. 326333, June 2011.
- [107] J. Valenzuela, J. Wang, and N. Bissinger, "Real-time intrusion detection in power system operations," *IEEE Trans. Power Syst.*, vol. 28, no.2, pp. 1052-1062, May 2013.
- [108] L.Che, X. Liu and Z. Li, "Mitigating false data attacks induced overloads using a corrective dispatch scheme," *IEEE Trans. Smart Grid*, vol. 1, no. 1, pp. 1-1, Mar. 2018.
- [109] C. Rakpenthai, S. Premrudeepreechacharn, S. Uatrongjit, and N. R. Watson, "An optimal PMU placement method against measurement loss and branch outage," *IEEE Trans. Power Del.*, vol. 22, no. 1, pp. 101107, Jan. 2007.
- [110] Y. M. Deng, Y. He, and B. M. Zhang, "A branch-estimation-based state estimation method for radial distribution systems," *IEEE Trans. Power Del.*, vol. 17, no. 4, pp. 1057-1062, Oct. 2002.
- [111] J. Chen, Y. Dong, and H. P. Zhang, "Distribution system state estimation: A survey of some relevant work," in *Proc. IEEE CCC'06*, June 2016.
- [112] A. Anwar, A. Mahmood, and M. Ahmed, "False data injection attack targeting the LTC transformers to disrupt smart grid operation," in *Proc. ICST Secure Comm. 14*, May 2015.
- [113] Y. Isozaki et al., "Detection of cyber attacks against voltage control in distribution power grids with PVs," *IEEE Trans. Smart Grid*, vol. 7, no. 4, pp. 1824-1835, July 2016.
- [114] A. Teixeira, G. Dn, H. Sandberg, R. Berthier, R. B. Bobba, and A. Valdes, "Security of smart distribution grids: data integrity attacks on integrated volt/VAR control and countermeasures," in *Proc. ACC'14*, June 2014.
- [115] M. A. Rahman and H. M. Rad, "False data injection attacks against nonlinear state estimation in smart power grids," in *Proc. IEEE PES GM'13*, July 2013.
- [116] G. Hug and J. A. Giampapa, "Vulnerability assessment of AC state estimation with respect to false data injection cyber-attacks," *IEEE Trans. Smart Grid*, vol. 3, no. 3, pp. 1362-1370, Sep. 2012.

- [117] L. Jia, R. J. Thomas, and L. Tong, "On the nonlinearity effects on malicious data attack on power system," in *Proc. IEEE PES GM'12*, July 2012.
- [118] G. Liang, J. Zhao, F. Luo, S. R. Weller, and Z. Y. Dong, "A review of false data injection attacks against modern power systems," *IEEE Trans. Smart Grid*, vol. 8, no. 4, pp. 1630-1638, July 2017.
- [119] R. Moslemi, A. Mesbahi, and J. M. Velni, "Design of robust profitable false data injection attacks in multi-settlement electricity markets," *IET GENER. TRANSM. DIS.*, vol. 12, no. 6, pp. 1263-1270, July 2018.
- [120] X. Liu and Z. Li, "False data attacks against AC state estimation with incomplete network information." *IEEE Trans. Smart Grid*, vol. 8, no. 5, pp. 2239-2248, June 2017.
- [121] X. Liu and Z. Li, "Local topology attacks in smart grids," *IEEE Trans. Smart Grid*, vol. 8, no. 6, pp. 2617-2626, Apr. 2017.
- [122] J. W. Kang, I. Y. Joo, and D. H. Choi, "False data injection attacks on contingency analysis: attack strategies and impact assessment," in *Proc. the IEEE*, Feb. 2018.
- [123] K. Zhou, L. Cai, and J. Pan, "Optimal combined heat and power system scheduling in smart grid," in *Proc. IEEE INFOCOM'14*, Apr. 2014.
- [124] Z. Li, W. Wu, M. Shahidehpour, J. Wang, and B. Zhang, "Combined heat and power dispatch considering pipeline energy storage of district heating network," in *Proc. IEEE PES GM'17*, July 2017.
- [125] H. Chen, Y. Yu, and X. Jiang, "Optimal scheduling of combined heat and power units with heat storage for the improvement of wind power integration," in *Proc. IEEE PES APPEEC'16*, Oct. 2016.
- [126] J. Aghaei et al., "Optimal robust unit commitment of CHP plants in electricity markets using information gap decision theory," *IEEE Trans. Smart Grid*, vol. 8, no. 5, pp. 2296-2304, Sept. 2017.
- [127] G. Zhang, Y. Cao, Y. Cao, D. Li, L. Wang, "Optimal energy management for microgrids with combined heat and power (chp) generation energy storages and renewable energy sources", *Energies*, vol. 10, no. 9, 2017.
- [128] P. Denholm *et al.*, "The value of energy storage for grid applications," *Contract*, vol. 303, pp. 275-300, 2013.
- [129] I. K. Song, "Operation schemes of smart distribution networks with distributed energy resources for loss reduction and service restoration," *IEEE Trans. Smart Grid*, vol. 4, no. 1, pp. 367374, Jan. 2013.

- [130] L. F. Ochoa, A. Keane, and G. P. Harrison, "Minimizing the reactive support for distributed generation: enhanced passive operation and smart distribution networks," *IEEE Trans. Power Syst.*, vol. 26, no. 4, pp. 2134-2142, Nov. 2011.
- [131] Z. Wang, C. Gu, F. Li, P. Bale, and H. Sun, "Active demand response using shared energy storage for household energy management," *IEEE Trans. Smart Grid*, vol. 4, no. 4, pp. 1888-1897, Dec. 2013.
- [132] A. Azizivahed, S. Ghavidel, M. J. Ghadi, L. Li, and J. Zhang, "New energy management approach in distribution systems considering energy storage," in *Proc. ICEMS'17*, Aug. 2017.
- [133] C. Zhao, S. Dong, and Y. Song, "Optimal home energy management system with mixed types of loads," *CSEE JPES*, vol. 1, no. 4, pp. 29-37, Dec. 2015.
- [134] P. Zhuang and H. Liang, "Energy storage management in smart homes based on resident activity of daily life recognition," in *Proc. IEEE SmartGridComm'15*, Nov. 2015.
- [135] International Energy Agency, "Global EV Outlook 2016: Beyond one million cars," 2016.
- [136] C. Guille and G. Gross, "A conceptual framework for the vehicle-to-grid (V2G) implementation," *Energy Policy*, vol. 37, no. 11, pp. 4379-4390, Nov. 2009.
- [137] H. F. Farahani, H. A. Shayanfar and M. S. Ghazizadeh, "Modeling of stochastic behavior of plug-in hybrid electric vehicle in a reactive power market," *Elect. Eng.*, vol. 96, no. 1, pp. 1-13, Mar. 2014.
- [138] A. Saber and G. Venayagamoorthy, "Optimization of vehicle-to-grid scheduling in constrained parking lots", in *Proc. IEEE PES GM'09*, July 2009.
- [139] M. Nikkhah Mojdehi and P. Ghosh, "An on-demand compensation function for an EV as a reactive power service provider," *IEEE Trans. Veh. Technol.*, vol. 65, no. 6, pp. 4572-4583, Jun. 2016.
- [140] L. Zhang and Y. Li, "A game-theoretic approach to optimal scheduling of parking-lot electric vehicle charging," *IEEE Trans. Veh. Technol.*, vol. 65, no. 6, pp. 4068-4078, Jun. 2016.
- [141] C. Wu, H. Mohsenian-Rad and J. Huang, "Vehicle-to-aggregator interaction game," *IEEE Trans. Smart Grid*, vol. 3, no. 1, pp. 434-442, Mar. 2012.
- [142] S. I. Vagropoulos and A. G. Bakirtzis, "Optimal bidding strategy for electric vehicle aggregators in electricity markets," *IEEE Trans. Power Syst.*, vol. 28, no. 4, pp. 4031-4041, Nov. 2013.

- [143] Y. Ota et al., "Effect of autonomous distributed vehicle-to-grid (V2G) on power system frequency control," in *Proc. CISIA'10*, June 2010.
- [144] A. K. Farraj, and D. Kundur, "On using energy storage systems in switching attacks that destabilize smart grid systems," in *Proc. IEEE ISGT'15*, Aug. 2015.
- [145] L. D. Albright, "Controlling greenhouse ventilation inlets by pressure difference," *Hort. Technology*, vol. 5, no. 3, pp. 260-264, Sept. 1995.
- [146] L. D. Albright, "Controlling greenhouses environment," *Acta. Horticulturae*, vol. 1, no. 578, pp. 47-54, June 2002.
- [147] C. Lamnatou and D. Chemisana, "Solar radiation manipulations and their role in greenhouse claddings: Fresnel lenses, NIR- and UV-blocking materials," *Renew. Sust. Energ. Rev.*, no.18, pp. 271-287, Feb. 2013.
- [148] J. E. CASKEY, "A Markov chain model for the probability of precipitation occurrence in intervals of various length," *Mon. Weather Rev.*, vol. 91, no. 6, pp. 298-301, June 1963.
- [149] W. Tushar, S. Huang, C. Yuen, B. Zhang, and D. B. Smith, "Synthetic generation of PV states for smart grid: A multiple segment Markov chain approach," in *Proc. IEEE ISGT'14*, Oct. 2014.
- [150] I. Teodorescu, "Maximum likelihood estimation for Markov Chains," *arXivpreprint arXiv:0905.4131*, 2009.
- [151] T. Guo and M. I. Henwood, "An algorithm for combined heat and power economic dispatch," *IEEE Trans. Power Syst.*, vol. 11, no. 4, pp. 1778-1784, Nov. 1996.
- [152] O. Linkevics and A. Sauhats, "Formulation of the objective function for economic dispatch optimisation of steam cycle CHP plants," in *Proc. IEEE Russia Power Tech.*, June 2005.
- [153] D. Xie, Y. Lu, and J. Sun, "Optimal operation of a combined heat and power system considering real-time energy prices," *IEEE Access*, vol. 4, pp. 3005-3015, June 2016.
- [154] A. Millner, "Modelling lithium ion battery degradation in electric vehicles," in *Proc. IEEE CITRES'10*, Sep. 2010.
- [155] F. Zhao, C. Zhang, and B. Sun, "Initiative optimization operation strategy and multi-objective energy management method for combined cooling heating and power," *IEEE/CAA J. Autom. Sinica*, vol. 3, no. 4, pp. 385-393, Nov. 2016.
- [156] D. Khiatani and U. Ghose, "Weather forecasting using Hidden Markov Model," in *Proc. IC3TSN'17*, Oct. 2017

- [157] A. I. Sarwat, A. Domijan, M. H. Amini, A. Damnjanovic, and A. Moghadasi, "Smart grid reliability assessment utilizing Boolean driven Markov Process and variable weather conditions," in *Proc. NAPS'15*, Oct. 2015.
- [158] Y. Lin, M. Hu, X. Yin, J. Guo, and Z. Li, "Evaluation of Lithium Batteries Based on Continuous Hidden Markov Model," in *Proc. QRS-C'17*, July 2017.
- [159] B. Da Lio, A. V. Guglielmi and L. Badia, "Markov models for electric vehicles: the role of battery parameters and charging point frequency," in *Proc. CAMAD'15*, Sept. 2015.
- [160] Z. Nie, F. Gao, C. B. Yan and X. Guan, "Realizability guaranteed multi-timescale optimization decision for home energy management," in *Proc. IEEE CASE'17*, Jan. 2017.
- [161] S. C. Hyeong, P. J. Fard, and S. I. Marcus, "Multitime scale Markov decision processes," *IEEE Trans. Autom. Control*, vol. 48, no. 6, pp. 976-987, June 2003.
- [162] D. Shen, C. Lim, P. Shi, and P. Bujlo, "Energy management of fuel cell hybrid vehicle based on partially observable Markov decision process," *IEEE Trans. Control. Syst. Technol.*, vol. 28, no. 2, pp. 318-330, March 2020.
- [163] I. Hussain, M. A. Ali, and G. H. Lee, "Performance and economic analyses of linear and spot fresnel lens solar collectors used for greenhouse heating in south Korea," *Energy*, vol. 90, no. 2, pp. 122-131, Oct. 2015.
- [164] R. S. Sutton and A. G. Barto, *Reinforcement Learning: An Introduction*, MIT Press, Cambridge, Mass., Feb. 1998.
- [165] C. Szepesvari, "Reinforcement learning algorithms for MDPs a survey," *Technical Report TR09-13*, Department of Computing Science, University of Alberta, Mar. 2009.
- [166] J. Chakravorty and A. Mahajan, "Sufficient conditions for the value function and optimal strategy to be even and quasi-convex," *IEEE Trans. Autom. Control*, Feb. 2018.
- [167] Bonnyville Forest Nursery Inc., <http://www.bonnyvilleforestnursery.com>.
- [168] Pomphrey Industries Corporation, <http://pomphreyindustries.co/>.
- [169] S. Peterson, J. Apt, and J. Whitacre, "Lithium ion battery cell degradation resulting from realistic vehicle and vehicle- to-grid utilization," *J. Pwr Sources*, vol.195, pp. 2385-2392, Nov. 2009.
- [170] Zone II Rates-Bchydro. Accessed: July 11, 2017. [Online]. Available: <https://www.bchydro.com/accounts-billing/rates-energy-use/electricity-rates/zone-2-rates.html>.

- [171] ATCOEnergy. Accessed: July 11, 2017. [Online]. Available: <http://www.atcoenergy.com/>.
- [172] R. K. Lam, D. H. Tran, and H. Yeh, "Economics of residential energy arbitrage in California using a PV system with directly connected energy storage," in *Proc. IEEE IGESC'15*, Nov. 2015.
- [173] J. V. de Souza et al., "Battery energy storage system allocation in distribution systems for power loss and operational costs reduction," in *Proc. IEEE PES ISGT'19*, Sept. 2019.
- [174] E. Chatzinikolaou and D. J. Rogers, "Hierarchical distributed balancing control for large-scale reconfigurable AC battery packs," *IEEE Trans. Power Electron.*, vol. 33, no. 7, pp. 5592-5602, July 2018.
- [175] J. Lian, J. Hansen, L. D. Marinovici, and K. Kalsi, "Hierarchical decentralized control strategy for demand-side primary frequency response," in *Proc. IEEE PESGM'16*, July 2016.
- [176] T. C. Green and M. Prodanovi, "Control of inverter-based microgrids," *Elect. Power Syst. Res.*, vol. 77, no. 9, pp. 1204-1213, Jul. 2007.
- [177] A. S. Gazafroudi et al., "A review of multi-agent based energy management systems," in *Proc. ISAmI'17*, June 2017.
- [178] H. E. Farag, E. F. El-Saadany, R. El-Shatshat, and A. Zidan, "A generalized power flow analysis for distribution systems with high penetration of distributed generation," *Elect. Power Syst. Res.*, vol. 81, no. 7, pp. 1499-1506, Jul. 2011.
- [179] N. Michelusi, L. Badia, R. Carli, L. Corradini, and M. Zorzi, "Energy management policies for harvesting-based wireless sensor devices with battery degradation," *IEEE Trans. Commun.*, vol. 61, no. 12, pp. 4934-4947, Dec. 2013.
- [180] B. Aksanli and T. Rosing, "Optimal battery configuration in a residential home with time-of-use pricing," in *Proc. IEEE SmartGridComm'13*, Oct. 2013.
- [181] Y. Ghiassi-Farrokhfal, S. Keshav, and F. Ciucu, "PV power shaping: An analytical approach," *IEEE Trans. Sustain. Energy*, vol. 6, no. 1, pp. 162-170, June 2015.
- [182] W. Tushar, S. Huang, and C. Yuen, "Synthetic generation of PV states for smart grid: a multiple segment Markov chain approach," in *Proc. IEEE ISGT'14*, Oct. 2014.
- [183] D. S. Bernstein, C. Amato, E. A. Hansen, and S. Zilberstein, "Policy iteration for decentralized control of Markov decision processes," *AAAI'09*, July 2009.

- [184] M. Zidar, P. S. Georgilakis, N. D. Hatziaargyriou, T. Capuder, and D. Skrlec, "Review of energy storage allocation in power distribution networks: applications, methods and future research," *IET GENER. TRANSM. DIS.*, vol. 10, no. 3, pp. 645-652, Feb. 2016.
- [185] B. A. E. Evan Nunen, "A set of successive approximation methods for discounted Markovian decision problems," *Oper. Res.*, vol. 20, pp. 203-208, Apr. 1976.
- [186] F. A. Oliehoek, "Decentralized POMDPs," in *Reinforcement Learning: State of the Art, Adaptation, Learning, and Optimization*, Springer, vol.12, pp. 471-503, 2012.
- [187] W. B. Hopp, B. C. Bean, and R. L. Smith, "A new optimality criterion for nonhomogeneous Markov decision processes," *Oper. Res.*, vol. 35, pp.875 -883, Mar. 1987.
- [188] IEEE PES AMPS DSAS Test Feeder. <http://sites.ieee.org/pes-testfeeders/resources/>.
- [189] Australia Government. <https://search.data.gov.au/>.
- [190] Measurement and Instrumentation Data Center. <https://www.nrel.gov/midc/spmd/>.
- [191] Tesla Powerwall. https://www.teslamotors.com/en_CA/POWERWALL.
- [192] Samsung SDI. <https://myess.samsungsdi.com/prod/prod.do#0>.
- [193] Pacific Gas and Electric Company, "Voltage tolerance boundary".
- [194] J. Wang, Y. Huang, H. Xie, and G. Tian, "Driving pattern recognition and energy management for extended range electric bus," in *Proc. IEEE VPPC'14*, Oct. 2014.
- [195] IEA, "Global EV Outlook 2018." Accessed: Jul. 11, 2019. [Online]. Available: www.iea.org.
- [196] UITP, "Public transport trends 2017." Accessed: Oct. 24, 2018. [Online]. Available: <https://www UITP.org/public-transport-trends>.
- [197] R. Li, Q. Wu and S. S. Oren, "Distribution locational marginal pricing for optimal electric vehicle charging management," *IEEE Trans. Power Syst.*, vol. 29, no. 1, pp. 203-211, Jan. 2014.
- [198] L. Bai, J. Wang, C. Wang, C. Chen, and F. Li, "Distribution locational marginal pricing (DLMP) for congestion management and voltage support," *IEEE Trans. Power Syst.*, vol. 33, no. 4, pp. 4061-4073, July 2018.
- [199] S. Huang, Q. Wu, S. S. Oren, R. Li, and Z. Liu, "Distribution locational marginal pricing through quadratic programming for congestion management in distribution networks," *IEEE Trans. Power Syst.*, vol. 30, no. 4, pp. 2170-2178, July 2015.

- [200] Z. Liu, Q. Wu, S. S. Oren, S. Huang, R. Li, and L. Cheng, "Distribution locational marginal pricing for optimal electric vehicle charging through chance constrained mixed-integer programming," *IEEE Trans. Smart Grid*, vol. 9, no. 2, pp. 644-654, March 2018.
- [201] D. Bertsimas, M. Sim, and M. Zhang, "Adaptive distributionally robust optimization", *Manag. Sci.*, vol. 65, no. 2, pp. 459-954, May 2018.
- [202] J. E. Hakegard, T. A. Myrvoll, and T. R. Skoglund, "Statistical modelling for estimation of OD matrices for public transport using Wi-Fi and APC aata," in *Proc. ITSC'18*, June 2018.
- [203] Y. Liu, L. Chu, N. Xu, Y. Jia, and Z. Xu, "A method to improve accuracy of velocity prediction using Markov model," in *Proc. ICONIP'17*, Oct. 2017.
- [204] Y. Liu and H. Liang, "An MHO approach for electric bus charging scheme optimization," in *Proc. IEEE PESGM'18*, Aug. 2018.
- [205] H. H. Abdeltawab and Y. A. I. Mohamed, "Mobile energy storage scheduling and operation in active distribution systems," *IEEE Trans. Ind. Electron.*, vol. 64, no. 9, pp. 6828-6840, Sept. 2017.
- [206] P. Zhuang, H. Liang, and M. Pomphrey, "Stochastic multi-timescale energy management of greenhouses with renewable energy sources," *IEEE Trans. Sustain. Energy*, vol. 10, no. 2, pp. 905-917, Apr. 2019.
- [207] W. Tushar, S. Huang, C. Yuen, J. A. Zhang, and D. B. Smith, "Synthetic generation of solar states for smart grid: a multiple segment Markov chain approach," in *Proc. IEEE PESISGT'14*, June 2014.
- [208] W. Li, Y. Li, H. Deng, and L. Bao, "Planning of electric public transport system under battery swap mode," *Sustainability*, vol. 10, no. 7, pp. 2528, July 2018.
- [209] Z. Chen, M. Sim, and P. Xiong, "Distributionally robust optimization for sequential decision making," *Optimization Online*, 2019.
- [210] M. N. Faqiry and S. Das, "Distributed bilevel energy allocation mechanism with grid constraints and hidden user information," *IEEE Trans. Smart Grid*, vol. 10, no. 2, pp. 1869-1879, March 2019.
- [211] S. Wang, S. Chen, and L. Wu, "Distributed generation hosting capacity evaluation for distribution systems considering the robust optimal operation of OLTC and SVC," *IEEE Trans. Sustain. Energy*, vol. 7, no. 3, pp. 1111-1123, July 2016.

- [212] Y. Guo, K. Baker, E. DallAnese, Z. Hu, and T. H. Summers, "Data-based distributionally robust stochastic optimal power flow-Part I: methodologies," *IEEE Trans. Power Syst.*, vol. 34, no. 2, pp. 1483-1492, March 2019.
- [213] E. Altman, *Constrained Markov Decision Processes*. Boca Raton, FL: Chapman and Hall, 1999.
- [214] A. Carpentier, and M. Valko, "Simple regret for infinitely many armed bandits," in *Proc. ICML'15*, June 2015.
- [215] J. Song, Y. Gao, H. Wang, and B. An, "Measuring the distance between finite markov decision processes". in *Proc. AAMAS'16*, May 2016.
- [216] R. T. Rockafellar, *Conjugate Duality and Optimization*. Philadelphia, PA, USA: Society for Industrial and Applied Mathematics, 1974.
- [217] W. Kuo, H. Lin, Z. Xu, and W. Zhang, "Reliability Optimization with the Lagrange-Multiplier and Branch-and-Bound Technique," *IEEE Trans. Rel.*, vol. 36, no. 5, pp. 624-630, Dec. 1987.
- [218] M. S. Bazaraa and J.J. Jarv, "Linear Programming and Network Flows," *John Wiley & Sones*, vol. 10, no. 1, pp. 1-219, 1977.
- [219] St. Albert Transit/StAT. <https://stalbert.ca/city/transit/>
- [220] Measurement & Instrumentation Data Center. <https://www.nrel.gov/midc/spmd/>.
- [221] IEEE PES AMPS DSAS. <https://site.ieee.org/pes-testfeeders/resources/>.
- [222] Batteries BYD. <http://www.byd.com/en/NewEnergy.html>.
- [223] Energy Storage Units GE. <https://www.ge.com/content/dam/gepower-renewables>.
- [224] IESO Canada. <http://www.ieso.ca/Power-Data>.
- [225] F. Nielsen, "K-MLE: a fast algorithm for learning statistical mixture models," in *Proc. IEEE ICASSP'12*, Mar. 2012.
- [226] W. B. Haskell, R. Jain, and D. Kalathil, "Empirical dynamic programming," *math.OC*, vol. 1, no. 1, pp. 402-429, Nov. 2013.
- [227] The National Institute of Technology and Standards, "Cybersecurity for smart grid systems." Accessed: June 12, 2018. [Online]. Available: <http://www.nist.gov>.
- [228] X. Yu and Y. Xue, "Smart grids: a cyber-physical systems perspective," in *Proc. the IEEE*, May 2016.

- [229] K. Zetter, "Inside the cunning, unprecedented hack of Ukraines power grid." Accessed: July 6, 2018. [Online]. Available: <https://wired.com>.
- [230] C. K. Das et al., "Overview of energy storage systems in distribution networks: placement sizing operation and power quality," *Renew. Sustain. Energy Rev.*, vol. 91, pp. 1205-1230, Aug. 2018.
- [231] C. N. Lu, J. H. Teng, and W. H. E. Liu, "Distribution system state estimation," *IEEE Trans. Power Syst.*, vol. 10, no. 1, pp. 229-240, Nov. 1995.
- [232] M. Bazrafshan and N. Gatsis, "Comprehensive modeling of three-phase distribution systems via the bus admittance matrix," *IEEE Trans. Power Syst.*, vol. 33, no. 2, pp. 2015-2029, Mar. 2018.
- [233] M. Abdel-Akher, K. Mohamed Nor, and A. H. Abdul-Rashid, "Development of unbalanced three-phase distribution power flow analysis using sequence and phase components," in *Proc. MEPSC'08*, Mar. 2008.
- [234] H. Ahmadi, J. R. Marti, and A. von Meier, "A linear power flow formulation for three-phase distribution systems," *IEEE Trans. Power Syst.*, vol. 31, no. 6, pp. 5012-5021, June 2016.
- [235] "Distribution State Estimation," ETAP. Accessed: Dec. 4, 2018. [Online]. Available: <https://etap.com/product/distribution-state-estimation>.
- [236] G. Gray, J. Simmins, G. Rajappan, G. Ravikumar, and S. Khaparde, "Making distribution automation work: Smart data is imperative for growth," *IEEE Power & Energy Mag.*, vol. 14, no. 1, pp. 5867, Jan. 2016.
- [237] D. Atanackovic and V. Dabic, "Deployment of real-time state estimator and load flow in BC Hydro DMS - challenges and opportunities," in *Proc. IEEE PES GM'13*, July 2013.
- [238] S. Lefebvre, J. Prvost, and L. Lenoir, "Distribution state estimation: a necessary requirement for the smart grid," in *Proc. IEEE PES GM'14*, July 2014.
- [239] M. Baran and T. McDermott, "Distribution system state estimation using AMI data," in *Proc. IEEE PES PSCE'09*, Mar. 2009.
- [240] V. Thornley, N. Jenkins, S. White, "State estimation applied to active distribution networks with minimal measurements," in *Proc. PSCC'05*, June 2005.
- [241] J. V. Milanovi et al., "International industry practice on power-quality monitoring," *IEEE Trans. Power Del.*, vol.29, no.2, pp 130-142, 2014.

- [242] A. G. Exposito, A. Abur, P. Rousseaux, A. D. I. V. Jaen, and C. G. Quiles, "On the use of PMUs in power system state estimation," in *Proc. PSCC'11*, Aug. 2011.
- [243] M. E. Baran and A. W. Kelley, "A branch-current-based state estimation method for distribution systems," *IEEE Trans. Power Syst.*, vol. 10, no. 1, pp. 483-491, Dec. 1995.
- [244] F. C. Schweppe and J. Wildes, "Power system static-state estimation, Part I: Exact model," *IEEE Trans. Power App. Syst.*, vol. 89, no. 1, pp. 120-125, Sept. 1970.
- [245] M. Pau, P. A. Pegoraro, and S. Sulis, "Efficient branch-current-based distribution system state estimation including synchronized measurements," *IEEE Trans. Instrum. Meas.*, vol. 62, no. 9, pp. 2419-2429, July 2013.
- [246] C. Muscas, M. Pau, P. A. Pegoraro, and S. Sulis, "Effects of measurements and pseudomeasurements correlation in distribution system state estimation," *IEEE Trans. Instrum. Meas.*, vol. 63, no. 12, pp. 2813-2823, Oct. 2014.
- [247] H. Wang and N. Schulz, "A revised branch current-based distribution system state estimation algorithm and meter placement impact," *IEEE Trans. Power Syst.*, vol. 19, no. 1, pp. 2072-213, Dec. 2004.
- [248] A. Filip, "Linear approximation to $\sqrt{x^2 + y^2}$ having equiripple error characteristics," *IEEE Trans. Audio and Electroacoust.*, vol. 13, no. 51, pp. 167-171, Sept. 2016.
- [249] R. Singh, B. C. Pal, and R. B. Vinter, "Measurement placement in distribution system state estimation" *IEEE Trans. Power Syst.*, vol. 24, no. 2, pp. 668-675, June 2009.
- [250] A. Abur and A. G. Exposito, "Power system state estimation: theory and implementation," *FL, Boca Raton: CRC Press*, 2004.
- [251] E. Handschin, F. C. Schweppe, J. Kohlas, and A. Fiechter, "Bad data analysis for power system state estimation," *IEEE Trans. Power App. Syst.*, vol. 94, no. 2, pp. 329-337, 1975.
- [252] M. C. Almeida and L. F. Ochoa, "An improved three-phase AMB distribution system state estimator," *IEEE Trans. Power Syst.*, vol. 32, no. 2, pp. 1463-1473, Oct. 2017.
- [253] H. Rahimi-Eichi, U. Ojha, F. Baronti, and M. Chow, "Battery management system: an overview of its application in the smart grid and electric vehicles," *IEEE Ind. Electron. Mag.*, vol. 7, no. 2, pp. 4-16, June 2013.
- [254] M. Bazrafshan and N. Gatsis, "Comprehensive modeling of three-phase distribution systems via the bus admittance matrix," *IEEE Trans. Power Syst.*, vol. 33, no. 2, pp. 2015-2029, March 2018.

- [255] S. Chen, Z. Wei, G. Sun, N. Lu, Y. Sun, Y. Zhu, "Multi-area distributed three-phase state estimation for unbalanced active distribution networks," *J. Modern Power Syst. Clean Energy*, vol. 5, no. 5, pp. 767-776, Sep. 2016.
- [256] P. Zhuang, R. Deng, and H. Liang, "False data injection attacks against state estimation in multiphase and unbalanced smart distribution systems," *IEEE Trans. Smart Grid*, vol. 10, no. 6, pp. 6000-6013, Nov. 2019.
- [257] Y. Guo, W. Wu, B. Zhang, and H. Sun, "An efficient state estimation algorithm considering zero injection constraints," *IEEE Trans. Power Syst.*, vol. 28, no. 3, pp. 2651-2659, Aug. 2013.
- [258] A. Majumdar and B. C. Pal, "A three-phase state estimation in unbalanced distribution networks with switch modelling," in *Proc. IEEE CMI'16*, Jan. 2016.
- [259] H. Qian, J. Zhang, J. Lai, and W. Yu, "A high-efficiency grid-tie battery energy storage system," *IEEE Trans. Power Electron.*, vol. 26, no. 3, pp. 886-896, March 2011.
- [260] X. Zhang, Y. Wang, C. Liu, and Z. Chen, "A novel approach of remaining discharge energy prediction for large format lithium-ion battery pack," *J. Power Sources*, vol. 343, no. 1, pp. 216-225, March 2017.
- [261] J. Kim, J. Shin, C. Chun, and B. H. Cho, "Stable configuration of a Li-Ion series battery pack based on a screening process for improved voltage/SOC balancing," *IEEE Trans. Power Electron.*, vol. 27, no. 1, pp. 411-424, Jan. 2012.
- [262] R. Xiong, H. He, F. Sun, and K. Zhao, "Evaluation on state of charge estimation of batteries with adaptive Extended Kalman Filter by experiment approach," *IEEE Trans. Veh. Technol.*, vol. 62, no. 1, pp. 108-117, Jan. 2013.
- [263] Z. Song, H. Wang, J. Hou, H. Hofmann, and J. Sun, "Combined state and parameter estimation of Lithium-Ion battery with active current injection," *IEEE Trans. Power Electron.*, vol. 35, no. 4, pp. 4439-4447, Apr. 2020.
- [264] X. Lin et al., "State of charge estimation error due to parameter mismatch in a generalized explicit lithium ion battery model," in *Proc. ASME DSCC'11*, Nov. 2011.
- [265] L. Liu and Z. Xi, "False data injection attack sequence design against quantized networked control systems," in *Proc. IEEE ICUS'19*, Oct. 2019.
- [266] X. Lin and A. G. Stefanopoulou, "Analytic bound on accuracy of battery state and parameter estimation," *J. Electrochem. Soc.*, vol. 162, no. 9, pp. 1879-1891, July 2015.
- [267] Z. Chen, Y. Fu, and C. C. Mi, "State of charge estimation of Lithium-Ion batteries in electric drive vehicles using Extended Kalman Filtering," *IEEE Trans. Veh. Technol.*, vol. 62, no. 3, pp. 1020-1030, March 2013.

- [268] H. He et al., "State-of-charge estimation of the Lithium-Ion battery using an adaptive extended Kalman Filter based on an improved Thevenin model," *IEEE Trans. Veh. Technol.*, vol. 60, no. 4, pp. 1461-1469, May 2011.
- [269] N. Zhu, D. Betaille, J. Marais, and M. Berbineau, "Extended Kalman Filter (EKF) innovation-based integrity monitoring scheme with C/N0 weighting," in *Proc. IEEE RTSI'18*, Sept. 2018.
- [270] Z. Xi, M. Dahmardeh, B. Xia, Y. Fu, and C. Mi, "Learning of battery model Bias for effective state of charge estimation of Lithium-Ion batteries," *IEEE Trans. Veh. Technol.*, vol. 68, no. 9, pp. 8613-8628, Sept. 2019.
- [271] K. Sarrafan, K. Muttaqi, and D. Sutanto, "Real-time estimation of model parameters and state-of-charge of lithiumion batteries in electric vehicles using recursive least-square with forgetting factor," in *Proc. IEEE PEDES'18*, Dec. 2018.
- [272] K. L. Morrow et al., "Topology perturbation for detecting malicious data injection," in *Proc. IEEE HICSS'12*, Jan. 2012.
- [273] Y. L. Mo et al., "False data injection attacks against state estimation in wireless sensor networks," in *Proc. IEEE CDC'10*, Dec. 2010.
- [274] R. Singh, B. C. Pal, and R. B. Vinter, "Measurement placement in distribution system state estimation," *IEEE Trans. Power Syst.*, vol. 24, no. 2, pp. 668-675, June 2009.
- [275] G. Rancilio et al., "Modeling a large-scale battery energy storage system for power grid application analysis," *ENERGIES*, vol. 12, no. 17, pp. 3312-3338, Aug. 2019.
- [276] *Center for Advanced Life Cycle Engineering*. Accessed: Dec. 17, 2019. [Online]. Available: <https://web.calce.umd.edu/batteries/data.htm>.
- [277] MathWorks, *Power Electronics Control Design With Simulink/Battery Modeling*. Accessed: Dec. 17, 2019. [Online]. Available: <https://www.mathworks.com/solutions/power-electronics-control.html>.